RATES OF TECTONIC AND MAGMATIC PROCESSES IN THE NORTH CASCADES CONTINENTAL MAGMATIC ARC

by

Jennifer E. Piontek Matzel

B.S. Geology
Saint Norbert College, 1995

M.S. Geological Sciences, 1999
The University of Texas at Austin

SUBMITTED TO THE DEPARTMENT OF EARTH, ATMOSPHERIC, AND PLANETARY SCIENCES IN PARTIAL FULFILLMENT OF THE REQUIREMENTS FOR THE DEGREE OF

DOCTOR OF PHILOSOPHY
AT THE
MASSACHUSETTS INSTITUTE OF TECHNOLOGY

SEPTEMBER 2004

Signature of Author: _____
Department of Earth, Atmospheric, and Planetary Sciences
September 15, 2004

Certified by: _____
Samuel A. Bowring
Professor of Geology
Thesis Supervisor

Accepted by: _____
Maria T. Zuber
E.A. Griswold Professor of Geophysics and Planerary Science
Department Head

RATES OF TECTONIC AND MAGMATIC PROCESSES IN THE NORTH CASCADES CONTINENTAL MAGMATIC ARC

by

Jennifer E. Piontek Matzel

Submitted to the Department of Earth, Atmospheric, and Planetary Sciences at the Massachusetts Institute of Technology on September 15, 2004 in Partial Fulfillment of the Requirements for the Degree of Doctor of Philosophy in Geology

ABSTRACT

Continental magmatic arcs are among the most dynamic geologic systems, and documentation of the magmatic, thermal, and tectonic evolution of arcs is essential for understanding the processes of magma generation, ascent and crustal growth. The primary goal of this research is to determine rates of tectonic and magmatic processes in the mid to deep crustal levels of the crystalline core of the Cretaceous North Cascades arc. This region was selected for study because it preserves a ~10-40 km depth-section through the arc which allows an assessment of magmatic and structural processes over a range of crustal levels. The relatively young age of the arc (ca. 100-45 Ma) and the inherent high-precision of U-Pb zircon dates permit absolute uncertainties of <100 ky.

Meta-supracrustal rocks of the Cascades core record some of the highest pressures obtained in the North American Cordillera. The timing of deposition and metamorphism of the 9-12 kbar Swakane Gneiss constrain tectonic burial models and the timescales of large crustal displacements within an arc setting. These models involve rapid burial (~7 mm/yr) of a fore- or back-arc basin from ca. 73-68 Ma. Nd isotopic signatures of all meta-clastic terranes of the Cascades core reflect mixing of arc- and craton-derived sediment, and the Swakane Gneiss has the most isotopically-evolved signature of these terranes. Nd isotopic signatures of plutons that intrude the core lack evidence of melting of this isotopically-evolved unit. $^{40}Ar/^{39}Ar$ and U-Pb thermochronologic data define regional cooling patterns that suggest mid- to Late Cretaceous exhumation coincident with contraction and crustal thickening at the deepest levels of the core, followed by Early Tertiary extension.

High-precision U-Pb geochronology reveals internal complexities inherent in the construction of an intrusive magmatic system. The Mount Stuart batholith was constructed over a ca. 5.6 Myr time period with four punctuated intervals of magma emplacement, whereas the Tenpeak intrusion was emplaced in a more continuous process over ca. 2.7 Myr time period. U-Pb zircon dates from two elongate intrusions, the Seven-Fingered Jack and Entiat suites, suggest that they were constructed from multiple magmatic sheets that were partially homogenized at the level of emplacement.

Thesis Supervisor: Samuel A. Bowring
Title: Professor of Geology

ACKNOWLEDGEMENTS

First and foremost, I would like to that my supervisor, Sam Bowring, for his guidance, enthusiasm for science and for always challenging me to take my work to the next level. I am also grateful to Bob Miller, my mentor in the field, for his support and interest in this project. Thanks also to my committee of Tim Grove, Kip Hodges and Greg Hirth for constructive feedback throughout this process, and to Malcolm Pringle for assistance in the Ar lab.

It was a special treat to work in the North Cascades because of the helpful and enthusiastic collaborators that I refer to as the Cascades Working Group (Scott Paterson, Melissa Boysun, Markus Albertz, and Helge Alsleben from USC, Donna Whitney and Pete Valley from the University of Minnesota, Harold Stowell, Carlos Zulaga, and Doug Tinkham from the University of Alabama, and Bob Miller, Jonathon Miller and Scott McPeek from San Jose State University). Your thoughtful discussions, field assistance, and encouragement are greatly appreciated.

I am also grateful to my lab-mates for providing such a fun and challenging working environment. Thanks go to (in rough chronological order) Mark Martin, Kathy Keefe, Greg Hoke, Mark Schmitz, Karen Viskupic, Julie Baldwin, Blair Schoene, Becky Flowers, Jahan Ramezani, Jim Crowley, Dan Condon, Frank Dudas, Danny MacPhee, Greg Weiss, Paul Bovet, and Cara Johnson. I don't know how I would have survived this without all of you. Special thanks also go to Karen Viskupic and Julie Baldwin – my office mates of almost 5 years. Your input and interest made all the difference. Thanks to all of the G&G students that I've overlapped with for providing a supportive and productive environment. I'm also grateful for all of Pat Walsh's assistance. Thanks for looking out for me.

Finally, I would like to thank my family for all of their love and encouragement - especially Eric for always being positive, enthusiastic and supportive. I couldn't have done this without you.

TABLE OF CONTENTS

INTRODUCTION

Much of the intermediate-composition continental crust exposed today is the result of the interaction of subduction-related basaltic magmas with pre-existing crust in continental magmatic arcs (CMAs). However, this dynamic tectonic setting and its deep crustal evolution, in particular, are not well understood. Magma, volatiles, and heat are transferred upward from the mantle through the "filter" of the continental crust, and the timescales of the construction of magmatic intrusions dictate the rate at which heat is transferred. Unraveling the magmatic and thermal history of CMAs is essential to understanding the maturation of arcs and ultimately the generation of continental crust.

Recent advances in geochronological techniques have made it possible to address questions related to the evolution of CMAs with high-precision temporal constraints. In the following chapters, I have applied high-precision, U-Pb and $^{40}Ar/^{39}Ar$ geo- and thermochronology and isotope geochemistry to document the tectonic, thermal and magmatic evolution of the North Cascades arc. Although these studies focus on the evolution of a narrow time-slice (ca. 100-45 Ma) through a single arc, the results will form a basis for which other arcs can be compared.

The metamorphic and igneous core of the North Cascades (Cascades core) records the Cretaceous to Paleogene history of magmatism, deformation and crustal growth along a segment of the North American margin (Monger et al., 1982; Tabor et al., 1989). The Cascades core lies at the southern termination of the Canadian Coast Belt, and comprises Paleozoic to Mesozoic accreted terranes of oceanic and island-arc affinity that have undergone amphibolite-facies metamorphism during the mid-Cretaceous (Misch, 1966; Tabor et al., 1989; Tabor et al., 1987b). These terranes were sutured together during final, NE-SW-oriented contraction as the Insular superterrane collided with the Intermontane superterrane (Journeay and Friedman, 1993; Monger et al., 1982; Rubin et al., 1990), and provide the framework in which ca. 96-45 Ma arc plutons intrude.

The North Cascades arc presents a unique opportunity to study the tectonic, thermal and magmatic evolution of CMAs for several reasons. Cretaceous plutons in the North Cascades crystallized at ~10 to 30 km depth, and thus provide a window into

magmatic and tectonic processes at a large range of depths within the arc (Miller and Paterson, 2001b). These plutons were also emplaced episodically from ca. 96-46 Ma, permitting comparisons of magma emplacement styles, composition and geochemical characteristics over the life of the arc. Excellent exposure in this >30 km depth-section through the arc allows an analysis of the duration, episodicity and rates at which individual intrusions were constructed as well as burial and exhumation processes at a range of crustal levels. In addition, the relatively young age of the arc (~100-45 Ma) combined with the inherent high precision of U-Pb zircon dates provide the potential of resolving absolute ages with uncertainties of less than 100 ky. Finally, the geochronologic and isotopic data presented here can be integrated with numerous published structural, petrologic and geochemical studies.

Meta-supracrustal terranes of the North Cascades magmatic arc record some of the highest pressures obtained in the North American Cordillera. However, the timing of burial of these supracrustal rocks and high-pressure metamorphism are unclear. The terranes that comprise the Cascades core are thought to have been assembled prior to the emplacement of ca. 96-45 Ma plutons. This assumption fails to explain the origin and tectonic affinity of the deepest level terrane, the 9-12 kbar Swakane Gneiss, because even though this terrane is thought to have occupied a lower crustal position during mid-Cretaceous magmatism, the gneiss does not contain arc-related plutons, unlike all other terranes of the North Cascades. In Chapter 1, U-Pb analyses from detrital zircons from the Swakane Gneiss indicate that its protolith was deposited as late as 72.5±0.6 Ma, much younger than previous age estimates and well after the juxtaposition of the other arc terranes that comprise the Cascades core. The Swakane protolith was then metamorphosed at 9-12 kbar (Valley et al., 2003) and intruded by ca. 68 Ma peraluminous leucogranite sheets that may represent partial melt derived from deeper levels of the gneiss at near- to post-peak P-T conditions (Boysun, 2004; Boysun and Paterson, 2003; Valley et al., 2003). These data suggest rapid burial of the Swakane protolith to depths of ca. 35 km in <5 Myr (i.e. ~7mm/yr), and a variety of tectonic mechanisms that can account for this rapid burial are discussed in Chapter 1.

In Chapter 2, the spatial and temporal variability in Nd isotope signatures across the Cascades core are discussed. New Nd data from 46 samples spatially distributed

within the Cascades core are compared with existing Nd data from igneous rocks of the Coast Belt to address questions related to crustal growth in this region and the influence of input from the North American craton. Meta-clastic rocks have ε_{Nd} values that lie between those of arc-derived and craton-derived sediment reflecting a mixture of these two sources. ε_{Nd} values of the plutons that intrude that Cascades core reflect mixing of mantle-derived melt and melt derived by anatexis of isotopically juvenile, lower crustal terranes.

In chapter 3, new $^{40}Ar/^{39}Ar$ and U-Pb sphene and zircon data are integrated with the existing thermochronologic database from the region to facilitate discussion of the evolution of this laterally-segmented and variably-exhumed arc. Patterns of cooling are interpreted as representing mid- to Late Cretaceous exhumation coincident with contraction and crustal thickening at the deepest levels of the core, followed by Early Tertiary extension. The combined Late Cretaceous and Tertiary extension resulted in the exposure of heterogeneous crustal depths over short distances at the present-day surface. These patterns suggest that the timing of peak metamorphism and greatest burial depth were more variable both along strike and across the arc than previously recognized, and point out the need to distinguish between the magnitudes of Cretaceous and Tertiary exhumation in order to develop better models of the evolution of this region.

The last two chapters focus on the duration, tempo, and rates at which individual intrusions are constructed. In chapter 4, U-Pb zircon and sphene data from the Mount Stuart and Tenpeak intrusions constrain the intrusive and cooling histories of these two contrasting magma systems. Construction of the Tenpeak intrusion appears to have been a more continuous process that occurred over a ca. 2.7 Myr time span. Texturally distinct phases and internal sheeting are well-documented in the Tenpeak intrusion and significant homogenization of different magma pulses is lacking. In contrast, the Mount Stuart batholith appears to have been constructed over four discrete time periods during a ca. 5.6 Myr time span. This intrusion exhibits gradational contacts between magma pulses of differing composition, and similar textures and magmatic fabrics between pulses that are significantly different in age. The differences in evolution of these two magmatic systems may reflect different rates of magma generation and/or segregation from their source region. Alternatively, the deeper-level Tenpeak system may represent a

"filter" between lower crustal zones of magma generation and mixing, and upper crustal zones of large, relatively homogeneous intrusions such as the Mount Stuart batholith.

The final chapter documents the timescales of construction of two elongate, internally-sheeted magmatic systems, the Seven-Fingered Jack and Entiat intrusive suites. Prior to this study, the magmatic sheets that comprise these elongate bodies were assumed to be co-magmatic and described as a single, Entiat pluton (Miller and Paterson, 2001a; Paterson and Miller, 1998; Tabor et al., 1987a). However, U-Pb zircon dates from several sheets indicate that this suite was emplaced over at least three distinct time periods. At the northwestern end of the body, the oldest sheets are coeval with the Triassic Dumbell plutons and should be considered part of that suite. Sheets with ca. 90-92 Ma crystallization ages form the Seven-Fingered Jack suite and extend from the northwestern tip of the body and potentially most of the length of the body. Sheets with ca. 71-73 Ma crystallization ages comprise the Entiat intrusive suite and make up the more homogeneous southeastern end of the body. The recognition of an approximately 20 Myr time lag between emplacement of the Seven-Fingered Jack and Entiat suites indicates that the multiple thin sheets that form the northwestern end could not have formed preheated pathways for the emplacement of later, more homogeneous sheets as proposed in previous models for the construction of the intrusion (i.e., Miller and Paterson, 2001a). The presence of inherited zircon in several of the Entiat and Seven-Fingered Jack samples suggests that the formation of these magmatic sheets involved multiple intrusion and partial homogenization of sheets at the level of emplacement.

The data from these studies represent a significant contribution to the understanding of the tectonic, magmatic and thermal evolution of the Cascades core. The timing of rapid burial and high-pressure metamorphism of the Swakane Gneiss provide information about the timescales of large vertical displacements of crust within an arc setting and constrain tectonic burial models. Integration of new thermochronologic data with existing data from the core define cooling patterns that point to different exhumation mechanisms occurring simultaneously at a range of depths in the arc. The application of high-precision geochronologic techniques to the study of intrusive magmatic systems, in particular, reveal internal complexities inherent in the genesis of a "pluton" and require careful reconsideration of thermal and mechanical models for their construction.

REFERENCES

Boysun, M. A., 2004, Statistical distribution of leucocratic melts in the Swakane terrane, North Cascades Crystalline Core, WA [M.S. thesis]: University of Southern California, Los Angeles, 60 p.

Boysun, M. A., and Paterson, S. R., 2003, Partial melting and melt collection and transport in the Swakane terrane, North Cascades crystalline core, WA: Geological Society of America Abstracts with Programs, v. 35, p. 223.

Journeay, J. M., and Friedman, R. M., 1993, The Coast Belt thrust system: Evidence of Late Cretaceous shortening in southwest British Columbia: Tectonics, v. 12, p. 1301-1302.

Miller, R. B., and Paterson, S. R., 2001a, Construction of mid-crustal sheeted plutons: Examples from the north Cascades, Washington: Geological Society of America Bulletin, v. 113, p. 1423-1442.

Miller, R. B., and Paterson, S. R., 2001b, Influence of lithological heterogeneity, mechanical anisotropy, and magmatism on the rheology of an arc, North Cascades, Washington: Tectonophysics, v. 342, p. 351-370.

Misch, P., 1966, Tectonic evolution of the Northern Cascades of Washington State: a west-cordilleran case history: Canadian Institute of Mining and Metallurgy, v. Special volume 8, p. 101-148.

Monger, J. W. H., Price, R. A., and Tempelman-Kluit, D. J., 1982, Tectonic accretion and the origin of the two major metamorphic and plutonic welts in the Canadian Cordillera: Geology, v. 10, p. 70-75.

Paterson, S. R., and Miller, R. B., 1998, Mid-crustal magmatic sheets in the Cascades Mountains, Washington: implications for magma ascent: Journal of Structural Geology, v. 20, p. 1345-1363.

Rubin, C. M., Saleeby, J. B., Cowan, D. S., Brandon, M. T., and McGroder, M. F., 1990, Regionally extensive mid-Cretaceous west-vergent thrust system in the northwestern Cordillera: Implications for continent-margin tectonism: Geology, v. 18, p. 276-280.

Tabor, R. W., Frizzell, V. A., Jr., Whetten, J. T., Waitt, R. B., Jr., Swanson, D. A., Byerly, G. R., Booth, D. B., Hetherington, M. J., and Zartman, R. E., 1987a, Geologic map of the Chelan 30' by 60' Quadrangle, Washington: U. S. Geological Survey, scale 1:100,000.

Tabor, R. W., Haugerud, R. A., Brown, E. H., Babcock, R. S., and Miller, R. B., 1989, Accreted Terranes of the North Cascades Range, Washington, International Geologic Congress Trip T307: Washington, D.C., American Geophysical Union, 62 p.

Tabor, R. W., Zartman, R. E., and Frizzell, V. A., Jr., 1987b, Possible tectonostratigraphic terranes in the North Cascades crystalline core, Washington, *in* Schuster, J. E., ed., Selected Papers on the Geology of Washington: Anaheim, CA, United States, Washington Division of Geology and Earth Resources, p. 107-127.

Valley, P. M., Whitney, D. L., Paterson, S. R., Miller, R. B., and Alsleben, H., 2003, Metamorphism of the deepest exposed arc rocks in the Cretaceous to Paleogene Cascades belt, Washington: evidence for large- scale vertical motion in a continental arc: Journal of Metamorphic Geology, v. 21, p. 203-220.

Chapter1

PROTOLITH AGE OF THE SWAKANE GNEISS, NORTH CASCADES, WA: EVIDENCE OF RAPID UNDERTHRUSTING OF SEDIMENTS BENEATH AN ARC

Submitted to Tectonics, August 2003

Jennifer E. P. Matzel and Samuel A. Bowring
Department of Earth, Atmospheric and Planetary Sciences
Massachusetts Institute of Technology, Cambridge, MA 02139

Robert B. Miller
Department of Geology
San Jose State University, San Jose, CA 95192

ABSTRACT

The metamorphic core of the North Cascades largely comprises island arc and oceanic terranes juxtaposed prior to ca. 96 Ma magmatism. However, the tectonic affinity of the structurally deepest terrane, the 9-12 kbar Swakane Gneiss, is distinctly different from other terranes in the core; it is not intruded by arc-related plutons, contains abundant Precambrian zircons. New U-Pb analyses of detrital zircons from the Swakane Gneiss yield dates from 73 Ma to 1610 Ma with a dominant Late Cretaceous population. These data indicate that the Swakane protolith was deposited as late as 72.6±0.6 Ma, the $^{206}Pb/^{238}U$ date of the youngest detrital grain. Following deposition, the gneiss was intruded by peraluminous leucogranite sheets that may represent partial melt derived from the gneiss at near- to post-peak P-T conditions. One sheet yielded a U-Pb crystallization age of 68.36±0.07 Ma, which indicates that the gneiss was deeply buried within 5 Myr of deposition. Two possible mechanisms considered for this rapid burial (~7mm/yr) are overthrusting of a fore- or back-arc basin by older crystalline rock or underthrusting of trench sediments during low-angle subduction. The model involving overthrusting of a fore- or back-arc basin is most consistent with thermobarometric and isotopic data and the regional geologic setting of the Cascades core. Rapid burial of the Swakane protolith is coincident with burial of sediments that formed the Pelona, Orocopia and Rand schists of southern California; however, differences in peak metamorphic temperatures indicate that conditions of burial must have varied along the plate margin.

INTRODUCTION

Continental magmatic arcs commonly preserve evidence of significant crustal thickening as a result of contractional deformation. In such settings, vertical displacements of crust on the order of 20 km to >30 km have been documented [e.g. Clarke et al., 2000; Grove et al., 2003; Valley et al., 2003; Whitney et al., 1999]. However, the rates and durations of vertical motion are usually not well-constrained, and mechanisms proposed to account for tectonic burial are controversial. Along the northwestern edge of North America, the >1500 km long Coast Plutonic Complex records the history of Cretaceous to Paleogene arc magmatism and intra-arc shortening

which resulted in burial of supracrustal rocks to moderately high pressures [McGroder, 1991; Monger et al., 1982; Rubin et al., 1990; Whitney et al., 1999]. The crystalline core of the North Cascades forms the southernmost extent of this arc and comprises several amphibolite-facies terranes, including the Swakane Gneiss (Figures 1 and 2) [Misch, 1966; Tabor et al., 1989; Tabor et al., 1987b]. The core is bounded by high-angle Tertiary faults on the west and northeast [Misch, 1966] and a mid-Cretaceous thrust in the south (Figure 1) [Miller, 1985]. These faults mark transitions between weakly-metamorphosed regions to regions of amphibolite-grade metamorphism and Late Cretaceous to Eocene cooling ages. The Swakane Gneiss and overlying terranes were exhumed from >30 km depth and represent some of the deepest level rocks exposed within the North American Cordillera [Paterson et al., 2004; Valley et al., 2003; Whitney et al., 1999].

The generally accepted tectonic model for this region involves juxtaposition of oceanic and island arc terranes, including the Swakane Gneiss, by 96 Ma followed by episodic intrusion of arc plutons (96-46 Ma), dextral transpression (73-58 Ma), and then transtension (55-45 Ma) [Miller and Bowring, 1990; Tabor et al., 1989; Umhoefer and Miller, 1996]. This model fails to explain two important observations about the origin and tectonic affinity of the Swakane Gneiss: 1) although the Swakane terrane is at the center of, and occupied a position deep within, a long-lived continental magmatic arc, it is devoid of arc-related intrusive rocks, and 2) unlike other terranes in the North Cascades core, the Swakane Gneiss contains abundant Early to mid-Proterozoic zircons and yields mid- to Late Proterozoic Nd depleted mantle model ages [Mattinson, 1972; Rasbury and Walker, 1992]. These distinct features of the Swakane terrane raise the possibility that it may have been tectonically emplaced as an exotic slice late in the history of the North Cascades core.

The timing of deposition and subsequent high-P metamorphism of the Swakane terrane can provide insight into the timescales of large vertical displacements of crust within an arc setting. The relationship of this distinctive high-P terrane to the other fault-bounded terranes in the North Cascades core constrain the development of tectonic models. U-Pb dates obtained in this study from detrital zircons in the Swakane Gneiss indicate that its protolith was deposited as late as 72.5±0.6 Ma, much younger than

previous age estimates and well after the juxtaposition of the other arc terranes that comprise the North Cascades core. The Swakane protolith was then metamorphosed to 9-12 kbar [Valley et al., 2003] and intruded by peraluminous leucogranite sheets that may represent partial melt derived from the gneiss at near- to post-peak P-T conditions [Boysun, 2004; Boysun and Paterson, 2003; Valley et al., 2003]. One of these peraluminous sheets yields a crystallization age of 68.36±0.07 Ma. These data suggest rapid burial of the Swakane protolith to depths of ca. 35 km in <5 Myr, and thus require a reassessment of tectonic models involving the assembly of the North Cascades core.

GEOLOGIC SETTING

Tabor et al. [1987b, 1989] delineated several tectonostratigraphic terranes within the Cascades core (Figure 2). These terranes underwent amphibolite facies-metamorphism and contractional deformation, and all terranes, except the Swakane terrane, were intruded by 96-46 Ma plutons. Following tectonic assembly, the core was cut by the post-metamorphic, high-angle, Tertiary Entiat fault, which divides the core into the Wenatchee and Chelan blocks (Figure 1) [Haugerud et al., 1991]. The Swakane terrane crops out in both blocks (Figure 2).

The Swakane terrane is composed entirely of the Swakane Gneiss, a predominantly quartzofeldspathic biotite ± garnet and muscovite gneiss with subordinant garnet amphibolite, garnet + hornblende + biotite gneiss, garnet + kyanite ± staurolite gneiss, calc-silicate, quartzite and meta-peridotite [Cater, 1982; Paterson et al., 2004; Sawyko, 1994; Tabor et al., 1987a; Tabor et al., 1987b; Valley et al., 2003; Waters, 1932]. The protolith of the gneiss has been interpreted as either a sequence of arc-derived clastic sediments or a thick pile of predominantly silicic volcanic rock [Cater, 1982; Mattinson, 1972; Sawyko, 1994; Tabor et al., 1987a; Tabor et al., 1987b; Waters, 1932; Whitney et al., 1999]. Although no plutons intrude the Swakane Gneiss, several generations of thin (<3 m) peraluminous leucogranite sheets containing muscovite ± garnet ± tourmaline are present at the deepest exposed crustal levels. These sheets are compositionally and mineralogically unlike the tonalitic sheets and plutons that intrude the other terranes of the crystalline core. The restriction of the sheets to the deepest structural level, their composition, geochemistry and small size suggest that they were

locally derived from partial melting of the gneiss [Boysun, 2004; Boysun and Paterson, 2003; Valley et al., 2003]; however direct evidence of in situ partial melting at the presently exposed crustal level in the Chelan block is lacking [Boysun, 2004; Valley et al., 2003].

In both the Wenatchee and Chelan blocks, the Swakane Gneiss is structurally overlain by the Napeequa Complex (formally known as rocks of the Napeequa River area) of the Chelan Mountains terrane. The Napeequa Complex comprises a heterogeneous assemblage of primarily amphibolite and quartzite with significant amounts of marble, metaperidotite, and biotite schist [Cater, 1982]. Both the Swakane Gneiss and Napeequa Complex exhibit peak P-T conditions of 9-12 kbar and 640-740 °C and were metamorphosed along clockwise P-T paths [Sawyko, 1994; Valley et al., 2003]. The contact between these units in the Chelan block is defined by the mid-crustal Dinkelman decollement in which the Swakane Gneiss forms the footwall [Alsleben, 2000; Paterson et al., 2004]. The dominant sense of motion along the decollement is top-to-NNE shear, which is, in part, responsible for exhumation of the gneiss under decreasing temperature conditions [Alsleben, 2000; Paterson et al., 2004]. This top-to-NNE shear was pervasive in the Swakane Gneiss and formed both high temperature ductile structures and late brittle features. In the Napeequa Complex, top-to-NNE shear overprints sparse kinematic indicators that show early WSW-directed thrusting [Paterson et al., 2004], but very little evidence of top-to-the-WSW directed motion is preserved in the Swakane Gneiss [Alsleben, 2000]. It has been proposed that the original contact between the Swakane Gneiss and Napeequa Complex was a SW-directed thrust [Hurlow, 1992; Tabor et al., 1987a] that was reactivated by N- to NNE-directed shear during exhumation [Paterson et al., 2004]. Since there is little evidence of early top-to-WSW kinematics in the Swakane Gneiss, the sense of motion during burial is unconstrained and may have been accomplished along a thrust contact that is no longer exposed.

The other moderate-P, metasupracrustal units in the Chelan Mountains terrane include the Cascade River unit and the correlative Holden assemblage (Figure 2), which are part of a Triassic arc sequence [Tabor et al., 1989]. These units comprise metavolcanic and metasedimentary rock (amphibolite and hornblende-biotite schist) with local metaconglomerate, metapelite and calc-silicate rock [Brown et al., 1994; Dragovich

et al., 1989; Dragovich and Norman, 1995; Miller et al., 1994; Tabor et al., 1989]. Contact relationships between the Cascade River-Holden units and the Napeequa Complex are not clearly defined. The Cascade River-Holden arc sequence has been proposed to have either formed unconformably on the oceanic Napeequa Complex [Tabor et al., 1989] or was overthrust by the Napeequa Complex [Brown et al., 1994; Dragovich et al., 1989]. Peak P-T conditions determined from the Cascade River unit reached 8-9 kbar and ~650°C [Brown et al., 1994; Miller et al., 1993]. Farther east, paragneisses that were likely derived from both the Napeequa Complex and Cascade River unit protoliths [Tabor et al., 1989] are extensively injected by orthogneiss sheets in the Skagit Gneiss Complex [Haugerud et al., 1991]. Peak P-T results from metapelitic outcrops within the Skagit Gneiss Complex are 9-10 kbar and >700°C [Whitney, 1992; Whitney et al., 1999]. The timing of burial metamorphism of these units with respect to the Swakane Gneiss is discussed below.

PREVIOUSLY PUBLISHED GEOCHRONOLOGIC DATA

The protolith age and tectonic affinity of the Swakane Gneiss have been investigated in two previous studies. Three multi-grain zircon fractions from Swakane biotite gneiss yielded highly discordant U-Pb data with Middle Proterozoic Pb-Pb dates [Mattinson, 1972]. Mattinson's preferred interpretation was that all zircons crystallized >1650 Ma, were metamorphosed ca. 415 Ma and then metamorphosed again between 60 Ma to 90 Ma. This interpretation was based in part on U-Pb data from regions outside the North Cascades core that were assumed to share a common history. However, interpretation of the Swakane data alone is ambiguous because of the high degree of discordance of the U-Pb data. Rasbury and Walker [1992] obtained U-Pb zircon dates from biotite gneiss with ca 1.4 Ga and ca. 1.6 Ga Pb-Pb dates and Nd depleted mantle model ages of 1.18 Ga and 1.27 Ga. Based on these U-Pb and Nd data, they suggest that the Swakane Gneiss is a metaclastic rock derived predominantly from Middle Proterozoic rocks. As a result of these two studies, the protolith of the Swakane Gneiss was thought to be at least Paleozoic in age and had been juxtaposed with the other terranes that comprise the North Cascades prior to the intrusion of Cretaceous plutons [Cater, 1982;

Tabor et al., 1987a; Tabor et al., 1989; Tabor et al., 1987b]. The fact that the Swakane Gneiss lacks Cretaceous or younger arc plutons is difficult to explain by this model.

Mattinson [1972] also obtained a $^{206}Pb/^{238}U$ zircon date from a pegmatitic sheet that cuts across the Swakane Gneiss. The pegmatite was proposed to be generated by melting of the gneiss at ca. 69 Ma, the $^{206}Pb/^{238}U$ date obtained from one multigrain zircon fraction. The ca. 69 Ma date is in general agreement with data obtained in this study; however, the uncertainties are not reported, making it difficult to compare in detail.

Previous constraints on the timing of the juxtaposition of the Swakane Gneiss and Napeequa Complex were derived from an 84±1 Ma (U-Pb zircon) foliated granodiorite sill that crops out along the Swakane-Napeequa contact in the Wenatchee block [Hurlow, 1992]. Based on previous mapping, Hurlow [1992] suggested that the sill intruded the Swakane-Napeequa contact after the terranes were juxtaposed [Hurlow, 1992]. Alternatively, the sill may have been faulted against the Swakane Gneiss, a proposal that is consistent with observations a short distance along strike where other intrusive sheets in the Napeequa Complex are truncated by the Dinkelman decollement [Paterson et al., 2004]. This interpretation of the field relationships suggest that the only timing constraint imposed by the crystallization age of the sill is that it pre-dates the latest motion along the Napeequa-Swakane contact, rather than providing a minimum age of the terranes.

RESULTS

Protolith Age

Zircon of varying sizes, shapes and clarity were recovered from a sample of biotite gneiss (SW3B) collected from an outcrop in the Chelan block that contains abundant leucogranite sheets (see Figure 2 for sample localities). All leucogranite sheets were carefully avoided during sampling. Representative zircons were analyzed according to methods outlined in Appendix A, and the data are reported at the 2σ uncertainty level in Table 1 and Figure 3. All analyses were performed on single zircon grains, and all grains were heavily abraded to ~50-70% of their original size in order to remove any potential metamorphic overgrowths. These analyses yield dates that range from the Late

Cretaceous to the Middle Proterozoic, reflecting a variety of zircon sources that contributed to the Swakane protolith. Analyses from Middle Proterozoic zircon grains are moderately to severely discordant (5.8%-75.9%) and yield $^{207}Pb/^{206}Pb$ dates from 1177.9±1.3 Ma to 1610.8±1.4 Ma. All but one of the analyses that yield Mesozoic or younger dates have error ellipses that overlap concordia. The youngest zircon grains are generally characterized by low radiogenic Pb contents (0.5 to 8 ppm), making the $^{206}Pb/^{238}U$ date the most precise. These dates range from 72.5±0.6 Ma to 191.6±0.2 Ma. A large sub-population of the zircons analyzed (9 of 24) have $^{206}Pb/^{238}U$ dates from 72.5±0.6 Ma to 74.4±0.2 Ma.

A second sample of biotite gneiss (SW8) was collected higher in the section from an outcrop that lacks leucogranite sheets (Figure 2). Eight single zircon analyses yield dates that range from 1635.1±1.6 Ma to 83.7±1.2 Ma (Table 1; Figure 3). Analyses that yield Middle Proterozoic $^{207}Pb/^{206}Pb$ dates are moderately to severely discordant (8.5-76.1%). All analyses from Cretaceous grains (except z1) are normally to reversely discordant. These analyses are characterized by low ratios of radiogenic to common Pb which leads to large uncertainties and scatter about concordia because of the common Pb correction.

Zircon grains from a garnet-kyanite gneiss sample (SW2) contain abundant inclusions of biotite, graphite, garnet, quartz, feldspar, and rutile which are generally restricted to the rim of the grain. The $^{206}Pb/^{238}U$ dates of six abraded zircons range from 97.0±0.4 Ma to 159.5±0.3 Ma (Table 1; Figure 3). All analyses are slightly discordant which may reflect incomplete removal of metamorphic rims.

Timing of Metamorphism

Because of the lack of minerals such as monazite that could potentially date metamorphism directly, our approach to constraining the timing of metamorphism focused instead on determining the age of peraluminous leucogranite sheets that post-date the initiation of foliation in the gneiss. Several generations of these sheets intrude the Swakane Gneiss with some concordant to host rock foliation, whereas others cut foliation but are also deformed [Boysun, 2004; Boysun and Paterson, 2002]. The composition, geochemistry, and size of these sheets suggest that they are derived from partial melting

of the gneiss below the presently exposed crustal level [Boysun, 2004; Boysun and Paterson, 2002; Valley et al., 2003]. If locally derived, their crystallization ages give an estimate of the timing of metamorphism. A more direct approach to determining the timing of peak metamorphism such as dating the thin metamorphic overgrowths on detrital zircons by ion probe methods was not attempted because of the low probability of collecting unambiguous data. Uncertainties on ion probe analyses of Late Cretaceous to Paleocene age are unlikely to be better than 2% (1σ) [e.g., Grove et al., 2003]. These relatively large uncertainties make it unlikely that the age of metamorphism would be resolvable from the ages of the youngest detrital grains.

A medium-grained leucogranite sheet (SW1) that cuts across foliation in the gneiss was collected from the Wenatchee block (Figure 2). Several zircon analyses lie on or near concordia with $^{206}Pb/^{238}U$ dates that range from 68.3±0.2 Ma to 86.2±1.0 Ma (Table 1). Six of the eleven analyses yield $^{206}Pb/^{238}U$ dates that overlap within uncertainty (Figure 4) whereas the other five analyses yield five distinctly different dates. The six concordant and equivalent analyses are interpreted to date zircon that crystallized within the leucogranite sheet and yield a concordia age [i.e. Ludwig, 1998] of 68.36±0.07 Ma (MSWD of concordance and equivalence = 0.55; including decay constant errors). The other five analyses were likely derived from zircon with cores inherited from the gneiss and overgrowths that grew during crystallization of the sheet. Zircon grains were analyzed from eight other leucogranite sheets in the Chelan block (see Boysun, [2004]), but all samples yielded a distribution of inherited zircon dates rather than primary crystallization ages.

DISCUSSION

Swakane Protolith

In order to interpret the petrologic significance of the zircon analyses, zircon grains representing the range of morphologies from samples SW3B and SW2 were imaged using cathodoluminescence (CL) techniques (Figures 5 and 6; Appendix A). In nearly all cases, the imaged zircon grains have fine-scale oscillatory-zoned cores surrounded by rims that exhibit chaotic zonation. An oscillatory zonation pattern results from growth of zircon in the presence of melt where oscillations are controlled by an

interplay between the stage of crystal growth, nature of the crystal-liquid interface, degree of supersaturation of the melt, rates of diffusion, and state of oxidation [Corfu et al., 2003; Hanchar and Miller, 1993; Hoskin, 2000; Mattinson et al., 1996; Vavra, 1990]. In extremely rare cases from eclogite facies rocks, oscillatory growth zonation has been observed in metamorphic rims on inherited zircon, which may be related to crystallization in local melt or supercritical fluids developed at peak metamorphic conditions [Gebauer et al., 1997]. The Swakane Gneiss samples, however, lack evidence of local melting, and the fact that nearly all of the imaged zircon grains display oscillatory growth zonation indicates that the detritus that formed the Swakane protolith was predominantly derived from an igneous source. Only SW3B analysis z25 displays sector growth zonation typical of metamorphic zircon [Corfu et al., 2003]. The presence of chaotically-zoned rims in both samples is best explained by recrystallization or dissolution and reprecipitation along grain boundaries during a metamorphic event [Corfu et al., 2003; Hoskin and Schaltegger, 2003].

Several zircons were plucked from the grain mount after imaging, heavily abraded to remove the rim, and then analyzed (SW3B z19-z27). These grains exhibited a wide range of crystallization dates with the oldest having a $^{207}Pb/^{206}Pb$ date of 1610.8±1.4 Ma and the youngest having a $^{206}Pb/^{238}U$ date of 73.3±1.0 Ma (Figure 5). The observation that even the youngest zircons analyzed have oscillatory-zoned cores is consistent with the interpretation that these grains were derived from an igneous rock. The grains were likely incorporated into the protolith as either a ca. 73 Ma volcanic-clastic component or as sediments derived from a nearby igneous source. There is no evidence of in situ partial melting at the presently exposed crustal level in the Chelan block [Alsleben, 2000; Boysun, 2004; Valley et al., 2003], and leucogranite sheets produced during melting of the gneiss rarely crystallized primary zircon [Boysun, 2004]. Therefore, it is unlikely that zircon with oscillatory growth zonation could have crystallized within small melt pods produced during metamorphism of the gneiss.

The fact that all of the imaged zircons displayed chaotically-zoned rims regardless of the age of their core suggests that the rim grew during metamorphism of the Swakane protolith. CL images of zircon grains from the garnet-kyanite gneiss sample display relatively thick overgrowths (Figure 6). These rims were unlikely to have been

completely removed during abrasion, and the most reasonable interpretation of the discordant SW2 zircon analyses is that they represent mixtures of detrital core and metamorphic overgrowth. In contrast, metamorphic rims on zircon from the biotite gneiss are much thinner (Figure 5) and were most likely completely removed by abrasion which reduced the grains to 50-70% of their original size. The dates determined from these grains are unlikely to represent mixtures of detrital core and metamorphic overgrowth. These geochronological data then place a maximum age for the deposition of the deepest parts of the Swakane Gneiss at 72.5±0.6 Ma, the $^{206}Pb/^{238}U$ date of the youngest detrital grain.

The question of whether the Swakane protolith was a sedimentary rock (arkose or greywacke) or a predominantly silicic volcanic rock has been long debated [Cater, 1982; Mattinson, 1972; Miller et al., 2000; Sawyko, 1994; Tabor et al., 1987a; Tabor et al., 1987b; Waters, 1932; Whitney et al., 1999]. These new geochronological data not only constrain the timing of deposition of the Swakane protolith, but also the nature of the protolith itself. The main piece of evidence used to support the hypothesis that the Swakane protolith is predominantly a silicic volcanic rock is the "remarkable homogeneity" of the Swakane Gneiss [Cater, 1982; Hopson, pers. comm. in Mattison, 1972; Sawyko, 1994]. Cater [1982] argued that the accumulation of a nearly uniform pile of arkose on the order of the Swakane Gneiss is unlikely; however, the lack of stratigraphic markers within the gneiss makes it difficult to estimate the degree of structural duplication or its original stratigraphic thickness. The wide distribution of zircon dates from the biotite gneiss and garnet-kyanite gneiss obtained in this study (Table 1; Figure 3) indicates that sources of several different ages contributed to the Swakane protolith. If the protolith of the Swakane biotite gneiss was a silicic volcanic rock, then the geochronologic data require that it either inherited zircons from a highly diverse crustal column or was contaminated by sediment from a wide range of sources at the surface. It is unlikely that Precambrian zircon grains were derived from transport through the crust during eruption because Precambrian crust is not present in the crustal column until much farther east of the arc [Coney et al., 1980; Patchett and Gehrels, 1998]. This suggests that Precambrian zircons were incorporated into the Swakane

protolith from sediment at the surface. This supports a model in which the Precambrian zircons were incorporated into the Swakane protolith from sediment at the surface.

Source terranes for sediment of the appropriate age are present throughout the northwest US Cordillera. The ages of the Precambrian zircons are broadly consistent with derivation from the Yavapai and Mazatzal terranes of the southwestern US [e.g., Bowring and Karlstrom, 1990]. Sources of Jurassic and Cretaceous zircons are present to the east in the Blue Mountains terranes, Idaho batholith and Okanogan Complex [Miller et al., 1992 and references therein; Parrish et al., 1988; Walker, 1986], and to the north and west in the Jurassic and Cretaceous arc sequences of the western Coast Belt [Journeay and Friedman, 1993]. The youngest zircon grains in the Swakane Gneiss are essentially coeval with plutons in these source terranes and may have been derived from their volcanic cover.

Potential sedimentary protoliths of the appropriate age for the Swakane Gneiss are present, but not abundant, in the region. Within the Methow Basin (Figure 2), the areally restricted Pipestone Canyon Formation is an early Maastrichtian (71-68 Ma) sequence of non-marine plutonic- and volcanic-clastic conglomerate and sandstone that contains substantial detritus from the 111-114 Ma Okanogan batholith [Peterson et al., 1997]. To the west in the Georgia Basin (Figure 7), the uppermost stratigraphic unit of the Nanaimo Group, the Gabriola Formation, is also a Maastrichtian unit comprised of massive, thick-bedded, coarse- to fine-grained sandstone deposited in a foreland basin [Mustard and Monger, 1991; Mustard et al., 1995]. The detrital zircon population of the Gabriola Formation includes Precambrian zircon, zircon of late Mesozoic age with Precambrian inheritance, concordant 87 Ma zircon, and a predominant 72-73 Ma population of zircon [Mustard et al., 1995]. This detrital zircon population is similar to that of the Swakane Gneiss and suggests that the Swakane protolith may have been deposited in the same basin or a basin of similar tectonic setting and age.

Potential Cretaceous Analogs in the US Cordillera

During the same time period that the protolith of the Swakane Gneiss was deposited and rapidly buried, sediment along the southwestern margin of the North American craton also followed a similar pattern of deposition followed by rapid burial.

These sediments formed the protoliths for what are now collectively known as the Pelona, Orocopia, and Rand (POR) schists of southern California (Figure 7). The Pelona and Orocopia schists were buried at approximately the same time as the Swakane sediments with detrital zircons as young as 70±1 Ma and were exhumed to shallow crustal levels during Late Cretaceous to early Tertiary time [Grove et al., 2003; Jacobson, 1990; Jacobson et al., 2000]. In addition to a Late Cretaceous detrital zircon population, the Pelona and Orocopia schists also contain zircons of Early Cretaceous, Triassic, and Middle to Early Proterozoic age that are proposed to have been derived from the Mojave Desert and Transverse Ranges of southern California [Grove et al., 2003; Jacobson et al., 2000]. The Pelona and Orocopia schists are sometimes correlated with schists that crop out farther north including the Rand, Portal Ridge, and Sierra de Salinas schists [Ehlig, 1981; Haxel and Dillon, 1978]. However, recent U-Pb data suggest that the protoliths of the northern schists were deposited up to 10 Myr earlier than the Pelona and Orocopia schists [Barth et al., 2003; Grove et al., 2000; Grove et al., 2003; Jacobson et al., 2000; Jacobson et al., 2002].

The POR schists are interpreted to be correlatives of the Franciscan Complex or Great Valley Group and are comprised of homogeneous quartzofeldspathic schist with related pelitic and mafic schists, calc-silicate, and meta-ultramafic rocks similar to the Swakane Gneiss [Burchfiel and Davis, 1981; Crowell, 1981; Dickinson, 1981; Yeats, 1968]. These schists are thought to underlie a large region beneath southern California and into Arizona [Cheadle et al., 1986; Ehlig, 1981; Haxel and Dillon, 1978; Malin et al., 1995].

A comparison of metamorphic conditions indicates that peak pressures of 8-10 kbar determined from the POR schists [Graham and Powell, 1984; Jacobson, 1995] overlap the 9-12 kbar pressure range calculated for the Swakane Gneiss [Sawyko, 1994; Valley et al., 2003]. The POR schists, however, generally yield significantly lower temperatures of 470-570 °C [Graham and Powell, 1984] as compared to the 670-730 °C temperatures calculated from the Swakane Gneiss [Sawyko, 1994; Valley et al., 2003]. The Sierra de Salinas and Portal Ridge schists are higher grade (i.e. mineral assemblage includes garnet, sillimanite and potassium-feldspar) [Ross, 1976], but detailed thermobarometry has not been carried out.

Burial and exhumation mechanisms of the POR schists are actively debated [c.f Grove et al., 2003; Haxel et al., 2002]. Late Cretaceous protolith ages and Paleocene cooling dates derived from the schists are interpreted to require underthrusting of these units beneath the Cretaceous arc to depths >20 km and exhumation to mid-crustal depths in less than 13±10 Myr [Grove et al., 2003]. Tectonic mechanisms proposed to account for their burial include shallow subduction of trench and/or accretionary complex sediments, burial during collision of an exotic microcontinent, or overthrusting of either a fore-arc or back-arc basin [c.f. Grove et al., 2003; Haxel et al., 2002]. Several of these models invoke shallow subduction as the driving mechanism for burial. The burial mechanism of the Swakane Gneiss need not be the same as that of the POR schists, but the similarity in timing of burial and exhumation point to similar processes occurring along the margin of North America during the Late Cretaceous to Eocene.

Timing of Regional Burial

In order to evaluate potential mechanisms that could be responsible for rapid burial of the Swakane Gneiss, its depositional and burial history must be placed into a regional context. Our new geochronologic data indicate that the Swakane Gneiss was deeply buried between 72.5±0.6 Ma, the age of the youngest detrital grain, and 68.36±0.07 Ma, the crystallization age of a cross-cutting peraluminous sheet. The chemical composition of these peraluminous sheets suggests that were locally derived from partial melting of the gneiss, which indirectly ties their age to the timing of peak metamorphism [Boysun and Paterson, 2003]. Post-peak metamorphic cooling of the Swakane Gneiss is constrained by a hornblende $^{40}Ar/^{39}Ar$ date of 57.9±0.5 Ma [Chapter 3], a hornblende K-Ar date of 50.8±2.8 Ma [Tabor et al., 1987a], and biotite $^{40}Ar/^{39}Ar$ dates of 49-46 Ma [Paterson et al., 2004]. The cooling and exhumation history of the Swakane Gneiss is described in detail in Paterson et al. [2004].

The available data indicate that burial of the Swakane Gneiss post-dates deep burial of all other terranes of the Cascades core. In the Wenatchee block and southern Chelan block (Figure 2), burial of the Swakane Gneiss occurred at least 20 Myr after peak metamorphism of the Napeequa Complex and Cascade River unit. In contrast, burial of the Swakane Gneiss may post-date burial of the Napeequa Complex, Cascade

River unit-Holden assemblage, and Skagit Gneiss Complex in the northern Chelan block by as little as 3 Myr to as many as 15 Myr (see below).

This diachronous burial history is defined by multiple lines of evidence [Brown and Walker, 1993; Miller et al., 1993]. In the Wenatchee block, the timing of deep burial of the Napeequa Complex is constrained by the presence of several plutons that were emplaced into the complex at 7-10 kbar between 96 Ma to 91 Ma [Dawes, 1993; Tabor et al., 1987a; Walker and Brown, 1991; Zen, 1985; Zen and Hammarstrom, 1984]. The pluton emplacement pressures were derived by Al-in-hornblende barometry and garnet-biotite-muscovite-plagioclase barometry [Dawes, 1993], and they agree with both qualitative indicators of high-pressure crystallization such as the presence of magmatic epidote [Dawes, 1993; Zen, 1985; Zen and Hammarstrom, 1984] and peak pressures of 9-11 kbar determined from their host rocks [Valley et al., 2003]. The presence of these 7-10 kbar plutons indicate that the Napeequa Complex in the Wenatchee block must have occupied a mid-to lower-crustal position by 96 Ma, which pre-dates burial of the Swakane Gneiss by at least 20 Myr.

In the southern Chelan block, the burial history of the Napeequa Complex and Cascade River unit is constrained, in part, by geochronologic and geobarometric data from the Entiat and Seven Fingered Jack intrusive suites [Chapter 5]. These sheeted intrusions consist of numerous tonalite to gabbro sheets emplaced at ca. 90-92 Ma (Seven-Fingered Jack suite) and ca. 71-73 Ma (Entiat suite) [Chapter 5]. Dawes [1993] used Al-in-hornblende barometry to determine emplacement pressures of 6-7 kbar at 18 locations from both suites. The lack of a discernible difference between emplacement pressures of ca. 90-92 Ma tonalite and ca. 71-73 Ma tonalite suggests that the Seven-Fingered Jack and Entiat suites and their host rocks, the Napeequa Complex and Cascade River unit, were at ~6-7 kbar pressures throughout the Late Cretaceous. This supposition is supported by the presence of magmatic epidote in several sheets [Dawes, 1993] and a 7 kbar pressure calculated from a metapelitic Napeequa schist (GASP barometry) adjacent to the southwestern margin of the Entiat intrusion [Valley et al., 2003].

In contrast, deep burial of the Napeequa Complex and Cascade River unit in the northwestern Chelan block occurred between 88 Ma and 76 Ma [Brown and Walker, 1993; Miller et al., 1993]. Pelitic wall rocks of the 91-88 Ma Eldorado Orthogneiss,

which intrudes the Napeequa Complex, Cascade River unit, and Skagit paragneisses contain andalusite replaced by kyanite indicating shallow emplacement of the Eldorado orthogneiss followed by regional burial metamorphism. Zoned garnets from these wall rocks indicate a pressure increase of 5-6 kbar [Brown and Walker, 1993; Miller et al., 1993]. The pressure increase likely occurred before the intrusion of the magmatic epidote-bearing Marble Creek pluton at ca. 76 Ma [Miller et al., 1993]. Further constraints on the timing of deep burial of these units is derived from the 7-10 kbar emplacement pressures of the 68 Ma Diablo orthogneiss from within the Skagit Gneiss Complex [Wernicke and Getty, 1997]. Therefore, burial metamorphism in the northern Chelan block occurred at least 3 Myr to potentially 15 Myr before deep burial of the Swakane Gneiss. The question remains as to whether the burial history of the Napeequa Complex, Cascade River unit, and Skagit Gneiss Complex in the northern Chelan block is tectonically linked to the moderate to high pressure metamorphism of the Swakane Gneiss.

Rapid Burial Mechanisms

Previous tectonic models of the assembly of the Cascades core assumed that the Swakane Gneiss was juxtaposed with the surrounding terranes during mid-Cretaceous thrusting and before intrusion of ca. 96 Ma plutons [McGroder, 1991; Misch, 1966; Tabor et al., 1987b]. The lack of arc plutons in the Swakane Gneiss is difficult to explain by this model. The recognition of a ca. 73 Ma protolith age of the Swakane Gneiss invalidates earlier assumptions about the timing of juxtaposition and requires that the tectonic model for the assembly of the core be modified. Any satisfactory tectonic model must account for the rapid burial of the Swakane protolith (~35 km in <5 Myr = ~7mm/yr)), rapid heating of the gneiss to peak metamorphic temperatures of 670-730°C, and timing of burial metamorphism that post-dates metamorphism in other parts of the core by at least 20 Myr.

We consider two types of mechanisms that could accommodate rapid burial of the Swakane protolith: 1) overthrusting of a fore-arc or back-arc basin or, 2) underthrusting of trench sediments or accretionary complex by subduction. These mechanisms are similar to those proposed for rapid burial of the POR schist protoliths [c.f. Grove et al.,

2003; Haxel et al., 2002], and a schematic illustration of these mechanisms, modified from Haxel et al., [2002], is depicted in Figure 8. The first mechanism (i.e., overthrusting of a fore- or back-arc basin) appears most compatible with thermobarometric and isotopic data and the regional geologic setting. The current data are not sufficient, however, to distinguish between the variations on the first mechanism depicted in the top two panels of Figure 8.

Closure of a Fore-arc or Back-arc Basin

The Cascades core and surrounding regions document a prolonged history of contractional deformation. The transition to dextral transpression between 73 to 58 Ma [Umhoefer and Miller, 1996] may have initiated closure of basins, crustal thickening, and thrusting of the Swakane protolith beneath the arc. During this time period, contractional deformation within the Cascades core is recorded at deep levels in a narrow belt of the Chelan block [Miller and Paterson, 2003]. Farther inboard of the arc in parts of the Shuswap core complex of the southern Omineca Belt (Figure 1), contraction and metamorphism are attributed to the development of a foreland-propagating fold-thrust belt with progressive westward underthrusting of basement [e.g., Parrish, 1995].

If the Swakane protolith was deposited in a fore-arc setting, burial may have been accommodated by underthrusting of sediments beneath a northeast-dipping thrust fault (Figure 8a). This setting is consistent with sparse evidence of early top-to-the-SSW kinematics on the Dinkelman decollement, which has been proposed to be a reactivated thrust [Paterson et al., 2004]. In addition, sediments of similar age and range of detrital zircon dates, such as the Gabriola Formation, are present in the fore-arc setting [Mustard et al., 1995]. However, the lack of clear evidence of the direction of motion during burial suggests that deposition of the Swakane protolith in a back-arc setting cannot be ruled out. The "back-arc" model is depicted in Figure 8b and mirrors the model shown in Figure 8a. Top-to-the-NNE shear has overprinted much of the earlier history on the Dinkelman decollement, and rather than being a reactivated thrust, it may instead be a late structure that excised the original thrust contact. The primary advantage of a back-arc setting for the deposition and burial of the Swakane protolith is the potential for high heat flow in the back-arc, which is necessary to explain the rapid heating (~700°C in <5

Myr) and relatively high-T metamorphism observed from the Swakane Gneiss. Numerical models of mantle flow patterns in a subduction zone predict that hot asthenosphere is drawn from the back arc into the mantle wedge corner during subduction [Andrews and Sleep, 1974; Bodri and Bodri, 1978; Furukawa, 1993]. The upwelling of hot mantle into the mantle wedge results in temperatures >800°C at the base of the crust underlying the arc and can result in adiabatic decompression melting on the upwelling limb of the mantle wedge [Gaetani and Grove, 2003].

Haxel et al. [2002] also discusses a model that combines elements of the fore-arc and back-arc models (not shown in Figure 8). The salient feature of this "Haxel" model is that the basin in which the protolith was deposited formed one of a series of small, short-lived basins that rapidly filled with sediment from the local area and shortly thereafter were deformed by transpression. This model is commonly linked to a back-arc setting; however, as it is described by Haxel et al. [2002], these small basins are not restricted to the back-arc and their position simply reflects their relationship to a crustal fragment outboard of the schist/gneiss package that rifted from the margin and then shortly thereafter recollided.

This model is difficult to apply in detail to the evolution of the North Cascades because a series of small basins has not been recognized as such. However, the implication that Swakane protolith may have been deposited in a small, short-lived, rapidly-filled basin is supported by Nd isotopic data from the Swakane Gneiss and plutons that intrude the other terranes of the crystalline core [Chapter 2]. The Swakane Gneiss is an isotopically-evolved unit with the lowest ε_{Nd} values (as low as -6 ε_{Nd} at 73 Ma) observed in the Cascades core and has mid to Late Proterozoic Nd depleted mantle model ages [Rasbury and Walker, 1992; Chapter 2]. If the Swakane Gneiss formed a regionally extensive unit beneath the arc (as predicted by the shallow subduction model shown in Figure 8c), the ca. 50-46 Ma plutons that intrude the core after burial of the gneiss might be expected to have significantly lower ε_{Nd} signatures than the ε_{Nd} signatures of plutons that pre-date burial of the gneiss because of interaction with the isotopically-evolved layer. However, the ε_{Nd} values derived from the ca. 50-46 Ma plutons are similar to those of the lowest ε_{Nd} values from the ca. 96-88 Ma plutons.

These data instead favor a model whereby the Swakane protolith formed in a small, regionally-restricted basin, and thus only represents a small sliver within the arc.

The great depth to which the Swakane Gneiss was buried also requires a large lateral translation beneath the arc. Localized burial on a steeply-dipping shear zone would negate the need for lateral translation, but there is no evidence that a steeply-dipping structure was active within the North Cascades at that time and burial on such a structure is incompatible with the shallowly-dipping foliation and gently-plunging lineation preserved in the gneiss and overlying units [Paterson et al., 2004]. The question remains as to whether these rapid rates of both lateral and vertical motion can be accounted for in a thrust-loading type of model such as the one discussed above. The short time period between deposition and burial of the gneiss requires a vertical burial rate of ~7 mm/yr. This rate is at least twice as fast as rates determined by GPS and structural and stratigraphic mapping studies in fold and thrust belts [Burbank et al., 1992; DeCelles, 1994; Lamb, 2000; Mazzotti and Hyndman, 2002]. However, rates of crustal thickening and vertical motion in an arc setting are not as well-documented, and rates determined from limited fold and thrust belt cases may not be sufficiently comparable to arcs [e.g. Paterson and Tobisch, 1992].

Burial by Subduction

A second mechanism that could account for the rapid burial of the Swakane protolith is underthrusting of trench and/or accretionary complex sediments (Figure 8c) as has been proposed for southern California. In this model, the ultimate driving force for underplating sediments is low-angle, shallow, northeast-dipping subduction of the Farallon plate during the Laramide orogeny. The low-angle subduction is proposed to have tectonically eroded the lowermost North American continental crust and underlying mantle lithosphere prior to accretion of the schist [Burchfiel and Davis, 1981; Crowell, 1981; Hamilton, 1987; Jacobson et al., 1996; Malin et al., 1995; Yeats, 1968; Yin, 2002]. This model predicts that the Swakane Gneiss forms a regionally extensive layer beneath the Cascades core and is only exposed within a tectonic window.

This model can easily account for rapid burial rates. For a 30°subduction angle and the slowest modeled plate motion determined for this region in the early Tertiary

(~10 cm/yr) [Page and Engebretson, 1984], the Swakane protolith could be buried to depths of 40 km in less than a Myr. Several aspects of this model, however, make it incompatible with the burial and metamorphism history of the Swakane Gneiss. First, burial by low-angle, shallow subduction is incompatible with the high-grade metamorphism that the Swakane Gneiss experienced. Low-angle subduction effectively prevents circulation of hot asthenosphere in the mantle wedge by placing cold slab material directly beneath the arc [Saleeby, 2003]. Although it is possible that the early, low-T/high-P history of the rocks could have been erased by later thermal events, the ~5 Myr time period over which these rocks reached their peak metamorphic conditions precludes this possibility. Second, Nd isotopic data from plutons that intrude the crystalline core of the North Cascades after burial of the gneiss suggest that the gneiss did not form a regionally extensive layer beneath the arc as discussed in the previous section. Third, it is unlikely that shallow subduction occurred at the latitude of the North Cascades. Classic Laramide structures attributed to shallow, low-angle subduction are not present farther north than the latitude of the Idaho batholith [Allmendinger, 1992; Miller et al., 1992], and erosion of subcontinental mantle (required by this model to place subducted sediments in contact with lower crust) did not occur farther north than the southernmost Sierra Nevada batholith [Dodge et al., 1986; Dodge et al., 1988; Ducea, 2001; Ducea and Saleeby, 1996; Ducea and Saleeby, 1998; Lee et al., 2001; Saleeby, 2003]. Tectonic models that propose rapid transport of rocks along the continental margin during the Late Cretacous to early Tertiary (i.e., the Baja-BC hypothesis) could result in northward transport of the Swakane Gneiss from a region of flat subduction. However, the protolith ages of schist underplated during flat subduction in southern California show a trend of older protolith ages to the northwest [Barth et al., 2003], implying that the Swakane Gneiss would have had to originate at the latitude of the Pelona and Orocopia schists. The differences between their peak metamorphic conditions would have to be explained by an additional mechanism.

CONCLUSIONS

The geochronological data presented here indicate that the protolith age of the Swakane Gneiss is much younger than previously thought and that the Swakane Gneiss

was not accreted prior to voluminous, mid-Cretaceous arc magmatism. This conclusion is a significant departure from previous models of the assembly of the North Cascades core. Zircon grains in the gneiss were derived from a variety of sources including Precambrian continental crust and Jurassic to Cretaceous arc rocks. Burial of the Swakane protolith was rapid and is most likely accounted for by thrusting of older crystalline rocks over a fore- or back-arc basin. This rapid burial occurred as much as 20 Myr after deep burial of the Napeequa Complex in the Wenatchee block and the Napeequa Complex and Cascade River unit in the southwestern Chelan block, and anywhere from 15 to 3 Myr after deep burial of the northeastern Napeequa Complex, Cascade River unit and Skagit Gneiss. Rapid burial of the Swakane sediments is coincident with burial of arc-derived sediments of the POR schists; however, differences in peak metamorphic temperatures indicate that conditions of burial must have varied along the plate margin.

APPENDIX A: ANALYTICAL METHODS

Mineral separation was carried out according to standard crushing, heavy liquid, and magnetic separation techniques. Zircon grains were picked in ethanol under a binocular microscope and sorted by their morphology, color, clarity, and inclusion characteristics. Representative zircons were selected for image analysis. These grains were mounted in epoxy and polished to approximately half their original thickness. Cathodoluminescence (CL) imaging was carried out on grain mounts on the MIT JEOL 733 Superprobe electron microscope. Image analysis was conducted with a 15 keV accelerating voltage and 10 to 30 nA beam current depending on the intensity of luminescence. In select cases, zircon grains were removed from the grain mount after CL imaging for U-Pb analysis. These zircons were selected because of their clearly oscillatory growth-zoned cores.

All zircons selected for U-Pb analysis were air-abraded, washed in 3M HNO_3 at 50°C for 12 hours, and ultrasonicated for 1 hour. Following this cycle of cleaning, the zircons were ultrasonicated in 3M HNO_3 for an additional hour. Each zircon was photographed to estimate sample weight, pipetted with acetone into 300 μL Teflon FEP capsules, washed again in 3M HNO_3 at 75°C for 3 hours, and finally rinsed 3 times with

3M HNO_3. Zircons were dissolved in 120 μL HF with a mixed ^{205}Pb-^{233}U-^{235}U spike and trace HNO_3 at 220°C for 48 hours, dried to salts, and redissolved in 120 μL 6M HCl at 180°C for at least 12 hours. Pb and U were separated from the sample using an HCl-based anion exchange procedure modified after Krogh [1973] and collected in a single beaker for isotope analysis.

Pb and U were analyzed by conventional thermal ionization mass spectrometry on the MIT VG Sector 54 multicollector mass spectrometer. Each mixed Pb and U sample was loaded onto previously degassed single Re filaments with a silica gel-H_3PO_4 mixture [Gerstenberger and Haase, 1997]. Pb isotopes were measured either: (1) for ^{207}Pb ion beams $>5x10^{-14}$ A, in a two-cycle dynamic routine with ^{204}Pb in the axial Daly detector and ^{205}Pb through ^{208}Pb in H1-H4 faraday detectors during the first cycle and ^{205}Pb in the Daly detector and ^{206}Pb through ^{208}Pb in the H1-H3 faraday detectors during the second cycle, providing real-time Daly gain measurement; or (2) for ^{207}Pb ion beams $<5x10^{-14}$ A, by peak-jumping all ion beams into the axial Daly detector in ion-counting mode. Uranium isotopes were measured as UO_2^+ in static mode with masses 270, 267, and 265 in the axial, L1, and L2 faraday collectors, respectively. Pb isotope fractionation was monitored throughout the study by daily analysis of the NBS-981 common Pb standard whereas U fractionation was monitored and corrected by use of the double spike.

ACKNOWLEDGEMENTS

This research was supported by NSF grants EAR-9980623 to S.B. and EAR-9628280 to R.M. We thank Donna Whitney, Scott Paterson, and Melissa Boysun for thoughtful discussion about the Swakane Gneiss and burial rates/mechanisms. We also thank Chris Andronicos, Marty Grove, and Mihai Ducea for constructive reviews.

REFERENCES

Allmendinger, R.W., Fold and thrust tectonics of the Western United States exclusive of the accreted terranes, in *The Cordilleran Orogen: Conterminous U.S.*, vol. The Geology of North America v.G-3, edited by B.C. Burchfiel, P.W. Lipman and M.L. Zoback, pp. 583-607, The Geological Society of America, Boulder, 1992.

Alsleben, H., Structural analysis of the Swakane terrane, North Cascades core, Washington, M.S. thesis, San Jose State University, San Jose, 2000.

Andrews, D.J., and N.H. Sleep, Numerical modelling of tectonic flow behind island arcs, *The Geophysical Journal of the Royal Astronomical Society, 38*, 237-251, 1974.

Barth, A.P., J.L. Wooden, M. Grove, C.E. Jacobson, and J.N. Pedrick, U-Pb zircon geochronology of rocks in the Salinas Valley region of California: A reevaluation of the crustal structure and origin of the Salinian block, *Geology, 31*, 517-520, 2003.

Bodri, L., and B. Bodri, Numerical investigation of tectonic flow in island-arc areas, *Tectonophysics, 50*, 163-175, 1978.

Bowring, S.A., and K.E. Karlstrom, Growth, stabilization, and reactivation of Proterozoic lithosphere in the Southwestern United States, *Geology, 18*, 1203-1206, 1990.

Boysun, M.A., Statistical distribution of leucocratic melts in the Swakane terrane, North Cascades Crystalline Core, WA, M.S. thesis, 60 pp., University of Southern California, Los Angeles, 2004.

Boysun, M.A., and S.R. Paterson, Melt injection in the Swakane biotite gneiss, North Cascades core: Implications for melting and dike emplacement in deep crust, *Geological Society of America Abstracts with Programs, 34*, 374, 2002.

Boysun, M.A., and S.R. Paterson, Partial melting and melt collection and transport in the Swakane terrane, North Cascades crystalline core, WA, *Geological Society of America Abstracts with Programs, 35*, 223, 2003.

Brown, E.H., J.A. Cary, B.E. Dougan, J.D. Dragovich, S.M. Fluke, and D.P. McShane, Tectonic evolution of the Cascades crystalline core in the Cascade River area, Washington, *Washington Division of Geology and Earth Resources Bulletin, 80*, 93-113, 1994.

Brown, E.H., and N.W. Walker, A magma-loading model for Barrovian metamorphism in the Southeast Coast Plutonic Complex, British Columbia and Washington, *Geological Society of America Bulletin, 105*, 479-500, 1993.

Burbank, D.W., J. Verges, J.A. Munoz, and P. Bentham, Coeval hindward- and forward-imbricating thrusting in the south-central Pyrenees, Spain: timing and rates of shortening and deposition, *Geological Society of America Bulletin, 104*, 3-17, 1992.

Burchfiel, B.C., and G.A. Davis, Mojave desert and environs, in *The Geotectonic Development of California*, vol. Rubey Volume 1, edited by W.G. Ernst, pp. 217-252, Prentice-Hall, Englewood Cliffs, New Jersey, 1981.

Cater, F.W., Intrusive rocks of the Holden and Lucerne quadrangles, Washington: the relation of depth zones, composition, textures, and emplacement of plutons, *U. S. Geological Survey Professional Paper, 1220*, 108, 1982.

Cater, F.W., and D.F. Crowder, Geologic map of the Holden Quadrangle, Snohomish and Chelan counties, Washington, in *Geologic Quadrangle Map - U. S. Geological Survey*, U. S. Geological Survey, Washington D.C., 1967.

Cater, F.W., and T.L. Wright, Geologic map of the Lucerne Quadrangle, Chelan County, Washington, in *Geologic Quadrangle Map - U. S. Geological Survey*, U.S. Geological Survey, Washington, D.C., 1967.

Cheadle, M.J., B.L. Czuchra, T. Byrne, C.J. Ando, J.E. Oliver, L.D. Brown, S. Kaufman, P.E. Malin, and R.A. Phinney, The deep crustal structure of the Mojave Desert, California, from COCORP seismic reflection data, *Tectonics, 5*, 293-320, 1986.

Clarke, G.L., K.A. Klepeis, and N.R. Daczko, Cretaceous high-P granulites at Milford Sound, New Zealand: metamorphic history and emplacement in a convergent margin setting, *Journal of Metamorphic Geology, 18*, 359-374, 2000.

Coney, P.J., D.L. Jones, and J.W.H. Monger, Cordilleran suspect terranes, *Nature, 288*, 329-333, 1980.

Corfu, F., J.M. Hanchar, P.W.O. Hoskin, and P. Kinny, Atlas of Zircon Textures, in *Zircon*, vol. Reviews in Mineralogy and Geochemistry 53, edited by J.M. Hanchar and P.W.O. Hoskin, pp. 468-500, Mineralogical Society of America and Geochemcial Society, Washinton, D.C., 2003.

Crowell, J.C., An outline of the tectonic history of southeastern California, in *The Geotectonic Development of California*, vol. Rubey Volume 1, edited by W.G. Ernst, Prentice-Hall, Englewood Cliffs, New Jersey, 1981.

Dawes, R.L., Mid-crustal, Late Cretaceous plutons of the North Cascades: petrogenesis and implications for the growth of continental crust, PhD thesis, 272 pp., University of Washington, Seattle, 1993.

DeCelles, P.G., Late Cretaceous-Paleocene synorogenic sedimentation and kinematic history of the Sevier thrust belt, northeast Utah and southwest Wyoming, *Geological Society of America Bulletin, 106*, 32-56, 1994.

Dickinson, W.R., Plate tectonics and the continental margin of California, in *The Geotectonic Development of California*, vol. Rubey Volume 1, edited by W.G. Ernst, Prentice-Hall, Englewood Cliffs, New Jersey, 1981.

Dodge, F.C.F., L.C. Calk, and R.W. Kistler, Lower crustal xenoliths, Chinese Peak lava flow, central Sierra Nevada, *Journal of Petrology, 27*, 1986.

Dodge, F.C.F., J.P. Lockwood, and L.C. Calk, Fragments of mantle and crust beneath the Sierra Nevada batholith: xenoliths in a volcanic pipe near Big Creek, California, *Geological Society of America Bulletin, 100*, 938-947, 1988.

Dragovich, J.D., J.A. Cary, and E.H. Brown, Stratigraphic and structural relations of the Cascade River schist, North Cascades, Washington, *Geological Society of America Abstracts with Programs, 21*, 74, 1989.

Dragovich, J.D., and D.K. Norman, Geologic map of the west half of the Twisp 1:100,000 Quadrangle, Washington, in *Open-File Report - Washington Division of Geology and Earth Resources*, pp. 63, 1995.

Ducea, M., The California arc: Thick granitic batholiths, eclogitic residues, lithospheric-scale thrusting, and magmatic flare-ups, *GSA Today, 11*, 4-10, 2001.

Ducea, M., and J.B. Saleeby, Buoyancy sources for a large, unrooted mountain range, the Sierra Nevada, California: Evidence from xenolith thermobarometry, *Journal of Geophysical Research, 101*, 8229-8244, 1996.

Ducea, M., and J.B. Saleeby, The age and origin of a thick mafic-ultramafic keel from beneath the Sierra Nevada batholith, *Contributions to Mineralogy and Petrology, 133*, 169-185, 1998.

Ehlig, P.L., Origin and tectonic history of the basement terrane of the San Gabriel Mountains, central Transverse Ranges, in *The Geotectonic Development of California*, vol. Rubey Volume 1, edited by W.G. Ernst, Prentice-Hall, Englewood Cliffs, New Jersey, 1981.

Furukawa, Y., Magmatic processes under arcs and formation of the volcanic front, *Journal of Geophysical Research, 98*, 8309-8319, 1993.

Gaetani, G.A., and T.L. Grove, Experimental constraints on melt generation in the Mantle wedge, in *Inside the Subduction Factory*, vol. Geophysical Monograph 138, edited by J. Eiler, pp. 107-133, American Geophysical Union, 2003.

Gebauer, D., H.P. Schertl, M. Brix, and W. Schreyer, 35 Ma old ultrahigh-pressure metamorphism and evidence for very rapid exhumation in the Dora Maira Massif, Western Alps, *Lithos, 41*, 5-24, 1997.

Gerstenberger, H., and G. Haase, A highly effective emitter substance for mass spectrometric Pb isotope ratio determinations, *Chemical Geology, 136*, 309-312, 1997.

Graham, C.M., and R. Powell, A garnet-hornblende geothermometer: Calibration, testing, and application to the Pelona Schist, Southern California, *Journal of Metamorphic Geology, 2*, 13-31, 1984.

Grove, M., C.E. Jacobson, and A.P. Barth, Temporal and spatial trends of Late Cretaceous-early Tertiary underplating beneath Southern California and Southwest Arizona, *Geological Society of America Abstracts with Programs, 32*, 46, 2000.

Grove, M., C.E. Jacobson, A.P. Barth, and A. Vucic, Temporal and spatial trends of Late Cretaceous - early Tertiary underplating of Pelona and related schist beneath southern California and southwestern Arizona, in *Tectonic Evolution of Northwestern Mexico and the Southwestern USA*, vol. Special Paper 374, edited by S.E. Johnson, S.R. Paterson, J.M. Fletcher, G.H. Girty, D.L. Kimbrough and A. Martín-Barajas, pp. 381-406, Geological Society of America, Boulder, Colorado, 2003.

Hamilton, W., Mesozoic geology and tectonics of the Big Maria Mountains region, southeastern California, in *Mesozoic Rocks of Southern Arizona and adjacent areas*, vol. 18, edited by W.R. Dickinson and M.A. Klute, pp. 33-47, Arizona Geological Society Digest, 1987.

Hanchar, J.M., and C.F. Miller, Zircon zonation patterns as revealed by cathodoluminescence and backscattered electron images: implications for interpretation of complex crustal histories, *Chemical Geology, 110*, 1-13, 1993.

Haugerud, R.A., P. Vanderheyden, R.W. Tabor, J.S. Stacey, and R.E. Zartman, Late Cretaceous and Early Tertiary plutonism and deformation in the Skagit Gneiss Complex, North Cascade Range, Washington and British Columbia, *Geological Society of America Bulletin, 103*, 1297-1307, 1991.

Haxel, G.B., and J.T. Dillon, The Pelona-Orocopia Schist and Vincent-Chocolate Mountain thrust system in southern California, in *Mesozoic Paleogeography of the Western United States*, vol. Pacific

Coast Symposium 2, edited by D.G. Howell and K.A. McDougall, pp. 453-469, Society of Economic Paleontologists and Mineralogists, 1978.

Hopson, C.A., and J.M. Mattinson, Chelan Migmatite Complex, Washington: Field evidence for mafic magmatism, crustal anatexis, mixing and protodiapiric emplacment, in *Geologic Field Trips in the Pacific Northwest*, edited by D.A. Swanson and R.A. Haugerud, pp. 2K-1 - 2K-21, Geological Society of America, Boulder, 1994.

Hoskin, P.W.O., Patterns of chaos: fractal statistics and the oscillatory chemistry of zircon, *Geochimica et Cosmochimica Acta, 64*, 1905-1923, 2000.

Hoskin, P.W.O., and U. Schaltegger, The composition of zircon and igneous and metamorphic petrogenesis, in *Zircon*, vol. Reviews in Mineralogy and Geochemistry 53, edited by J.M. Hanchar and P.W.O. Hoskin, pp. 27-62, Mineralogical Society of America and Geochemcial Society, Washington, D.C., 2003.

Hurlow, H.A., Structural and U/Pb geochronologic studies of the Pasayten Fault, Okanogan Range Batholith, and southeastern Cascades crystalline core, Washington, PhD thesis, 180 pp., University of Washington, Seattle, 1992.

Jacobson, C.E., The $^{40}Ar/^{39}Ar$ geochronology of the Pelona Schist and related rocks, southern California, *Journal of Geophysical Research, 95*, 509-528, 1990.

Jacobson, C.E., Qualitative thermobarometry of inverted metamorphism in the Pelona and Rand Schists, southern California, using calciferous amphibole in mafic schist, *Journal of Metamorphic Geology, 13*, 79-92, 1995.

Jacobson, C.E., A.P. Barth, and M. Grove, Late Cretaceous protolith age and provenance of the Pelona and Orocopia Schists, southern California: Implications for evolution of the Cordilleran margin, *Geology, 28*, 219-222, 2000.

Jacobson, C.E., M. Grove, A.P. Barth, J.N. Pedrick, and A. Vucic, "Salmon tectonics" as a possible explanation for Laramide sedimentation and underplating of schist in southern California and southwestern Arizona, *Geological Society of America Abstracts with Programs, 34*, 510, 2002.

Jacobson, C.E., F.R. Oyarzabal, and G.B. Haxel, Subduction and exhumation of the Pelona-Orocopia-Rand schists, southern California, *Geology, 24*, 547-550, 1996.

Journeay, J.M., and R.M. Friedman, The Coast Belt thrust system: Evidence of Late Cretaceous shortening in southwest British Columbia, *Tectonics, 12*, 1301-1302, 1993.

Lamb, S., Active deformation in the Bolivian Andes, South America, *Journal of Geophysical Research, 105*, 25627-25653, 2000.

Lee, C.-T., Q. Yin, R.L. Rudnick, and S.B. Jacobsen, Preservation of ancient and fertile lithospheric mantle beneath the southwestern United States, *Nature, 411*, 69-73, 2001.

Ludwig, K.R., On the treatment of concordant uranium-lead ages, *Geochimica et Cosmochimica Acta, 62*, 665-676, 1998.

Malin, P.E., E.D. Goodman, T.L. Henyey, Y.G. Li, D.A. Okaya, and J.B. Saleeby, Significance of seismic reflections beneath a tilted exposure of deep continental crust, Tehachapi Mountains, California, *Journal of Geophysical Research, 100*, 2069-2087, 1995.

Mattinson, J., C.M. Graubard, D.L. Parkinson, and W.C. McClelland, U-Pb reverse discordance in zircons and the role of fine-scale oscillatory zoning and sub-microscopic transport of Pb, *American Geophysical Union, Geophysical Monograph, 95*, 355-370, 1996.

Mattinson, J.M., Ages of zircons from the Northern Cascade Mountains, Washington, *Geological Society of America Bulletin, 83*, 3769-3783, 1972.

Mazzotti, S., and R.D. Hyndman, Yakutat collision and strain transfer across the northern Canadian Cordillera, *Geology, 30*, 495-498, 2002.

McGroder, M.F., Reconciliation of two-sided thrusting, burial metamorphism, and diachronous uplift in the Cascades of Washington and British Columbia, *Geological Society of America Bulletin, 103*, 189-209, 1991.

Miller, D.M., T.H. Nilsen, and W.L. Bilodeau, Late Cretaceous to early Eocene geologic evolution of the U.S. Cordillera, in *The Cordilleran Orogen: Conterminous U.S.*, vol. The Geology of North America v. G-3, edited by B.C. Burchfield, P.W. Lipman and M.L. Zoback, pp. 205-260, The Geological Society of America, Boulder, 1992.

Miller, R.B., The Ophiolitic Ingalls Complex, North Central Cascade Mountains, Washington, *Geological Society of America Bulletin, 96*, 27-42, 1985.

Miller, R.B., and S.A. Bowring, Structure and chronology of the Oval Peak batholith and adjacent rocks: Implications for the Ross Lake fault zone, North Cascades, Washington, *Geological Society of America Bulletin, 102*, 1361-1377, 1990.

Miller, R.B., E.H. Brown, D.P. McShane, and D.L. Whitney, Intra-arc crustal loading and its tectonic implications, North Cascades crystalline core, Washington and British Columbia, *Geology, 21*, 255-258, 1993.

Miller, R.B., R.A. Haugerud, F. Murphy, and L.S. Nicholson, Tectonostratigraphic framework of the northeastern Cascades, *Washington Division of Geology and Earth Resources Bulletin, 80*, 73-92, 1994.

Miller, R.B., and S.R. Paterson, Evolution of the hinterland to the Cretaceous Northwest Cascades thrust system: Modes of shortening in the Cascades core, Washington, *Geological Association of Canada - Mineralogical Association of Canada Program with Abstracts, 28*, 2003.

Miller, R.B., S.R. Paterson, S.M. DeBari, and D.L. Whitney, North Cascades Cretaceous crustal section: changing kinematics, rheology, metamorphism, pluton emplacement and petrogenesis from 0 to 40 km depth, in *Guidebook for geological field trips in southwestern British Columbia and northern Washington*, edited by G.J. Woodsworth, J.L.E. Jackson, J.L. Nelson and B.C. Ward, pp. 229-278, Geological Association of Canada, Vancouver, 2000.

Misch, P., Tectonic evolution of the Northern Cascades of Washington State: a west-cordilleran case history, *Canadian Institute of Mining and Metallurgy, Special volume 8*, 101-148, 1966.

Monger, J.W.H., R.A. Price, and D.J. Tempelman-Kluit, Tectonic accretion and the origin of the two major metamorphic and plutonic welts in the Canadian Cordillera, *Geology, 10*, 70-75, 1982.

Mustard, P.S., and J.W.H. Monger, Upper-Cretaceous Tertiary Georgia Basin, British Columbia: forearc or foreland, *Abstracts with Programs, Geological Association of Canada Annual Meeting, 16*, A88, 1991.

Mustard, P.S., R.R. Parrish, and V. McNicoll, Provenance of the Upper Cretaceous Nanaimo Group, British Columbia: Evidence from U-Pb analyses of detrital zircons, in *Stratigraphic Evolution of Foreland Basins*, vol. 52, edited by S.L. Dorobek and G.M. Ross, pp. 65-76, SEPM Special Publication, 1995.

Page, B.M., and Engebretson, Correlation between the geologic record and computed plate motions for central California, *Tectonics, 3*, 133-155, 1984.

Parrish, R.R., S.D. Carr, and D.L. Parkinson, Eocene extensional tectonics and geochronology of the southern Omineca Belt, British Columbia and Washington, *Tectonics, 7*, 181-212, 1988.

Patchett, P.J., and G.E. Gehrels, Continental influence on Canadian Cordilleran terranes from Nd isotopic study, and significance for crustal growth processes, *Journal of Geology, 106*, 269-280, 1998.

Paterson, S.R., R.B. Miller, H. Alsleben, D.L. Whitney, P.M. Valley, and H. Hurlow, Driving mechanisms for >40 km of exhumation during contraction and extension in a continental arc, Cascades core, Washington, *Tectonics, 23*, 10.1029/2002TC001440, 2004.

Paterson, S.R., and O.T. Tobisch, Rates of processes in magmatic arcs: Implications for the timing and nature of pluton emplacement and wall rock deformation, *Journal of Structural Geology, 14*, 291-300, 1992.

Peterson, J.J., J.B. Mahoney, and R.A. Haugerud, Constraints on Late Cretaceous movement on the Pasayten Faul:; the Pipestone Canyon Formation, Washington, *Geological Society of America Abstracts with Programs, 29*, 278, 1997.

Rasbury, T.E., and N.W. Walker, Implications of Sm-Nd model ages and single grain U-Pb zircon geochronology for the age and heritage of the Swakane Gneiss, Yellow Aster Complex, and Skagit Gneiss, North Cascades, Washington, *Geological Society of America Abstracts with Programs, 24*, A28, 1992.

Ross, D.C., Reconnaissance geologic map of the pre-Cenozoic basement rocks, northern Santa Lucia range, Monteray County, California, U.S. Geological Survey, 1976.

Rubin, C.M., J.B. Saleeby, D.S. Cowan, M.T. Brandon, and M.F. McGroder, Regionally extensive mid-Cretaceous west-vergent thrust system in the northwestern Cordillera: Implications for continent-margin tectonism, *Geology, 18*, 276-280, 1990.

Saleeby, J.B., Segmentation of the Laramide Slab: evidence from the southern Sierra Nevada region, *Geological Society of America Bulletin, 115*, 655-668, 2003.

Sawyko, L.T., III, The geology and petrology of the Swakane biotite gneiss, North Cascades, Washington, M.S. thesis, 134 pp., University of Washington, Seattle, 1994.

Tabor, R.W., V.A. Frizzell, Jr., J.T. Whetten, R.B. Waitt, Jr., D.A. Swanson, G.R. Byerly, D.B. Booth, M.J. Hetherington, and R.E. Zartman, Geologic map of the Chelan 30' by 60' Quadrangle, Washington, in *Miscellaneous Investigations Series*, pp. 33 (1 sheet), U. S. Geological Survey, Washington, D.C., 1987a.

Tabor, R.W., R.A. Haugerud, E.H. Brown, R.S. Babcock, and R.B. Miller, *Accreted Terranes of the North Cascades Range, Washington*, 62 pp., American Geophysical Union, Washington, D.C., 1989.

Tabor, R.W., R.E. Zartman, and V.A. Frizzell, Jr., Possible tectonostratigraphic terranes in the North Cascades crystalline core, Washington, in *Selected Papers on the Geology of Washington*, vol. 77, edited by J.E. Schuster, pp. 107-127, Washington Division of Geology and Earth Resources, Anaheim, CA, United States, 1987b.

Umhoefer, P.J., and R.B. Miller, Mid-Cretaceous thrusting in the southern Coast Belt, British Columbia and Washington, after strike-slip fault reconstruction, *Tectonics, 15*, 545-565, 1996.

Valley, P.M., D.L. Whitney, S.R. Paterson, R.B. Miller, and H. Alsleben, Metamorphism of the deepest exposed arc rocks in the Cretaceous to Paleogene Cascades belt, Washington: evidence for large-scale vertical motion in a continental arc, *Journal of Metamorphic Geology, 21*, 203-220, 2003.

Vavra, G., On the kinematics of zircon growth and its petrogenetic significance: a cathodoluminescence study, *Contributions to Mineralogy and Petrology, 106*, 90-99, 1990.

Walker, N.W., U/Pb geochronologic and petrologic studies in the Blue Mountains Terrane, northeastern Oregon and westernmost-central Idaho: implications for pre-Tertiary tectonic evolution, PhD thesis, 224 pp., University of California, Santa Barbara, 1986.

Walker, N.W., and E.H. Brown, Is the southeast Coast Plutonic Complex the consequence of accretion of the Insular Superterrane: Evidence from U-Pb zircon geochronometry in the Northern Washington Cascades, *Geology, 19*, 714-717, 1991.

Waters, A.C., A petrologic and structural study of the Swakane Gneiss, Entiat Mountains, Washington, *Journal of Geology, 40*, 604-633, 1932.

Wernicke, B., and S.R. Getty, Intracrustal subduction and gravity currents in the deep crust: Sm-Nd, Ar-Ar, and thermobarometric constraints from the Skagit Gneiss Complex, Washington, *Geological Society of America Bulletin, 109*, 1149-1166, 1997.

Whitney, D.L., High-pressure metamorphism in the western Cordillera of North America: An example from the Skagit Gneiss, North Cascades, *Journal of Metamorphic Geology, 10*, 71-85, 1992.

Whitney, D.L., R.B. Miller, and S.R. Paterson, P-T-t evidence for mechanisms of vertical tectonic motion in a contractional orogen: north-western US and Canadian Cordillera, *Journal of Metamorphic Geology, 17*, 75-90, 1999.

Yeats, R.S., Southern California structure, seafloor spreading, and history of the Pacific Basin, *Geological Society of America Bulletin, 79*, 1693-1702, 1968.

Yin, A., Passive-roof thrust model for the emplacement of the Pelona-Orocopia schist in southern California, *Geology, 30*, 183-186, 2002.

Zen, E.-a., Implications of magmatic epidote-bearing plutons on crustal evolution in the accreted terranes of northwestern North America, *Geology, 13*, 266-269, 1985.

Zen, E.-a., and J.M. Hammarstrom, Magmatic epidote and its petrologic significance, *Geology, 12*, 515-518, 1984.

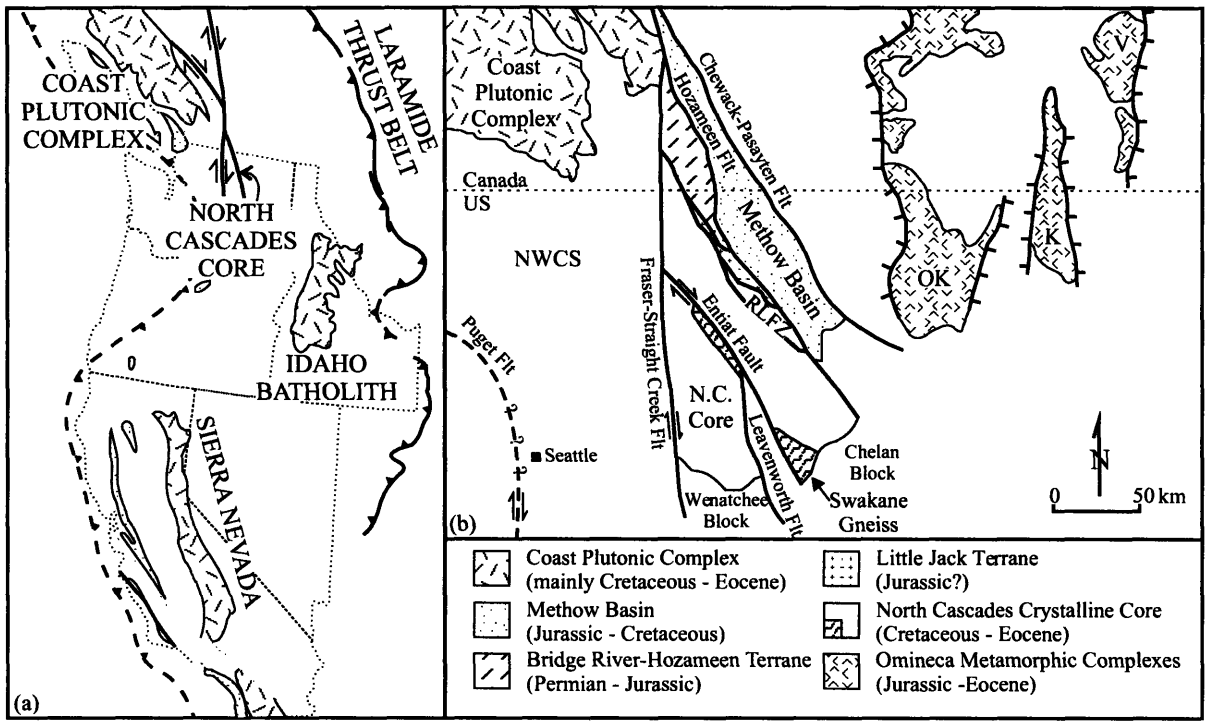

Figure 1. (a) Simplified paleogeographic map of the western U.S. emphasizing Cretaceous to Tertiary features; (b) simplified geologic map of the North Cascades, southern Canadian Coast Mountains, and Omineca metamorphic complexes after Miller and Bowring [1990] and Tabor et al. [1989]. Abbreviations are as follows: K, Kettle Dome; NWCS, Northwest Cascades Thrust System (Cretaceous); OK, Okanogan Complex; RLFZ, Ross Lake Fault Zone; and V, Valhalla Complex.

Figure 2. Simplified geologic map of the Cascades core after Haugerud et al., [1991], Brown and Walker [1993] and Hopson and Mattinson [1994]. Sample localities are marked by white dots. Plutons are shown in a random dashed pattern. The largest dashes denote ca. 96-88 Ma plutons; intermediate dashes denote ca. 79-65 Ma plutons; and the smallest dashes denote ca. 50-46 Ma plutons. Heavy lines represent faults whereas light lines represent depositional or intrusive contacts. Abbreviations are as follows: DD, Dinkelman Detachment; EN, Entiat intrusive suite; SFJ, Seven-Fingered Jack intrusive suite; and WRSZ, White River shear zone.

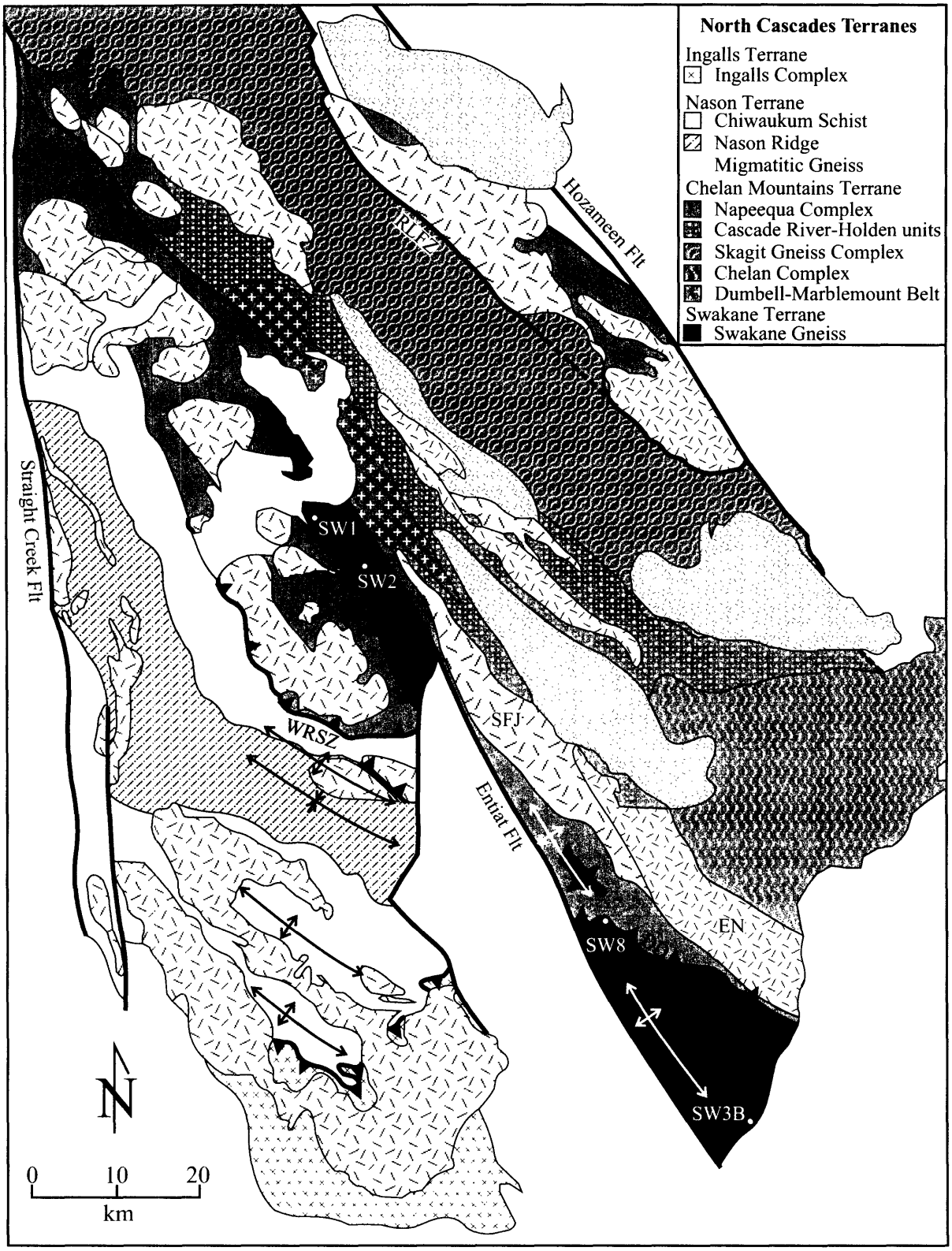

Figure 2. Caption on opposite page.

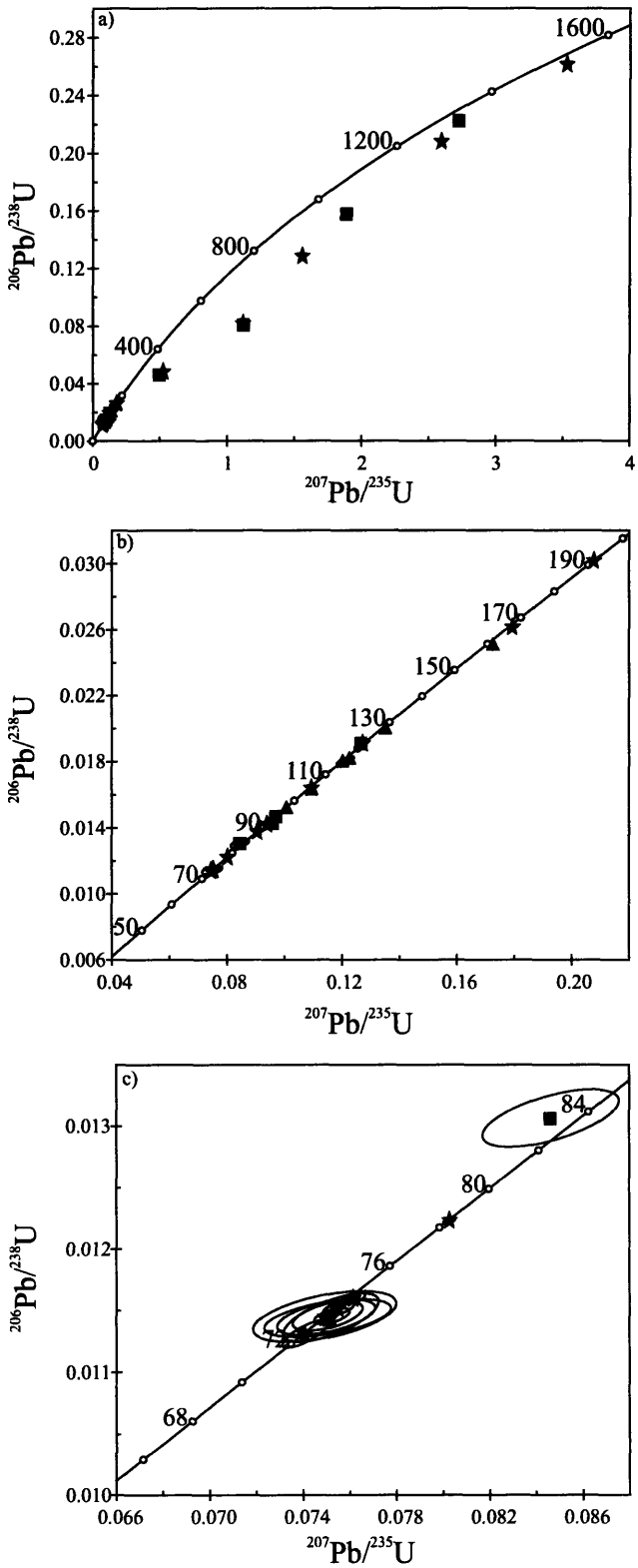

Figure 3. U-Pb concordia diagrams for zircon analyses from the Swakane terrane with a) all analyses shown, b) focusing in on Jurassic to Late Cretaceous analyses, and c) focusing in on the population of youngest zircon analyses. Stars represent data from sample SW3B. Squares represent data from sample SW8. Triangles represent data from sample SW2.

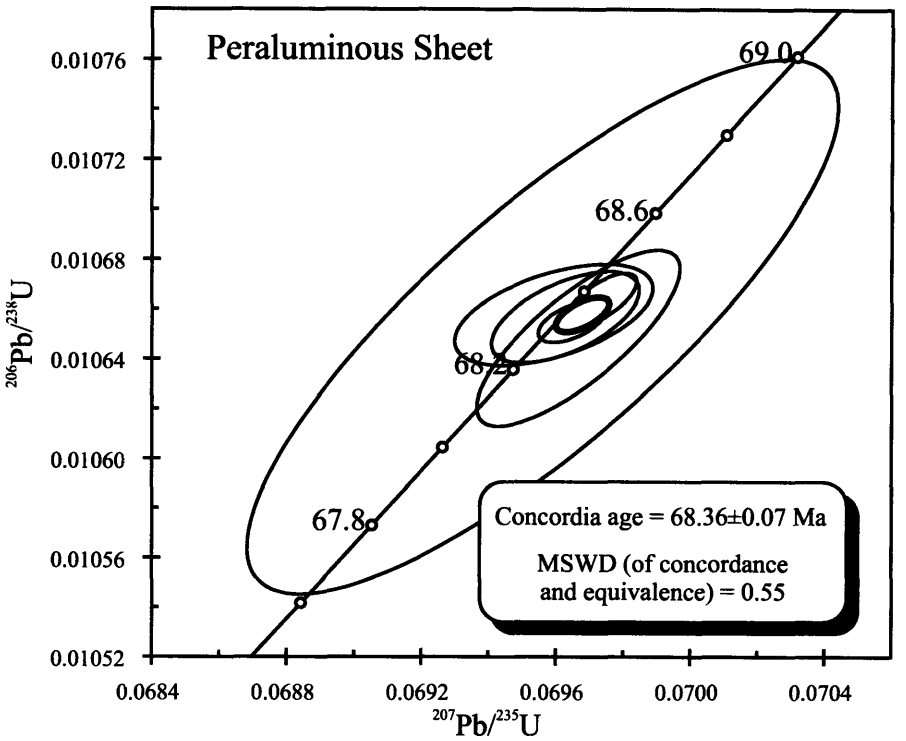

Figure 4. U-Pb concordia diagram showing zircon analyses that represent the crystallization age of a peraluminous leucogranite sheet. The concordia ellipse is shaded in light grey.

Figure 5. Cathodoluminescence images of zircon grains from the Swakane biotite gneiss (sample SW3B) that were analyzed after imaging. The number in the upper left corner of each panel corresponds to the fraction number in table 1, and its U-Pb date is shown in the upper right corner.

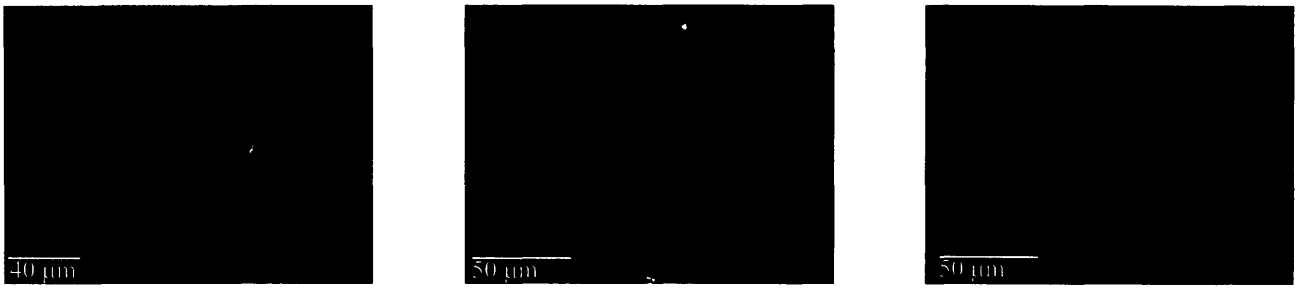

Figure 6. Representative cathodoluminescence images from Swakane garnet-kyanite gneiss.

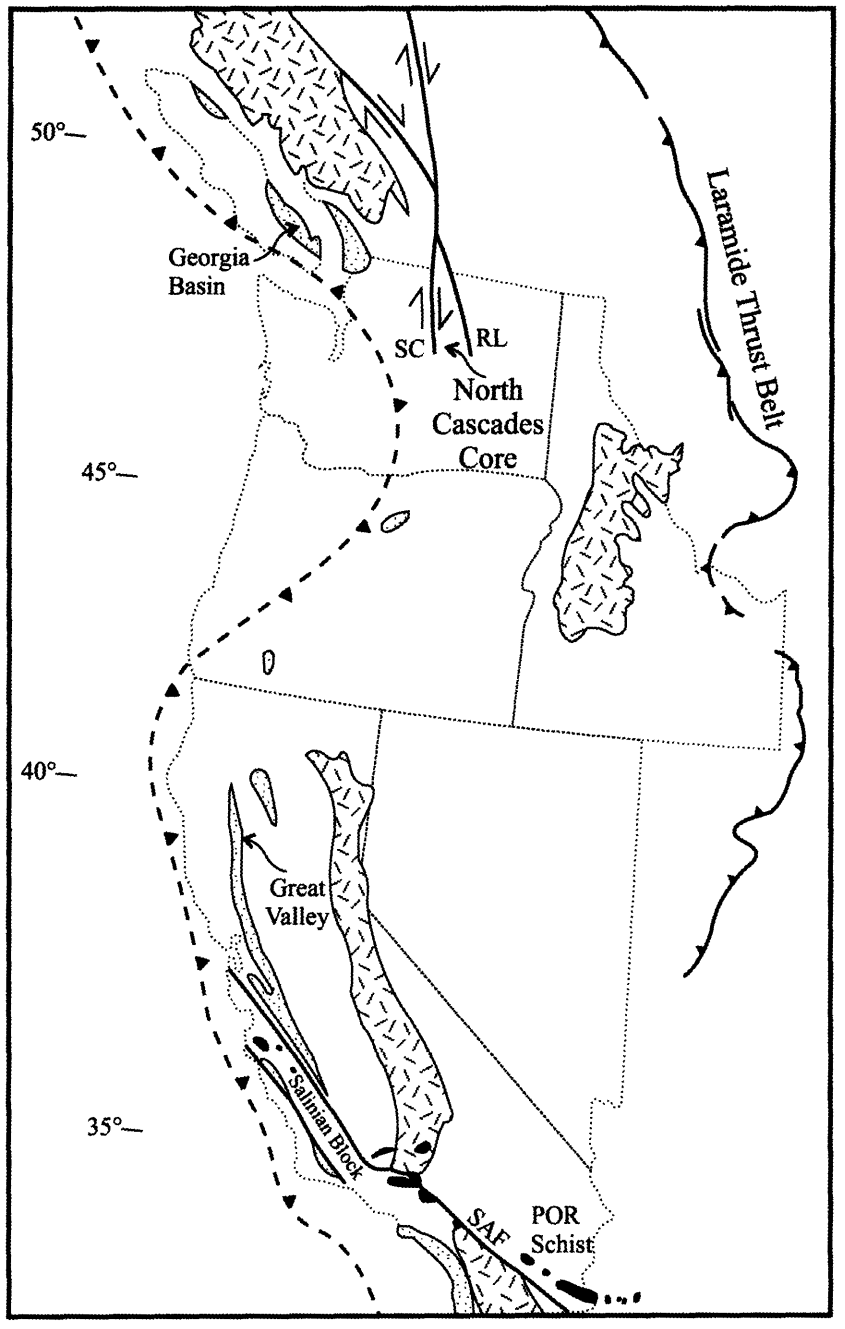

Figure 7. Paleogeographic and tectonic map of the western US Cordillera during the latest Cretaceous to middle Eocene time after Burchfiel [1992]. The western margin of North America is depicted by a bold, dashed line. Fore-arc basins are depicted with a stippled pattern. Arc plutonic rocks are depicted with a cross-hatched pattern. The Pelona, Orocopia and Rand schist group is shown in solid black. Other abbreviations include: SAF, San Andreas fault; SC, Straight Creek fault; RL, Ross Lake fault zone.

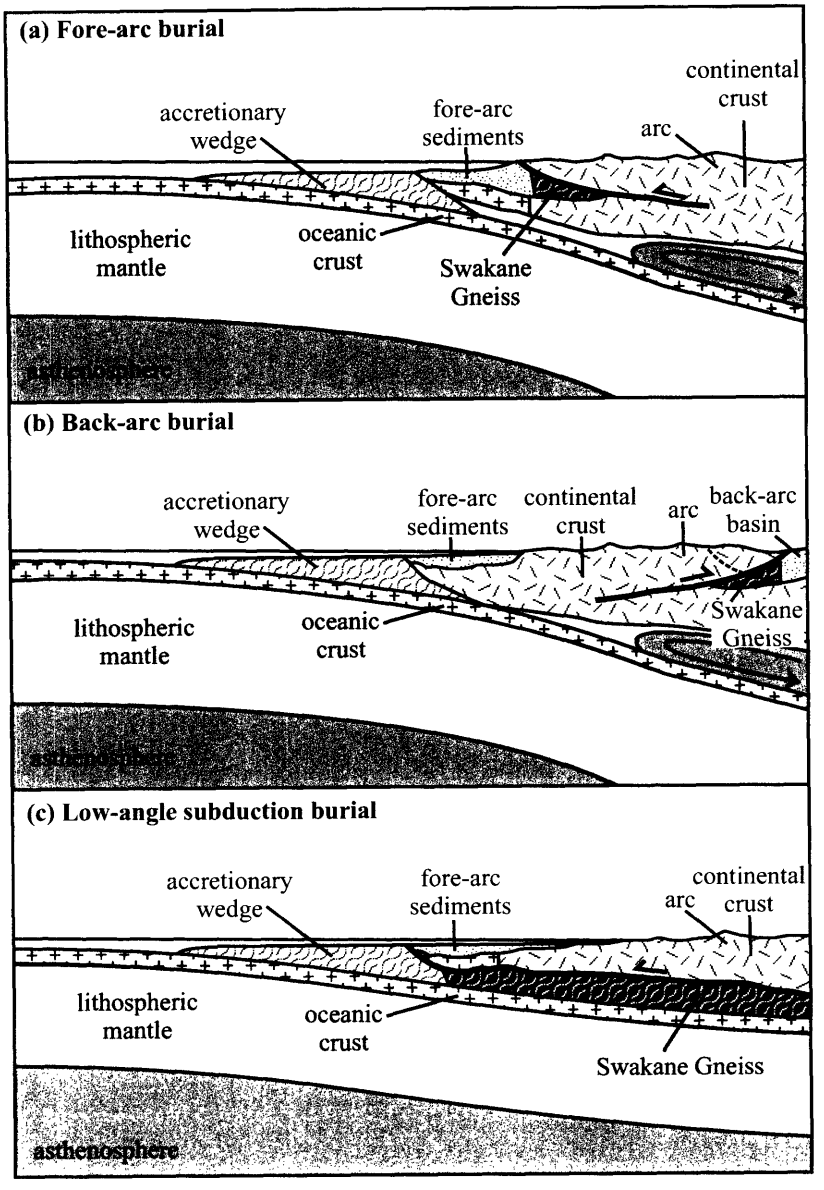

Figure 8. Schematic diagram of potential burial mechanisms for the Swakane Gneiss after Haxel et al. [2002]. See text for discussion of models. Heavy black lines represent thrust faults responsible for burial of sediments. Light arrow in the sub-arc mantle wedge represents flow lines.

Table 1: U-Pb isotopic data from zircon from the Swakane terrane.

	Composition						Isotopic Ratios								Dates (Ma)				
Frac[a]	Wt (μg)[b]	U (ppm)	Pb (ppm)	Th[c] / U	Pb*[d] / Pbc	Pbc[d] (pg)	$^{206}Pb/^{204}Pb$[e]	$^{208}Pb/^{206}Pb$[f]	$^{206}Pb/^{238}U$[f]	% err[g]	$^{207}Pb/^{235}U$[f]	% err[g]	$^{207}Pb/^{206}Pb$[f]	% err[g]	$^{206}Pb/^{238}U$[h]	$^{207}Pb/^{235}U$[h]	$^{207}Pb/^{206}Pb$[h]	corr. coef.	Discord-ance
SW3B: BIOTITE GNEISS																			
z1	36.2	252.0	11.9	0.051	392.3	1.1	25709	0.064	0.048215	(.12)	0.52671	(.13)	0.079229	(.06)	303.6	429.6	**1177.9**	0.880	75.9
z2	13.2	214.0	6.4	0.338	44.8	1.9	2918	0.108	0.030161	(.08)	0.20761	(.16)	0.049922	(.14)	**191.6**	191.5	191.4	0.513	-0.1
z3	12.8	206.6	2.9	0.310	19.4	1.9	1284	0.099	0.014245	(.17)	0.09403	(.33)	0.047878	(.28)	**91.2**	91.3	93.2	0.543	2.2
z4	15.4	78.8	1.4	0.546	6.6	3.2	423	0.176	0.016385	(.48)	0.10945	(.61)	0.048450	(.35)	104.8	105.5	**121.3**	0.813	13.7
z6	10.8	138.0	1.6	0.459	9.8	1.8	631	0.147	0.011600	(.33)	0.07611	(.59)	0.047588	(.47)	**74.3**	74.5	78.8	0.613	5.7
z9	10.6	44.6	0.5	0.456	2.8	2.0	196	0.146	0.011437	(1.10)	0.07472	(2.58)	0.047385	(2.21)	**73.3**	73.2	68.7	0.527	-6.8
z10	6.5	288.5	5.3	0.229	9.9	3.5	677	0.073	0.019069	(.30)	0.12716	(.45)	0.048365	(.32)	**121.8**	121.5	117.2	0.702	-3.9
z11	3.5	503.8	103.9	0.177	145.5	2.5	9461	0.063	0.207816	(.08)	2.59148	(.10)	0.090441	(.06)	1217.2	1298.2	**1434.9**	0.800	16.6
z12	3.5	478.8	92.7	0.206	107.8	3.0	6944	0.076	0.193348	(.09)	2.35285	(.12)	0.088258	(.08)	1139.5	1228.4	**1388.1**	0.773	19.5
z13	3.8	82.0	0.9	0.334	2.1	1.7	153	0.107	0.011452	(1.44)	0.07494	(3.34)	0.047458	(2.85)	**73.4**	73.4	72.4	0.531	-1.4
z14	4.3	633.8	7.7	0.317	18.9	1.7	1249	0.101	0.012228	(.16)	0.08027	(.26)	0.047610	(.19)	**78.4**	78.4	79.9	0.680	2.0
z15	4.6	78.9	0.9	0.384	3.6	1.2	250	0.123	0.011453	(.84)	0.07505	(1.63)	0.047527	(1.34)	**73.4**	73.5	75.8	0.575	3.2
z16	6.0	83.3	1.0	0.404	8.0	0.7	531	0.129	0.011516	(.39)	0.07550	(.72)	0.047553	(.58)	**73.8**	73.9	77.1	0.603	4.3
z17	4.3	116.1	1.5	0.857	4.3	1.5	263	0.274	0.011310	(.79)	0.07409	(1.07)	0.047515	(.69)	**72.5**	72.6	75.3	0.764	3.7
z18	8.6	113.5	1.3	0.405	6.6	1.7	441	0.130	0.011458	(.46)	0.07525	(.83)	0.047630	(.65)	**73.4**	73.7	80.9	0.624	9.3
z19*	2.4	336.4	4.0	0.482	2.2	4.2	157	0.155	0.011440	(1.40)	0.07517	(2.23)	0.047656	(1.63)	**73.3**	73.6	82.3	0.682	10.9
z20*	1.8	540.5	48.0	0.159	47.6	1.8	2838	0.163	0.081736	(.12)	1.11898	(.14)	0.099290	(.08)	506.5	762.5	**1610.8**	0.841	71.2
z21*	0.1	279.6	3.8	0.351	3.5	1.6	244	0.112	0.013732	(.87)	0.09018	(3.02)	0.047628	(2.74)	**87.9**	87.7	80.9	0.442	-8.8
z22*	2.0	110.4	1.3	0.571	3.1	0.8	208	0.184	0.011448	(1.03)	0.07531	(2.63)	0.047713	(2.29)	**73.4**	73.7	85.1	0.501	13.8
z23*	0.6	517.5	7.3	0.474	3.2	1.3	219.98	0.151	0.013750	(.97)	0.09026	(1.67)	0.04761	(1.30)	**88.0**	87.7	79.8	0.634	-10.4
z24*	0.8	10.0	0.1	0.247	7.8	1.8	534.78	0.079	0.01422	(.37)	0.09366	(.49)	0.04776	(.30)	**91.0**	90.9	87.3	0.787	-4.30
z25*	1.8	5.7	0.1	0.290	9.9	1.5	667.77	0.093	0.02612	(.30)	0.17920	(.45)	0.04976	(.32)	**166.2**	167.4	183.6	0.706	9.58
z26*	1.4	17.7	2.2	0.098	134.6	1.7	8840.90	0.054	0.12857	(.05)	1.55864	(.07)	0.08792	(.05)	779.7	953.9	**1380.8**	0.719	46.17
z27*	1.0	10.3	2.7	0.159	80.0	3.3	5234.40	0.050	0.261793	(.06)	3.52690	(.08)	0.09771	(.05)	1499.0	1533.3	**1580.9**	0.758	5.80
SW8:BIOTITE GNEISS																			
z1	10.4	106.1	1.6	0.486	22.7	0.7	1431	0.155	0.014684	(.15)	0.09696	(.24)	0.047894	(.19)	**94.0**	94.0	94.0	0.649	0.0
z2	2.9	1924.6	85.5	0.032	360.8	0.7	24165	0.041	0.046214	(.06)	0.49471	(.07)	0.077639	(.05)	291.2	408.1	**1137.6**	0.765	76.1
z3	3.9	85.5	1.6	0.324	4.8	1.3	333	0.103	0.019072	(.61)	0.12653	(.84)	0.048116	(.55)	**121.8**	121.0	105.0	0.760	-16.1
z5	2.4	88.8	1.2	0.420	2.1	1.3	150	0.133	0.013067	(1.47)	0.08463	(2.83)	0.046971	(2.29)	**83.7**	82.5	47.8	0.594	-75.7
z6	1.5	301.1	25.9	0.130	28.3	1.4	1730	0.136	0.080693	(.13)	1.11920	(.16)	0.100593	(.08)	500.3	762.6	**1635.1**	0.846	72.1
z7	1.9	377.3	58.1	0.110	84.5	1.3	5591	0.049	0.157750	(.07)	1.88573	(.11)	0.086698	(.08)	944.3	1076.1	**1353.8**	0.705	32.5
z8	1.9	524.4	115.4	0.194	109.7	1.9	7145	0.063	0.222134	(.09)	2.72126	(.11)	0.088849	(.05)	1293.1	1334.3	**1400.9**	0.856	8.5
z9	1.8	268.3	3.6	0.148	3.7	1.7	273	0.048	0.014281	(.75)	0.09567	(.96)	0.048588	(.57)	91.4	92.8	**128.0**	0.808	28.8

Table 1 continued: U-Pb isotopic data from zircon from the Swakane terrane.

	Composition						Isotopic Ratios								Dates (Ma)				
Frac[a]	Wt (μg)[b]	U (ppm)	Pb (ppm)	Th[c] / U	Pb*[d] / Pbc	Pbc[d] (pg)	^{206}Pb[e] / ^{204}Pb	^{208}Pb[f] / ^{206}Pb	^{206}Pb[f] / ^{238}U	% err[g]	^{207}Pb[f] / ^{235}U	% err[g]	^{207}Pb[f] / ^{206}Pb	% err[g]	^{206}Pb[h] / ^{238}U	^{207}Pb[h] / ^{235}U	^{207}Pb[h] / ^{206}Pb	corr. coef.	Discord-ance
SW2: GARNET-KYANITE GNEISS																			
z1	2.1	383.8	6.7	0.208	4.3	3.3	305	0.067	0.018133	(.68)	0.12229	(1.06)	0.048915	(.78)	115.84	117.15	**143.7**	0.681	19.6
z2	1.4	224.0	4.4	0.300	4.8	1.3	332	0.096	0.019958	(.61)	0.13486	(.88)	0.049007	(.60)	127.39	128.45	**148.2**	0.730	14.2
z3	0.4	684.6	12.1	0.289	3.2	1.4	230	0.093	0.017997	(.91)	0.12050	(1.43)	0.048560	(1.05)	114.99	115.52	**126.6**	0.682	9.3
z4	1.1	495.3	7.7	0.210	5.6	1.5	392	0.068	0.016269	(.52)	0.10947	(.75)	0.048800	(.51)	104.03	105.48	**138.2**	0.730	24.9
z5	3.0	544.5	8.2	0.315	9.9	2.5	661	0.101	0.015154	(.35)	0.10067	(.77)	0.048183	(.66)	96.95	97.40	**108.2**	0.526	10.5
z6	0.7	1042.7	27.5	0.532	13.1	1.4	819	0.172	0.025053	(.25)	0.17222	(.35)	0.049857	(.24)	159.51	161.35	**188.4**	0.732	15.5
SWPEG1: PERALUMINOUS SHEET																			
z1	15.0	1018.7	9.9	0.049	73.0	2.0	5158	0.016	0.010664	(.08)	0.06974	(.12)	0.047429	(.09)	**68.4**	68.4	70.9	0.680	3.6
z3	2.7	984.4	9.7	0.091	28.9	0.9	2027	0.029	0.010658	(.16)	0.06959	(.35)	0.047359	(.30)	**68.3**	68.3	67.4	0.522	-1.4
z5	4.2	632.5	6.1	0.044	3.3	7.8	252	0.014	0.010653	(.82)	0.06956	(1.03)	0.047359	(.58)	**68.3**	68.3	67.4	0.824	-1.4
z9	11.3	743.5	7.2	0.053	126.5	0.6	8920	0.017	0.010655	(.06)	0.06965	(.12)	0.047408	(.10)	**68.3**	68.4	69.8	0.557	2.2
z11	2.0	772.0	7.6	0.080	10.8	1.4	773	0.026	0.010648	(.27)	0.06967	(.35)	0.047450	(.22)	**68.3**	68.4	72.0	0.790	5.1
z12	3.4	613.0	8.0	0.271	2.6	10.5	188	0.086	0.013402	(1.15)	0.08803	(2.05)	0.047639	(1.64)	**85.8**	85.7	81.4	0.603	-5.4
z13	2.5	250.6	2.7	0.173	2.2	3.0	168	0.058	0.011350	(1.30)	0.07845	(2.20)	0.050126	(1.67)	**72.8**	76.7	200.8	0.650	64.1
z14	7.1	844.1	9.3	0.171	69.8	0.9	4761	0.055	0.011603	(.06)	0.07617	(.09)	0.047615	(.07)	**74.4**	74.5	80.2	0.656	7.3
z15	2.9	534.4	5.2	0.062	20.8	0.7	1478	0.020	0.010657	(.14)	0.06963	(.26)	0.047387	(.21)	**68.3**	68.3	68.8	0.583	0.6
z16	1.9	922.2	9.4	0.109	23.6	0.7	1652	0.035	0.011000	(.13)	0.07195	(.23)	0.047440	(.18)	**70.5**	70.5	71.4	0.611	1.3
z17	1.3	542.6	5.9	0.338	10.3	0.7	689	0.108	0.010915	(.29)	0.07133	(.50)	0.047397	(.39)	**70.0**	70.0	69.2	0.641	-1.1

[a] All zircon fractions (i.e. z1, z2) are composed of single abraded zircons. Asterisk denotes grains that were imaged by cathodoluminescence before abrasion.

[b] Sample weights were estimated to within 40% using measured grain dimensions and a nominal density of 4.5 g/cm^3 for zircon.

[c] Th contents calculated from radiogenic ^{208}Pb and the $^{207}Pb/^{206}Pb$ date of the sample, assuming concordance between U-Th-Pb systems.

[d] Pb* and Pbc represent radiogenic Pb and common Pb respectively.

[e] Measured ratio corrected for fractionation and spike contribution; Pb fractionation was 0.12 ±0.04%/a.m.u. for Faraday detector or 0.20 ± 0.04%/a.m.u. for Daly detector analysis, based on daily analysis of NBS-981.

[f] Measured ratios corrected for fractionation, spike, and blank; nominal U blank = 0.1 pg ± 50% (2 σ); all common Pb attributed to blank; measured laboratory Pb composition: $^{206}Pb/^{204}Pb$ = 19.10±0.05, $^{207}Pb/^{204}Pb$ = 15.71±0.05, $^{208}Pb/^{204}Pb$ = 38.65 ± 0.05 (2σ).

[g] Numbers in parentheses are the % errors reported at the 2 σ confidence interval, propagated using the algorithms of Ludwig (1980).

[h] Isotopic ages calculated using the decay constants of Jaffey et al. (1971): $\lambda(^{235}U) = 9.8485 \times 10^{-10}$ yr^{-1} and $\lambda(^{238}U) = 1.55125 \times 10^{-10}$ yr^{-1}. date reported at the 2 σ confidence interval. Dates in bold are the best estimates of the age of the zircon.

Chapter 2

SPATIAL AND TEMPORAL VARIATIONS IN Nd ISOTOPIC SIGNATURES ACROSS THE CRYSTALLINE CORE OF THE NORTH CASCADES, WA: IMPLICATIONS FOR THE TECTONIC EVOLUTION OF A MAGMATIC ARC

ABSTRACT

The crystalline core of the North Cascades lies at the southern termination of the Coast Belt and records the Cretaceous to Paleogene history of terrane accretion and crustal growth along the North American continental margin. The nature and extent of involvement of Precambrian continental crust in the evolution of the North Cascades has been largely unconstrained. Arc plutons that intrude the Cascades core provide probes of this crustal architecture. Sm-Nd data from metamorphic terranes of the North Cascades, excluding the Swakane terrane, yield ε_{Nd} values in the mid-Cretaceous that range from +9.4 to -2.7 and indicate that involvement of evolved crustal material in the formation of these terranes was minimal. Amphibolites from the Napeequa Complex and Chiwaukum Schist yield near-depleted mantle ε_{Nd} values in the mid-Cretaceous, which suggest that these terranes have an oceanic affinity. Meta-clastic rocks from the Chiwaukum Schist and Nason Ridge Migmatitic Gneiss have ε_{Nd} values that lie between those of arc-derived and craton-derived sediment reflecting a mixture of these two sources. Initial ε_{Nd} values of the Swakane Gneiss also reflect mixing of craton-derived and arc-derived sources with a relatively more significant component of craton-derived sediments. ε_{Nd} values of plutons that intrude the Cascades core reflect mixing of mantle-derived melt and melt derived by anatexis of isotopically juvenile terranes. The range of initial ε_{Nd} values observed from the plutons is strongly influenced by local variations in the Nd signature of the crustal source. Initial ε_{Nd} values of Chelan block plutons decreased over time suggesting melting from increasingly more evolved crustal sources. These temporal variations in Nd signatures are also observed between the northern and southern Coast Plutonic Complex, and may reflect changes in the sources of crustal melting along the length of the Cretaceous arc.

INTRODUCTION

The Coast Belt, which forms the northwestern cordillera of North America, represents a classic example of growth of continental crust by accretion of terranes that have had only a short crustal residence time and, thus, are isotopically juvenile terranes (Coney et al., 1980; Monger et al., 1982; Patchett and Gehrels, 1998; Samson et al.,

1989). At the southernmost extent of the Coast Belt, the crystalline core of the North Cascades (Cascades core) records the Cretaceous to Paleogene history of crustal growth along this segment of the continental margin. It has long been known that metamorphic terranes of the Cascades core contain Precambrian zircons (Mattinson, 1972); however, the nature and extent of this Precambrian "inheritance" is largely unconstrained. For example, were these Precambrian zircons derived from an exotic sliver of Precambrian crust entrained within the arc or sediment transported west from the North American margin? Plutons that intrude the Cascades core provide probes of this crustal architecture.

In this chapter, I discuss the evolution of magmatism at the southern termination of the Coast Belt based primarily on Nd isotopic data from granitoid rocks and their host terranes. New Nd data from 46 samples spatially distributed within the Cascades core are compared with existing Nd data from igneous rocks of the southern Coast Belt to address questions related to crustal growth in this region and the influence of input from the North American craton. The approximately 50 Myr history of magmatism in the Cascades core offers an exceptional opportunity to evaluate both spatial and temporal variations in Nd isotope evolution.

HISTORY OF CRUSTAL AMALGAMATION

The Cascades core makes up the southernmost extent of the Coast Belt, one of the five physiographic provinces of the Canadian Cordillera (Fig. 1) (Monger et al., 1982). These physiographic provinces record the history of amalgamation of terranes to the North American craton during mid-Jurassic orogenesis. The Omineca Crystalline Belt records suturing of the Intermontane superterrane to the ancient North American margin (Rocky Mountain Belt) whereas, the Coast Belt records suturing of the Insular and Intermontane superterranes (Monger et al., 1982).

The Coast Belt is underlain primarily by the Coast Plutonic Complex, a long, narrow belt about 1700 km long and 50-175 km wide, composed of discrete to coalescing plutons, migmatite, gneiss and lesser, variably-metamorphosed volcanic and sedimentary rocks (Friedman et al., 1995). The plutons are predominantly quartz diorite, tonalite, and diorite (Woodsworth et al., 1991), and they range in age from Silurian to Miocene,

although ~95% of the bodies are Jurassic to Eocene in age (Friedman and Armstrong, 1995; van der Heyden, 1992; Van der Heyden, 1989; Woodsworth et al., 1991). In the southern Coast Belt, the Coast Plutonic Complex intrudes small, early Mesozoic arc (Harrison and Cadwallader) and oceanic (Bridge River) terranes, which may have equivalents in the North Cascades.

The Cascades core is dominated by Paleozoic to Mesozoic accreted terranes of oceanic and island-arc affinity that have undergone amphibolite-facies metamorphism (Misch, 1966; Tabor et al., 1989; Tabor et al., 1987b). These terranes were sutured together and form the framework into which Cretaceous to Paleogene plutons intrude. The Cascades core is offset from the main part of the Coast Belt by the Tertiary, N-trending, strike-slip, Fraser-Straight Creek fault and bound on the east by the Ross Lake fault zone (Fig. 1) (Misch, 1966). The southeastern boundary is obscured by Tertiary basin fill and the Columbia River Basalt Group. The major internal structure of the core is the post-metamorphic, high-angle, Tertiary Entiat fault, which divides the core into the Wenatchee and Chelan blocks (Fig. 2).

The crystalline core of the North Cascades can be divided into four separate tectonostratigraphic terranes following Tabor et al. (1987b, 1989): 1) Chelan Mountains terrane, 2) Nason terrane, 3) Swakane terrane, and 4) Ingalls terrane. The **Chelan Mountains terrane** comprises most of the Chelan block and has been further subdivided. The *Napeequa Complex* (i.e., "rocks of the Napeequa River area" of Cater and Crowder (1967)) and the associated Twisp Valley schist (Adams, 1964) are comprised of mainly quartz-rich mica schist, quartzite, and amphibolite with minor calc-silicate rock, marble, and meta-ultramafic rock (Miller and Paterson, 2001; Tabor et al., 1989). This association of rock types has been interpreted as a chert- and basalt-rich, oceanic unit assembled in an accretionary wedge (Brown et al., 1994; Haugerud et al., 1991; Miller et al., 1994; Miller et al., 1993; Tabor et al., 1989), and is potentially equivalent to the Mississippian to Jurassic Bridge River complex in southwestern British Columbia (Tabor et al., 1989). Peak P-T conditions in the Napeequa Complex reached 9-11 kbar and 640-740°C (Valley et al., 2003). The timing of peak metamorphism is not well-established; however, 96-91 Ma plutons that intrude the Napeequa Complex yield emplacement pressures of 8-10 kbar and contain magmatic epidote which is consistent with high

pressure crystallization (Dawes, 1993; Walker and Brown, 1991; Zen and Hammarstrom, 1984). These data suggest that the Napeequa Complex occupied a mid- to lower-crustal position during mid-Cretaceous arc magmatism.

The other metasupracrustal units in the Chelan Mountains terrane include the *Cascade River unit* and the correlative *Holden assemblage* (Fig. 2), which are part of a Triassic arc sequence (Tabor et al., 1989). These units comprise metavolcanic and metasedimentary rock (amphibolite and hornblende-biotite schist) with local metaconglomerate, metapelite and calc-silicate rock (Dragovich et al., 1989; Dragovich and Norman, 1995; Tabor et al., 1989). Contact relationships between the Cascade River-Holden (CR-H) units and the Napeequa Complex are not clearly defined. The CR-H arc sequence has been proposed to have either formed unconformably on the oceanic Napeequa Complex (Tabor et al., 1989) or was overthrust by the Napeequa Complex (Brown et al., 1994; Dragovich et al., 1989). In the eastern Coast Belt (British Columbia), the Upper Triassic Cadwallader Group, which is potentially correlative to the CR-H arc sequence, is faulted against the Bridge River complex, a potential correlative of the Napeequa Complex (Rusmore, 1987; Rusmore and Woodsworth, 1991; Tabor et al., 1989).

The CR-H units are intruded by the tonalitic, strongly-deformed, Triassic Dumbell plutons and the Marblemount Meta Quartz Diorite to form what is known as the *Marblemount-Dumbell belt* (Fig. 2). A ca. 220 Ma U-Pb zircon data represents the crystallization age of this belt (Mattinson, 1972). These intrusive rocks form the roots of the Holden-Cascades River arc (Miller et al., 1994; Tabor et al., 1989).

In the northeastern Chelan block, the Napeequa Complex and CR-H units are extensively injected by granodiorite to hornblende quartz diorite orthogneiss bodies, forming the *Skagit Gneiss Complex* (Fig. 2) (Haugerud et al., 1991). U-Pb zircon analyses yield ca. 60-90 Ma crystallization ages from the orthogneiss bodies and ca. 47-44 Ma crystallization ages from late, lineated leucogranite dikes (Haugerud et al., 1991). Screens and rafts of paragneiss of probable Napeequa Complex and CR-H unit affinity are widespread in the Skagit Gneiss Complex (Tabor et al., 1988). The Skagit Gneiss Complex strikes directly into the *Chelan Complex*, a metaplutonic migmatite complex (Hopson and Mattinson, 1994); however, the boundary between these units is obscured

by the crosscutting, Eocene Cooper Mountain pluton. Several differences between the Chelan Complex and the Skagit Gneiss Complex indicate that these complexes form distinct units with independent histories (Hopson and Mattinson, 1994). In contrast to the Skagit Gneiss Complex, the Chelan Complex lacks paragneiss screens and contains greater proportions of mafic and ultramafic rock (Hopson and Mattinson, 1994). The Chelan Complex also appears to be significantly older than the Skagit Gneiss Complex with metatonalite bodies that yield crystallization dates in the range of 120-110 Ma (Mattinson, 1972). These crystallization dates suggest that the Chelan Complex is temporally more closely related to the 114-111 Ma Okanogan Range batholith (Hurlow and Nelson, 1993) that extends to the north of the Chelan Complex (Fig. 2) than to the other rocks of the Cascades core (Hopson and Mattinson, 1994). Overall, the Chelan Mountains terrane appears to form a complex, N-trending antiform with the Skagit migmatitic gneiss in its core (Tabor et al., 1989).

The **Nason terrane** comprises the bulk of the Wenatchee block and is made up of the Nason Ridge Migmatitic Gneiss and Chiwaukum Schist. The Chiwaukum Schist, an interlayered metapelitic and metapsammitic unit, underlies the Napeequa Complex along the White River shear zone (Fig. 2) (Miller and Paterson, 2001; Tabor et al., 1987a; Van Diver, 1967). Pressures calculated from Chiwaukum metapelitic schist increase from 3 kbar near the Mount Stuart batholith to 9 kbar near the White River shear zone (Bendixen, 1994; Brown and Walker, 1993; Evans and Berti, 1986). At the deepest levels of this terrane in the core of a regional antiform, the Chiwaukum Schist grades into the Nason Ridge Migmatitic Gneiss. The protolith of the gneiss is likely the same rock that forms the Chiwaukum Schist; however, the Nason Ridge Migmatitic Gneiss has been extensively injected by tonalitic to trondhjemitic magma (Tabor et al., 1987a). The composition, metamorphic history and associated plutons suggest that the Chiwaukum Schist may be the lateral equivalent of the Settler Schist in southwestern British Columbia (Evans and Berti, 1986; Magloughlin, 1986; Misch, 1977; Monger, 1991) or the Late Jurassic Cayoosh assemblage (Miller et al., 2003).

The Swakane Gneiss is the only unit that makes up the **Swakane terrane**, which crops out in both the Wenatchee and Chelan blocks. It is a meta-supracrustal unit consisting predominantly of homogeneous quartzofeldspathic biotite ± garnet and

muscovite gneiss with local garnet amphibolite, garnet + hornblende + biotite gneiss, garnet + kyanite ± staurolite gneiss, calc-silicate, quartzite and meta-peridotite (Cater, 1982; Paterson et al., 2004; Sawyko, 1994; Tabor et al., 1987a; Valley et al., 2003; Waters, 1932). Peak P-T conditions reached 9-12 kbar and 670-730 °C (Valley et al., 2003), making it the deepest unit in the Cascades core. The Swakane Gneiss is unique in the Cascades core because it lacks arc related plutons, although the base of the section is intruded by thin peraluminous, granitic sheets. Until recently, the protolith age of the Swakane Gneiss was inferred to be Proterozoic based on the presence of Precambrian zircon grains (Mattinson, 1972; Tabor et al., 1987b); however this age assignment was problematic because of the lack of arc-related plutons in a unit that was assumed to have occupied a lower crustal position during mid-Cretaceous magmatism. New U-Pb geochronology from detrital zircons in the Swakane Gneiss (Chapter 1) indicates that the protolith age of the Swakane Gneiss is ca. 73 Ma, much younger than previously thought. Therefore, this terrane was not part of the crustal architecture of the Cascades core until after voluminous mid-Cretaceous magmatism.

The final terrane that comprises the Cascades core is the **Ingalls terrane**, which is solely composed of the Late Jurassic Ingalls ophiolite (Miller, 1985). The ophiolite was thrust over the Nason terrane along the Windy Pass thrust. Latest motion along the thrust was concurrent with the emplacement of the 96-91 Ma Mount Stuart batholith (Matzel et al., 2002; Miller and Paterson, 1992). The Ingalls ophiolite sequence represents the shallowest level rocks involved in the Cascades core metamorphism and deformation. Metamorphic grade ranges from prehnite-pumpellyite facies in the southern, low grade part of the sequence, to amphibolite facies in the structurally lower part near the Windy Pass thrust (Miller and Paterson, 2001).

MAGMATIC HISTORY

Arc magmas intruded the Cascades core from at least 96 Ma until ca. 46 Ma (Miller et al., 1989). Magmatism occurred in three distinct pulses including the most voluminous 96-88 Ma (Group I) pulse, a 78-65 Ma (Group II) pulse, and a 50-46 Ma (Group III) pulse. Both the Wenatchee and Chelan blocks experienced 96-88 Ma magmatism; however only the Chelan block contains plutons from the Group II and

Group III pulses at the presently exposed crustal level. The compositions of plutons vary from gabbro to granodiorite (Cater, 1982), and this variation is not restricted to a given block. The plutons can be divided into two compositional series – a gabbro to tonalite series and a tonalite to granodiorite series (see Dawes, 1993). Both series are observed in the Group I plutons, but the Group II plutons predominantly fall in the gabbro to tonalite series and the Group III plutons predominantly fall in the tonalite to granodiorite series. In fact, the Group III plutons generally lack mafic endmembers, and the single-most characteristic feature of this group is the presence of considerable K-feldspar (Cater, 1982). Table 1 lists the plutons sampled in this study along with their predominant rock type(s) and their respective crystallization ages.

Sm-Nd ISOTOPIC DATA

Analytical Techniques

Analyzed samples encompass the entire age and compositional range of plutons in the Cascades core, and provide regional coverage of the host metamorphic terranes. Approximately 100 mg of powdered whole rock from each sample was spiked with a mixed ^{149}Sm-^{150}Nd tracer and completely dissolved in 3 mL of concentrated HF and 0.5 mL of 7M HNO_3 in Teflon pressure vessels at 220°C for five days. These solutions were dried down, and completely redissolved in 6M HCl by fluxing on a hotplate at 120°C for 24-48 hours. Separation of Nd and Sm was carried out using a standard two-stage column chemistry procedure. The REE were isolated using a cation-exchange resin followed by separation of Nd from Sm using the LN-spec resin. Once separated, Sm was loaded on to single Ta filaments with approximately 1 μL of 1M H_3PO_4 and analyzed as metal ions in static mode. Nd was loaded on to triple Re filaments with approximately 1 μL of 0.1M H_3PO_4 and analyzed as metal ions in dynamic multicollector mode with a ^{144}Nd signal intensity of approximately $1.5x10^{-11}$ A. Sm and Nd data were fractionation corrected with an exponential law, normalizing to $^{152}Sm/^{147}Sm=1.783$ and $^{146}Nd/^{144}Nd=0.7219$ respectively. Details of internal and external reproducibility of the data are given in the caption to table 2. The uncertainty on calculated initial ε_{Nd} values for all samples is between 0.1 to 0.2 ε_{Nd} units.

Host Terrane Data

During mid-Cretaceous times, ε_{Nd} values of the terranes in the Cascades core (excluding the Swakane terrane) cover an approximately 10 epsilon unit range from near depleted mantle values (+8.6) to slightly negative values (-1.9) (Table 2; Fig. 3). The trajectories of ε_{Nd} evolution are relatively flat with the difference between present day ε_{Nd} values and ε_{Nd} values back-calculated to 96 Ma generally being less than one epsilon unit. This suggests little fractionation of Sm from Nd after the formation of these terranes. The flat Nd isotope evolution trajectories also mean that uncertainties in the age of a given terrane make little difference in the calculated initial ε_{Nd} value. Data from all samples are given in table 2, and sample localities are plotted on figure 2.

The host terrane data can be broken out into four groups: 1) deformed pre-96 Ma plutons, 2) Napeequa Complex of the Chelan Mountains terrane, 3) Nason terrane, and 4) Swakane terrane. The pre-96 Ma plutons include the ca. 220 Ma Dumbell Gneiss from the Marblemount-Dumbell belt within the Chelan block and the ca. 138 Ma Methow Gneiss and ca. 118 Ma Alta Lake Complex along the eastern margin of the Cascades core. A hornblende tonalite gneiss from the Dumbell Gneiss unit yields an initial ε_{Nd} value of +7.6 and an ε_{Nd} value of +6.8 at 96 Ma (the timing of the earliest magmatism in the Cascades core) (Fig. 3). Samples of the Methow Gneiss and Alta Lake Complex yield similar initial ε_{Nd} values of +6.0 and +5.3 respectively.

Amphibolites and hornblende-biotite schists of the Napeequa Complex show a broader range of ε_{Nd} values at 96 Ma than the pre-96 Ma plutons (Fig. 3). The most positive ε_{Nd} value measured in this study (+8.6) was obtained from a Napeequa amphibolite from the Wenatchee block. The ε_{Nd} value of this sample increased slightly with time (present day ε_{Nd} = +9.4) indicating LREE depletion during its formation. Other amphibolite samples from the Napeequa Complex have ε_{Nd} values at 96 Ma of +8.0 to +5.1 (Fig. 3) and have ε_{Nd} values that decrease to the present day. A hornblende-biotite schist sample yields the lowest ε_{Nd} value of the Napeequa Complex at +3.4 (Fig. 3).

Samples from the Nason terrane exhibit the broadest range of ε_{Nd} values from +7.7 to -1.9 (Fig. 3). These samples include amphibolite (+7.7) and garnet-biotite schist

(+2.6, -1.9) from the Chiwaukum Schist and garnet-biotite gneiss (+0.6) from the Nason Ridge Migmatitic Gneiss.

The Swakane terrane samples exhibit the most negative ε_{Nd} values obtained in this study with values that range from -0.6 to ~-6.1 (Fig. 3). These values were measured from garnet-biotite gneisses distributed throughout the Swakane Gneiss in the Chelan block.

Pluton Data

Plutons from the Cascades core exhibit a more limited range of initial ε_{Nd} data than values from the host terranes (Table 2, Fig. 4). The Group I plutons display the broadest range of ε_{Nd} values, from +6.3 to +2.0; however, Group I plutons from the Chelan block generally have higher initial ε_{Nd} values (+6.3 to +4.6) than Group I plutons from the Wenatchee block (+5.1 to +2.0) (Fig. 4). This difference in initial ε_{Nd} value between the two crustal blocks does not correlate with rock type. Initial ε_{Nd} values of gabbro or diorite from a given pluton are generally more positive than tonalite from the same pluton, as is to be expected, but gabbro or diorite samples are only higher than tonalite samples by about one ε_{Nd} unit or less (Fig. 5). This trend means that samples of tonalite and granodiorite from the Chelan block have more positive initial ε_{Nd} values than the most mafic rocks sampled from the Wenatchee block. Initial ε_{Nd} values from granodiorites exhibit nearly the full range of ε_{Nd} values observed in the Group I plutons (Fig. 5).

Initial ε_{Nd} values from Group II plutons (only present in the Chelan block) form a tight cluster (+4.9 to +3.8) that is less positive than initial ε_{Nd} values from the Group I plutons from the Chelan block (+6.3 to +4.6) with little overlap between groups (Fig. 4). Again, this difference in ε_{Nd} value does not correlate with rock type. The most positive mafic sample from Group II is only slightly more positive than the most negative tonalite sample from the Chelan block Group I plutons.

Initial ε_{Nd} values from the Group III plutons form two distinct clusters on an ε_{Nd} versus time plot (Fig. 4). Five samples from plutons within the Chelan block have initial ε_{Nd} values that range from +2.9 to +1.5, whereas two samples from plutons within the

Ross Lake fault zone and a leucogranite dike that cuts the Skagit Gneiss Complex have initial ε_{Nd} values of +5.2 to +5.0. The samples with lower ε_{Nd} values are granodioritic whereas samples with higher ε_{Nd} values are granitic (Golden Horn batholith and a leucocratic dike) or trondhjemitic (Ruby Creek Heterogeneous Plutonic Belt).

DISCUSSION

Host Terranes

The ε_{Nd} values of the terranes that comprise the Cascades core reflect variations in the sources that contributed to each terrane. Overall, the positive and near depleted mantle-like values of most samples preclude the involvement of significant amounts of old, radiogenically-enriched, continental crust. A limit on the extent of contamination by old continental crust can be estimated by simple two-component mixing between end members with MORB-like and continental crustal characteristics. Calculations using ε_{Nd} of +10 and 10 ppm to represent the juvenile end-member and ε_{Nd} of -15 and 30 ppm for old crustal material (DePaolo et al., 1991) suggest that amount of old crustal material in the host terranes averaged ~10%. The pre-96 Ma pluton samples represent parts of the Late Triassic and Early Cretaceous arc sequences, and their initial ε_{Nd} values are only slightly lower than the depleted mantle at 96 Ma. In the case of the Dumbell Gneiss, its depleted mantle model age (ca. 260 Ma) is similar to its U-Pb crystallization age (ca. 220 Ma). These observations suggest that the pre-96 Ma plutons were derived from sources that had a short crustal residence time. This interpretation of the Nd results is the same as the interpretation of Nd data from similarly-aged samples of the southern Coast Plutonic Complex (Cui and Russell, 1995; Friedman et al., 1995). The southern Coast Plutonic Complex samples have initial ε_{Nd} values that range from +2.4 to +8.0, and 80% of the samples fall between +4 and +8 (Fig. 4).

The Napeequa Complex also has positive, near depleted mantle values during the mid-Cretaceous. Amphibolite samples yield the highest ε_{Nd} values obtained in this study and support the interpretation that the Napeequa Complex is predominantly an oceanic unit (Brown et al., 1994; Miller et al., 1993; Tabor et al., 1989; Tabor et al., 1987b). The Complex has been interpreted to have formed in an accretionary wedge because of the tectonic interleaving of units (Brown et al., 1994; Miller et al., 1993; Tabor et al., 1989;

Tabor et al., 1987b). If a clastic component was present in the accretionary wedge, the Nd data suggest that it was derived from isotopically juvenile crust, not evolved continental crust.

The Chiwaukum Schist and Nason Ridge Migmatitic Gneiss display the largest range of ε_{Nd} values observed from a given terrane. Amphibolite interlayered with garnet-biotite schist of the Chiwaukum Schist yielded the most positive ε_{Nd} value of this group, and these results are similar to those obtained by Magloughlin (1993). High ε_{Nd} values and its MORB-type geochemical signature are consistent with an oceanic derivation of the amphibolite (Magloughlin, 1993; Metzger and Miller, 1994). Clastic-derived units of the Chiwaukum Schist and Nason Ridge Migmatitic Gneiss yield much lower ε_{Nd} values at 96 Ma than the amphibolite (Table 2; Fig. 3). Two possible end-member sources include sediment derived locally from the Jurassic arc or nearby terranes, and sediment derived from cratonic North America. A local arc source is consistent with geochemical data from the schist (Anderson and Paterson, 1991; Magloughlin, 1993), and a reasonable estimate of the ε_{Nd} values of such sediment is between +5 and +8, the ε_{Nd} values of Early Permian to Middle Jurassic terranes of the southern Coast Belt (Cui and Russell, 1995; Friedman et al., 1995). Sediment derived from cratonic North America may be expected to have ε_{Nd} values of -14 to -22 (Boghossian et al., 1996). Meta-clastic rocks of the Nason terrane have ε_{Nd} values that fall between ε_{Nd} values expected from these two sources, and a reasonable interpretation of the Nason terrane data is that the meta-clastic units were derived from a mixture of both arc and cratonic sources. Additional evidence supporting involvement of a cratonic sedimentary component comes from a potential correlative of the Chiwaukum Schist, the Settler Schist in southern British Columbia, which contains detrital Precambrian zircons (Gabites, 1985) and inherited Precambrian zircons contained within a leucocratic sheet that intrudes the Nason Ridge Migmatitic Gneiss (S. Bowring, unpublished data). However, the fact that ε_{Nd} values from the Nason terrane are only slightly lower than ε_{Nd} values expected from arc-derived sediments suggests that the cratonic component was a relatively minor input.

The Swakane Gneiss forms the most isotopically evolved unit in the Cascades core and the southern Coast Belt with ε_{Nd} values at 73 Ma that are near zero to

moderately negative (Table 2; Fig. 3). As is the case for clastic units of the Nason terrane, the protolith of the Swakane biotite gneiss likely formed as a mixture of arc-derived and craton-derived sediments. The abundance of Precambrian detrital grains (Chapter 1) and lower ε_{Nd} values as compared to the Nason terrane samples indicate that the craton-derived sedimentary component was volumetrically more significant in the Swakane Gneiss than in the Nason terrane. The origin and tectonic affinity of this high-P, meta-supracrustal terrane has been the subject of much recent study (Matzel et al., in review; Paterson et al., 2004; Valley et al., 2003). The recognition that the Swakane Gneiss has a protolith age of ca. 73 Ma indicates that the underthrusting of this isotopically evolved unit to the base of the arc only occurred after the most voluminous mid-Cretaceous magmatism. Several mechanisms have been proposed to explain the rapid burial of the Swakane protolith (Matzel et al., in review). One such model proposes that the protolith of the gneiss was deposited in an accretionary wedge and then subducted beneath the arc. This model predicts that the Swakane Gneiss forms a regionally extensive layer beneath the arc. Other proposed mechanisms infer that the protolith of the gneiss was deposited in a small back-arc or fore-arc basin that was then overthrust during contraction of the arc. In this case, the Swakane Gneiss would only form a laterally restricted section of the Cascades core. The addition of the Swakane Gneiss to the crustal architecture of the North Cascades and its effect on the ε_{Nd} signatures of plutons that intrude the Cascades core are discussed in the following section.

Plutons

Variations in the Nd data from the plutons can be explained by two end-member models: 1) the Nd signatures are inherited from crustal sources with different ε_{Nd} values, or 2) the Nd signatures result from mixing between varying volumes of crust versus mantle melt. In all likelihood these processes do not operate independently of one another, and the relative effects of each are difficult to separate. In the case of the most mafic samples, a mantle source is almost certainly required as melting of a crustal source will produce melts that are tonalitic or more felsic in composition.

The initial ε_{Nd} values of the plutons analyzed in this study overlap those of the terranes they intrude during the mid-Cretaceous (Fig. 4). We could hypothesize that the Nd signatures of the plutons resulted from mixing of very small volumes of melt derived from Precambrian continental crust with mantle-derived mafic melt; however this hypothesis is unlikely to result in the large volumes of tonalitic magma present in the Cascades core. In addition, there is little evidence for inheritance of Precambrian zircon in any of these plutons. A much more reasonable explanation for the range of initial ε_{Nd} values observed from the North Cascades plutons is that these plutons were derived from melts of the isotopically juvenile arc terranes with input from the depleted mantle reservoir.

This interpretation of the Nd data is supported by geochemical studies from these plutons. Mafic complexes, sheets and enclaves found in the Group I and II plutons have the geochemical signature of mantle-derived, high-alumina basalts that evolved to water-rich hornblende-bearing magmas at the base of the crust and into the lower and middle crust (Dawes, 1993; DeBari et al., 1998). The geochemistry of the tonalite cannot be explained by simple fractional crystallization from basalt, but rather can be explained by mixing of a mafic, mantle-derived component and silicic (trondhjemitic to tonalitic) melt of a garnet bearing mafic source (Dawes, 1993; DeBari et al., 1998; Miller et al., 2000). The crustal source must have contained residual garnet because the REE patterns of the tonalite shows strong LREE enrichment and HREE depletion (DeBari et al., 1998; Miller et al., 2000). DeBari et al. (1998) estimated that this crustal melting occurred near the base of an overthickened crustal section at pressures of 15-17 kbar. Granodioritic plutons that comprise the Group III plutons are composed predominantly of crustal melt that also was derived from a garnet-bearing source (Dawes, 1993). These plutons have high $\delta^{18}O$ (White et al., 1988) and are thought to have been derived from metamorphosed equivalents of either a plagioclase- and lithic-rich greywacke or altered basalt or both (Dawes, 1993). Although mafic compositions do not comprise a significant proportion of the Group III plutons, the involvement of mafic magmas is inferred from the presence of mafic enclaves, and these mafic magmas likely supplied the heat necessary to generate crustal melts.

Mixing between crustal and mantle-derived melts is clearly indicated by the geochemistry, but variations in the Nd isotopic signature of the plutons appear to be dominated by the ε_{Nd} value of the crustal component. Evidence for this interpretation comes from an examination of pairs of gabbro and contemporaneous tonalite samples from individual plutons (Fig. 5). For example, gabbro and tonalite from the ca. 91 Ma phases of the Mount Stuart batholith have initial ε_{Nd} values of +3.8 and +3.6, respectively, and diorite and tonalite from the ca. 96 Ma phases have initial ε_{Nd} values of +3.6 and +2.0, respectively. This relationship is also observed from gabbro-tonalite pairs from the Tenpeak pluton and Black Peak batholith. These gabbro-tonalite pairs indicate that the mixing that produces the entire range of compositions observed in a pluton results in no more than a 1.6 epsilon unit difference in the ε_{Nd} values of the end-members of individual plutons. The crustal Nd signature also appears to dominate the ε_{Nd} values of the Group II plutons. A sample of the Riddle Peaks gabbro has an initial ε_{Nd} value of +4.9 whereas two samples of tonalite from the coeval Cardinal Peak pluton (Cater, 1982; McPeek et al., 2002; Parent, 1999) have initial ε_{Nd} values of +4.0 and +3.8.

The fact that gabbro from each suite of plutons has initial ε_{Nd} values that are significantly lower than the depleted mantle indicates that these mafic magmas must contain a component of crustal melt, but this component must be volumetrically minor in order to maintain its mafic composition. Mantle melt typically has a low Nd concentration when compared to crustal melt because of the incompatibility of REEs in typical mantle minerals. The comparatively high Nd concentration of the crustal melt may have overwhelmed the Nd budget of the mantle-derived melt exerting a leveraging effect on the overall Nd signature of the gabbro. When comparing gabbro-tonalite associations from different plutons, ε_{Nd} signatures from a given pluton do not overlap other gabbro-tonalite pairs even though these pairs are compositionally similar (Fig. 5). I would infer from this relationship that the Nd signature of a given pluton, even the most mafic component, is controlled by local variations in the Nd signature of its crustal component.

Of the crustal terranes that we have Nd data from in the Cascades core, the Napeequa Complex and potentially the deepest structural levels of the Chiwaukum Schist/Nason Ridge Migmatitic Gneiss have P-T-t estimates that indicate that these rocks

were deep within the crust during the time period when the bulk of the arc magmatism took place (Valley et al., 2003). More importantly, these units have more evolved end-members than the pre-96 Ma arc terranes, and if melts of the Napeequa Complex and Nason terrane were mixed with a depleted mantle melt, this mixing would result in the Nd signatures that we observe in the arc plutons. Both the Napeequa Complex and Nason Ridge Migmatitic Gneiss contain small-scale leucosomes produced by in situ melting of biotite schists and abundant sheets of tonalitic magma making up an estimated 30% of the outcrop area (Miller and Paterson, 2001). The ultimate source of the tonalitic sheets is not known, but a reasonable explanation is that they are derived from somewhat deeper levels of the terranes or other unexposed juvenile terranes.

If we examine the Nd signatures of plutons from the Chelan block, an interesting pattern emerges. The intitial ε_{Nd} values of plutons in each age group systematically decrease with time (Fig. 4). The exceptions to this trend are samples from Group III that intrude the Ross Lake fault zone on the eastern edge of the Cascades core. Once again, the fact that mixing between mantle-derived mafic melt and crustal melt produces less than a 1.6 epsilon unit difference in ε_{Nd} values between end-members of a given pluton (Fig. 5) suggests that the ~5 epsilon unit trend in ε_{Nd} values from the Chelan block plutons is more likely produced by variations in the Nd signature of the crustal source. This interpretation implies that an increase or decrease in the input of mantle melts is not resolvable in the data. It also suggests that crustal melts produced to the east of the Ross Lake fault zone have a distinctly different crustal source than those inside the Cascades core.

The interpretation that the decreasing ε_{Nd} trend of the Chelan block plutons results from changes in the Nd signature of the crustal component leads to the interesting possibility that deep burial of the Swakane Gneiss, the most isotopically-evolved terrane in the Cascades core, may have influenced the evolution of the Nd signatures of Group III plutons. One tectonic model proposed to account for rapid burial of the Swakane Gneiss involves underthrusting of sediments beneath the arc during shallow, low-angle subduction (c.f. Chapter 1). If this model is correct, then the Swakane Gneiss would form a regionally extensive layer beneath the Cascades core. Could underplating of the gneiss after the intrusion of the Group II plutons be responsible the low initial ε_{Nd} values

of the Group III plutons? Nd data from Wenatchee block plutons suggest that these special circumstances are not required. Group I plutons from the Wenatchee block show the entire range of ε_{Nd} values that are observed in the Chelan block. This suggests that whatever crustal source melted to form the group III plutons in the Chelan block also underlay the Wenatchee block prior to 96 Ma and likely contributed to the oldest Wenatchee block plutons.

The process that caused a shift to melting of different crustal sources in the Chelan block over time is unclear. Continued convergence during the Cretaceous almost certainly modified the crustal architecture of the North Cascades, and this modification may have caused a change in the sources available for melting. The Wenatchee Block was exhumed to mid to upper crustal levels before the emplacement of Group II plutons, and thus occupied a higher structural position during Group II and Group III magmatism. As crustal magmatism continued over the life of the arc, the fertility of different crustal sources would also be expected to evolve.

Based on the Nd data obtained in this study, several parallels may be drawn between the Cascades core and the Coast Plutonic Complex (CPC). In the southern CPC, most plutons are Late Jurassic to Late Cretaceous in age (ca. 100-180 Ma), and have initial ε_{Nd} values that are similar to the pre-96 Ma plutons of the North Cascades (Cui and Russell, 1995; Friedman et al., 1995). The southern CPC exhibits a relatively restricted range of initial ε_{Nd} values from +2.4 to +8.0 with ~80% of the samples between +4 and +8 (Fig. 4) (Cui and Russell, 1995; Friedman et al., 1995). These high, positive initial ε_{Nd} values, which overlap the ε_{Nd} values of the terranes that the southern CPC intrudes (Samson et al., 1989; Samson et al., 1990), indicate that the southern CPC samples were not significantly contaminated by old, isotopically-evolved, continental material (Cui and Russell, 1995; Friedman et al., 1995). Like the petrogenetic models presented here for the generation of the Cascades core plutons, models for the formation of the southern CPC involve mixing of mantle melt with anatectic melt of the isotopically juvenile Alexander, Wrangellia and Stikine terranes (Cui and Russell, 1995; Friedman et al., 1995).

The Nd data from the northern CPC illustrate a distinctly different picture of the evolution of the batholith. Plutons from the northern CPC are typically Late Cretaceous

to Eocene in age (ca. 70-45 Ma) (Gehrels et al., 1991), therefore a direct comparison between the northern CPC and the Group III plutons of the Cascades core can be made. Initial ε_{Nd} values from the northern CPC ~2-7 epsilon units lower than the lowest ε_{Nd} value measured from the Group III plutons and range from -0.2 to -5.4 with crystallization ages between 49 Ma and 68 Ma (Fig. 4) (Arth et al., 1988; Samson et al., 1991). The Alexander, Wrangellia and Stikine terranes have ε_{Nd} values of ~0 to +10 during the Eocene (Samson et al., 1989; Samson et al., 1990), therefore the initial ε_{Nd} values of the plutons are too low for the plutons to have been derived from anatexis of the nearby arc terranes or by mixing of depleted mantle melts with melts of the terranes (Samson et al., 1991). The Nd data from the northern CPC therefore require a component of old, evolved, continental crust in their genesis unlike the Group III plutons from the Cascades Core (Samson et al., 1991). These data are supported by the presence of an inherited, Proterozoic Pb component in zircons from many of the northern CPC plutons (Gehrels et al., 1990). Samson et al. (1991) proposed that the evolved crustal component was likely derived from the Yukon-Tanana terrane in a model where the plutons formed as a delayed result of the underthrusting of the Alexander-Wrangellia terrane beneath the Yukon-Tanana and Stikine terranes during mid-Cretaceous orogenesis.

CONCLUSIONS

The ε_{Nd} values obtained in this study indicate that only a minor component of Precambrian crustal material could have been involved in the genesis of the host terranes and plutons of the North Cascades core. Amphibolites from both the Napeequa Complex and Chiwaukum Schist have near depleted mantle values, suggesting that these terranes have an oceanic affinity. Meta-clastic rocks from the Chiwaukum Schist and Nason Ridge Migmatitic Gneiss have ε_{Nd} values that lie between those of arc-derived and craton-derived sediment reflecting a mixture of these two sources. Initial ε_{Nd} values of the Swakane Gneiss also reflect mixing of craton-derived and arc-derived sources with a relatively more significant component of craton-derived sediments in the Swakane Gneiss than in the Nason terrane samples.

ε_{Nd} values of the plutons that intrude that Cascades core reflect mixing of mantle-derived melt and melt derived by anatexis of isotopically juvenile terranes. Mixing of the

mantle and crustal-derived melts results in less than a 1.6 epsilon unit difference between the compositional end-members of individual plutons. This suggests that the range of initial ε_{Nd} values observed from the plutons is more strongly influenced by local variations in the Nd signatures of the crustal source rather than varying amounts of crustal versus mantle input.

Chelan block plutons show a trend of lower initial ε_{Nd} values with decreasing crystallization age suggesting melting from more evolved crustal sources over the life of the arc. However, plutons that intruded the Wenatchee block exhibit the entire range of ε_{Nd} values observed from plutons in the Chelan block even though the Wenatchee block plutons all intruded during the 96-84 Ma pulse of magmatism. This suggests that the evolution of Nd signatures in the Chelan block plutons may reflect differences in the depth of crustal melting and the availability of more evolved crustal sources. These temporal variations in Nd signatures are also observed between the northern and southern Coast Plutonic Complex, and may reflect changes in crustal melting along the length of the Late Cretaceous to Eocene arc.

REFERENCES

Adams, J. B., 1964, Origin of the Black Peak Quartz Diorite, Northern Cascades, Washington: American Journal of Science, v. 262, p. 290-306.

Anderson, J. L., and Paterson, S. R., 1991, Emplacement of the Cretaceous Mt. Stuart batholith, central Cascades, Washington: Geological Society of America Abstracts with Programs, v. 23, p. A387.

Arth, J. G., Barker, F., and Stern, T. W., 1988, Coast Batholith and Taku plutons near Ketchikan, Alaska; petrography, geochronology, geochemistry, and isotopic character: American Journal of Science, v. 288-A, p. 461-489.

Bendixen, J., 1994, Thermobarometry and structural history of the pelitic Chiwaukum Schist, northern Cascades, Washington [M.S. thesis]: University of Southern California, Los Angeles.

Boghossian, N. D., Patchett, P. J., Ross, G. M., and Gehrels, G. E., 1996, Nd isotopes and the source of sediments in the miogeocline of the Canadian Cordillera: Journal of Geology, v. 104, p. 259-277.

Brown, E. H., Cary, J. A., Dougan, B. E., Dragovich, J. D., Fluke, S. M., and McShane, D. P., 1994, Tectonic evolution of the Cascades crystalline core in the Cascade River area, Washington: Washington Division of Geology and Earth Resources Bulletin, v. 80, p. 93-113.

Brown, E. H., and Walker, N. W., 1993, A magma-loading model for Barrovian metamorphism in the Southeast Coast Plutonic Complex, British Columbia and Washington: Geological Society of America Bulletin, v. 105, p. 479-500.

Cater, F. W., 1982, Intrusive rocks of the Holden and Lucerne quadrangles, Washington: the relation of depth zones, composition, textures, and emplacement of plutons: U. S. Geological Survey Professional Paper, v. 1220, p. 108.

Cater, F. W., and Crowder, D. F., 1967, Geologic map of the Holden Quadrangle, Snohomish and Chelan counties, Washington: U. S. Geological Survey.

Coney, P. J., Jones, D. L., and Monger, J. W. H., 1980, Cordilleran suspect terranes: Nature, v. 288, p. 329-333.

Cui, Y., and Russell, J. K., 1995, Nd-Sr-Pb isotopic studies of the southern Coast Plutonic Complex, southwestern British Columbia: Geological Society of America Bulletin, v. 107, p. 127-138.
Dawes, R. L., 1993, Mid-crustal, Late Cretaceous plutons of the North Cascades: petrogenesis and implications for the growth of continental crust [PhD thesis]: University of Washington, Seattle, 272 p.
DeBari, S. M., Miller, R. B., and Paterson, S. R., 1998, Genesis of tonalitic plutons in the Cretaceous magmatic arc of the North Cascades: mixing of mantle-derived mafic magmas and melts of a garnet-bearing lower crust: Geological Society of America Abstracts with Programs, v. 30, p. 257-258.
Dellinger, D. A., and Hopson, C. A., 1986, Age-depth compositional spectrum through the diapiric Duncan Hill Pluton, North Cascades, Washington: Geological Society of America Abstracts with Programs, v. 18, p. 100-101.
DePaolo, D. J., Linn, A. M., and Schubert, G., 1991, The continental crustal age distribution: methods of determining mantle separation ages from Sm-Nd isotopic data and application to the Southwestern United States: Journal of Geophysical Research, v. 96, p. 2071-2088.
Dragovich, J. D., Cary, J. A., and Brown, E. H., 1989, Stratigraphic and structural relations of the Cascade River schist, North Cascades, Washington: Geological Society of America Abstracts with Programs, v. 21, p. 74.
Dragovich, J. D., and Norman, D. K., 1995, Geologic map of the west half of the Twisp 1:100,000 Quadrangle, Washington, scale 1:100,000.
Evans, B. W., and Berti, J. W., 1986, Revised metamorphic history for the Chiwaukum Schist, North Cascades, Washington: Geology, v. 14, p. 695-698.
Fawcett, T. C., Burmester, R. F., Housen, B. A., and Iriondo, A., 2003, Tectonic implications of magnetic fabrics and remanence in the Cooper Mountain pluton, North Cascade Mountains, Washington: Canadian Journal of Earth Sciences, v. 40, p. 1335-1356.
Friedman, R. M., and Armstrong, R. L., 1995, Jurassic and Cretaceous geochronology of the southern Coast Belt, British Columbia, 49° to 51°N, *in* Miller, D. M., and Busby, C., eds., Jurassic magmatism and tectonics of the North American Cordillera: Boulder, Geological Society of America, p. 95-139.
Friedman, R. M., Mahoney, J. B., and Cui, Y., 1995, Magmatic evolution of the southern Coast Belt: constraints from Nd-Sr isotopic systematics and geochronology of the southern Coast Plutonic Complex: Canadian Journal of Earth Sciences, v. 32, p. 1681-1698.
Gabites, J. E., 1985, Geology and geochronometry of the Cogburn Creek-settler Creek area, northeast of Harrison Lake, B.C. [MS thesis]: University of British Columbia, Vancouver, 153 p.
Gehrels, G. E., McClelland, W. C., Samson, S. D., Patchett, P. J., and Brew, D. A., 1991, U-Pb geochronology of Late Cretaceous and Early Tertiary plutons in the northern Coast Mountains Batholith: Canadian Journal of Earth Sciences, v. 28, p. 899-911.
Gehrels, G. E., McClelland, W. C., Samson, S. D., Patchett, P. J., and Jackson, J. L., 1990, Ancient continental margin assemblage in the northern Coast Mountains, southeast Alaska and northwest Canada: Geology, v. 18, p. 208-211.
Haugerud, R. A., Vanderheyden, P., Tabor, R. W., Stacey, J. S., and Zartman, R. E., 1991, Late Cretaceous and Early Tertiary plutonism and deformation in the Skagit Gneiss Complex, North Cascade Range, Washington and British Columbia: Geological Society of America Bulletin, v. 103, p. 1297-1307.
Hopson, C. A., and Mattinson, J. M., 1994, Chelan Migmatite Complex, Washington: Field evidence for mafic magmatism, crustal anatexis, mixing and protodiapiric emplacment, *in* Swanson, D. A., and Haugerud, R. A., eds., Geologic Field Trips in the Pacific Northwest: Boulder, Geological Society of America, p. 2K-1 - 2K-21.
Hurlow, H. A., 1992, Structural and U/Pb geochronologic studies of the Pasayten Fault, Okanogan Range Batholith, and southeastern Cascades crystalline core, Washington [PhD thesis]: University of Washington, Seattle, 180 p.
Hurlow, H. A., and Nelson, B. K., 1993, U-Pb zircon and monazite ages for the Okanogan Range Batholith, Washington: Implications for the magmatic and tectonic evolution of the southern Canadian and northern United States Cordillera: Geological Society of America Bulletin, v. 105, p. 231-240.

Magloughlin, J. F., 1986, Metamorphic petrology, structural history, geochronology, tectonics and geothermometry/geobarometry in the Wenatchee Ridge area, North Cascades, Washington [MS thesis]: University of Washington, Seattle, 343 p.

Magloughlin, J. F., 1993, A Nason Terrane trilogy: I, Nature and significance of pseudotachylyte: II, Summary of the structural and tectonic history: III, Major and trace element geochemistry and strontium and neodymium isotope geochemistry of the Chiwaukum Schist, amphibolite, and meta-tonalite gneiss of the Nason Terrane [PhD thesis]: University of Minnesota, Minneapolis, 325 p.

Mattinson, J. M., 1972, Ages of zircons from the Northern Cascade Mountains, Washington: Geological Society of America Bulletin, v. 83, p. 3769-3783.

Matzel, J., Bowring, S. A., and Miller, R. B., 2002, Timescales of pluton construction and the crystallization history of the Mt Stuart Batholith, North Cascades, WA: EOS, Transactions of the American Geophysical Union, Fall Meeting Supplement, v. 83, p. T11E-09.

Matzel, J., Bowring, S. A., and Miller, R. B., in review, Reassessing tectonic models for the assembly of the North Cascades arc, WA, in light of a Late Cretaceous protolith age of the Swakane Gneiss: Tectonics.

McPeek, S. L., Miller, R. B., Miller, J. S., and Matzel, J. P., 2002, Significance of fabric development in the gabbroic Riddle Peaks Pluton, North Cascades, Washington: Geological Society of America Abstracts with Programs, v. 34, p. 96.

Metzger, E. P., and Miller, R. B., 1994, Trace element geochemistry of mafic igneous rocks from the Ingalls ophiolite complex, Washington: tectonic implications: Geological Society of America Abstracts with Programs, v. 26, p. 188-189.

Miller, R. B., 1985, The Ophiolitic Ingalls Complex, North Central Cascade Mountains, Washington: Geological Society of America Bulletin, v. 96, p. 27-42.

Miller, R. B., and Bowring, S. A., 1990, Structure and chronology of the Oval Peak batholith and adjacent rocks: Implications for the Ross Lake fault zone, North Cascades, Washington: Geological Society of America Bulletin, v. 102, p. 1361-1377.

Miller, R. B., Bowring, S. A., and Hoppe, W. J., 1988, New evidence for extensive Paleogene plutonism and metamorphism in the crystalline core of the North Cascades: Geological Society of America Abstracts with Programs, v. 20, p. 432-433.

Miller, R. B., Bowring, S. A., and Hoppe, W. J., 1989, Paleocene plutonism and its tectonic implications, North Cascades, Washington: Geology, v. 17, p. 846-849.

Miller, R. B., Haugerud, R. A., Bowring, S. A., Dragovich, J. D., McClelland, W. C., Raviola, F. P., and Matzel, J., in review, A synthesis of the Ross Lake fault system and its implications for the Baja British Columbia model.

Miller, R. B., Haugerud, R. A., Murphy, F., and Nicholson, L. S., 1994, Tectonostratigraphic framework of the northeastern Cascades: Washington Division of Geology and Earth Resources Bulletin, v. 80, p. 73-92.

Miller, R. B., Matzel, J. P., Paterson, S. R., and Stowell, H., 2003, Cretaceous to Paleogene Cascades Arc: Structure, metamorphism, and timescales of magmatism, burial, and exhumation of a crustal section, *in* Swanson, T. W., ed., Western Cordillera and Adjacent Areas: Boulder, Colorado, Geological Society of America, p. 107-135.

Miller, R. B., and Paterson, S. R., 1992, Tectonic implications of syn-emplacement and postemplacement deformation of the Mount Stuart batholith for mid-Cretaceous orogenesis in the North Cascades: Canadian Journal of Earth Sciences, v. 29, p. 479-485.

Miller, R. B., and Paterson, S. R., 2001, Influence of lithological heterogeneity, mechanical anisotropy, and magmatism on the rheology of an arc, North Cascades, Washington: Tectonophysics, v. 342, p. 351-370.

Miller, R. B., Paterson, S. R., DeBari, S. M., and Whitney, D. L., 2000, North Cascades Cretaceous crustal section: changing kinematics, rheology, metamorphism, pluton emplacement and petrogenesis from 0 to 40 km depth, *in* Woodsworth, G. J., Jackson, J. L. E., Nelson, J. L., and Ward, B. C., eds., Guidebook for geological field trips in southwestern British Columbia and northern Washington: Vancouver, Geological Association of Canada, p. 229-278.

Miller, R. B., Whitney, D. L., and Geary, E. E., 1993, Tectonostratigraphic terranes and the metamorphic history of the northeastern part of the crystalline core of the North Cascades: Evidence from the Twisp Valley Schist: Canadian Journal of Earth Sciences, v. 30, p. 1306-1323.

Misch, P., 1966, Tectonic evolution of the Northern Cascades of Washington State: a west-cordilleran case history: Canadian Institute of Mining and Metallurgy, v. Special volume 8, p. 101-148.
Misch, P., 1977, Dextral displacements at some major strike faults in the North Cascades: Geological Association of Canada Abstracts with Programs, v. 2, p. 37.
Monger, J. W. H., 1991, Correlation of Settler Schist with Darrington Phyllite and Shuksan Greenschist and its tectonic implications, Coast and Cascade mountains, British Columbia and Washington: Canadian Journal of Earth Sciences, v. 28, p. 447-458.
Monger, J. W. H., Price, R. A., and Tempelman-Kluit, D. J., 1982, Tectonic accretion and the origin of the two major metamorphic and plutonic welts in the Canadian Cordillera: Geology, v. 10, p. 70-75.
Parent, L. A., 1999, Petrology and petrogenesis of the Cardinal Peak pluton, North Cascades Washington [M.S. thesis]: San Jose State University, San Jose, California, 119 p.
Patchett, P. J., and Gehrels, G. E., 1998, Continental influence on Canadian Cordilleran terranes from Nd isotopic study, and significance for crustal growth processes: Journal of Geology, v. 106, p. 269-280.
Paterson, S. R., Miller, R. B., Alsleben, H., Whitney, D. L., Valley, P. M., and Hurlow, H., 2004, Driving mechanisms for >40 km of exhumation during contraction and extension in a continental arc, Cascades core, Washington: Tectonics, v. 23, p. 10.1029/2002TC001440.
Petro, G. T., Housen, B. A., and Iriondo, A., 2002, Tectonic significance of paleomagnetism of the Eocene Golden Horn Batholith: Geological Society of America Abstracts with Programs, v. 34, p. 96.
Rusmore, M. E., 1987, Geology of the Cadwallader Group and the Intermontane-Insular superterrane boundary, southwestern British Columbia: Canadian Journal of Earth Sciences, v. 24, p. 2279-2291.
Rusmore, M. E., and Woodsworth, G. J., 1991, Coast Plutonic Complex: a mid-Cretaceous contractional orogen: Geology, v. 19, p. 941-944.
Samson, S. D., McClelland, W. C., Patchett, P. J., Gehrels, G. E., and Anderson, R. G., 1989, Evidence from neodymium isotopes for mantle contributions to Phanerozoic crustal genesis in the Canadian Cordillera: Nature, v. 337, p. 705-709.
Samson, S. D., Patchett, J. P., Gehrels, G. E., and Anderson, R. G., 1990, Nd and Sr isotopic characterization of the Wrangellia terrane and implications for crustal growth of the Canadian Cordillera: Journal of Geology, v. 98, p. 749-762.
Samson, S. D., Patchett, P. J., McClelland, W. C., and Gehrels, G. E., 1991, Nd and Sr isotopic constraints on the petrogenesis of the west side of the northern Coast Mountains Batholith, Alaskan and Canadian Cordillera: Canadian Journal of Earth Sciences, v. 28, p. 939-946.
Sawyko, L. T., III, 1994, The geology and petrology of the Swakane biotite gneiss, North Cascades, Washington [M.S. thesis]: University of Washington, Seattle, 134 p.
Tabor, R. W., Booth, D. B., Vance, J. A., Ford, A. B., and Ort, M. H., 1988, Preliminary geologic map of the Sauk River 30 by 60 minute Quadrangle, Washington: U. S. Geological Survey, 0196-1497.
Tabor, R. W., Frizzell, V. A., Jr., Whetten, J. T., Waitt, R. B., Jr., Swanson, D. A., Byerly, G. R., Booth, D. B., Hetherington, M. J., and Zartman, R. E., 1987a, Geologic map of the Chelan 30' by 60' Quadrangle, Washington: U. S. Geological Survey, scale 1:100,000.
Tabor, R. W., Haugerud, R. A., Brown, E. H., Babcock, R. S., and Miller, R. B., 1989, Accreted Terranes of the North Cascades Range, Washington, International Geologic Congress Trip T307: Washington, D.C., American Geophysical Union, 62 p.
Tabor, R. W., Zartman, R. E., and Frizzell, V. A., Jr., 1987b, Possible tectonostratigraphic terranes in the North Cascades crystalline core, Washington, *in* Schuster, J. E., ed., Selected Papers on the Geology of Washington: Anaheim, CA, United States, Washington Division of Geology and Earth Resources, p. 107-127.
Valley, P. M., Whitney, D. L., Paterson, S. R., Miller, R. B., and Alsleben, H., 2003, Metamorphism of the deepest exposed arc rocks in the Cretaceous to Paleogene Cascades belt, Washington: evidence for large- scale vertical motion in a continental arc: Journal of Metamorphic Geology, v. 21, p. 203-220.
van der Heyden, P., 1992, A Middle Jurassic to early Tertiary Andean-Sierran arc model for the Coast Belt of British Columbia: Tectonics, v. 11, p. 82-97.
Van der Heyden, P. A. H., 1989, U-Pb and K-Ar geochronometry of the Coast plutonic complex, 53°N to 54°N, British Columbia, and implications for the Insular-Intermontane superterrane boundary [PhD thesis]: The University of British Columbia, Vancouver.

Van Diver, B. B., 1967, Contemporaneous faulting-metamorphism in Wenatchee Ridge area, Northern Cascades, Washington: American Journal of Science, v. 265, p. 132-150.

Walker, N. W., and Brown, E. H., 1991, Is the southeast Coast Plutonic Complex the consequence of accretion of the Insular Superterrane: Evidence from U-Pb zircon geochronometry in the Northern Washington Cascades: Geology, v. 19, p. 714-717.

Waters, A. C., 1932, A petrologic and structural study of the Swakane Gneiss, Entiat Mountains, Washington: Journal of Geology, v. 40, p. 604-633.

White, L. D., Maley, C. A., Barnes, I., and Ford, A. B., 1988, Oxygen isotopic data for plutonic rocks and gneisses of the Glacier Peak Wilderness and vicinity, northern Cascades, Washington, 0196-1497.

Woodsworth, G. W., Anderson, R. G., and Armstrong, R. L., 1991, Plutonic regimes, *in* Gabrielse, H., and Yorath, C. J., eds., Geology of the Cordilleran Orogen in Canada, Geological Survey of Canada, p. 491-531.

Zen, E.-a., and Hammarstrom, J. M., 1984, Magmatic epidote and its petrologic significance: Geology, v. 12, p. 515-518.

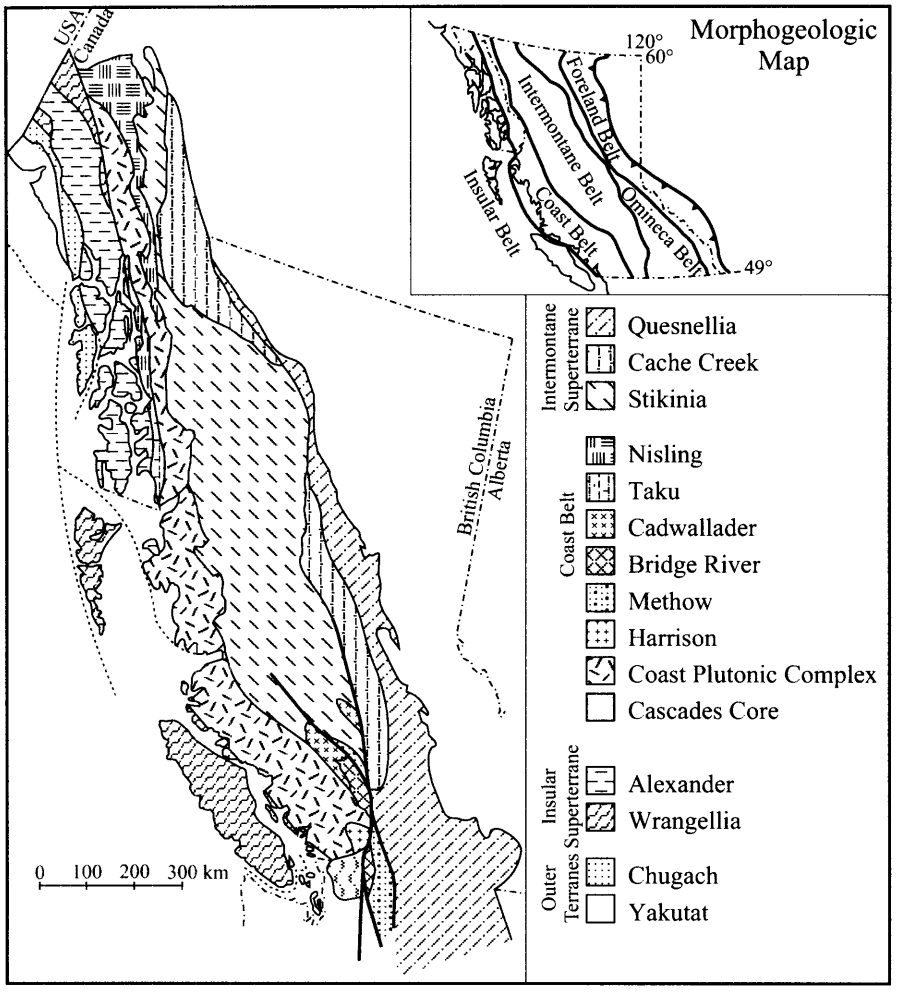

Figure 1. Simplified terrane map of the northwestern North American Cordillera after Friedman et al. (1995) and Mahoney et al., (1995). Inset shows the five physiographic provinces of the Canadian Cordillera.

Figure 2. Simplified geologic map of the Cascades core after Haugerud et al., (1991), Brown and Walker (1993) and Hopson and Mattinson (1994). Plutons are shown in a random dashed pattern. The largest dashes denote ca. 96-88 Ma plutons; intermediate dashes denote ca. 79-65 Ma plutons; and the smallest dashes denote ca. 50-46 Ma plutons. Early Cretaceous plutons adjacent to the eastern margin of the core are filled with a plus sign pattern. Sample localities are represented by red dots numbered according to table 1. Heavy lines represent faults whereas light lines represent depositional or intrusive contacts. Abbreviations are as follows: A, Alma Creek pluton; ALC, Alta Lake Complex; BL, Bench Lake pluton; BP, Black Peak pluton; BR, Bearcat Ridge pluton; CL, Cyclone Lake pluton; CPB, Cloudy Pass batholith; MB, Mount Buckindy pluton; CV, Chaval pluton; CO, Cooper Mountain batholith; CP, Cardinal Peak pluton; DC, Downey Creek intrusion; DD, Dinkelman Detachment; DF, Dirtyface pluton; DH, Duncan Hill pluton; EN, Entiat intrusive suite; EL, Eldorado pluton; GH, Golden Horn pluton; H, Haystack pluton; HL, Hidden Lake pluton; JL, Jordan Lake pluton; MC, Marble Creek pluton; MSB, Mount Stuart batholith; MG, Methow Gneiss; NRG, Nason Ridge Migmatitic Gneiss; OP, Oval Peak pluton; RC, Railroad Creek pluton; RP, Riddle Peaks pluton; SC, Sloan Creek pluton; SFJ, Seven-Fingered Jack intrusive suite; SM, Sulphur Mountain pluton; TP, Tenpeak pluton; WRG, Wenatchee Ridge Gneiss; and WRSZ, White River shear zone.

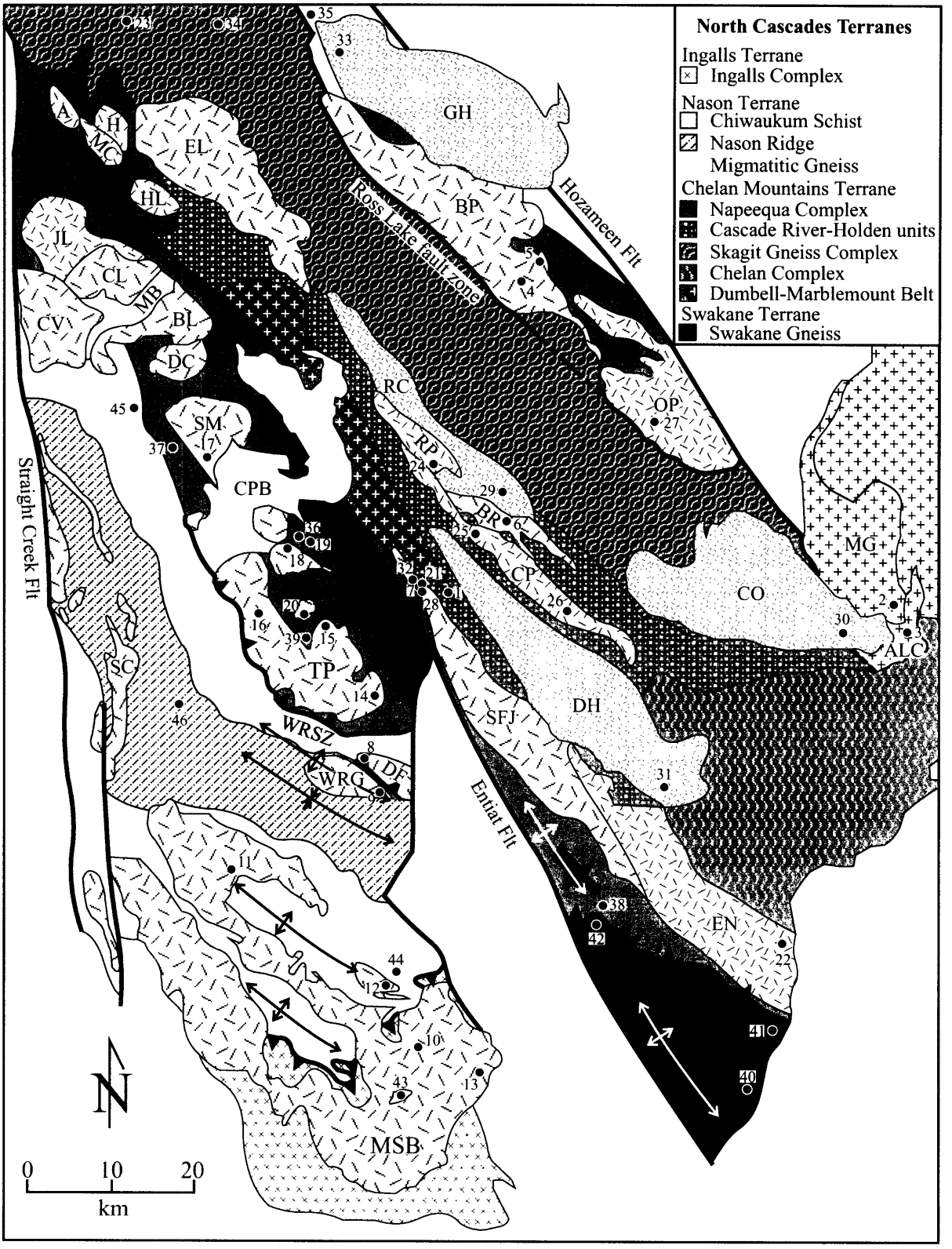

Figure 2. Caption on opposite page

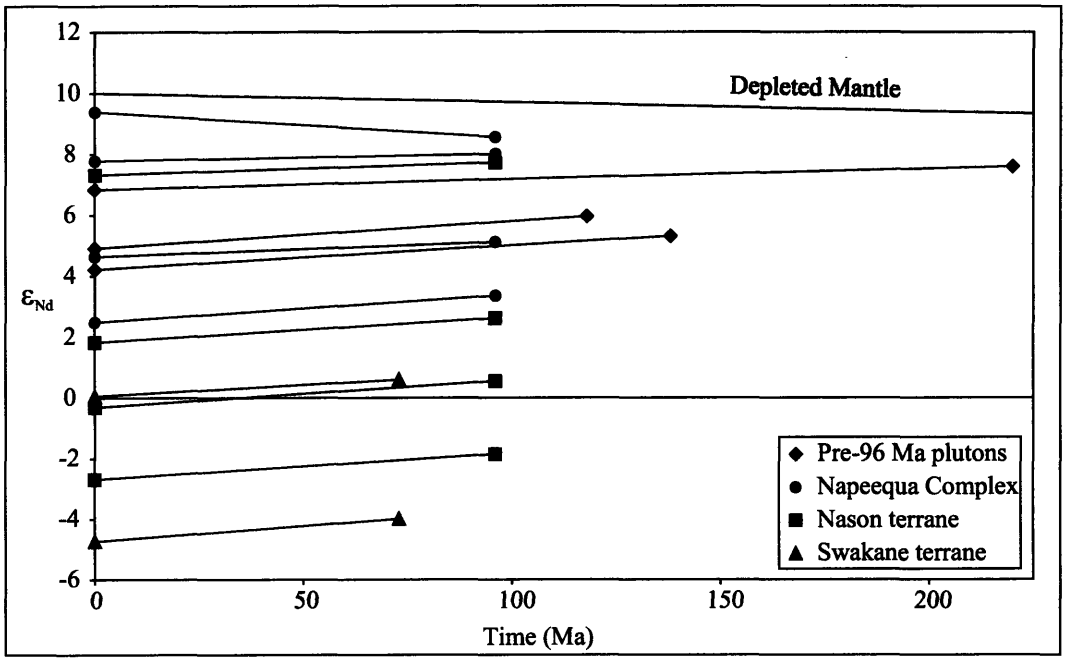

Figure 3. ε_{Nd} values from samples of metamorphic host terranes versus time.

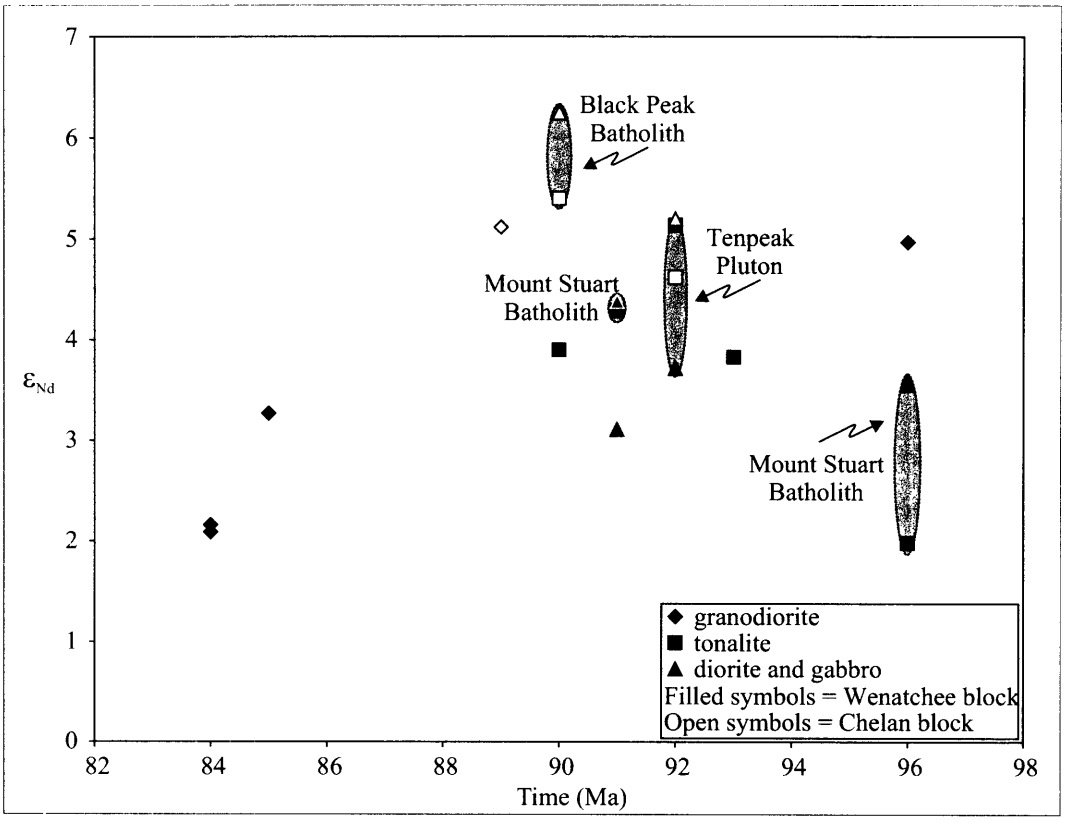

Figure 5. Compositional variation in ε_{Nd} values of Group I plutons.

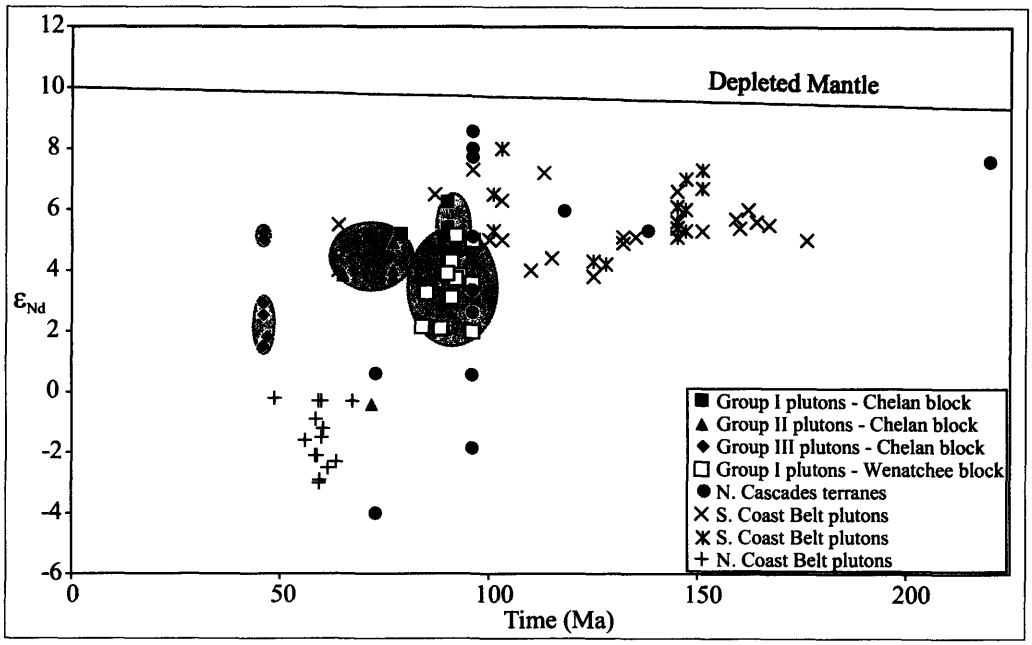

Figure 4. ε_{Nd} values from all samples in this study compared to ε_{Nd} values from other Coast Belt plutons (data from Cui and Russell, 1995; Friedman et al., 1995; Samson et al., 1991). Shaded regions represent clusters of Group I, Group II, and Group III plutons.

Table 1. Sample, rock type, location and age.

	ID	Sample	Pluton/Unit	Rock Type	Age (Ma)	Reference
>96 Ma plutons	1	DB1	Dumbell Gneiss	Tonalite gneiss	220	Mattinson, 1972
	2	MT1	Methow Gneiss	Granitic gneiss	118	Miller et al., in review
	3	AL1	Alta Lake Complex	Trondhjemite	138	Miller et al., in review
Group I Plutons	4	SCP	Black Peak	Tonalite	90	Miller et al., in review
	5	MAF	Black Peak	Gabbro	90	Miller et al., in review
	6	LU-13-1	Bearcat Ridge	Tonalite	89	Miller et al., in review
	7	EN42	Entiat	Tonalite	92	Chapter 5
	8	DF1	Dirtyface	Diorite	91	Hurlow, 1992
	9	WRO2	Wenatchee Ridge	Trondhjemite	93	Matzel, unpub. data
	10	MS2	Mount Stuart	Gabbro	91	Chapter 4
	11	MS5	Mount Stuart	Tonalite	96	Chapter 4
	12	MS17C	Mount Stuart	Diorite	96	Chapter 4
	13	MS31	Mount Stuart	Tonalite	91	Chapter 4
	14	TP11	Tenpeak	Tonalite	92	Chapter 4
	15	TP30	Tenpeak	Diorite	92	Chapter 4
	16	TP-524-1	Tenpeak	Tonalite	90	Chapter 4
	17	SP3	Sulphur Mtn	Granodiorite	96	Walker and Brown, 1991
	18	HP1	High Pass	Granodiorite	88	Matzel, unpub. data
	19	BC1	Buck Creek	Granodiorite	84	Hurlow, 1992
	20	CM1	Clark Mtn	Granodiorite	85	Walker, unpub.data
Group II Plutons	21	EN41	Entiat	Gabbro	79	Chapter 5
	22	EN23	Entiat	Tonalite	73	Chapter 5
	23	NHO1	Newhalem Orthogneiss	Tonalite	65	Haugerud et al., 1991
	24	Ho-64-1	Riddle Peaks	Gabbro	77	McPeek et al., 2002
	25	PI-110-2	Cardinal Peak	Tonalite	77	McPeek et al., 2002
	26	PM-165-1	Cardinal Peak	Tonalite	77	McPeek et al., 2002
	27	OP-D	Oval Peak	Tonalite	65	Miller and Bowring, 1990
Group III Plutons	28	LLP	Larch Lakes	Granodiorite	47	Bowring, unpub. data
	29	RC1	Railroad Creek	Granodiorite	46	Bowring, unpub. data
	30	CMB	Cooper Mtn	Granodiorite	48	Fawcett et al., 2003
	31	DH5	Duncan Hill	Granodiorite	46	Dellinger and Hopson, 1986
	32	RM1	Rampart Mountain	Granodiorite	47	Cater, 1982
	33	GH1	Golden Horn	Granite	47	Petro et al., 2002
	34	NC19-1	Leucogranite Dike	Granite	46	Haugerud et al., 1991
	35	NC22-1	Ruby Creek Belt	Trondhjemite	48	Miller et al., 1988
Metamorphic Terranes	36	NQ2	Napeequa	Amphibolite	Jurassic?	Tabor et al., 1989
	37	NQ19	Napeequa	Amphibolite	Jurassic?	Tabor et al., 1989
	38	NQ21	Napeequa	Amphibolite	Jurassic?	Tabor et al., 1989
	39	NQ31	Napeequa	Biotite schist	Jurassic?	Tabor et al., 1989
	40	SW3B	Swakane	Biotite gneiss	73	Chapter 1
	41	SW4	Swakane	Biotite gneiss	73	Chapter 1
	42	SW8	Swakane	Biotite gneiss	73	Chapter 1
	43	CW13	Chiwaukum	Garnet-biotite schist	Jurassic?	Miller et al., 2003
	44	CW19	Chiwaukum	Amphibolite	Jurassic?	Miller et al., 2003
	45	CW24	Chiwaukum	Garnet-biotite schist	Jurassic?	Miller et al., 2003
	46	BG2B	Nason Ridge Gneiss	Garnet-biotite gneiss	Jurassic?	Miller et al., 2003

Table 2. Sm-Nd isotopic data.

	ID	Sample No.	Sm (ppm)*	Nd (ppm)*	$\frac{^{147}Sm^{\dagger}}{^{144}Nd}$	$\frac{^{143}Nd^{\ddagger}}{^{144}Nd}$		$\varepsilon_{Nd(0)}^{\#}$	$\varepsilon_{Nd(t)}^{\#}$	T_{DM} (Ma)$^{\&}$
>96 Ma plutons	1	DB1	2.71	9.62	0.1700	0.512989	±3	6.84	7.60	261
	2	MT1	2.33	11.09	0.1269	0.512890	±4	4.91	5.96	303
	3	AL1	1.50	6.70	0.1351	0.512854	±4	4.22	5.31	397
Group I plutons	4	SCP	2.05	11.34	0.1094	0.512863	±3	4.39	5.40	292
	5	MAF	2.60	10.85	0.1448	0.512928	±3	5.66	6.25	298
	6	LU-13-1	3.17	20.55	0.0932	0.512840	±2	3.95	5.12	282
	7	EN41	2.35	6.81	0.2087	0.512912	±4	5.34	5.20	-
	8	EN42	2.91	11.95	0.1475	0.512845	±4	4.04	4.62	487
	9	DF1	2.97	11.93	0.1505	0.512770	±3	2.57	3.11	679
	10	WRO2	8.02	42.43	0.1142	0.512784	±4	2.85	3.83	421
	11	MS2	2.89	12.04	0.1450	0.512832	±4	3.78	4.38	498
	12	MS5	2.41	12.63	0.1153	0.512688	±4	0.98	1.98	567
	13	MS17C	2.72	11.12	0.1478	0.512790	±3	2.96	3.56	609
	14	MS31	2.58	11.55	0.1348	0.512821	±3	3.57	4.29	457
	15	TP11	1.85	9.59	0.1164	0.512853	±4	4.2	5.14	327
	16	TP30	3.67	17.90	0.1240	0.512785	±4	2.87	3.72	463
	17	TP-524-1	4.25	23.64	0.1087	0.512786	±4	2.88	3.90	397
	18	SP3	4.32	20.90	0.1251	0.512848	±3	4.09	4.97	366
	19	HP1	2.38	14.30	0.1005	0.512692	±4	1.06	2.09	491
	20	BC1	5.32	28.72	0.1120	0.512702	±3	1.25	2.16	530
	21	CM1	4.12	22.68	0.1098	0.512757	±3	2.33	3.27	441
Group II plutons	22	EN23	2.96	14.73	0.1214	0.512582	±3	-1.1	-0.41	772
	23	NHO1	4.39	17.67	0.1501	0.512815	±4	3.45	3.84	573
	24	Ho-64-1	3.79	12.39	0.1847	0.512885	±3	4.81	4.93	854
	25	PI-110-2	3.72	18.13	0.1240	0.512797	±4	3.1	3.82	443
	26	PM-165-1	4.56	24.06	0.1145	0.512803	±3	3.22	4.03	394
	27	OP-D	2.88	15.22	0.1146	0.512804	±3	3.23	3.92	393
Group III plutons	28	LLP	2.73	12.91	0.1280	0.512710	±4	1.41	1.82	610
	29	RC1	4.63	25.26	0.1108	0.512762	±3	2.42	2.92	439
	30	CMB	4.12	22.11	0.1126	0.512690	±3	1.02	1.51	550
	31	DH5	4.36	23.25	0.1133	0.512742	±3	2.04	2.53	478
	32	RM1	3.15	15.26	0.1248	0.512747	±4	2.12	2.54	529
	33	GH1	5.93	32.23	0.1113	0.512881	±3	4.73	5.23	272
	34	NC19-1	4.97	21.74	0.1382	0.512878	±3	4.69	5.03	367
	35	NC22-1	1.00	4.50	0.1342	0.512877	±4	4.67	5.04	351
Metamorphic Terranes	36	NQ2	6.27	21.22	0.1786	0.513037	±3	7.78	8.00	136
	37	NQ19	5.41	20.68	0.1583	0.512876	±3	4.64	5.11	496
	38	NQ21	2.92	6.67	0.2648	0.513119	±4	9.39	8.56	155
	39	NQ31	17.20	82.01	0.1268	0.512766	±3	2.49	3.35	509
	40	SW3B	2.83	14.58	0.1173	0.512325	±3	-6.11	-5.37	1137
	41	SW4	3.88	16.94	0.1385	0.512641	±3	0.06	0.60	825
	42	SW8	9.16	47.64	0.1162	0.512395	±3	-4.74	-3.99	1017
	43	CW13	4.14	19.39	0.1291	0.512500	±3	-2.69	-1.86	982
	44	CW19	4.66	17.12	0.1646	0.513013	±3	7.32	7.72	167
	45	CW24	3.50	15.99	0.1322	0.512732	±4	1.83	2.62	601
	46	BG2B	5.57	26.68	0.1263	0.512622	±3	-0.31	0.55	746

*Concentrations determined by isotope dilution.

†Internal errors in measured $^{147}Sm/^{144}Nd$ are ≤0.1% (2σ s.e.).

‡Measured $^{143}Nd/^{144}Nd$ with internal error (2σ s.d.); long-term reproducibility of Nd isotopic standards is ≤20 ppm (2σ s.d.), which propagate into an average reproducibility of $\varepsilon_{Nd(t)}$ of approximately ±0.5 epsilon units.

#ε_{Nd} calculated with $(^{147}Sm/^{144}Nd)_{CHUR}=0.1967$ and $(^{143}Nd/^{144}Nd)_{CHUR}=0.512638$; $\varepsilon_{Nd(t)}$ calculated at the crystallization or protolith age listed in table 1 except when the protolith age was not sufficiently well-known (i.e. Chiwaukum Schist, Nason Ridge Gneiss and Napeequa Complex) where $\varepsilon_{Nd(t)}$ was calculated at 96 Ma.

&$T_{DM}(Ma)=\{(1/\lambda_{147})*\ln[((^{143}Nd/^{144}Nd)_{sample}-(^{143}Nd/^{144}Nd)_{DM})/((^{147}Sm/^{144}Nd)_{sample}-(^{147}Sm/^{144}Nd)_{DM}))+1]*1000\}$; present day $(^{143}Nd/^{144}Nd)_{DM}=0.513151$, $(^{147}Sm/^{144}Nd)_{DM}=0.2137$.

Chapter 3

EVIDENCE FOR LATERAL SEGMENTATION AND VARIABLE RATES OF EXHUMATION FROM U-Pb and $^{40}Ar/^{39}Ar$ THERMOCHRONOLOGY OF THE CRETACEOUS CORE OF THE NORTH CASCADES ARC, WA

ABSTRACT

The metamorphic core of the North Cascades arc records the burial and exhumation history of the southern termination of the Coast Plutonic Complex. New hornblende, muscovite and biotite $^{40}Ar/^{39}Ar$ data and titanite and zircon U-Pb data are integrated with the existing thermochronologic database from the region to define core-wide cooling and exhumation patterns and document discontinuities in cooling histories related to post-metamorphic fault systems. In general, the youngest cooling ages and the greatest amount of exhumation are approximately centered on the regions that preserve the highest metamorphic pressures (Paterson et al., 2004; Wernicke and Getty, 1997; Whitney et al., 1999). Cooling patterns can be broken into NW-trending lateral segments between fault boundaries. New data from opposing sides of one such fault boundary, the White River shear zone, indicate that the shear zone was active during the Late Cretaceous. Hornblende cooling dates are similar in age on either side of the shear zone whereas biotite cooling dates are ~10 Myr to 15 Myr younger to the northeast in the Tenpeak intrusion. The difference between biotite cooling dates across the shear zone diminishes to the north of the Tenpeak intrusion consistent with field observations that the amount of slip on the shear zone also decreases to the north. Similarly, early Tertiary biotite cooling dates are not significantly different across the northern contact between the Napeequa Complex and the Swakane Gneiss, two of the most deeply buried units in the North Cascades. These data contrast with K-Ar and $^{40}Ar/^{39}Ar$ hornblende and biotite dates from the Chelan block that show at least a 10 Myr difference in age between the Napeequa Complex and the Swakane Gneiss (Paterson et al., 2004; this study). These cooling patterns suggest that exhumation began in the North Cascades by ca. 90 Ma and was coincident with contraction and crustal thickening. A second phase of exhumation was accommodated by Tertiary N-S extension. The combined Late Cretaceous and Tertiary exhumation resulted in heterogeneous crustal depths exposed over short distances at the present erosional level. These patterns suggest that the timing of peak metamorphism and greatest burial depth are more variable both along strike and across the arc than previously recognized.

INTRODUCTION

Metamorphosed supracrustal rocks of the crystalline core of the North Cascades (Cascades core) record some of the highest pressures obtained in the North American Cordillera (Brown and Walker, 1993; Valley et al., 2003; Whitney, 1992; Whitney et al., 1999). P-T paths constructed from mineral assemblages and reaction textures indicate that the metamorphic and thermal evolution of this magmatic arc was strongly influenced by large-scale vertical tectonic motion (Whitney et al., 1999). P-T paths are broadly similar along the length of the arc (Whitney et al., 1999); however, the timing of burial and exhumation are not well-constrained and may vary along the length of the arc. Burial and crustal thickening began during the mid-Cretaceous with the collision of the Intermontane and Insular superterranes (Journeay and Friedman, 1993; McGroder, 1991; Monger et al., 1982; Rubin et al., 1990) and continued until ca. 68 Ma in some parts of the core (Miller and Paterson, 2001b; Miller et al., 1993; Chapter 1). Subsequent exhumation followed nearly isothermal decompression paths of up to 5 kbar (Wernicke and Getty, 1997; Whitney, 1992; Whitney et al., 1999), and was accomplished both by erosion and extension along a low-angle normal fault (Paterson et al., 2004). Similar metamorphic histories have been reported from other contractional magmatic arcs (e.g. Cretaceous arcs of Fiordland, New Zealand and Japan, and the Late Jurassic to Early Cretaceous arc of the North American Cordillera), suggesting similar burial and exhumation mechanisms that may be common to arcs (Whitney et al., 1999).

This study is focused on gaining a better understanding of patterns of cooling and exhumation throughout the Cascades core. Comparatively few detailed studies of the cooling and exhumation histories of magmatic arcs exist, and numerical models that aim to explain the evolution of such systems do not account for simultaneous crustal thickening, exhumation and the advection of heat by magmatism as occurs in contractional arcs. A case study such as this is useful in exploring the potential for different exhumation mechanisms occurring simultaneously within an arc. New $^{40}Ar/^{39}Ar$ and U-Pb titanite and zircon data add to the existing thermochronologic database from the region. In particular, thermochronologic data were obtained along several transects that cross major terrane boundaries in order to document discontinuities in cooling histories that might imply the position, significance and age of post-

metamorphic fault systems. All data are integrated into a core-wide view to facilitate discussion of the evolution of this laterally segmented and variably exhumed orogen.

GEOLOGIC SETTING

The Cascades core lies at the southern termination of the Coast Plutonic Complex (Fig. 1). It is comprised of Paleozoic to Mesozoic accreted terranes of oceanic and island-arc affinity that have undergone amphibolite-facies metamorphism (Misch, 1966; Tabor et al., 1989; Tabor et al., 1987b). These terranes were sutured together during final, NE-SW oriented contraction as the Insular superterrane collided with the Intermontane superterrane (Journeay and Friedman, 1993; Monger et al., 1982; Rubin et al., 1990). These terranes form the framework in which ca. 96-45 Ma arc plutons intrude.

The Cascades core is offset from the Coast Belt by the Tertiary, N-trending, strike-slip, Fraser-Straight Creek fault and bound on the east by the Ross Lake fault zone (Fig. 1) (Misch, 1966). The southern margin is obscured by Tertiary sediments and the Miocene Columbia River flood basalts. The major internal structure of the core is the post-metamorphic, high-angle, Tertiary Entiat fault, which divides the core into the Wenatchee and Chelan blocks (Fig. 2). The boundaries of the metamorphic core mark transitions between weakly-metamorphosed regions to regions of amphibolite-grade metamorphism and Late Cretaceous to Eocene cooling ages. The transition is abrupt across the NE margin (Baldwin et al., 1997; Haugerud et al., 1991; Kriens and Wernicke, 1990; Miller et al., 1993) but is more gradual along segments of the southern and W-NW margins (Brown and Walker, 1993; Duggan and Brown, 1994; Paterson et al., 1994).

Widespread thrusting and magmatism occurred along the length of the Coast-Belt-North Cascades system until ca. 85 Ma (Journeay and Friedman, 1993; Rubin et al., 1990; Rusmore and Woodsworth, 1991; Umhoefer and Miller, 1996). Within the core, regional but diachronous crustal loading associated with local thrusting and widespread folding that deformed earlier thrusts occurred until ca. 68 Ma (Miller et al., 1993; Paterson et al., 2004; Wernicke and Getty, 1997; Chapter 1). At the same time, parts of the metamorphic core along the southern and western margins were being exhumed. Localized magmatism continued within the Chelan block from ca. 79-45 Ma (Mattinson,

1972; Tabor et al., 1987a; Chapter 5) concurrent with exhumation of the deepest levels of the Cascades core (Wernicke and Getty, 1997; Whitney et al., 1999).

Miller and Paterson (2001b) constructed a schematic crustal section that shows the relationship between the various terranes that comprise the Wenatchee block (Fig. 3). They infer that this crustal section was established during the mid-Cretaceous assembly of the metamorphic core, although I have since shown that the Swakane Gneiss did not become part of the crustal section until after ca. 73 Ma (Chapter 1). At mid-crustal levels of this section, the Chiwaukum Schist, a meta-pelitic and psammitic unit, was intruded by the Mount Stuart batholith (Fig 2). Following emplacement of the ca. 93 Ma phases of the Mount Stuart batholith, the northwestern portion of the Mount Stuart region experienced a ~2-4 kbar regional increase in pressure (Brown and Walker, 1993; Evans and Berti, 1986; Evans and Davidson, 1999) attributed to loading by thrust sheets (Whitney et al., 1999) or shallower plutons (Brown and Walker, 1993).

At progressively deeper structural levels, the Chiwaukum Schist was extensively injected with tonalitic to trondhjemitic sheets forming the Nason Ridge Migmatitic Gneiss (Tabor et al., 1993). The deepest structural level of the Mount Stuart domain is preserved in a regional antiform in which the trondhjemitic Wenatchee Ridge Gneiss forms the core (Miller and Paterson, 2001b). The base of the Wenatchee Ridge Gneiss is not exposed, but Miller and Paterson (2001b) infer from thermobarometric data that during the mid-Cretaceous, the gneiss was underlain by the Napeequa Complex, a heterogeneous metamorphosed oceanic assemblage dominated by amphibolite and quartzite (metachert) (Cater and Crowder, 1967; Miller and Paterson, 2001b; Tabor et al., 1989).

The Napeequa Complex now structurally overlies the Chiwaukum Schist along the reverse-slip, White River shear zone. This shear zone is a post-peak metamorphic, NE-dipping, reverse fault marked in part by retrograde greenschist facies mylonites (Magloughlin, 1993; Van Diver, 1967). The shear zone divides the Wenatchee block into what are informally known as the Mount Stuart and Tenpeak domains. The amount of slip on the fault is poorly constrained. Limited K-Ar data from opposing sides of the shear zone at its SE end suggest a discontinuity in the crustal section.

The Swakane Gneiss represents the deepest structural level exposed in the Cascades core. The gneiss underlies the Napeequa Complex in the SW-dipping limb of a regional synform in the Wenatchee block, whereas it forms the core of a regional antiform in the Chelan block (Fig. 2). The contact between the Swakane Gneiss and the Napeequa Complex in the Chelan block is described as the Dinkelman decollement, and is thought to be a SW-directed thrust that was reactivated during top-to-N extension (Paterson et al., 2004).

Peak temperatures of regional metamorphism in the Wenatchee block were achieved just prior to, or at the same time as, voluminous ca. 96-88 Ma magmatism. These temperatures range from approximately 550-650°C near the Mount Stuart batholith (Brown and Walker, 1993; Evans and Berti, 1986; Stowell and Tinkham, 2003) to 650-675°C north of the White River shear zone (Valley et al., 2003). Peak temperatures in the Napeequa Complex and Swakane Gneiss in the Chelan block are broadly similar to each other, ranging from 640°C to 740°C (Valley et al., 2003); however, the peak temperature of the Swakane Gneiss was not obtained until after 73 Ma, the protolith age of the Swakane Gneiss (Chapter 1).

THERMOCHRONOLOGY RESULTS

Sampling Strategy

Hornblende, muscovite, and biotite were separated from samples collected in a broad N-S swath across the Wenatchee block and the southwest corner of the Chelan block (Fig. 2). Titanite and zircon were also separated from a limited number of samples for U-Pb analysis. These samples were selected to improve the lateral distribution of cooling dates in the region for the purpose of developing region-wide cooling patterns and as a qualitative evaluation of nearby K-Ar dates. In particular, sample selection focused on major terrane boundaries in order to document the timing of slip on key exhumational structures.

Samples from the Wenatchee block form a transect from mid-crustal (~3-4 kbar) depths to progressively deeper crustal levels from southwest to northeast. This transect crosses the southeastern part of the Nason–Chelan Mountains terrane boundary, which is marked by the White River shear zone. Samples were collected on either side of the

shear zone in order to compare and contrast cooling histories near the fault. These samples are compared with samples adjacent to the terrane boundary further to the NW to document the extent of the White River shear zone.

Samples were also analyzed from both the Wenatchee and Chelan blocks to better quantify differences in cooling history across the Napeequa-Swakane contact. Paterson et al. (2004) defined a distinct difference in cooling history between the Swakane terrane and the overlying Napeequa Complex of the Chelan Mountains terrane, which they attributed to exhumation by a low-angle normal fault called the Dinkelman decollement. It is unclear, however, whether this detachment surface extends along the same contact within the Wenatchee block. In addition, numerous tonalitic to granodioritic sheets intrude the Napeequa Complex, and are truncated by the Dinkelman decollement. U-Pb analyses of zircon from three sheets were obtained to provide an upper timing constraint for motion on the decollement.

Peak temperatures determined from the metamorphic terranes are in excess of the closure temperatures of the minerals analyzed by the $^{40}Ar/^{39}Ar$ method, therefore unless otherwise noted, the $^{40}Ar/^{39}Ar$ and K-Ar dates quoted in the text are interpreted as cooling ages through the nominal closure temperatures of ~500-550°C for hornblende, ~350-415°C for muscovite, and ~300-350°C for biotite (Hodges, 2003). U-Pb titanite analyses are also interpreted as cooling ages through a nominal closure temperature of ~600-650°C (Hodges, 2003). In contrast, the high closure temperature of zircon to Pb diffusion (>900°C; Hodges, 2003) indicates that U-Pb zircon analyses represent either igneous crystallization ages or timing of metamorphic growth.

$^{40}Ar/^{39}Ar$ Analytical Methods

Samples of biotite and muscovite weighing 60-100 mg and hornblende weighing 100-150 mg were washed in distilled water and methanol, and packed into an Al foil cylinder. The cylinders were then loaded into Al disks, shielded with Al foil and irradiated at the research nuclear reactor at McMaster University, Ontario, Canada. Corrections for interfering reactions were based on a combination of synthetic and natural salts. The neutron flux during irradiation was monitored with Taylor Creek sanidine

(28.34±0.16 Ma; Renne et al., 1998). The neutron flux parameter, *J*, varied with position along the length of the irradiation package, and is known to 0.2 to 0.4% precision.

Samples were analyzed at the Scottish Universities Environmental Research Centre (SUERC), East Kilbride, using double-vacuum resistance-furnace and step-heating procedures similar to those described in Singer et al. (1999). Isotopic measurements were performed on a MAP215-50 mass spectrometer using a Faraday cup collector. $^{40}Ar/^{39}Ar$ data were reduced using the ArArCALC routines of Koppers (2002), and ages were calculated assuming decay constants recommended by Steiger and Jager (1977). All data are reported at the 2σ uncertainty level. For each increment of gas extracted, a $^{40}Ar/^{39}Ar$ date was calculated assuming that the non-radiogenic $^{40}Ar/^{36}Ar$ component is that of atmosphere (295.5). The results for each step are plotted on a conventional release spectrum diagram as a function of cumulative $^{39}Ar_K$ released during the experiment.

$^{40}Ar/^{39}Ar$ Data Analysis

The incremental-heating method can aid in the interpretation of $^{40}Ar/^{39}Ar$ data by revealing correlations between the $^{40}Ar/^{39}Ar$ ratio of Ar released at certain temperatures and possible impurities in the mineral separate. Moreover, it is a powerful technique for identifying and correcting for excess ^{40}Ar contamination, which is defined as parent-less radiogenic Ar incorporated into the mineral during crystallization, introduced into the mineral lattice by subsequent diffusion or occluded within fluid or melt inclusions within the mineral (Kelley, 2002). The initial, low-temperature steps of all the data presented here contain only small amounts of radiogenic Ar and have correspondingly large uncertainties. For most samples, the initial low-temperature steps also yield lower apparent ages than later steps, which could be attributed to degassing of impurities. In particular, the presence of biotite in the hornblende separates is suggested by high K/Ca ratios observed in the initial hornblende degassing steps. Several hornblende samples have anomalously old, low-temperature steps which may be attributed to release of excess ^{40}Ar from defects and/or fluid/melt inclusions. The last one or possibly two steps of some mica samples have very low K/Ca ratios and anomalously old apparent ages, which may represent degassing of more retentive, high-Ca inclusions such as apatite or

hornblende. These anomalously old or young steps were excluded from calculation of a plateau date. In all cases, a weighted mean plateau date was calculated using three or more contiguous steps comprising at least 50% of the total $^{39}Ar_K$ released, each step of which yields an age within 2σ of the mean without contribution from the error in J (e.g., Dalrymple and Lanphere, 1974). The uncertainty on the plateau date includes the error associated with the J value, but does not include systematic error such as decay constant errors. These plateau dates are considered statistically valid if the MSWD (mean squares weighted deviate) of the mean lies within the 2σ uncertainty level of the expected value of 1.0 (Wendt and Carl, 1991).

Isotope correlation diagrams ($^{36}Ar/^{40}Ar$ vs. $^{39}Ar/^{40}Ar$) were also constructed. The data yield linear arrays reflecting mixtures of radiogenic and non-radiogenic components and, in ideal cases, may be regressed to determine $^{40}Ar/^{39}Ar$ isochron dates without the need to assume an initial $^{40}Ar/^{36}Ar$ ratio (Roddick et al., 1980). These isochron dates are considered statistically valid if the MSWD calculated from the regression of appropriate steps lies within the 2σ uncertainty level of the expected value of 1.0 (Wendt and Carl, 1991).

Weighted mean plateau and isochron dates from each sample are listed in Table 1, and the preferred age is shown in bold-face type. The selection of the preferred age is largely based on the initial $^{40}Ar/^{36}Ar$ ratio obtained from the isochron fits. If the initial $^{40}Ar/^{36}Ar$ is within uncertainty of the atmospheric value (295.5), then the assumption inherent in the calculation of a weighted mean plateau is validated, and I take the more precise plateau date as the best estimate of the cooling age. If the initial $^{40}Ar/^{36}Ar$ is greater than 295.5 outside of uncertainty, then I infer the presence of excess ^{40}Ar which makes the plateau date unreliable and accept the isochron date as the best estimate of the cooling age. In certain cases, the initial $^{40}Ar/^{36}Ar$ is slightly less than 295.5 outside of analytical uncertainty. No obvious geologic process can account for an initial ratio less than the atmospheric value, and this low ratio may instead be an analytical artifact of the analysis. In these cases, I refer to the weighted mean plateau date as the best estimate of the cooling age.

When a statistically significant plateau or isochron date cannot be determined from the data, but several steps approximate a plateau, then I quote this "pseudo-plateau"

as an approximate cooling age. Multiplication of the uncertainty on the weighted mean date by the square root of the MSWD gives a minimum estimate of the uncertainty attributed to the scatter of the data (York, 1969).

$^{40}Ar/^{39}Ar$ Results

For ease of discussion, $^{40}Ar/^{39}Ar$ results are presented in small groups according to their similarity in age and geographic position from south to north. The cooling ages determined from each data point are shown on a map of the Cascades core in Figure 2 and the data are reported in Table 1.

Southern Wenatchee Block

From the southern Wenatchee block, four samples were analyzed and all yield both weighted mean plateau and isochron dates with initial $^{40}Ar/^{36}Ar$ ratios within uncertainty of 295.5 (Fig. 4; Table 1). Biotite from the oldest, ca 96.0 Ma phases of the Mount Stuart batholith (U-Pb crystallization ages from Chapter 4) yielded 87.2±0.4 Ma (*MS5*) and 90.7±0.8 Ma (*MS17C*) $^{40}Ar/^{39}Ar$ dates. Biotite from Chiwaukum garnet-biotite schist (*CW7*) in the contact aureole of the Mount Stuart batholith yielded an 86.2±0.4 Ma date. Across strike to the northeast, muscovite from the Wenatchee Ridge Gneiss (*WRO2*) recorded an 86.9±0.4 Ma date from the deepest levels of the Wenatchee block southwest of the White River shear zone.

Tenpeak Intrusion and Host Rock

Across the White River shear zone directly to the north of the first set of samples, hornblende and biotite ages were determined from the 90-92 Ma Tenpeak intrusion and its host rock, the Napeequa Complex. Hornblende samples yielded complicated Ar release spectra, and only two hornblende samples (*TP19B* and *NQ31*) yielded both weighted mean plateau and isochron dates.

Regression of all but one step from hornblende sample *TP19B*, an amphibolite raft within the Tenpeak pluton, yields an isochron date with an initial $^{40}Ar/^{36}Ar$ within uncertainty of 295.5. Because the initial $^{40}Ar/^{36}Ar$ is within uncertainty of the atmospheric value, then the assumption inherent in a plateau analysis is validated. Five

of eight steps from *TP19B* define a weighted mean plateau date of 90.5±0.8 Ma (Fig. 5). I regard the weighted mean plateau date as the best estimate of the cooling age of the hornblende sample.

The release spectrum from hornblende of Napeequa Complex sample (*NQ31*) is complicated by an anomalously old first step and two anomalously old steps near the end of the step-heating experiment (Fig. 5). Six of eight steps yield an isochron date of 81.8±1.6 with an initial $^{40}Ar/^{36}Ar$ of 594.5±28.2. This isochron date best represents the cooling age of the sample. The high initial $^{40}Ar/^{36}Ar$ suggests the presence of an excess ^{40}Ar trapped component, making a plateau analysis invalid.

The steps from hornblende of tonalite sample *TP-524-1* form a cluster of radiogenic analyses on an isotope correlation diagram (Fig. 5). An isochron date of 94.5±1.7 Ma can be defined, but the initial $^{40}Ar/^{36}Ar$ is poorly constrained, and the isochron date is several Myr older than the U-Pb zircon crystallization age of that sample (89.74±0.09 Ma; Chapter 4). A statistically significant plateau date cannot be defined, but the last five steps approach a plateau with a mean date of ca. 88.9 Ma and a minimum uncertainty of ~3.1 Myr This pseudo-plateau hornblende date agrees with its U-Pb zircon crystallization age, and best approximates the cooling age of this sample.

The remaining two hornblende samples from the Tenpeak pluton (*TP31* and *TP11*) also exhibit complicated release spectrum (Figs. 5 and 6), and isotope correlation diagrams for these samples indicate contamination by excess ^{40}Ar. The $^{40}Ar/^{36}Ar$ of the non-radiogenic component of each sample is not well-constrained. As a consequence, geologically meaningful ages cannot be determined from the data.

Biotite dates from the southern Tenpeak pluton are approximately 15 to 20 Myr younger than hornblende cooling ages from the same or nearby samples and biotite cooling ages from the Mount Stuart region (Fig. 2). Data from biotite samples *TP31* and *TP-524-1* yield isochron dates with initial $^{40}Ar/^{36}Ar$ ratios within uncertainty of 295.5 (Fig. 6). The more precise plateau dates of 68.1±0.4 Ma and 75.2±0.4 Ma for samples *TP31* and *TP-524-1*, respectively, best represent the cooling age of each sample. An isochron date can also be defined from biotite sample *TP11*; however, the initial $^{40}Ar/^{36}Ar$ is lower than 295.5 outside uncertainty. As discussed in the previous section, no reasonable geologic process can result in an initial $^{40}Ar/^{36}Ar$ lower than the

atmospheric value of 295.5, and this low initial ratio is probably an artifact of the experimental analysis. Therefore, I assume that the non-radiogenic Ar component present in sample *TP11* is best approximated by the atmospheric value and use the weighted mean plateau date (67.0±0.6 Ma) as the best estimate of the biotite cooling age of this sample.

Nason-Chelan Mountains Terrane Boundary and the White River Shear Zone

Two additional sets of samples from the northernmost Tenpeak pluton, Chiwaukum Schist and Napeequa Complex constrain cooling histories from opposing sides of the Nason-Chelan Mountains terrane boundary. One set includes biotite from Chiwaukum garnet-biotite schist (*CW22B*) and hornblende from an amphibolite layer (*TP-749-1*) within the same outcrop (Fig. 2). These samples were collected about 1 km across strike southwest of the boundary. Data from the Chiwaukum samples are compared to hornblende and biotite from the northernmost Tenpeak intrusion collected ~1.25 km on the northeast side of the terrane boundary.

Only hornblende sample *TP-749-1* yielded a Late Cretaceous cooling age. Five of eight steps define an isochron, but the initial $^{40}Ar/^{36}Ar$ is significantly less than 295.5, and I must assume that the non-radiogenic Ar component is best approximated by the atmospheric value. Acknowledging this assumption, I use a plateau analysis to determine the cooling age of the sample. The first five steps on the Ar release spectrum show a gradual increase in apparent age (Fig. 7). The remaining three of eight steps comprise 77.1% of the $^{39}Ar_K$ and define a plateau of 88.5±1.0 Ma (Fig. 7). Biotite from the same outcrop exhibits a concave Ar release spectrum, and neither an isochron nor a plateau can be defined. The spectrum does approximate a plateau in the range of 30-32 Ma with a weighted mean of 30.9 Ma and a minimum uncertainty of ~1.0 Myr (Fig. 7). This sample was collected within ~3 km of the ca. 20-23 Ma Cloudy Pass batholith, and I would interpret the biotite systematics as partially reset by this intrusion.

From the northernmost Tenpeak pluton, hornblende from sample *TP27* exhibits a complicated release spectrum with no obvious plateau and a poorly-defined, nearly horizontal, linear trend on an isotope correlation diagram (Fig. 7). The data array does not constrain the $^{40}Ar/^{36}Ar$ of the non-radiogenic component, and as a result, a

geologically meaningful age cannot be obtained from this sample. In contrast, biotite from the same sample defines both an isochron and a plateau date. The intial $^{40}Ar/^{36}Ar$ is within uncertainty of 295.5; therefore it is valid to use the more precise plateau date of 23.0±0.2 Ma (Fig. 7). This date agrees within uncertainty of a K-Ar biotite date from the Cloudy Pass batholith (Tabor et al., 2002).

The second set of samples that constrains cooling histories on either side of the Nason-Chelan Mountains terrane boundary was collected ~12 km along strike to the north of samples *TP-749-1*, *CW22B* and *TP27* (Fig. 2). This set includes biotite from Chiwaukum garnet-biotite schist (*CW24*) collected ~1 km across strike southwest of the Chiwaukum-Napeequa contact, and hornblende and biotite from a Napeequa amphibolite (*NQ18*) collected ~0.5 km across strike northeast of the contact. These samples yield both isochron and plateau dates with initial $^{40}Ar/^{36}Ar$ ratios within uncertainty of the atmospheric value; therefore the more precise plateau dates represent the preferred cooling ages (Fig. 8). Four of seven steps from *NQ18* hornblende define a plateau date of 88.9±1.1 Ma. One step from the middle of the plateau has a significantly large uncertainty but accounts for only 0.3% of the $^{39}Ar_K$ released, and therefore this step has not been considered in calculation of the plateau date. *NQ18* biotite and *CW24* biotite yielded plateau dates of 68.8±0.6 Ma and 70.0±0.4 Ma, respectively. The similarity of biotite cooling ages from either side of the shear zone indicate that little, if any, differential motion occurred along this segment of the Nason-Chelan Mountains terrane boundary.

Chelan Mountains-Swakane Terrane Boundary (Wenatchee Block)

The next group of samples was collected from the deepest structural levels of the Wenatchee block across the Napeequa-Swakane contact (Fig. 2). Both hornblende and biotite were analyzed from a sample of Napeequa amphibolite (*NQ2*) collected ~1.3 km across strike from the Napeequa-Swakane contact. From the Swakane Gneiss, muscovite was analyzed from a 68.4 Ma deformed leucogranite sheet that cuts the gneiss (*SW1*; Chapter 1), and farther south, biotite was analyzed from garnet-kyanite gneiss (*SW2*).

NQ2 hornblende yielded both isochron and plateau dates. The plateau date of 79.1±0.9 Ma is the preferred cooling age. If three outliers are excluded from *NQ2* biotite

data, an isochron date of 57.0±0.7 Ma can be defined with an initial $^{40}Ar/^{36}Ar$ within uncertainty of 295.5. The Ar release spectrum from *NQ2* biotite is slightly concave, and a plateau with contiguous steps cannot be defined (Fig. 9). Therefore, the isochron date represents the best estimate of the cooling age of the biotite sample.

Biotite from Swakane garnet-kyanite gneiss (*SW2*) yielded both isochron and plateau dates of which the plateau date of 54.0±0.3 Ma is the preferred cooling age (Fig. 9). Muscovite from the leucogranite sheet that cuts the Swakane Gneiss (*SW1*) displays more complicated systematics. The first six steps yield anomalously low apparent ages and are outliers on an isotope correlation diagram (Fig. 9). Neither a plateau nor an isochron can be defined, but the last five steps approach a plateau with a weighted mean date of 58.3 Ma. Multiplication of the uncertainty on the weighted mean by the square root of the MSWD results in a minimum uncertainty of 0.8 Ma.

Chelan Mountains-Swakane Terrane Boundary (Chelan Block)

The final group of samples was collected from opposing sides of the Napeequa-Swakane contact in the Chelan block (i.e., the Dinkelman decollement). Hornblende from a Napeequa amphibolite in the upper plate of the decollement yielded a plateau date of 70.4±0.8 Ma (Fig. 10). This cooling age contrasts with hornblende from an amphibolite layer at the structurally deepest level of the Swakane Gneiss that yielded a plateau date of 57.9±0.5 Ma (Fig. 10). Biotite from the Swakane sample yielded a plateau date of 49.5±0.3 Ma.

U-Pb Results

Details of the preparation, dissolution, and analysis of zircon and titanite grains are given in Chapter 4. The data are presented in Table 2 and Figure 11. The first three samples were collected from tonalitic to granodioritic orthogneiss bodies that intrude the Napeequa Complex southwest of the Entiat intrusion and can be traced for several kilometers in length. The uppermost sheet (*LSh1*) is the largest and most homogeneous body, although internal contacts between texturally distinct phases are present. Six U-Pb zircon analyses obtained from near the center of this sheet spread out on a trend that is nearly parallel to concordia with $^{206}Pb/^{238}U$ dates ranging from 84.9±1.4 to 88.8±0.8 Ma.

The youngest analysis is a reasonable estimate of the crystallization age of this sheet, whereas the slightly older analyses may reflect inheritance of earlier crystallized portions of the sheet.

A structurally-lower orthogneiss sheet (*LSh2*) displays well-defined internal layering characterized by textural and compositional variations and zones of boudinaged host rock rafts (Paterson et al., 2004). Five U-Pb zircon analyses from a tonalitic layer in this sheet yield a large range of $^{206}Pb/^{238}U$ dates from 90.5±0.2 to 100±0.1 Ma. Three analyses overlap concordia, but the youngest and oldest analyses are discordant and may represent mixtures between mid-Cretaceous and Mesozoic(?) grains inherited from the Napeequa Complex. It is unlikely that any of these analyses represent the crystallization age of this sheet. The most reasonable interpretation is that the sheet is younger than the $^{206}Pb/^{238}U$ dates of the above analyses, although just how much younger is unconstrained.

The lowest orthogneiss sheet sampled (*LSh4*) also displays well-defined internal layering. U-Pb zircon analyses from a tonalitic layer in the sheet yield four concordant analyses with $^{206}Pb/^{238}U$ dates from 77.1±0.6 to 78.6±0.4 Ma and one highly discordant analysis (89%) with a Middle Proterzoic $^{207}Pb/^{206}Pb$ date. A minimum age for the crystallization of this sheet is best estimated by the youngest concordant analysis.

U-Pb titanite analyses from a Napeequa garnet amphibolite sample (*NQ21*) also yield Late Cretaceous $^{206}Pb/^{238}U$ dates from 70.4±0.4 to 71.5±0.1 Ma. This sample was collected from the Chelan block near the Dinkelman decollement, and the U-Pb dates likely reflect cooling of this block after peak metamorphism.

The final sample selected for U-Pb analysis is amphibolite of the Napeequa Complex (*NQ4*) collected in the Wenatchee block within ~200 m of the Napeequa-Swakane contact. Zircon grains analyzed from this sample are characterized by low Pb concentrations (0.2-0.4 ppm) and very low Th/U ratios (0-0.02). All three analyses plot slightly below concordia suggestive of U-Th disequilibrium. The crystallization age of these zircons is probably best represented by the $^{207}Pb/^{235}U$ dates at ca. 67 Ma.

DISCUSSION

Comparison of Published K-Ar and $^{40}Ar/^{39}Ar$ Data

The development of a core-wide view of cooling patterns in the North Cascades core requires assessment of all K-Ar and $^{40}Ar/^{39}Ar$ dates published from the region. This assessment must first address issues related to the quality of the K-Ar data. A critical evaluation of the K-Ar dates is necessary because it is possible to obtain spurious dates if one of several assumptions is not met. These assumptions include: 1) closed-system behavior of the sample for both K and Ar throughout the history of the sample, 2) an initial $^{40}Ar/^{36}Ar$ ratio equal to that of the atmosphere (i.e. 295.5), and 3) a pure mineral separate that lacks inclusions or any alteration products. Any later thermal disturbance or alteration of the minerals of interest violates the closed-system assumption, resulting in dates that fall somewhere between the ages of primary and secondary geologic events and have no geologic significance. The incorporation of excess, non-radiogenic ^{40}Ar at some time during the history of the mineral violates the assumption of a known initial $^{40}Ar/^{36}Ar$, resulting in anomalously old dates that, again, have no geologic significance.

In practice, it is difficult, if not impossible, to evaluate whether these assumptions are valid for a given K-Ar date. Unlike the incremental-heating method, no opportunity exists in the K-Ar method to identify or isolate excess ^{40}Ar contributions or inspect for potential impurities. In the North Cascades, most biotite K-Ar dates are ~10-15% younger than nearby $^{40}Ar/^{39}Ar$ biotite dates, and less than half of the K-Ar dates agree with nearby $^{40}Ar/^{39}Ar$ dates within uncertainty. However, the $^{40}Ar/^{39}Ar$ data presented here indicate that excess ^{40}Ar is not a widespread problem in the region. The K-Ar data are included in the complication for comparative purpose, but are given less weight when considering region-wide cooling patterns.

The accuracy of $^{40}Ar/^{39}Ar$ dates is dependent upon intercalibration between samples, neutron fluence monitors of known age, and primary $^{40}Ar/^{40}K$ (or other external standards) (e.g. Renne et al., 1998). Comparisons of $^{40}Ar/^{39}Ar$ dates determined with respect to different fluence monitors can result in a bias between dates if the monitors are not calibrated against each other. Renne et al. (1998) measured several intercalibration factors and developed a mathematical formulation to recalculate $^{40}Ar/^{39}Ar$ dates so that all dates can be referenced to the same primary standard. The information required to use

this mathematical formulation includes which flux monitor was analyzed and the age that was assigned to that monitor. Unfortunately, this information is not available for all of the North Cascades studies. When the information was available (i.e. Miller et al., in review; Paterson et al., 2004; Wernicke and Getty, 1997), I recalculated previously published $^{40}Ar/^{39}Ar$ dates to the primary standard GA-1550 at an age of 98.79±0.54 Ma (Renne et al., 1998). The revised dates are 0.5-1.5% older than the previously published ages which has little influence on the regional cooling pattern. Dates from the study by Evans and Davidson (1999) could not be recalculated, but are still considered in the discussion of core-wide cooling patterns with the knowledge that these dates may be ~1% too young when compared to the other $^{40}Ar/^{39}Ar$ dates.

Regional Cooling Patterns

All Late Cretaceous to early Tertiary K-Ar and $^{40}Ar/^{39}Ar$ dates available from the Cascades core are plotted on figure 12, and figures 13 and 14 show the data contoured for hornblende and biotite cooling ages respectively. Contours were not drawn across the Entiat fault because of significant differences in the thermal histories of the Wenatchee and Chelan blocks. These differences resulted, in part, because magmatism continued episodically in the Chelan block until ca. 45 Ma, whereas it had ceased in the Wentachee block by ca. 88 Ma (Tabor et al., 1987a). The difference in cooling history between the blocks is also a function of the relative amount of early Tertiary exhumation as discussed in the following sections. Significant crustal thickening and loading of plutons occurred throughout much of the core between 90 Ma and 72 Ma (Miller et al., 1993; Wernicke and Getty, 1997; Whitney et al., 1999). The region of youngest cooling ages and the greatest amount of exhumation is approximately centered on the region that records the highest metamorphic pressures (Paterson et al., 2004; Wernicke and Getty, 1997; Whitney et al., 1999).

Wenatchee Block

The new $^{40}Ar/^{39}Ar$ dates presented here support the previously noted general trend of decreasing hornblende, muscovite and biotite cooling dates across strike to the NNE (Figs. 13 and 14) (Brown and Walker, 1993; Paterson et al., 2004; Whitney et al., 1999).

In the Wenatchee block, K-Ar and $^{40}Ar/^{39}Ar$ dates post-date voluminous Late Cretaceous magmatism, therefore the dates likely reflect regional cooling trends as a result of exhumation. These trends are locally disrupted around the Miocene Cloudy Pass batholith and Mount Buckindy intrusion, as noted for biotite samples *CW22B* and *TP27*. Dates that yield Miocene or younger ages are not shown on figure 12, and were ignored for the purposes of contouring the hornblende and biotite dates.

This cooling pattern is superimposed on a baric gradient that increases from pressures of 3-4 kbar in the Chiwaukum Schist at the southwestern end of the Mount Stuart batholith (Evans and Berti, 1986; Plummer, 1980) to 7-9 kbar pressures in the core of the Wenatchee Ridge antiform (Brown and Walker, 1993) to 9-11 kbar peak pressures in the Napeequa Complex northeast of the Tenpeak pluton (Sawyko, 1994; Valley et al., 2003). This baric gradient forms the basis for construction of the mid-Cretaceous crustal section (Fig. 3) (Miller and Paterson, 2001b).

The decrease in cooling ages across strike within the Wenatchee block is compatible with the observation that rocks exhumed from the greatest depth (i.e. Napeequa Complex and Swakane Gneiss) have the youngest cooling ages. This suggests that exhumation of the Wenatchee block proceeded from the margin of the core inward (Paterson et al., 2004). Hornblende, muscovite and biotite dates from the deepest structural levels of the Mount Stuart domain suggest that exhumation began by ca. 90 Ma (Engels and Crowder, 1971; Evans and Davidson, 1999; this study). Hornblende and biotite K-Ar dates are within uncertainty of each other along the southwestern margin of the Mount Stuart batholith (Fig. 12). The similarity between hornblende and biotite dates and U-Pb zircon crystallization dates (Chapter 4) most likely reflects rapid cooling following emplacement into shallow level rocks.

The area from the northwestern, hook-shaped region of the Mount Stuart batholith to the White River shear zone experienced a ~2-4 kbar pressure increase (Brown and Walker, 1993; Stowell and Tinkham, 2003) after emplacement of the ca. 93 Ma portions of the Mount Stuart batholith (Evans and Davidson, 1999; Chapter 4). Biotite $^{40}Ar/^{39}Ar$ and titanite U-Pb dates from the northwestern hook-region of the Mount Stuart batholith and its host rock are consistent with relatively rapid cooling (~30-40°C/Myr) of this region after loading. The Chiwaukum Schist on the northwest side of the Mount Stuart

batholith records temperatures of 600-650°C following emplacement of ca. 96 Ma phases of the Mount Stuart batholith (Stowell and Tinkham, 2003). A biotite $^{40}Ar/^{39}Ar$ date from near that locality (sample *CW7*) indicates that the temperature had decreased to ≤350°C by 86.2±0.4 Ma (this study). Within the Mount Stuart batholith, secondary titanite growth is associated with breakdown of biotite to chlorite at ca. 89-86 Ma (Chapter 4), which also supports decreasing temperatures soon after loading. Hornblende $^{40}Ar/^{39}Ar$ dates from the Chiwaukum Schist and Nason Ridge Migmatitic Gneiss north of the batholith range from 86.7±3.0 Ma to 83.0±0.8 Ma (Evans and Davidson, 1999). Biotite $^{40}Ar/^{39}Ar$ dates range from 86.2±0.4 Ma to 80.6±0.4 Ma (Evans and Davidson, 1999; this study). The youngest cooling ages in the Mount Stuart domain were obtained from the deepest levels of the Nason Ridge Migmatitic Gneiss (Fig. 12).

Across strike to the NNE of the Mount Stuart batholith, rocks of the Tenpeak domain represent deeper levels of the crustal section. Hornblende K-Ar and $^{40}Ar/^{39}Ar$ dates from the Tenpeak pluton and its host rock, the Napeequa Complex, range from 90.5±0.8 Ma to 79.1±0.9 Ma (Engels et al, 1976; this study). U-Pb titanite cooling dates from the Tenpeak pluton are less than 1 Myr younger than their respective zircon crystallization ages of ca. 92-90 Ma, and overlap in age with the oldest hornblende $^{40}Ar/^{39}Ar$ date from the pluton (Chapter 4). The titanite and hornblende cooling dates exhibit a similar range in age as hornblende $^{40}Ar/^{39}Ar$ dates immediately to the SSW across the White River shear zone in the Nason Ridge Gneiss. The hornblende ages from the Tenpeak pluton are also similar in age to hornblende $^{40}Ar/^{39}Ar$ cooling ages of 88.5±0.9 Ma and 88.9±1.1 Ma obtained from Chiwaukum amphibolite (TP-749-1) and Napeequa amphibolite (NQ18), respectively, (Fig. 12; this study). This similarity of hornblende cooling ages on either side of the Nason-Chelan Mountains terrane boundary indicates that there was little to no differential movement on this boundary before the terranes cooled through 500-550°C (i.e., the hornblende closure temperature).

In contrast, biotite K-Ar and $^{40}Ar/^{39}Ar$ cooling ages are on average 10 Myr to 15 Myr younger in the Tenpeak pluton than in the Chiwaukum Schist and Nason Ridge Gneiss SSW of the shear zone (Fig. 12). This difference in cooling ages across the shear zone suggests that after ca. 85 Ma exhumation of the Tenpeak domain was most likely accommodated by uplift of these rocks in the hanging the White River shear zone

coupled with erosion. Biotite cooling ages from samples that straddle the Nason-Chelan Mountains terrane boundary to the north of the Tenpeak pluton, however, are not significantly different from each other, which imply that motion on the shear zone dies out to the NNW. This scenario is consistent with our field observations and observations made by Tabor et al. (2002) of a progressively decreasing width to the shear zone to the northwest of the Tenpeak pluton.

The Swakane Gneiss comprises the structurally deepest level in the Wenatchee block (Fig. 3), but the gneiss differs from the other units in the Cascades core in that it did not become part of the crustal section until after 73 Ma, the approximate depositional age of the Swakane protolith (Chapter 1). Whereas the other units in the crustal section record mid-Cretaceous metamorphism and mid- to late Cretaceous cooling and inferred exhumation, the Swakane Gneiss records much younger peak metamorphism and partial melting at ca. 68 Ma (Chapter 1) coincident with cooling of the Tenpeak pluton through the biotite closure temperature. The Napeequa Complex overlies the Swakane Gneiss along the SW-dipping limb of a regional synform. A hornblende $^{40}Ar/^{39}Ar$ date of 79.1±0.9 Ma was obtained from Napeequa amphibolite (*NQ2*) within 1.5 km of the Napeequa-Swakane contact (this study), but unfortunately, no hornblende dates are available from the Swakane Gneiss to make a comparison. A biotite $^{40}Ar/^{39}Ar$ date of 57.0±0.7 Ma was obtained from the same Napeequa sample (*NQ2*). This date is comparable to a ca. 58 Ma muscovite $^{40}Ar/^{39}Ar$ date from a leucogranite dike that cuts the gneiss. The Napeequa biotite date is also only ~3 Myr older than a 54.0±0.3 Ma $^{40}Ar/^{39}Ar$ biotite date obtained from Swakane garnet-kyanite gneiss (*SW2*) collected ~5 km to the south (this study). The similarity in age of the Napeequa and Swakane samples suggests continuity in cooling history across the Napeequa-Swakane contact. Metamorphic zircon was recovered from a sample of Napeequa amphibolite collected within ~200 m of the Napeequa-Swakane contact about 2 km along strike to the north of sample *NQ2*. U-Pb analyses were obtained for one single zircon and two multi-grain fractions (Table 2; Fig. 11). These analyses are interpreted to reflect growth of metamorphic zircon, perhaps related to fluid infiltration along the contact, at ca. 67 Ma.

On the northwestern margin of the core, the available K-Ar data appear to conflict with the hypothesis that exhumation began at the margins of the core in the mid-

Cretaceous. In the Jordan Lakes region (Fig. 2), Brown and Walker (1993) document a similar baric gradient to the Mount Stuart region. Peak metamorphic pressures increase from ~3 kbar in the northwestern part of the Wenatchee block to ~7-9 kbar near the Sulphur Mountain pluton (Fig. 2). Unlike the Mount Stuart region, however, hornblende, muscovite, and biotite K-Ar dates do not exhibit a coherent trend of decreasing age with increasing peak pressures (Fig. 12). The ca. 92 Ma Chauval pluton (Walker and Brown, 1991) exhibits K-Ar hornblende dates from 81.7±0.8 Ma to 63.8±1.4 Ma over an ~10 km distance (Tabor et al., 2002). K-Ar hornblende dates from other intrusions in the region range from 73.7±1.0 Ma to 58.9±0.6 Ma, and K-Ar biotite dates range from 61.4±0.6 Ma to 44.7±1.6 Ma (Tabor et al., 2002). Some of the published K-Ar dates published were not plotted on figure 12 because they were assumed to be reset by the Miocene Mount Buckindy intrusion (Tabor et al., 2002).

Nearly all of the thermochronologic data from this region were derived from intrusions in which the emplacement ages are poorly constrained. The Bench Lake and Downey Creek intrusions are described as swarms of gneissic, tonalitic to granodioritic, sills and dikes (Tabor et al., 2002). An apophysis of the Bench Lake intrusion yielded a U-Pb zircon date of ca. 96 Ma (Fluke, 1992). Discordant U-Pb zircon dates from the Jordan Lakes intrusion were interpreted as representing a ca. 73 Ma emplacement age with ca. 90 Ma inheritance (Tabor et al., 2002; Walker and Brown, 1991). The lack of a clear pattern of decreasing K-Ar dates with the increasing baric gradient may reflect a more prolonged history of magmatism in this region and widespread disturbance of the K-Ar system by Miocene dikes and intrusions.

Chelan Block

The Chelan block also displays a general trend of younger K-Ar and $^{40}Ar/^{39}Ar$ dates to the north (Fig. 12); however, a more distinct pattern of cooling dates is difficult to define. One reason for this difficulty is that thermochronologic data are lacking from the Skagit Gneiss Complex, which makes up much of the Chelan block. Based on data from one sample locality in the northern Skagit Gneiss Complex, Wernicke and Getty (1997) documented two phases of cooling that occurred slowly between 68-60 Ma at mid-crustal depths and amphibolite facies conditions, and then rapidly between 50-45 Ma

as indicated by hornblende and biotite $^{40}Ar/^{39}Ar$ dates that nearly overlap within uncertainty (Wernicke and Getty, 1997). Unfortunately, there are few thermochronologic data from the Skagit Gneiss Complex to the south to document the regional extent of these two proposed unroofing events.

Another reason that distinct cooling patterns are difficult to recognize in the Chelan block is because Late Cretaceous to Paleogene cooling patterns have been disrupted by shallow level Eocene magmatism. From ca. 45-50 Ma, several intrusions including the Duncan Hill, Railroad Creek, Golden Horn and Cooper Mountain plutons were emplaced at relatively shallow crustal levels of the Chelan block (Fig. 2) (Hopson and Dellinger, 1989). Hornblende and biotite K-Ar dates from these intrusions commonly agree within uncertainty and may reflect rapid cooling after emplacement into rocks at or near the biotite closure temperature (Engels et al., 1976).

The clearest evidence of a Late Cretaceous cooling and exhumation history similar to that of the Wenatchee block can be found in the southern Chelan block. Limited K-Ar data suggest that the oldest cooling ages are preserved in the Chelan Migmatite Complex, which forms the core of a broad regional antiform along the southeast margin of the Chelan block. The Chelan Complex is directly on strike with the Skagit Gneiss Complex, but the cooling histories of these two complexes appear to be significantly different. Hopson and Mattinson (1994) concluded that magma was emplaced into the Chelan Complex at 6-10 kbar between 100-120 Ma (U-Pb zircon crystallization dates) followed by cooling through the hornblende closure temperature by 70-80 Ma and the biotite closure temperature between 60-70 Ma. The contacts between the Chelan Complex, the 8-9 kbar Cascade River – Holden – Twenty-Five-Mile-Creek units (herein referred to as the Cascade River unit) and the 9-11 kbar Napeequa Complex are obscured by magmatism, as is also the case for the contact between the Cascade River unit and Napeequa Complex in the southern Chelan block. Limited U-Pb titanite analyses from amphibolite of the Napeequa Complex yield ca. 71 Ma dates (Table 2; Fig. 11), which overlap the hornblende K-Ar and $^{40}Ar/^{39}Ar$ dates from this unit within uncertainty. These U-Pb dates are also comparable to 70-87 Ma titanite dates from the Chelan Complex (Hopson and Mattinson, 1994; Mattinson, 1972). Both hornblende and biotite K-Ar and $^{40}Ar/^{39}Ar$ dates from the Napeequa Complex and the intervening ca. 71-

73 Ma portions of the Entiat intrusion overlap in age with the youngest dates from the Chelan Complex. Taken together, the U-Pb titanite and hornblende and biotite K-Ar and $^{40}Ar/^{39}Ar$ dates suggest continuity in the cooling and exhumation history between the Chelan and Napeequa complexes.

In contrast, the Swakane Gneiss displays a much younger cooling history than the overlying Napeequa Complex. In the Chelan block, the Swakane Gneiss lies in the core of a broad regional antiform, and the contact between the Swakane Gneiss and the Napeequa Complex is described as the Dinkelman decollement (Alsleben, 2000; Paterson et al., 2004; Valley et al., 2003). This low-angle normal fault truncates lithologic units in the Napeequa Complex, including tonalitic to trondhjemitic intrusive sheets, as it cuts up-section along strike in a SE direction (Paterson et al., 2004). U-Pb zircon analyses from three intrusive sheets (this Chapter) indicate that the sheets were emplaced during the Late Cretaceous and are as young as 77.1±0.6 Ma. Additional U-Pb zircon analyses from other intrusive sheets in the area yield discordant results that are interpreted to represent crystallization dates as young as 66.7±2.4 Ma (Paterson et al., 2004). These results suggest that the latest motion on the decollement occurred after ca. 67 Ma. Biotite $^{40}Ar/^{39}Ar$ dates from the Swakane Gneiss immediately below the decollement range from ca. 46-49 Ma and are ~10 Myr younger than biotite dates in the overlying Napeequa Complex (Paterson et al., 2004; this study). A single hornblende $^{40}Ar/^{39}Ar$ date of 57.9±0.5 Ma from the Swakane Gneiss also supports a ~10 Myr difference in cooling ages across the decollement (this chapter). Paterson et al. (2004) used the available thermochronologic data, along with assumptions about hornblende and biotite closure temperatures (510°C and 350°C, respectively) and a geothermal gradient (30°C/km), to estimate ≥4 km of excision along the decollement. The new thermochronologic data obtained in this study help tighten these constraints. If I use the same closure temperature estimates, but a lower geotherm of 20°C/km (see Chapter 6) and the more precise cooling ages from this study, I estimate at least 8 km of excision along the decollement. The thermochronologic data are also consistent with the observation that by ca. 45 Ma, the Swakane Gneiss was at the surface and supplying sediment to the Eocene Chumstick basin (Evans, 1994; Johnson, 1985).

The available hornblende and biotite K-Ar and $^{40}Ar/^{39}Ar$ dates from the northern and central parts of the Chelan block suggest that much of the Chelan block was not exhumed until the early Tertiary. Hornblende K-Ar and $^{40}Ar/^{39}Ar$ dates range from 50-58 Ma along the eastern edge of the Chelan block and in the Cascade River unit near the Duncan Hill and Cardinal Peak intrusions (Miller and Bowring, 1990; Miller et al., in review). Across the NE margin, high pressure rocks with Tertiary cooling ages in the Skagit Gneiss Complex contrast with an abrupt transition to low pressure rocks with Late Cretaceous cooling ages in the Ross Lake fault zone and the Methow Basin (Baldwin et al., 1997; Haugerud et al., 1991; Kriens and Wernicke, 1990; Miller et al., 1993).

Based on the available thermochronologic data, Paterson et al. (2004) speculated that the Swakane Gneiss and Skagit Gneiss Complex in the Chelan block and the Tenpeak domain of the Wenatchee block formed the footwall of a Cascades-wide system of younger Eocene exhumation in which the Dinkelman decollement formed one segment. The older, already partly-exhumed regions along the margins of the core (i.e., the Mount Stuart domain of the Wenatchee block, and the Napeequa Complex, Cascade River unit, and Chelan Complex in the Chelan block) were proposed to have formed the hanging wall. This model requires "bounding structures" along which the Eocene exhumation could be accommodated. These structures would ideally be marked by discrete Tertiary cooling and pressure gradients that have ~30-40 km of vertical separation. Paterson et al. (2004) proposed that the Ross Lake fault zone on the east and the White River shear zone on the west as two possible bounding structures. The new thermochronologic data present here, however, indicate that the White River shear zone could not be a bounding structure. Exhumation of the Tenpeak domain occurred in the latest Cretaceous to early Tertiary as indicated by biotite dates ranging from 75-54 Ma. These dates place the Tenpeak domain in the hanging wall of any proposed Cascades-wide Eocene extensional structure. There are no other obvious candidates for a western bounding structure. Significantly more thermochronologic data are needed from the Napeequa Complex, Cascade River unit and Skagit Gneiss Complex to document the extent of early Tertiary exhumation and identify any possible discontinuities in the regional cooling patterns.

Low Temperature Thermochronologic Data

Reiners et al. (2002) utilized (U-Th)/He and fission track methods on apatite and zircon to obtain data for low temperature (~70-180 °C) cooling and exhumation history of the Cascades Range. Their discussion of the "east flank" region covers the areas around the Mount Stuart batholith and Tenpeak pluton in the Wenatchee block. An age-elevation transect within the Mount Stuart batholith yields a relatively, slow apparent exhumation rate of 0.15-0.25 km/Myr through most of the Oligocene to Early Miocene (Reiners et al., 2002). Cooling ages in the southeastern Mount Stuart batholith indicate that exhumation was limited to <~2-3 km since the early Tertiary (Reiners et al., 2002) consistent with the observation from the higher temperature thermochronology that the Mount Stuart region had been exhumed through the biotite closure temperature by at least 85 Ma (Fig. 14). Differences between apatite fission track and apatite (U-Th)/He ages, also from the Mount Stuart region, require slow time-averaged cooling (~1-2 °C/Myr) in the early to mid-Tertiary. Reiners et al. (2002) argued that the distribution of the (U-Th)/He and apatite fission track ages from their entire study region support a general model of slow exhumation from the Eocene to the Late Miocene (≤0.25 km/Myr) and rapid Late Miocene exhumation. Their study area, however, did not include the northern Skagit Gneiss Complex which shows evidence of rapid exhumation in the early Eocene (Wernicke and Getty, 1997). Reiners et al. (2002) also note that their model is consistent with exhumation histories for the Coast Mountains which involve slow cooling and little to no exhumation from the Eocene through the Late Miocene, followed by accelerated exhumation beginning at ca. 10 Ma.

IMPLICATIONS OF THE THERMOCHRONOLOGIC DATA

Integration of all the available thermochronologic data defines distinct patterns of cooling and inferred exhumation of the Cascades core. These patterns can be explained by the following exhumation history, which is illustrated in schematic block diagrams in figure 15. Exhumation began in the Cascades core by ca. 90 Ma. This exhumation appears to have been accomplished by rotation of the Wenatchee block on a roughly NW-SE axis which resulted in a decrease in cooling ages from SW to NE. This exhumation was coincident with contraction and crustal thickening that continued until ca. 68 Ma

(Miller et al., 1993; Miller and Paterson, 2001a; Paterson et al., 2004). Along the margin of the core, slow exhumation (<1 mm/yr) may have been driven by erosion coupled with isostatic adjustments (Willett, 1999; Willett and Beaumont, 1994; Zeitler et al., 2001). Presumably, similar exhumation was occurring at higher crustal levels that have since been removed.

The Wenatchee block had cooled through the hornblende closure temperature (500-550°C) by ca. 85 Ma. After ca. 85 Ma, differential relief cause by high-angle faulting along the WRSZ may have led to accelerated erosion of the Tenpeak pluton and Napeequa Complex. The new $^{40}Ar/^{39}Ar$ dates determined from this study indicate that slip on this structure dies out to the NW. During this time period, sediments of the Swakane Gneiss were underthrust beneath the arc.

A second phase of exhumation is proposed to have begun with the transition to dextral transtension at ca. 55 Ma (Paterson et al., 2004; Umhoefer and Miller, 1996). This early Tertiary extension exhumed much of the Chelan block including the Swakane Gneiss and Skagit Gneiss Complex. Exhumation of the Swakane Gneiss was accomplished in part by top-to-N shear on the Dinkelman decollement (Alsleben, 2000; Paterson et al., 2004). The Ross Lake fault zone may have accommodated exhumation of the Skagit Gneiss Complex on its northeastern margin; however, structures that may have accommodated Eocene exhumation of the Skagit Gneiss Complex on its eastern and southern margins have not yet been recognized. Similar periods of Tertiary extension in other parts of the Coast Belt were proposed to have been driven by gravitational collapse of thickened crust during dextral shearing (Klepeis and Crawford, 1999; Parrish et al., 1988). Paterson et al. (2004) point out that gravitational collapse should produce NE-SW extension away from topographic highs rather than N-S extension. They call upon an additional mechanism of differential stretching or arching along the arc coupled with differential erosion to account for heterogeneous N-S extension (e.g. Wells et al., 1999). The proposed causes of the along strike variability may be related to tectonic thickening/stretching, spatially variable erosion rates or underthrusting of buoyant materials such as the Swakane Gneiss. The low-temperature thermochronologic data from the Cascades core indicate slow cooling and exhumation following Eocene

extension until the Late Miocene, which is consistent with exhumation histories determined from other parts of the Coast Mountains (Reiners et al., 2002).

Magnitudes of Cretaceous exhumation range from <10 km at the margins of the core to ~30-40 km at the center of the core. Paterson and Miller (2000) and Paterson et al. (2004) estimate a long-term exhumation rate from thermochronologic data from the Swakane Gneiss. Assuming exhumation from ~40 km depth in 25 Myr, they calculate a maximum exhumation rate of ~1.6 km/Myr. These rates are comparable to rates of 2.0 km/Myr estimated by Hollister (1982) from the Coast Plutonic Complex. If I use the same assumptions, but use the thermochronologic data from the Napeequa Complex instead, I calculate ~30 km of exhumation from ca. 91 Ma, the crystallization age of the 7-9 kbar Tenpeak pluton, and ca. 59 Ma, the biotite cooling age of the deepest level Napeequa sample. This results in a slower average exhumation rate of 0.9 km/Myr.

The thermochronologic data indicate that exhumation processes operated during both early thrust loading and crustal thickening and during later arc-oblique extension and crustal thinning. Variations in exhumation rates and mechanisms operating from the margins to deeper crustal levels of the arc contributed to laterally-segmented cooling patterns. The thermochronologic data also indicate that even though units such as the Napeequa Complex and Swakane Gneiss followed similar P-T paths, their burial and exhumation occurred over distinctly different time periods. The combined Late Cretaceous and Tertiary extension resulted in heterogeneous crustal depths exposed over short distances at the present day surface. Additional thermochronologic data from the Chelan block, in particular the Skagit Gneiss Complex, are necessary to fully explore the interplay between Cretaceous and Tertiary exhumation. These patterns suggest that the timing of peak metamorphism and greatest burial depth was more variable both along strike and across the arc than previously recognized, and point out the need to distinguish between the magnitudes of Cretaceous and Tertiary exhumation in order to develop better models of the development of this arc.

REFERENCES

Alsleben, H., 2000, Structural analysis of the Swakane terrane, North Cascades core, Washington [M.S. thesis]: San Jose State University, San Jose.

Baldwin, J. A., Whitney, D. L., and Hurlow, H. A., 1997, Metamorphic and structural evidence for significant vertical displacement along the Ross Lake fault zone, a major orogen-parallel shear zone in the Cordillera of western North America: Tectonics, v. 16, p. 662-681.

Brown, E. H., and Walker, N. W., 1993, A magma-loading model for Barrovian metamorphism in the Southeast Coast Plutonic Complex, British Columbia and Washington: Geological Society of America Bulletin, v. 105, p. 479-500.

Cater, F. W., and Crowder, D. F., 1967, Geologic map of the Holden Quadrangle, Snohomish and Chelan counties, Washington: U. S. Geological Survey.

Cherniak, D. J., and Watson, E. B., 2001, Pb diffusion in zircon: Chemical Geology, v. 172, p. 5-24.

Dragovich, J. D., and Norman, D. K., 1995, Geologic map of the west half of the Twisp 1:100,000 Quadrangle, Washington, scale 1:100,000.

Duggan, K. M., and Brown, E. H., 1994, Correlation of the Tonga Formation and the Chiwaukum Schist, North Cascades, Washington: Implications for Late Cretaceous orogenic mechanisms: Tectonics, v. 13, p. 1411-1424.

Engels, J. C., and Crowder, D. F., 1971, Late Cretaceous fission-track and potassium-argon ages of the Mount Stuart granodiorite and Beckler Peak stock, North Cascades, Washington: U.S. Geological Survey Professional Paper, v. 750-D, p. D39-D43.

Engels, J. C., Tabor, R. W., Miller, F. K., and Obradovich, J. D., 1976, Summary of K-Ar, Rb-Sr, U-Pb, Pb-alpha, and fission-track ages of rocks from Washington State prior to 1975 (exclusive of Columbia Plateau basalts): Miscellaneous Field Studies Map - U. S. Geological Survey.

Evans, B. W., and Berti, J. W., 1986, Revised metamorphic history for the Chiwaukum Schist, North Cascades, Washington: Geology, v. 14, p. 695-698.

Evans, B. W., and Davidson, G. F., 1999, Kinetic control of metamorphic imprint during synplutonic loading of batholiths: An example from Mount Stuart, Washington: Geology, v. 27, p. 415-418.

Evans, J. E., 1994, Depositional history of the Eocene Chumstick Formation: Implications of tectonic partitioning for the history of the Leavenworth and Entiat-Eagle Creek fault systems, Washington: Tectonics, v. 13, p. 1425-1444.

Fluke, S. M., 1992, Metamorphism and plutonism of the Mt. Buckindy-Snow King region, North Cascades, Washington [M.S. thesis]: Western Washington University, Bellingham, Washington, 100 p.

Frost, B. R., Chamberlain, K. R., and Schumacher, J. C., 2000, Sphene (titanite): phase relations and role as a geochronometer: Chemical Geology, v. 172, p. 131-148.

Haugerud, R. A., Vanderheyden, P., Tabor, R. W., Stacey, J. S., and Zartman, R. E., 1991, Late Cretaceous and Early Tertiary plutonism and deformation in the Skagit Gneiss Complex, North Cascade Range, Washington and British Columbia: Geological Society of America Bulletin, v. 103, p. 1297-1307.

Hodges, K. V., 2003, Geochronology and thermochronology in orogenic systems, *in* Rudnick, R. L., ed., Treatise on Geochemistry: Amsterdam, Elsevier, p. 263-292.

Hollister, L. S., 1982, Metamorphic evidence for rapid (2 mm/yr) uplift of a portion of the Central Gneiss Complex, Coast Mountains, B.C.: The Canadian Mineralogist, v. 20, p. 319-332.

Hopson, C. A., and Dellinger, D. A., 1989, Depth dependency of granite types, illustrated by tilted plutons in the North Cascades, Washington: Geological Society of America Abstracts with Programs, v. 21, p. 95.

Hopson, C. A., and Mattinson, J. M., 1994, Chelan Migmatite Complex, Washington: Field evidence for mafic magmatism, crustal anatexis, mixing and protodiapiric emplacment, *in* Swanson, D. A., and Haugerud, R. A., eds., Geologic Field Trips in the Pacific Northwest: Boulder, Geological Society of America, p. 2K-1 - 2K-21.

Hurtado, J. M., Jr., 2002, Tectonic evolution of the Thakkhola Graben and Dhaulagiri Himalaya, central Nepal [PhD thesis]: Massachusetts Institute of Technology, Cambridge, MA.

Jaffey, A. H., Flynn, K. F., Glendenin, L. E., Bentley, W. C., and Essling, A. M., 1971, Precision measurements of half-lives and specific activities of ^{235}U and ^{238}U: Physics Review, v. C4, p. 1889-1906.

Johnson, S. Y., 1985, Eocene strike-slip faulting and non-marine basin formation in Washington, *in* Biddle, K. T., and Christie-Blick, N., eds., Strike-slip deformation, basin formation, and sedimentation: San Antonio, TX, United States, Society of Economic Paleontologists and Mineralogists, p. 283-302.

Journeay, J. M., and Friedman, R. M., 1993, The Coast Belt thrust system: Evidence of Late Cretaceous shortening in southwest British Columbia: Tectonics, v. 12, p. 1301-1302.
Kelley, S., 2002, Excess argon in K-Ar and Ar-Ar geochronology: Chemical Geology, v. 188, p. 1-22.
Klepeis, K. A., and Crawford, M. L., 1999, High-temperature arc-parallel normal faulting and transtension at the roots of an obliquely convergent orogen: Geology, v. 27, p. 7-10.
Koppers, A. A. P., 2002, ArArCALC: Software for $^{40}Ar/^{39}Ar$ age calculations: Computers & Geosciences, v. 28, p. 605-619.
Kriens, B., and Wernicke, B. P., 1990, Nature of the contact zone between the North Cascades crystalline core and the Methow sequence in the Ross Lake area, Washington: Implications for Cordilleran tectonics: Tectonics, v. 9, p. 953-981.
Krogh, T. E., 1973, A low contamination method for hydrothermal decomposition of zircon and extraction of U and Pb for isotopic age determination: Geochimica et Cosmochimica Acta, v. 37, p. 485-494.
Magloughlin, J. F., 1993, A Nason Terrane trilogy: I, Nature and significance of pseudotachylyte: II, Summary of the structural and tectonic history: III, Major and trace element geochemistry and strontium and neodymium isotope geochemistry of the Chiwaukum Schist, amphibolite, and meta-tonalite gneiss of the Nason Terrane [PhD thesis]: University of Minnesota, Minneapolis, 325 p.
Mattinson, J. M., 1972, Ages of zircons from the Northern Cascade Mountains, Washington: Geological Society of America Bulletin, v. 83, p. 3769-3783.
McGroder, M. F., 1991, Reconciliation of two-sided thrusting, burial metamorphism, and diachronous uplift in the Cascades of Washington and British Columbia: Geological Society of America Bulletin, v. 103, p. 189-209.
Miller, R. B., and Bowring, S. A., 1990, Structure and chronology of the Oval Peak batholith and adjacent rocks: Implications for the Ross Lake fault zone, North Cascades, Washington: Geological Society of America Bulletin, v. 102, p. 1361-1377.
Miller, R. B., Brown, E. H., McShane, D. P., and Whitney, D. L., 1993, Intra-arc crustal loading and its tectonic implications, North Cascades crystalline core, Washington and British Columbia: Geology, v. 21, p. 255-258.
Miller, R. B., Haugerud, R. A., Bowring, S. A., Dragovich, J. D., McClelland, W. C., Raviola, F. P., and Matzel, J., in review, A synthesis of the Ross Lake fault system and its implications for the Baja British Columbia model.
Miller, R. B., and Paterson, S. R., 2001a, Construction of mid-crustal sheeted plutons: Examples from the north Cascades, Washington: Geological Society of America Bulletin, v. 113, p. 1423-1442.
Miller, R. B., and Paterson, S. R., 2001b, Influence of lithological heterogeneity, mechanical anisotropy, and magmatism on the rheology of an arc, North Cascades, Washington: Tectonophysics, v. 342, p. 351-370.
Misch, P., 1966, Tectonic evolution of the Northern Cascades of Washington State: a west-cordilleran case history: Canadian Institute of Mining and Metallurgy, v. Special volume 8, p. 101-148.
Monger, J. W. H., Price, R. A., and Tempelman-Kluit, D. J., 1982, Tectonic accretion and the origin of the two major metamorphic and plutonic welts in the Canadian Cordillera: Geology, v. 10, p. 70-75.
Parrish, R. R., Carr, S. D., and Parkinson, D. L., 1988, Eocene extensional tectonics and geochronology of the southern Omineca Belt, British Columbia and Washington: Tectonics, v. 7, p. 181-212.
Paterson, S. R., and Miller, R. B., 2000, Rates and durations of tectonic and magmatic processes in arcs: the Cretaceous Cascades core as a case study: Geological Society of America Abstracts with Programs, v. 32, p. 172.
Paterson, S. R., Miller, R. B., Alsleben, H., Whitney, D. L., Valley, P. M., and Hurlow, H., 2004, Driving mechanisms for >40 km of exhumation during contraction and extension in a continental arc, Cascades core, Washington: Tectonics, v. 23, p. 10.1029/2002TC001440.
Paterson, S. R., Miller, R. B., Anderson, J. L., Lund, S. P., Bendixen, J., Taylor, N., and Fink, T., 1994, Emplacement and evolution of the Mt. Stuart batholith, *in* Swanson, D. A., and Haugerud, R. A., eds., Geologic field trips in the Pacific Northwest: 1994 Geological Society of American Annual Meeting, Geological Society of America, p. 2F1-2F47.
Plummer, C. C., 1980, Dynamothermal contact metamorphism superposed on regional metamorphism in the pelitic rocks of the Chiwaukum Mountains area, Washington Cascades: Geological Society of America Bulletin, v. 91, p. 386-388.

Reiners, P. W., Ehlers, T. A., Garver, J. I., Mitchell, S. G., Montgomery, D. R., Vance, J. A., and Nicolescu, S., 2002, Late Miocene exhumation and uplift of the Washington Cascade Range: Geology, v. 30, p. 767-770.

Renne, P. R., Swisher, C. C., Deino, A. L., Karner, D. B., Owens, T. L., and DePaolo, D. J., 1998, Intercalibration of standards, absolute ages and uncertainties in $^{40}Ar/^{39}Ar$ dating: Chemical Geology, v. 145, p. 117-152.

Roddick, J. C., Cliff, R. A., and Rex, D. C., 1980, The evolution of excess argon in Alpine biotites: A ^{40}Ar-^{39}Ar analysis: Earth and Planetary Science Letters, v. 48, p. 185-208.

Rubin, C. M., Saleeby, J. B., Cowan, D. S., Brandon, M. T., and McGroder, M. F., 1990, Regionally extensive mid-Cretaceous west-vergent thrust system in the northwestern Cordillera: Implications for continent-margin tectonism: Geology, v. 18, p. 276-280.

Rusmore, M. E., and Woodsworth, G. J., 1991, Coast Plutonic Complex: a mid-Cretaceous contractional orogen: Geology, v. 19, p. 941-944.

Sawyko, L. T., III, 1994, The geology and petrology of the Swakane biotite gneiss, North Cascades, Washington [M.S. thesis]: University of Washington, Seattle, 134 p.

Singer, B. S., Hoffman, K. A., Chauvin, A., Coe, R. S., and Pringle, M. S., 1999, Dating transitionally magnetized lavas of the late Matuyama Chron: Toward a new $^{40}Ar/^{39}Ar$ timescale of reversals and events: Journal of Geophysical Research, v. 104, p. 679-693.

Stacey, J. C., and Kramers, J. D., 1975, Approximation of terrestrial lead isotope evolution by a two-stage model: Earth and Planetary Science Letters, v. 26, p. 207-221.

Steiger, R. H., and Jaeger, E., 1977, Subcommission on geochronology: Convention on the use of decay constants in geo- and cosmochronology: Earth and Planetary Science Letters, v. 36, p. 359-362.

Stowell, H. H., and Tinkham, D. K., 2003, Integration of phase equilibria modelling and garnet Sm-Nd chronology for construction of P-T-t paths: Examples from the Cordilleran Coast Plutonic Complex, USA, *in* Vance, D., Muller, W., and Villa, I., eds., Geochronology: Linking the Isotopic Record with Petrology and Textures, Geological Society of London, p. 119-145.

Tabor, R. W., Booth, D. B., Vance, J. A., and Ford, A. B., 2002, Geologic map of the Sauk River 30- by 60-minute quadrangle, Washington: U.S. Geological Survey, scale 1:100000.

Tabor, R. W., Frizzell, V. A., Jr., Booth, D. B., Waitt, R. B., Whetten, J. T., and Zartman, R. E., 1993, Geologic map of the Skykomish River 30- by 60-minute Quadrangle, Washington: U. S. Geological Survey, scale 1:100,000.

Tabor, R. W., Frizzell, V. A., Jr., Whetten, J. T., Waitt, R. B., Jr., Swanson, D. A., Byerly, G. R., Booth, D. B., Hetherington, M. J., and Zartman, R. E., 1987a, Geologic map of the Chelan 30' by 60' Quadrangle, Washington: U. S. Geological Survey, scale 1:100,000.

Tabor, R. W., Haugerud, R. A., Brown, E. H., Babcock, R. S., and Miller, R. B., 1989, Accreted Terranes of the North Cascades Range, Washington, International Geologic Congress Trip T307: Washington, D.C., American Geophysical Union, 62 p.

Tabor, R. W., Zartman, R. E., and Frizzell, V. A., Jr., 1987b, Possible tectonostratigraphic terranes in the North Cascades crystalline core, Washington, *in* Schuster, J. E., ed., Selected Papers on the Geology of Washington: Anaheim, CA, United States, Washington Division of Geology and Earth Resources, p. 107-127.

Umhoefer, P. J., and Miller, R. B., 1996, Mid-Cretaceous thrusting in the southern Coast Belt, British Columbia and Washington, after strike-slip fault reconstruction: Tectonics, v. 15, p. 545-565.

Valley, P. M., Whitney, D. L., Paterson, S. R., Miller, R. B., and Alsleben, H., 2003, Metamorphism of the deepest exposed arc rocks in the Cretaceous to Paleogene Cascades belt, Washington: evidence for large- scale vertical motion in a continental arc: Journal of Metamorphic Geology, v. 21, p. 203-220.

Van Diver, B. B., 1967, Contemporaneous faulting-metamorphism in Wenatchee Ridge area, Northern Cascades, Washington: American Journal of Science, v. 265, p. 132-150.

Walker, N. W., and Brown, E. H., 1991, Is the southeast Coast Plutonic Complex the consequence of accretion of the Insular Superterrane: Evidence from U-Pb zircon geochronometry in the Northern Washington Cascades: Geology, v. 19, p. 714-717.

Wells, M. L., Hoisch, T. D., Hanson, L. M., and Wolff, E. D., 1999, Rapid thrust burial and subsequent partial exhumation, hinterland of the Sevier Orogen: Geological Society of America Abstracts with Programs, v. 31, p. 107.

Wendt, I., and Carl, C., 1991, The statistical distribution of the mean squared weighted deviation: Chemical Geology, v. 86, p. 275-285.
Wernicke, B., and Getty, S. R., 1997, Intracrustal subduction and gravity currents in the deep crust: Sm-Nd, Ar-Ar, and thermobarometric constraints from the Skagit Gneiss Complex, Washington: Geological Society of America Bulletin, v. 109, p. 1149-1166.
Whitney, D. L., 1992, High-pressure metamorphism in the western Cordillera of North America: An example from the Skagit Gneiss, North Cascades: Journal of Metamorphic Geology, v. 10, p. 71-85.
Whitney, D. L., Miller, R. B., and Paterson, S. R., 1999, P-T-t evidence for mechanisms of vertical tectonic motion in a contractional orogen: north-western US and Canadian Cordillera: Journal of Metamorphic Geology, v. 17, p. 75-90.
Willett, S. D., 1999, Rheological dependence of extension in wedge models of convergent orogens: Tectonophysics, v. 305, p. 419-435.
Willett, S. D., and Beaumont, C., 1994, Subduction of Asian lithospheric mantle beneath Tibet inferred from models of continental collision: Nature, v. 369, p. 642-645.
York, D., 1969, Least squares fitting of a straight line with correlated errors: Earth and Planetary Science Letters, v. 5, p. 320-324.
Zeitler, P. K., Meltzer, A. S., Koons, P. O., Craw, D., Hallet, B., Chamberlain, C. P., Kidd, W. S. F., Park, S. K., Seeber, L., Bishop, M., and Shroder, J., 2001, Erosion, Himalayan geodynamics, and the geomorphology of metamorphism: GSA Today, v. 11, p. 4-9.

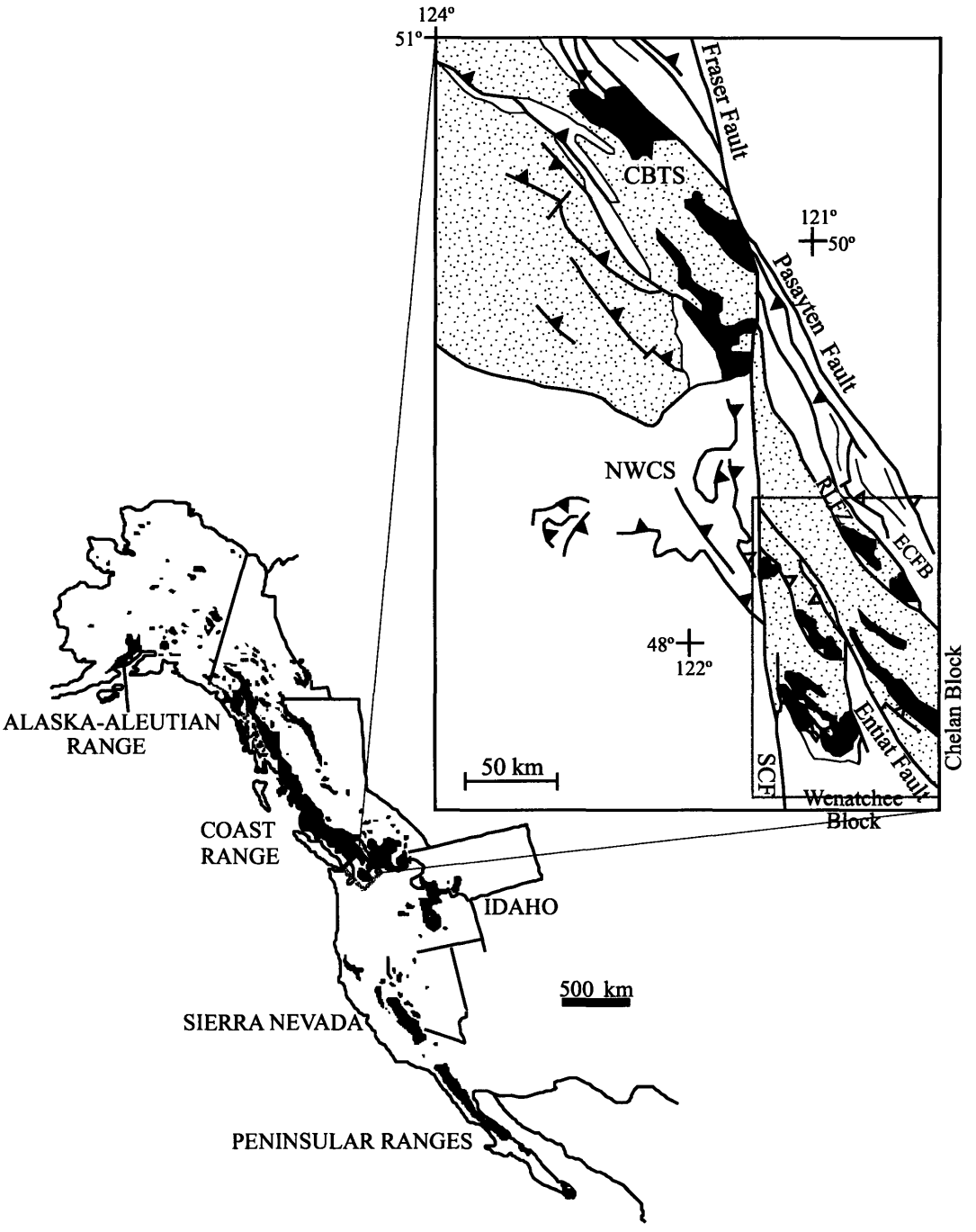

Figure 1. Sketch map of Mesozoic and Paleogene arc plutons in the western North American Cordillera (after Miller et al., 2000). Inset emphasizes distribution of metamorphic rocks (speckled pattern) and plutons (dark grey). Also shown are the Coast Belt thrust system (CBTS), lower-grade rocks of the Eastern Cascades fold belt (ECFB), and Northwest Cascades fault system (NWCS). The dextral Fraser-Straight Creek (SCF) fault offsets the Cascades core from the main part of the Coast Belt. The Ross Lake fault zone (RLFZ) marks the eastern boundary of the core. The Entiat fault is a Tertiary, high-angle fault that divides that Cascades core into the Wenatchee and Chelan blocks.

Figure 2. Geologic map of the Cascades core after Brown and Walker (1993) and Haugerud et al. (1991). Plutons are shown in a random dashed pattern. The largest dashes denote ca. 96-88 Ma plutons; intermediate dashes denote ca. 79-65 Ma plutons; and the smallest dashes denote ca. 50-46 Ma plutons. Heavy lines represent faults whereas light lines represent depositional or intrusive contacts. Abbreviations are as follows: A, Alma Creek; BL, Bench Lake; BP, Black Peak; BR, Bearcat Ridge; CL, Cyclone Lake; CO, Cooper Mountain; CP, Cardinal Peak; CPB, Cloudy Peak batholith; CV, Chaval; DC, Downey Creek; DD; Dinkelman decollement; DF, Dirtyface; DH, Duncan Hill; EN, Entiat; EL, Eldorado orthogneiss; GH, Golden Horn; H, Haystack; HL, Hidden Lake; JL, Jordan Lakes; MB, Mount Buckindy; MC, Marble Creek; MSB, Mount Stuart; OP, Oval Peak; RC, Railroad Creek; RLFZ, Ross Lake fault zone; RP, Riddle Peaks; SC, Sloan Creek; SG, Swakane Gneiss; SM, Sulphur Mountain; TP, Tenpeak; WRG, Wenatchee Ridge Gneiss. $^{40}Ar/^{39}Ar$ dates obtained in this study are shown with an "h" denoting hornblende, "m" denoting muscovite, and "b" denoting biotite.

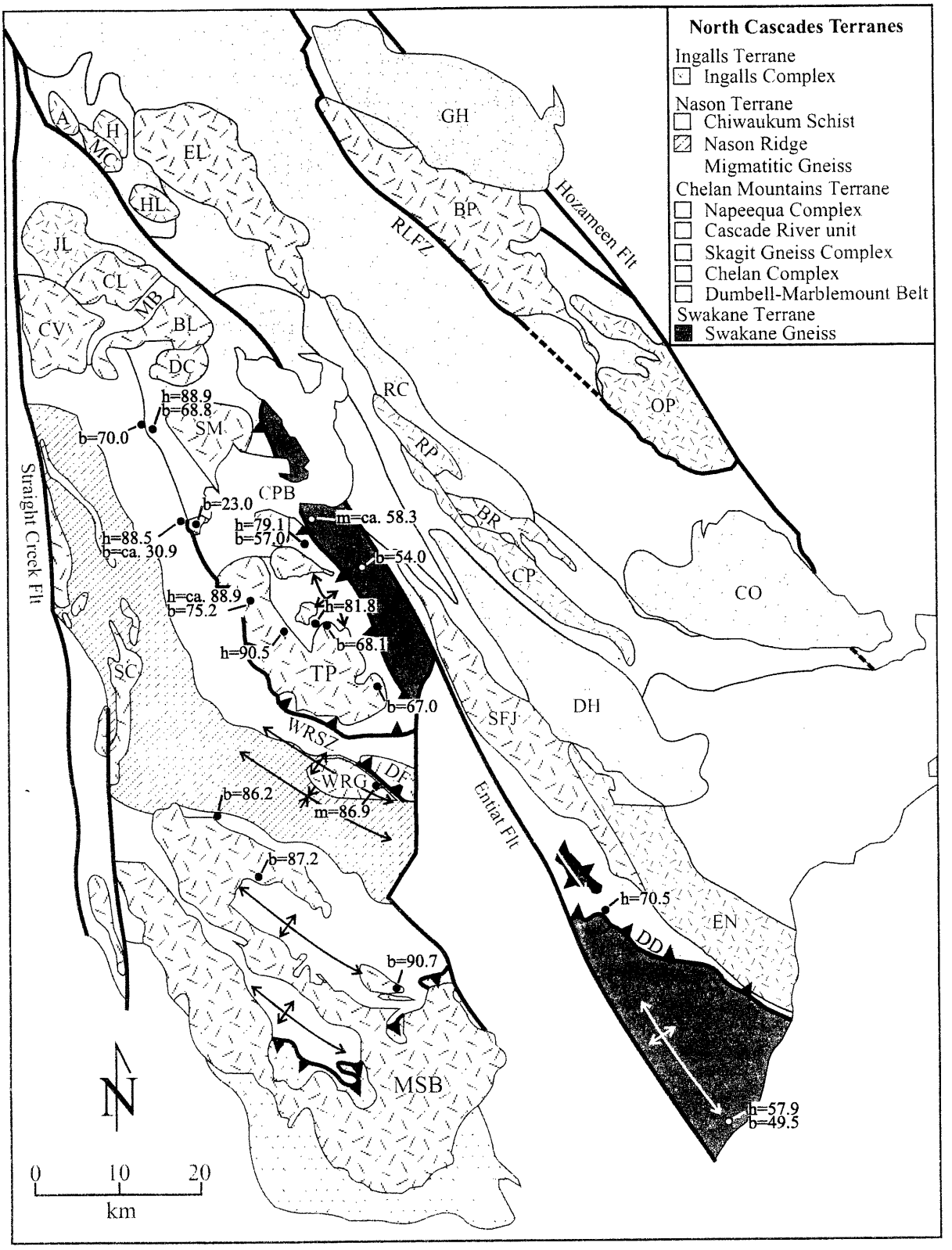

Figure 2. Caption on opposite page.

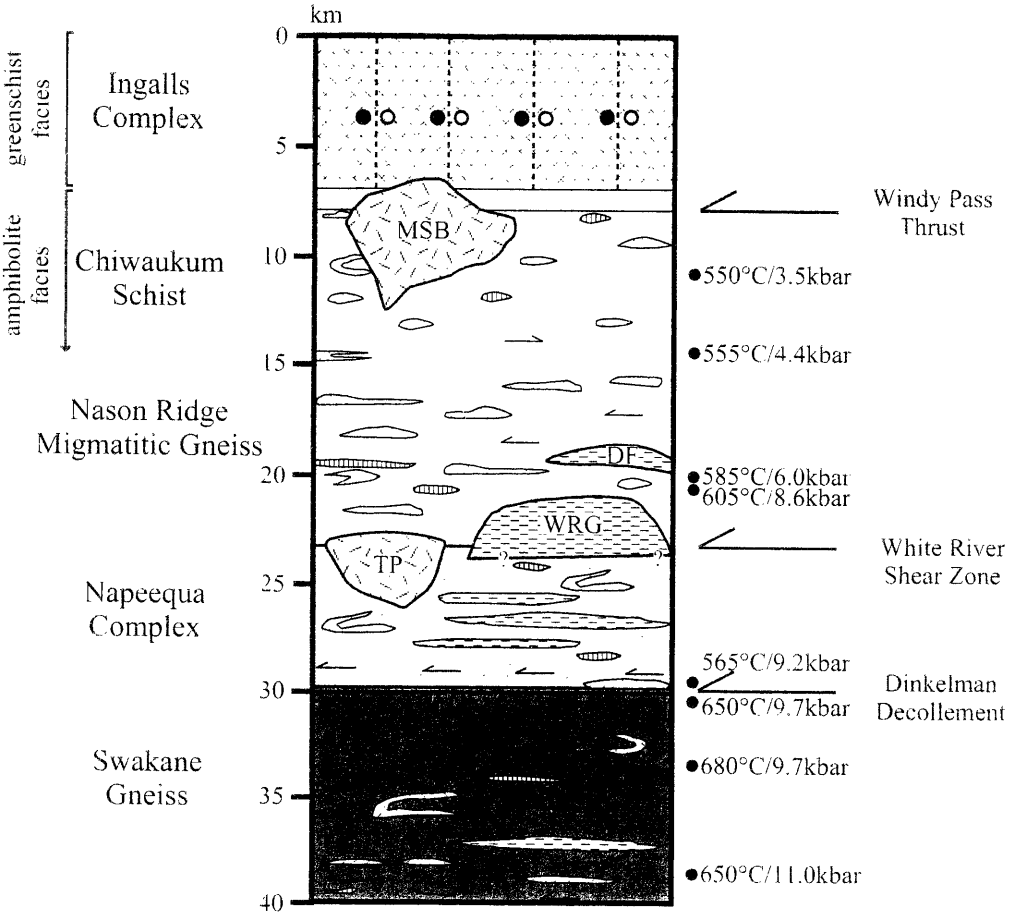

Figure 3. Schematic diagram of the North Cascades crustal section modified from Miller and Paterson (2001b). Random dashes denote plutons with mostly magmatic fabrics, whereas bold horizontal dashes denote intrusive rocks with strongly developed solid-state deformation and/or intense magmatic foliation. Other lenses in the Chiwaukum and Napeequa units are amphibolite, metaperidotite and minor marble, and half-arrows show areas with non-coaxial shear. Vertical dashed lines are faults in the Ingalls Complex. Numbers on right side of diagram list representative temperatures (°C) and pressures (kbar) summarized in Miller and Paterson (2001b). Abbreviations are the same as in figure 2.

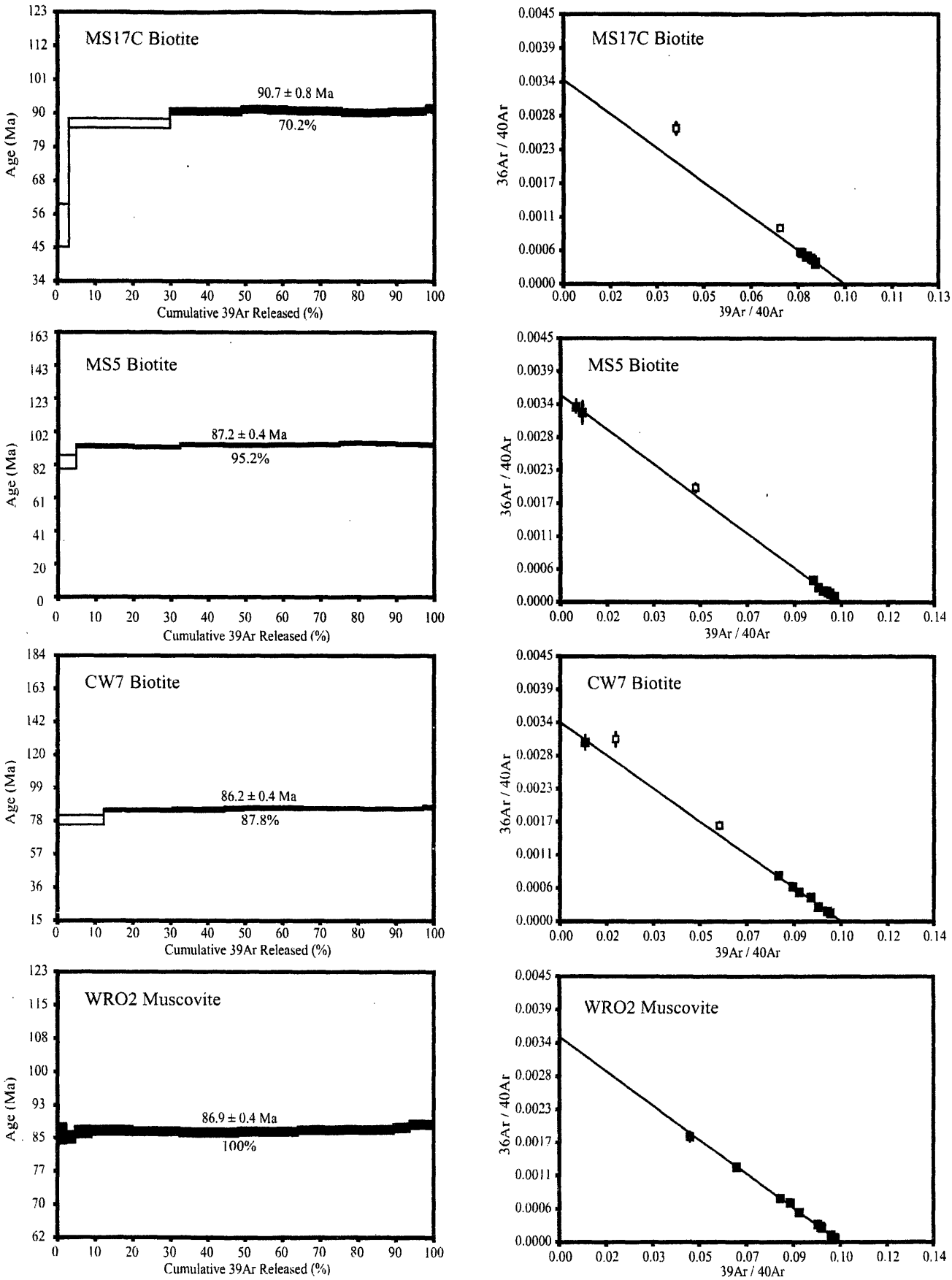

Figure 4. Ar release spectrum and inverse isochron plots from samples collected from the southern Wenatchee block. On Ar release spectra, filled black steps were included in regression, open steps were not. On isochron plots, filled squares are data points that are included in the linear regression, whereas open squares are data points that were not included.

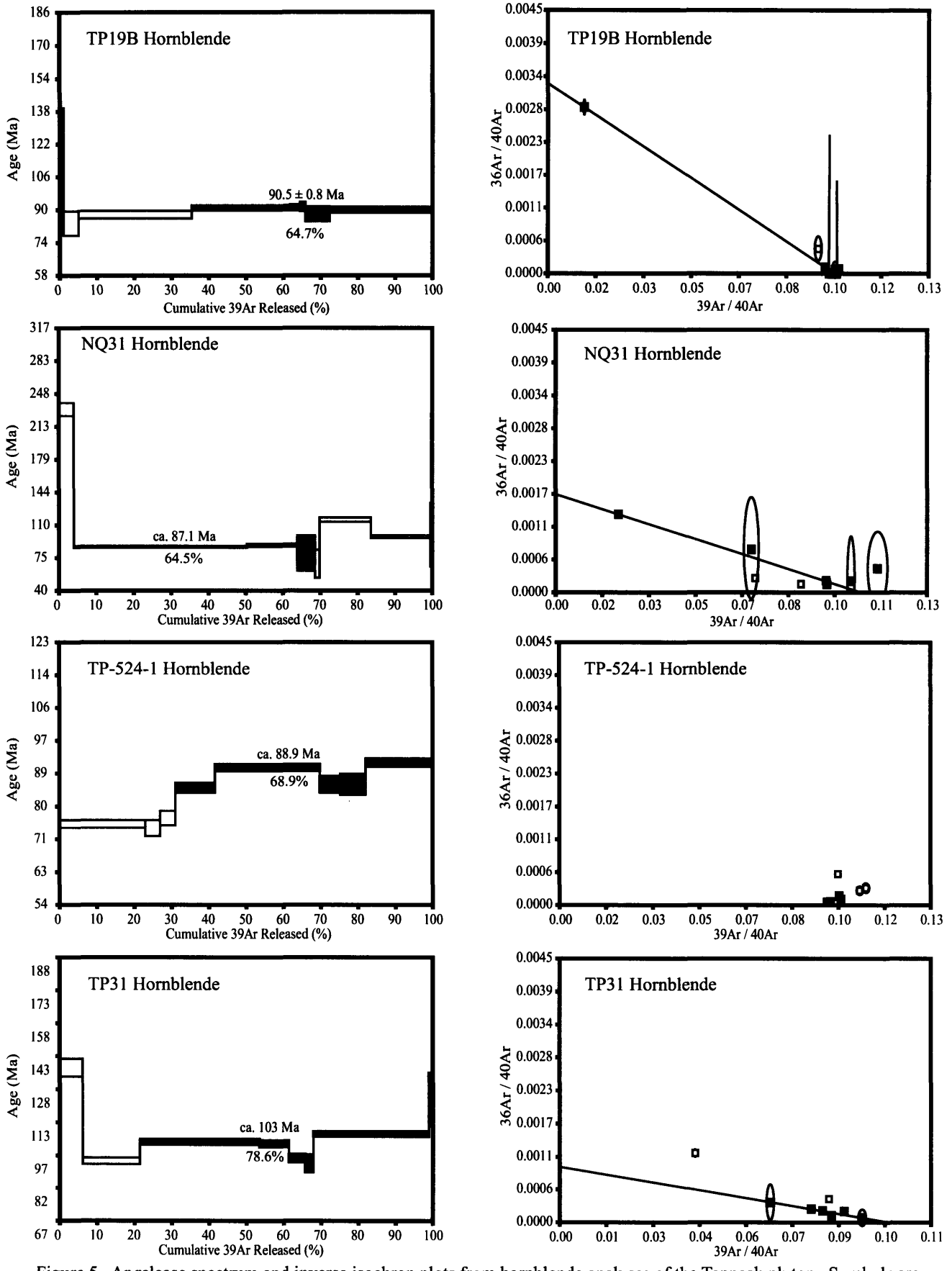

Figure 5. Ar release spectrum and inverse isochron plots from hornblende analyses of the Tenpeak pluton. Symbols are the same as figure 4.

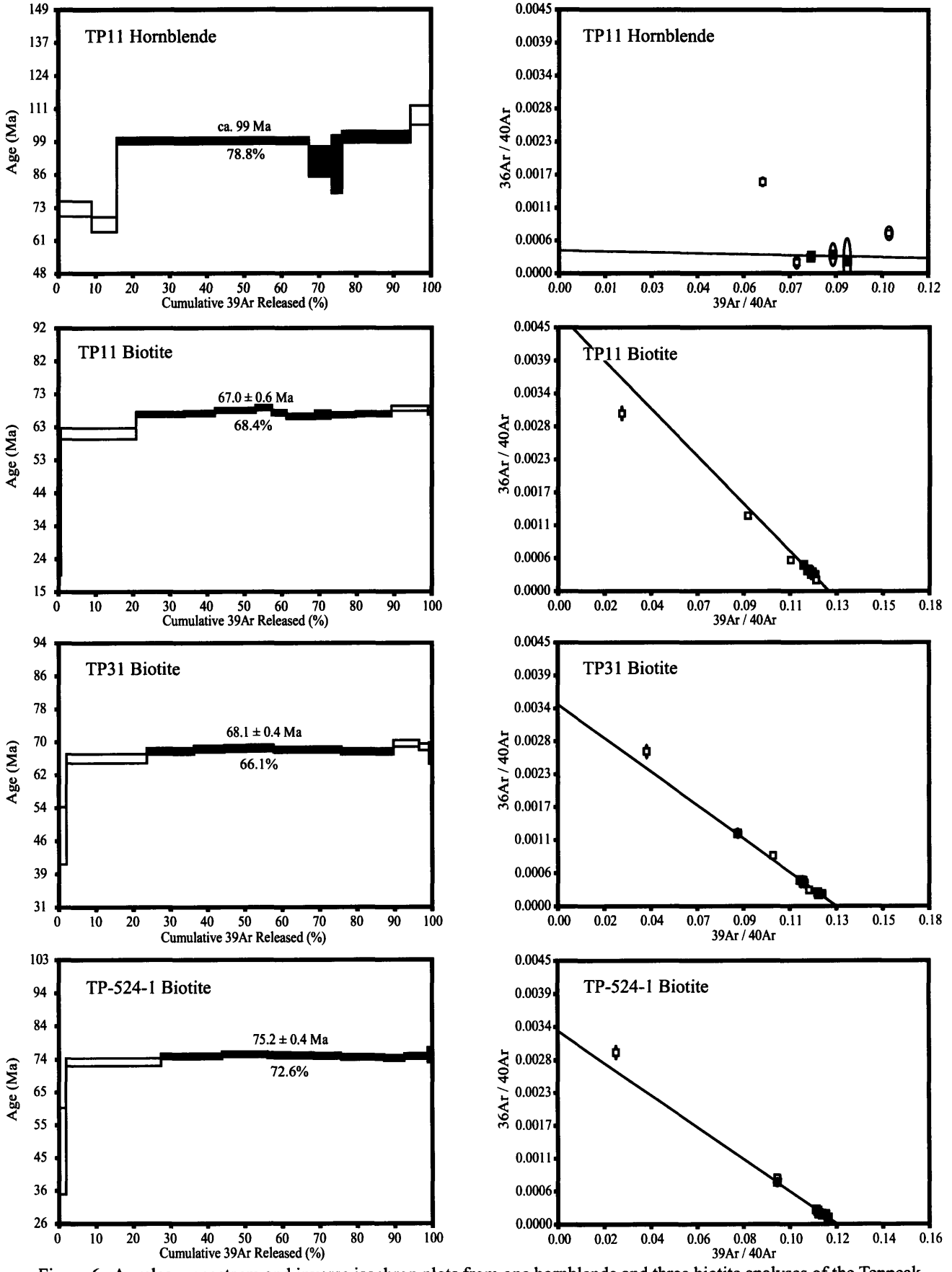

Figure 6. Ar release spectrum and inverse isochron plots from one hornblende and three biotite analyses of the Tenpeak pluton. Symbols are the same as figure 4.

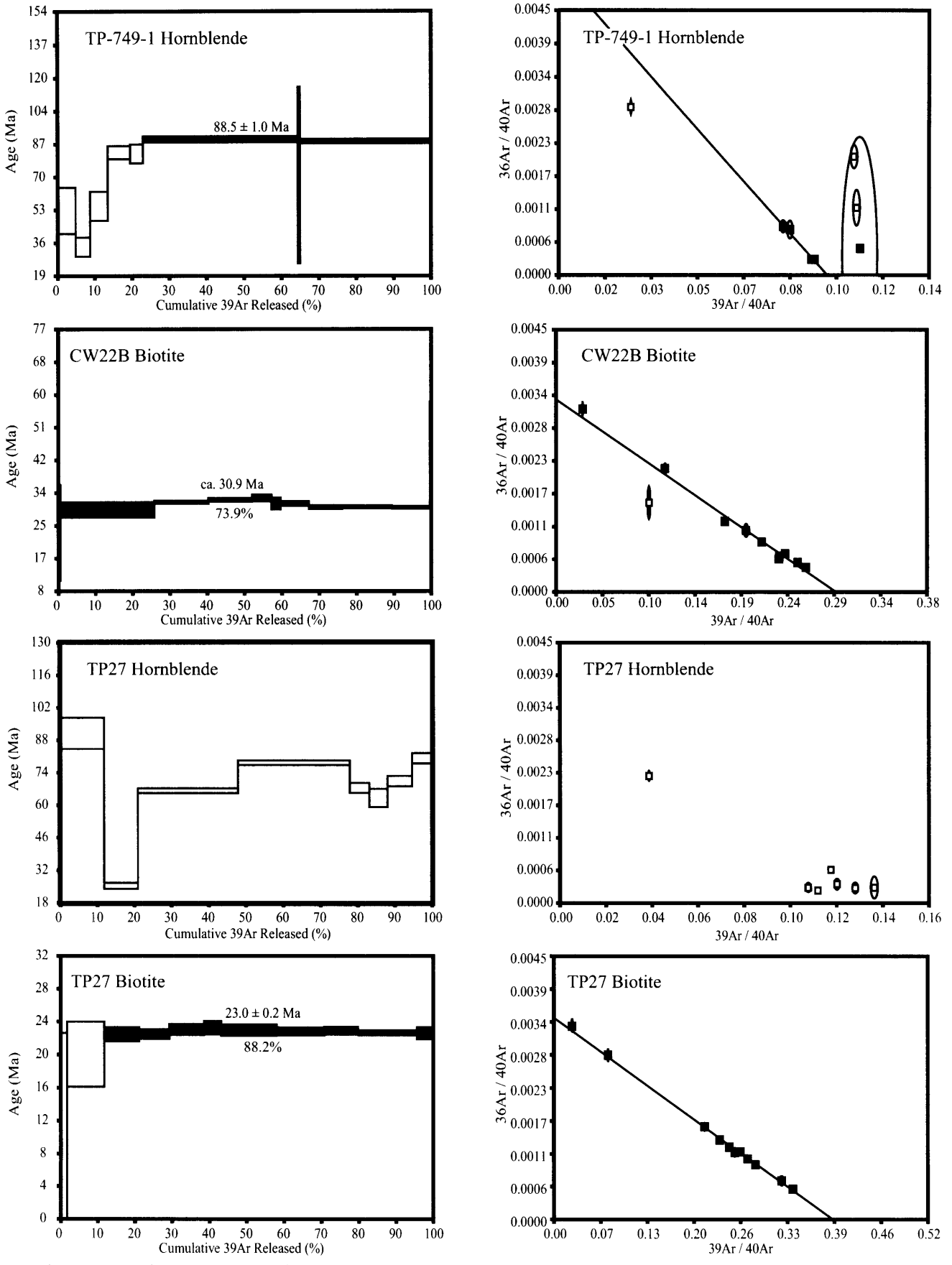

Figure 7. Ar release spectrum and inverse isochron plots from Chiwaukum amphibolite and biotite schist and from the northernmost Tenpeak pluton. Symbols are the same as figure 4.

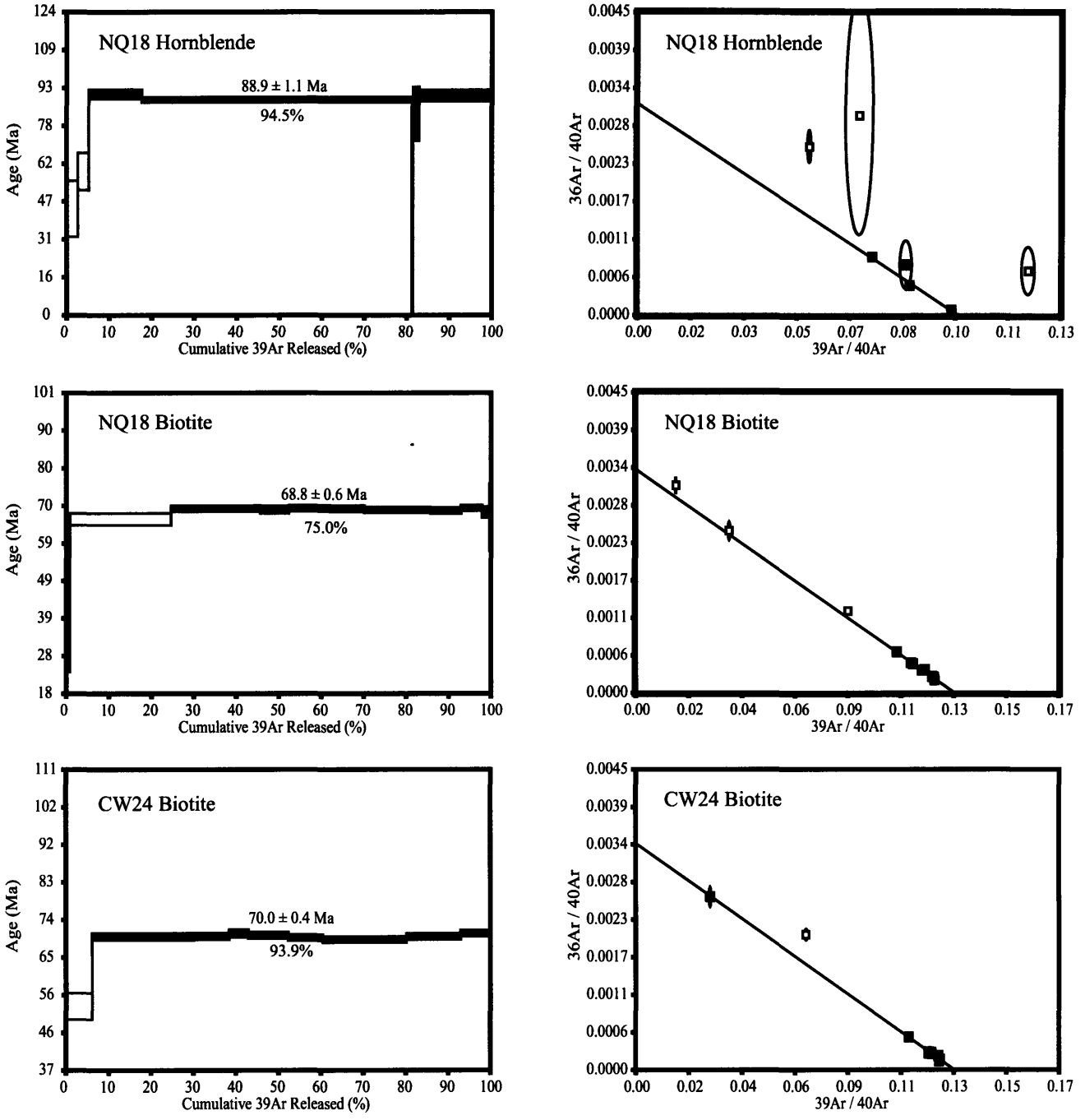

Figure 8. Ar release spectrum and inverse isochron plots from Napeequa amphibolite and Chiwaukum biotite schist. Symbols are the same as figure 4.

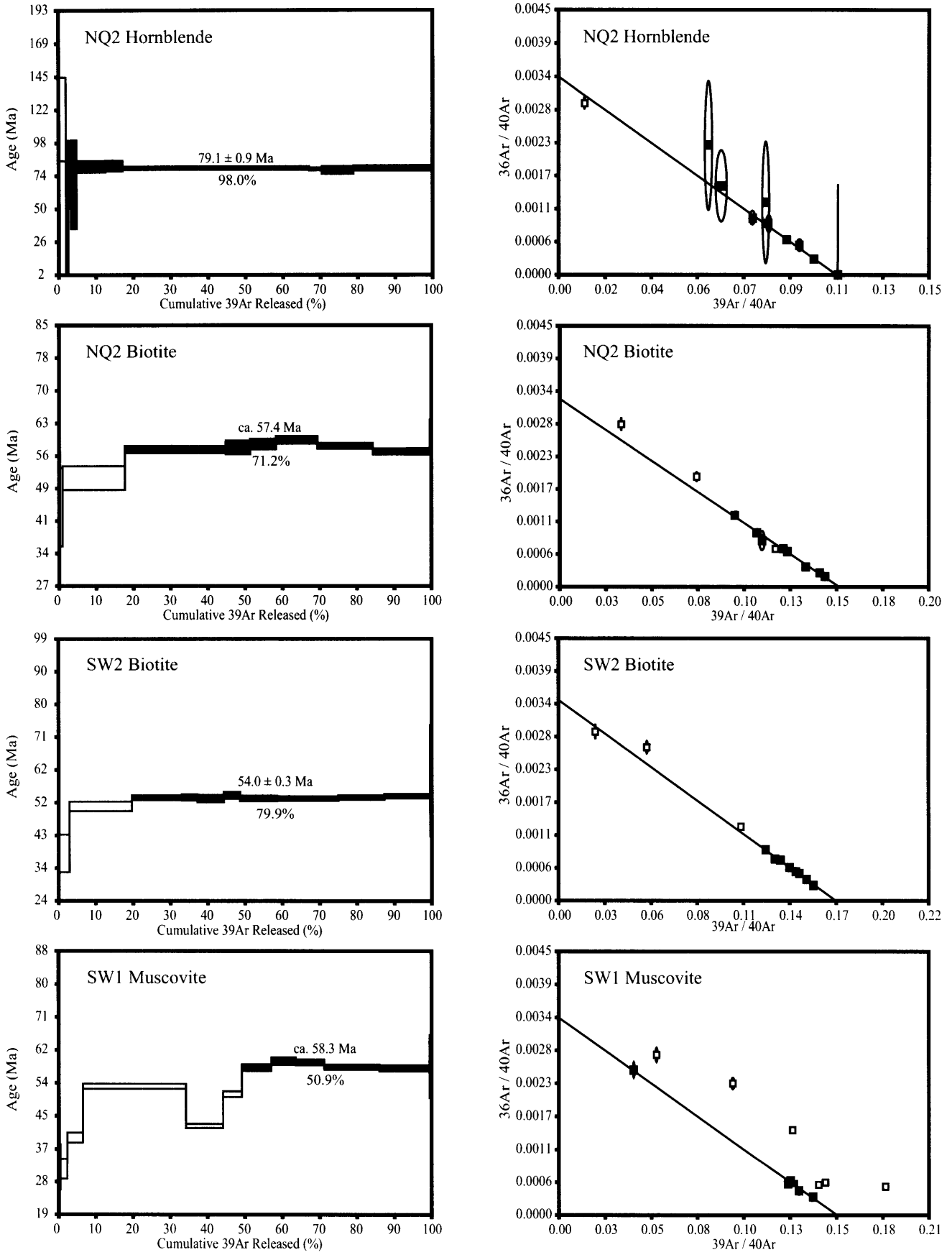

Figure 9. Ar release spectrum and inverse isochron plots from Napeequa amphibolite, Swakane garnet-kyanite gneiss and a leucogranite dike that crosscuts the Swakane Gneiss. All samples collected in the Wenatchee block. Symbols are the same as figure 4.

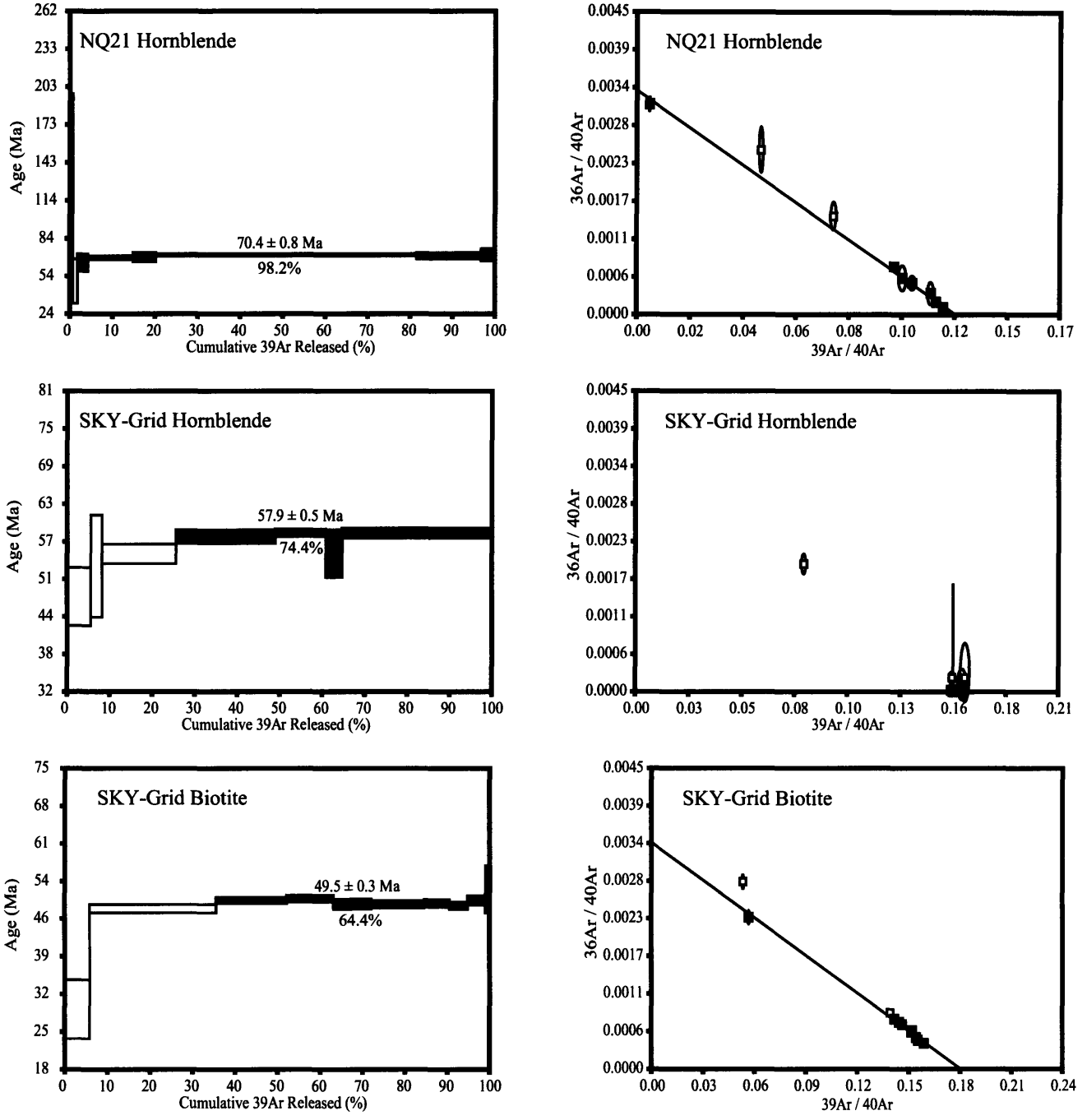

Figure 10. Ar release spectrum and inverse isochron plots from Napeequa and Swakane amphibolite samples collected in the Chelan block. Symbols are the same as figure 4.

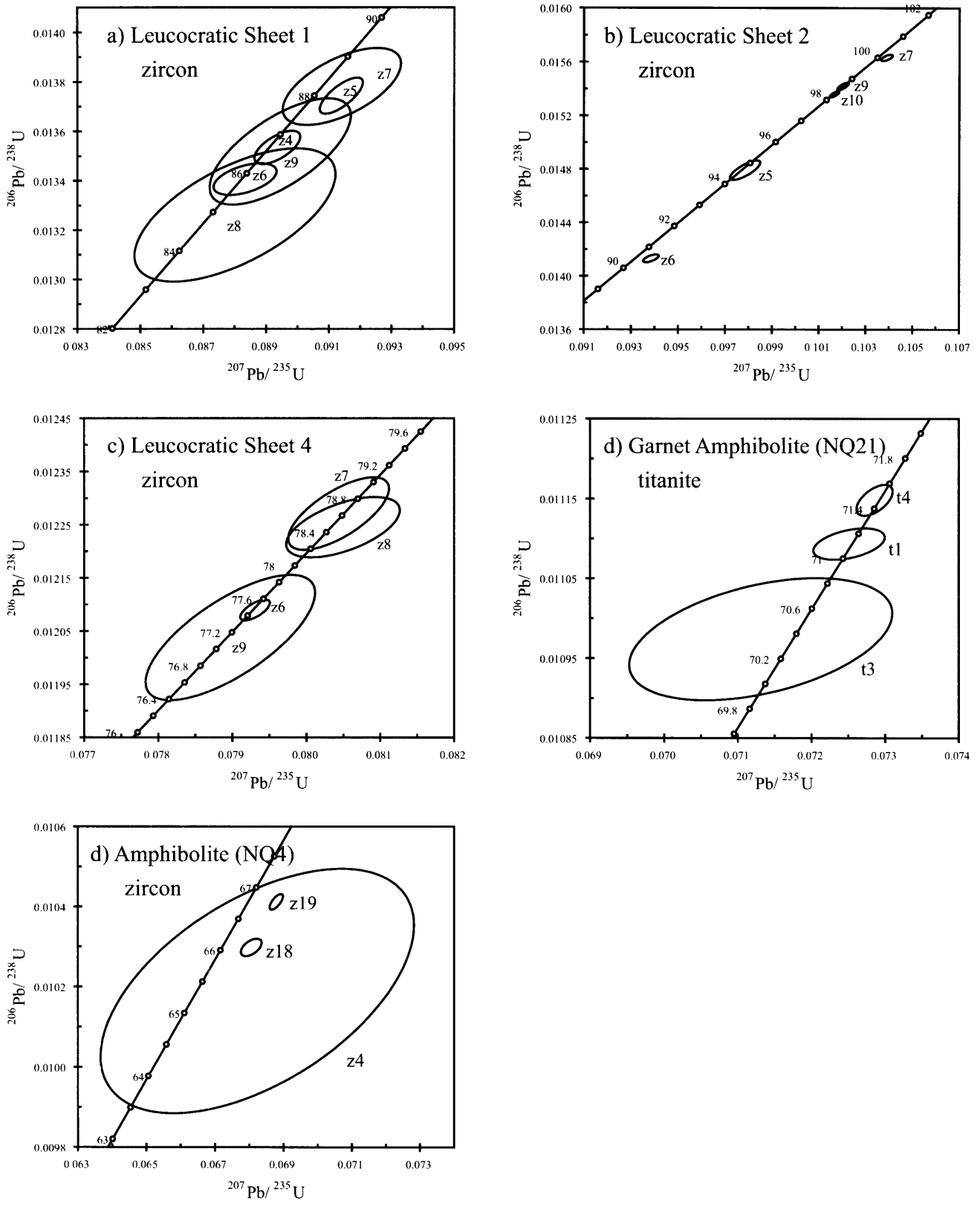

Figure 11. U-Pb concordia diagrams from leucocratic orthogneiss sheets (a-c) and Napeequa amphibolite (d-e).

Figure 2. Geologic map of the Cascades core after Brown and Walker (1993) and Haugerud et al. (1991). Plutons are shown in a random dashed pattern. The largest dashes denote ca. 96-88 Ma plutons; intermediate dashes denote ca. 79-65 Ma plutons; and the smallest dashes denote ca. 50-46 Ma plutons. Heavy lines represent faults whereas light lines represent depositional or intrusive contacts. Abbreviations are as follows: A, Alma Creek; BL, Bench Lake; BP, Black Peak; BR, Bearcat Ridge; CL, Cyclone Lake; CO, Cooper Mountain; CP, Cardinal Peak; CPB, Cloudy Peak batholith; CV, Chaval; DC, Downey Creek; DD; Dinkelman decollement; DF, Dirtyface; DH, Duncan Hill; EN, Entiat; EL, Eldorado orthogneiss; GH, Golden Horn; H, Haystack; HL, Hidden Lake; JL, Jordan Lakes; MB, Mount Buckindy; MC, Marble Creek; MSB, Mount Stuart; OP, Oval Peak; RC, Railroad Creek; RLFZ, Ross Lake fault zone; RP, Riddle Peaks; SC, Sloan Creek; SG, Swakane Gneiss; SM, Sulphur Mountain; TP, Tenpeak; WRG, Wenatchee Ridge Gneiss. $^{40}Ar/^{39}Ar$ dates obtained in this study are shown with an "h" denoting hornblende, "m" denoting muscovite, and "b" denoting biotite.

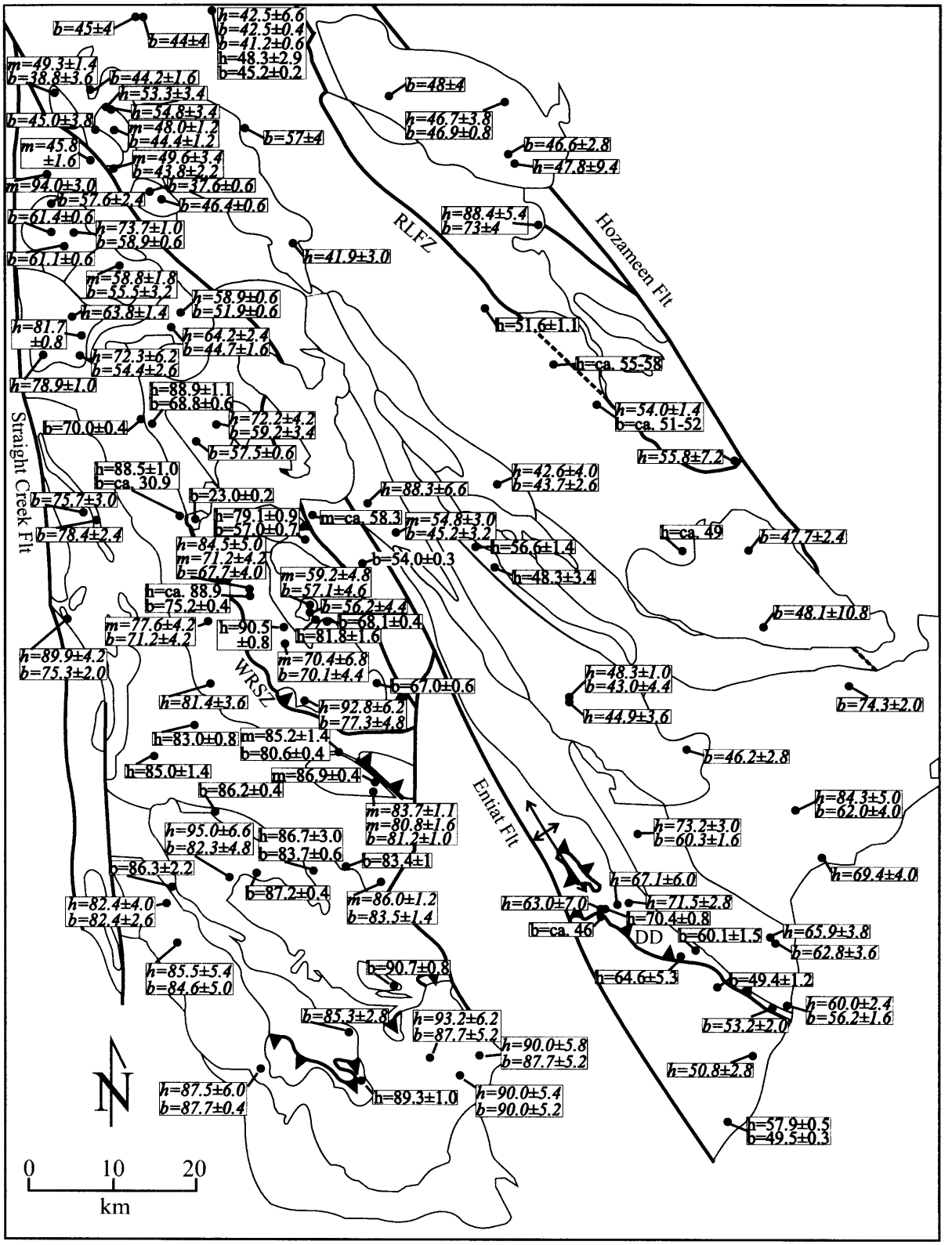

Figure 12. Caption on opposite page.

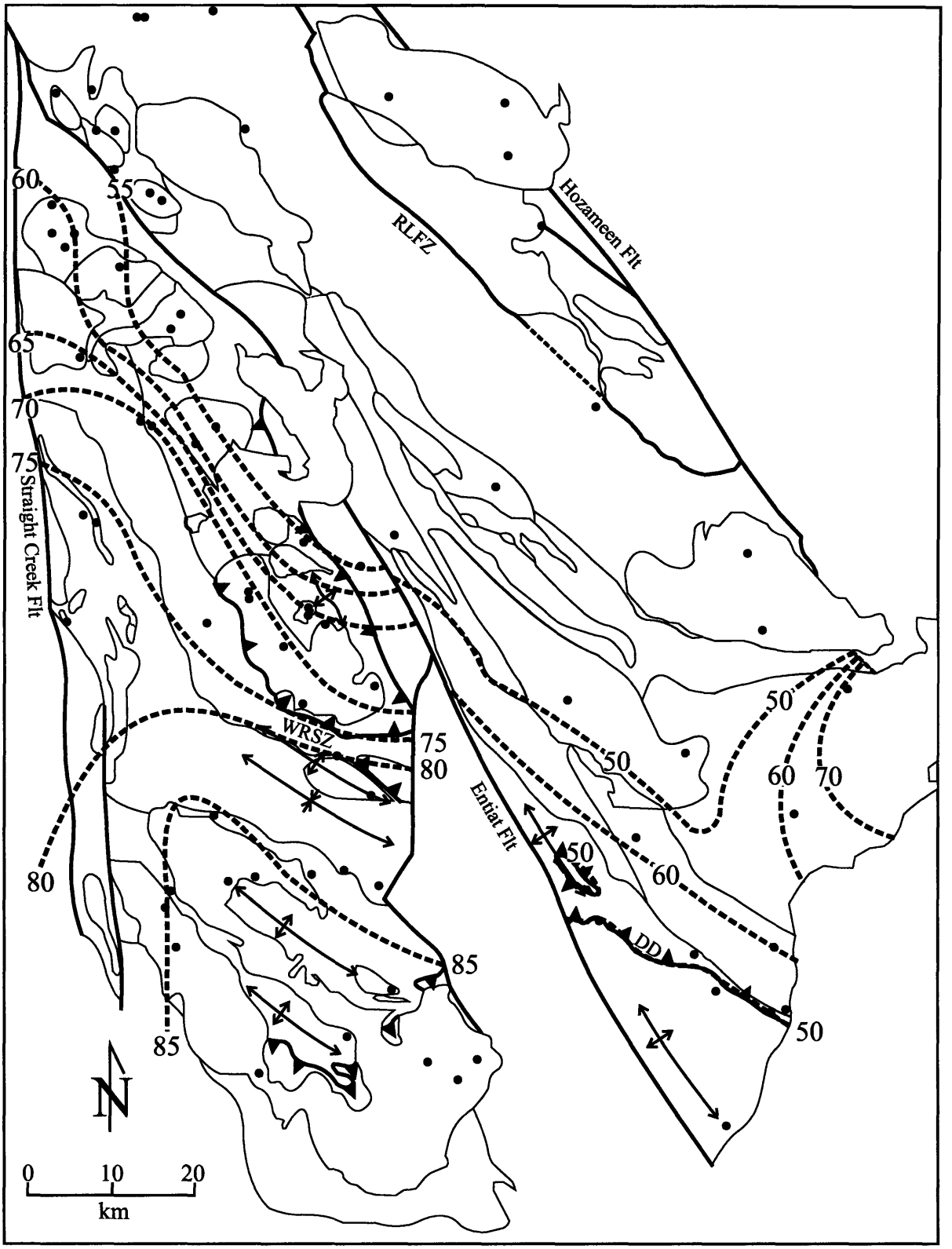

Figure 13. Geologic map of the Cascades core after Brown and Walker (1993) and Haugerud et al. (1991) emphasizing **biotite** K-Ar and $^{40}Ar/^{39}Ar$ dates. Heavy, dashed red lines are contours of the data. Data sources are the same as in figure 13.

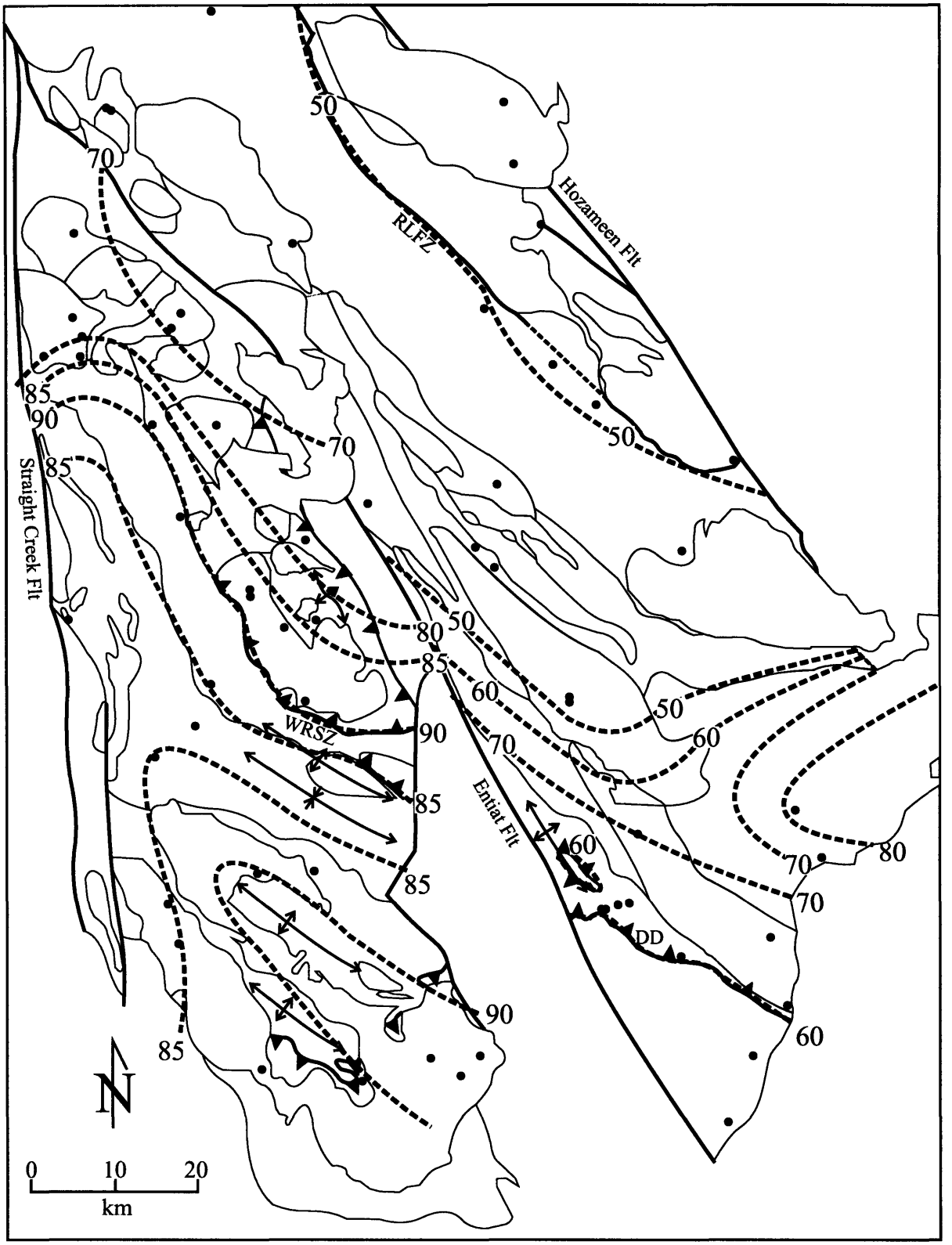

Figure 14. Geologic map of the Cascades core after Brown and Walker (1993) and Haugerud et al. (1991) emphasizing **hornblende** K-Ar and $^{40}Ar/^{39}Ar$ dates. Heavy, dashed red lines are contours of the data. Data sources are the same as in figure 13.

Step 1: Rotation of block during contraction (~90 Ma)

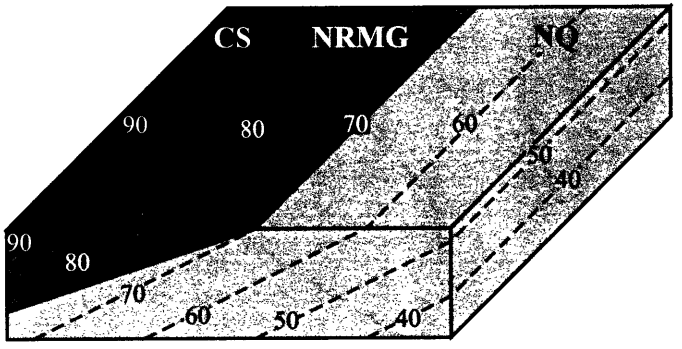

Step 2: Uplift and rotation of Tenpeak domain (ca. 85-70 Ma)

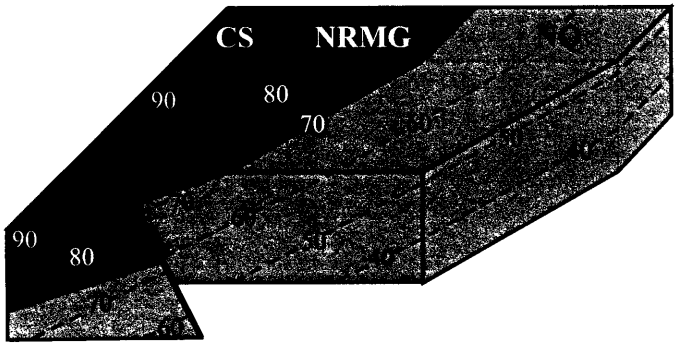

Step 3: Erosion of Tenpeak domain and underthrusting of Swakane Gneiss (ca.70 Ma)

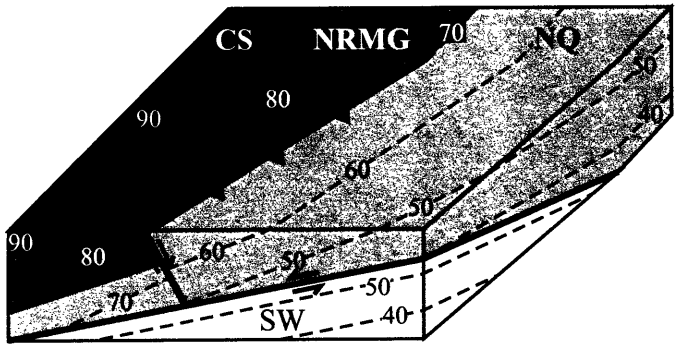

Step 4: Exhumation of Swakane Gneiss by low-angle normal faulting (ca. 50 Ma)

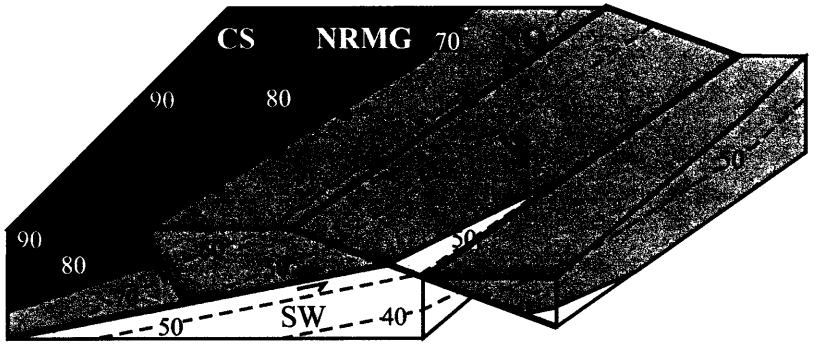

Figure 15. Schematic block diagrams that illustrate the tectonic evolution of the Wenatchee block. See text for details. Red dashed lines represent lines of equal biotite cooling ages (Ma). Abbreviations as follow: CS, Chiwaukum Schist; NR, Nason Ridge Migmatitic Gneiss; NQ, Napeequa Complex; SW, Swakane Gneiss.

Table 1. $^{40}Ar/^{39}Ar$ data.

Sample	Mineral	K/Ca	Total Fusion Age (Ma)	±	Plateau Age (Ma)	±	MSWD	# of steps included	$\%^{39}Ar_K$ on plateau	Isochron Age (Ma)	±	MSWD	# of steps included	initial $^{40}Ar/^{36}Ar$	±
MS17C	bt	13.8	88.4	0.9	**90.7**	**0.8**	0.55	8 of 10	70.2	90.8	2.4	0.64	8 of 10	293.1	50.6
MS5	bt	14.3	86.6	0.5	**87.2**	**0.4**	1.81	12 of 15	95.2	87.7	0.7	1.70	12 of 15	269.9	28.7
CW7	bt	0.83	85.0	0.5	**86.2**	**0.4**	1.44	9 of 11	87.8	86.2	0.6	1.63	9 of 11	295.8	10.7
WRO2	musc	21.1	86.8	0.4	**86.9**	**0.4**	1.63	11 of 11	100	87.1	0.4	1.45	12 of 12	287.5	8.5
TP19B	hbld	0.04	89.7	1.0	**90.5**	**0.8**	1.56	5 of 8	64.7	90.2	0.9	1.86	7 of 8	306.7	14.7
NQ31	hbld	0.06	98.0	1.4	87.1	1.1	1.42	3 of 8	64.5	**81.8**	**1.6**	1.57	6 of 8	594.5	28.2
TP524-1	hbld	0.09	84.7	0.6	88.9	0.7	20.76	5 of 8	68.9	94.5	1.7	1.38	5 of 8	-493.6	242.0
TP31	hbld	0.07	105.1	0.8	103.5	0.8	25.45	6 of 8	78.6	88.1	6.9	2.72	7 of 8	1053.5	381.1
TP11	hbld	0.05	94.6	1.2	99.0	1.3	4.06	4 of 7	78.8	26.5	30.9	0.84	4 of 7	2539.8	11537
TP11	bt	13.7	65.8	0.7	**67.0**	**0.6**	2.05	9 of 13	68.4	69.0	1.4	1.06	9 of 13	210.9	51.4
TP31	bt	21.3	67.3	0.4	**68.1**	**0.4**	0.79	6 of 11	66.1	68.3	0.6	1.10	8 of 11	315.7	39.4
TP-524-1	bt	0.50	74.2	0.5	**75.2**	**0.4**	0.73	9 of 11	72.6	75.1	0.7	0.82	9 of 11	302.2	37.7
TP-749-1	hbld	0.04	82.5	1.1	**88.5**	**1.0**	0.93	3 of 8	77.1	91.1	1.4	1.24	5 of 8	193.8	34.0
CW22B	bt	20.6	30.7	0.6	30.9	0.3	10.05	10 of 11	73.9	30.8	0.4	11.05	10 of 11	302.4	8.5
TP27	hbld	0.09	69.8	1.1	72.0	0.8	76.25	6 of 8	79.1	95.3	2.8	44.01	6 of 8	-530.3	137.1
TP27	bt	3.63	22.5	0.5	**23.0**	**0.2**	0.63	9 of 11	88.2	23.2	0.3	0.66	11 of 11	290.1	7.1
NQ18	hbld	0.04	86.6	1.2	**88.9**	**1.1**	2.20	4 of 7	94.5	88.3	1.4	1.83	4 of 7	317.9	27.1
NQ18	bt	1.17	68.0	0.7	**68.8**	**0.6**	0.50	8 of 11	75.0	68.7	0.9	0.58	8 of 11	289.7	27.1
CW24	bt	0.18	68.9	0.4	**70.0**	**0.4**	1.41	9 of 10	93.9	70.0	0.5	1.60	9 of 10	294.7	15.0
NQ2	hbld	0.04	79.5	1.4	**79.1**	**0.9**	0.59	9 0f 10	98.0	79.2	1.8	0.63	9 of 10	296.6	35.1
NQ2	bt	0.68	56.5	0.7	57.4	0.5	2.26	8 of 11	71.2	**57.0**	**0.7**	1.94	8 of 11	308.5	12.9
SW2	bt	54.8	53.1	0.4	**54.0**	**0.3**	0.69	8 of 11	79.9	54.1	0.7	0.76	8 of 11	290.7	19.4
SW1	musc	58.5	53.4	0.3	58.3	0.4	3.52	6 of 12	50.9	58.2	0.6	4.43	6 of 12	296.7	15.4
NQ21	hbld	0.05	70.5	1.0	**70.4**	**0.8**	1.73	7 of 9	98.2	70.4	0.8	2.04	7 of 9	300.3	11.8
SKY-Grid	hbld	0.08	56.5	0.6	**57.9**	**0.5**	1.25	4 of 7	74.4	58.9	2.2	0.05	4 of 7	-495.6	1423.3
SKY-Grid	bt	0.40	48.0	0.5	**49.5**	**0.3**	1.86	9 of 11	64.4	49.5	0.5	2.13	9 of 11	295.1	12.9

Table 2. U-Pb analyses from leucocratic orthogneiss sheets and Napeequa amphibolite.

	Composition						Isotopic Ratios								Dates (Ma)				
Frac[a]	Wt (μg)[b]	U (ppm)	Pb (ppm)	Th[c] / U	Pb*[d] / Pbc	Pbc[d] (pg)	$^{206}Pb^{e}/^{204}Pb$	$^{208}Pb^{f}/^{206}Pb$	$^{206}Pb^{f}/^{238}U$	% err[g]	$^{207}Pb^{f}/^{235}U$	% err[g]	$^{207}Pb^{f}/^{206}Pb$	% err[g]	$^{206}Pb^{h}/^{238}U$	$^{207}Pb^{h}/^{235}U$	$^{207}Pb^{h}/^{206}Pb$	corr. coef.	Discord-ance
LSH1: LEUCOCRATIC SHEET																			
z4	6.7	424.2	5.5	0.199	7.2	5.1	491	0.064	0.013536	(.40)	0.08936	(.67)	0.047880	(.51)	86.7	86.9	93.4	0.641	7.2
z5	2.9	340.2	4.5	0.204	3.0	4.2	216	0.066	0.013782	(.92)	0.09142	(1.68)	0.048108	(1.36)	88.2	88.8	104.6	0.596	15.8
z6	1.9	364.3	4.7	0.193	7.4	1.2	512	0.062	0.013407	(.39)	0.08833	(.92)	0.047784	(.81)	85.9	85.9	88.6	0.489	3.1
z7	2.0	319.1	4.2	0.187	6.1	1.3	425	0.060	0.013744	(.43)	0.09139	(.61)	0.048227	(.42)	88.0	88.8	110.5	0.736	20.5
z8	0.6	156.3	2.0	0.221	1.6	0.7	126	0.071	0.013261	(1.67)	0.08801	(2.97)	0.048133	(2.35)	84.9	85.6	105.8	0.612	19.9
z9	0.6	327.6	4.4	0.227	2.0	1.2	151	0.073	0.013519	(1.30)	0.08945	(2.05)	0.047989	(1.51)	86.6	87.0	98.8	0.678	12.4
LSH2: LEUCOCRATIC SHEET																			
z5	2.0	1015.5	14.6	0.260	7.0	4.1	473	0.083	0.014792	(.40)	0.09785	(.54)	0.047978	(.34)	94.7	94.8	98.1	0.773	3.6
z6	1.6	1448.7	18.9	0.075	17.2	1.7	1200	0.024	0.014132	(.17)	0.09385	(.28)	0.048164	(.22)	90.5	91.1	107.3	0.636	15.8
z7	2.3	721.8	10.3	0.023	24.3	1.0	1709	0.007	0.015633	(.12)	0.10390	(.19)	0.048200	(.15)	100.0	100.4	109.1	0.642	8.4
z9*	4.4	1014.0	14.6	0.061	19.1	3.3	1335	0.020	0.015420	(.14)	0.10203	(.19)	0.047987	(.12)	98.6	98.6	98.6	0.766	0.0
z10*	4.5	795.5	11.7	0.201	25.1	2.1	1675	0.064	0.015361	(.12)	0.10166	(.16)	0.048001	(.10)	98.3	98.3	99.3	0.763	1.0
LSH4: LEUCOCRATIC SHEET																			
z5	6.7	391.0	6.4	0.216	39.7	1.1	2519	0.098	0.016330	(.11)	0.15630	(.23)	0.069416	(.20)	104.4	147.5	911.2	0.522	89.2
z6	5.1	389.1	4.4	0.130	22.2	1.0	1513	0.041	0.012090	(.13)	0.07931	(.20)	0.047577	(.15)	77.5	77.5	78.3	0.675	1.1
z7	2.5	297.8	3.5	0.168	6.1	1.4	423	0.054	0.012271	(.45)	0.08044	(.69)	0.047542	(.50)	78.6	78.6	76.6	0.691	-2.7
z8	1.2	466.2	5.4	0.161	7.2	0.9	502	0.052	0.012245	(.38)	0.08050	(.78)	0.047677	(.65)	78.5	78.6	83.3	0.564	5.8
z9	1.4	367.4	4.1	0.099	3.4	1.6	247	0.032	0.012038	(.80)	0.07897	(1.18)	0.047581	(.83)	77.1	77.2	78.4	0.713	1.7
NQ21: GARNET AMPHIBOLITE																			
t1*	30.7	394.8	6.4	0.172	1.8	70.5	140.1	0.055	0.011093	(.15)	0.07251	(.55)	0.047406	(.50)	71.1	71.1	69.7	0.425	-2.1
t3	81.9	17.7	0.6	0.015	0.4	36.6	46.2	0.005	0.010974	(.57)	0.07131	(2.04)	0.047131	(1.88)	70.4	69.9	55.8	0.424	-26.1
t4*	33.8	286.7	3.3	0.003	6.1	15.9	451.6	0.001	0.011148	(.14)	0.07286	(.27)	0.047398	(.23)	71.5	71.4	69.4	0.566	-3.0
NQ4: AMPHIBOLITE																			
z4	4.3	22.5	0.2	-0.004	1.0	0.8	87	-0.001	0.010190	(2.44)	0.06824	(5.49)	0.048573	(4.65)	65.35	67.03	127.2	0.537	48.9
z18*	33.6	36.9	0.3	0.013	15.0	0.7	1065	0.004	0.010298	(.17)	0.06806	(.36)	0.047934	(.31)	66.05	66.86	96.0	0.525	31.3
z19*	42.8	44.5	0.4	0.017	17.1	1.0	1211	0.006	0.010412	(.15)	0.06879	(.23)	0.047918	(.16)	66.77	67.55	95.3	0.693	30.1

[a] An asterisk next to the fraction number (i.e., z1 for zircon or t1 for sphene) indicates a small multi-grain fraction.

[b] Sample weights were estimated to within 40% using measured grain dimensions and a nominal density of 4.5 g/cm^3 for zircon and 3.5g/cm^3 for sphene.

[c] Th contents calculated from radiogenic ^{208}Pb and the $^{207}Pb/^{206}Pb$ date of the sample, assuming concordance between U-Th-Pb systems.

[d] Pb* and Pbc represent radiogenic Pb and common Pb respectively.

[e] Measured ratio corrected for fractionation and spike contribution; Pb fractionation was 0.12 ±0.04%/a.m.u. for Faraday detector or 0.20 ± 0.04%/a.m.u. for Daly detector analysis, based on daily analysis of NBS-981.

[f] Measured ratios corrected for fractionation, spike, blank, and initial common Pb; nominal U blank = 0.1 pg ± 50% (2 σ); nominal Pb blank = 2.0 pg ± 50% (2σ) or where lower the total common Pb of the analysis ±10% (2σ); measured laboratory Pb composition: $^{206}Pb/^{204}Pb = 18.287$, $^{207}Pb/^{204}Pb = 15.61$, $^{208}Pb/^{204}Pb = 38.195 \pm 0.05$ (2σ); initial Pb composition from model of Stacey and Kramers (1975) at the nominal age of the fraction (i.e. 0.1 Ga).

[g] Numbers in parentheses are the % errors reported at the 2 σ confidence interval, propagated using the algorithms of Ludwig (1980).

[h] Isotopic ages calculated using the decay constants of Jaffey et al. (1971): $\lambda(^{235}U) = 9.8485 \times 10^{-10}$ yr^{-1} and $\lambda(^{238}U) = 1.55125 \times 10^{-10}$ yr^{-1}; error in $^{207}Pb/^{206}Pb$ date reported at the 2 σ confidence interval.

Chapter 4

TIMESCALES OF THE CONSTRUCTION OF INTRUSIVE MAGMATIC SYSTEMS AT DIFFERING CRUSTAL LEVELS: EXAMPLES FROM THE MOUNT STUART AND TENPEAK INTRUSIONS, NORTH CASCADES, WA

ABSTRACT

High-precision, U-Pb geochronology is used to document the duration and episodicity of the construction of two contrasting intrusive magmatic systems, the Mount Stuart and Tenpeak intrusions. Petrologic and textural variations, internal magmatic contacts and local magma mingling indicate that the Mount Stuart and Tenpeak intrusions were constructed from multiple batches of magma during the development of the North Cascades continental magmatic arc.

The shallow-level (<4 kbar) Mount Stuart batholith (MSB) was emplaced from ca. 96.4-90.8 Ma over four punctuated intervals. Within the MSB, internal contacts between magma pulses of differing composition are gradational, and contacts between tonalite pulses of differing age are difficult to delineate. The U-Pb zircon dates suggest a general NW to SE trend in the timing of emplacement. Magmatic fabrics vary smoothly between magma pulses of differing age suggesting a nearly constant strain field over the duration of magma emplacement. U-Pb dates from primary magmatic titanite are <1.5 Myr younger than the respective zircon crystallization age of the sample, indicating rapid cooling (~100°C/km) of the batholith after emplacement.

In contrast, the Tenpeak intrusion was emplaced from ca. 92.4-89.7 Ma with <0.5 Myr time intervals between magma pulses. Within the Tenpeak intrusion, texturally and compositionally distinct phases form well-defined internal magmatic contacts, and suggest only limited mixing between magma pulses. U-Pb titanite dates indicate that the oldest phases of the intrusion cooled below the solidus <1 Myr after emplacement.

Magmatism plays a key role in the thermal evolution of a magmatic arc as an efficient mechanism of heat transfer from the lower to upper crust. Time-averaged, minimum magma emplacment rates are 2.1×10^{-4} km^3/yr and 1.2×10^{-4} km^3/yr for the MSB and Tenpeak intrusion, respectively. These rates are comparable to estimates of other continental magmatic arcs. The differences between intrusive histories of these two magmatic systems may be tied to the rate at which magma is generated and/or segregated from its source region. Alternatively, the deep-level Tenpeak intrusion may serve as a conduit that supplied a more homogeneous upper level system. At the resolution of these dates, emplacment processes appear more episodic than continuous, which supports that idea that magma is emplaced in discrete batches. The geochronologic data from the MSB

and Tenpeak intrusion suggest that magma pulses in both systems remained distinct phases and challenge the view that these systems ever formed a single, convecting magma chamber.

INTRODUCTION

Much of the intermediate-composition continental crust exposed today is the result of the interaction of subduction-related basaltic magmas with pre-existing crust in continental magmatic arcs (CMAs). However, this dynamic tectonic setting, and in particular its deep crustal evolution, is not well understood. Heat and magma are transferred upward from the mantle through the "filter" of the continental crust. Unraveling the magmatic and thermal history of CMAs is essential to understanding the maturation of arcs and ultimately the generation of continental crust.

Recent advances in geochronological techniques have made it possible to address questions related to the magmatic and thermal evolution of CMAs with high-precision temporal constraints. Modern low-blank, high-precision U-Pb geochronology permits the determination of crystallization ages of igneous rocks to a precision approaching 0.1%, but application of these techniques to the study of CMAs has been underutilized. Specifically, unresolved issues include the duration, episodicity, and rates at which individual intrusions are constructed, and the scale of compositional and temporal heterogeneity of a given magmatic system. For example, are composite intrusions constructed by continuous emplacement of small batches of magma (e.g. Coleman et al., 2004; Glazner et al., 2004) or during more punctuated intervals? For this reason, I used high-precision U-Pb geo- and thermochronology to elucidate the magmatic and thermal history of two composite intrusions within the crystalline core of the Cretaceous North Cascades arc, the Mount Stuart batholith (MSB) and the Tenpeak pluton. This study is one of the first to provide a large number of precise temporal constraints that document the intrusive history of an individual magmatic system.

The North Cascades arc presents a unique opportunity to study the thermal and magmatic evolution of CMAs for several reasons. Cretaceous plutons in the North Cascades crystallized at ~10 to 30 km depth, and thus provide a window into magmatic and structural processes at a large range of depths within the arc (Miller and Paterson,

2001b). Excellent exposure in this >30 km depth-section through the arc allows an analysis of magma emplacement styles, thermal structure, and rates of magmatism at varying crustal levels. In addition, the relatively young age of the arc (~100-45 Ma) combined with the inherent high precision of U-Pb zircon dates allow the potential of resolving absolute ages with uncertainties of less than 100 ky. This precision, coupled with an intensive sampling regime, allow an assessment of the episodicity of arc magmatism at a high resolution. Although this study focuses on the evolution of a narrow time slice through a single arc, the results will form a basis for which other arcs can be compared.

The results presented here indicate that construction of the MSB occurred over a ca. 5.6 m.y time period with at least four punctuated intervals of magma emplacement. In contrast, the Tenpeak intrusion exhibits episodic emplacement over a ca. 2.7 Myr time span with much shorter intervals (<0.5 Myr) between magma pulses. The U-Pb zircon dates reveal the complexity in the construction of each magmatic system and caution against oversimplification in interpreting geochemical or structural patterns. The use of the term "pluton" for the Tenpeak intrusion, in particular, is misleading because it implies that different compositional and textural phases are co-magmatic and that the entire body was once a single, convecting magma chamber. I will argue that this is not the case for the Tenpeak or the MSB and will use the more general terms "intrusion" or "magmatic system" instead to reflect the internal complexities. Each system evolved with chemically, texturally, and temporally distinct phases which may be related through their source region and/or level of emplacement.

GEOLOGIC SETTING

The crystalline core of the North Cascades (Cascades core) lies at the southern termination of the 1700 km long Coast Plutonic Complex, which documents the Jurassic to Eocene history of arc magmatism in the Canadian Cordillera (Friedman and Armstrong, 1995; Friedman et al., 1995; van der Heyden, 1992; Van der Heyden, 1989; Woodsworth et al., 1991) and records the final suturing of the Insular superterrane to North America (Fig. 1) (Monger et al., 1982). The Coast Plutonic Complex forms one segment of the Mesozoic-Cenozoic arc that is exposed along the length of the western

margin of North and South America and comprises the largest single concentration of plutonic rock on the western North American margin (Friedman et al., 1995).

As part of this greater than 100 Myr history of arc magmatism, the North Cascades arc comprises predominantly Late Cretaceous to Eocene intrusions, of which the Mount Stuart and Tenpeak intrusions are volumetrically significant members. Both magmatic systems were emplaced into amphibolite facies metamorphic terranes of the Wenatchee crustal block, which comprises the western half of the Cascades core between the high-angle, Tertiary Entiat fault and the core-bounding, strike-slip, Straight Creek fault (Figs. 1 and 2). The Wenatchee block displays increasing peak metamorphic pressure from 3-4 kbar pressures in the Chiwaukum Schist at the southwestern end near the MSB (Fig. 2) (Evans and Berti, 1986; Plummer, 1980) through 7-9 kbar peak pressures in the Nason Ridge Migmatitic Gneiss and the Chiwaukum Schist at the core of the Wenatchee Ridge antiform (Brown and Walker, 1993) to 9-11 kbar peak pressures in the Napeequa Complex northeast of the Tenpeak intrusion (Valley et al., 2003). Miller and Paterson (2001) used this barometric gradient along with "unfolding" of major regional folds to construct a ~10-40 km crustal section through the Wenatchee block (Fig 3). The NE-dipping, reverse White River Shear Zone (WRSZ) forms a structural break along the southwestern margin of the Tenpeak intrusion and is marked, in part, by greenschist facies mylonites that clearly postdate peak metamorphism (Magloughlin, 1993; Van Diver, 1967). The WRSZ divides the Wenatchee block into two domains that may have experienced somewhat different metamorphic and exhumation histories (Brown and Walker, 1993; Miller et al., 1993; Chapter 3). These domains are informally referred to as the Mount Stuart and Tenpeak domains.

The Mount Stuart and Tenpeak intrusions are the largest of a suite of 96-84 Ma, tonalitic to granodioritic, intrusions that intrude the Wenatchee block including the Sulphur Mountain, High Pass, Clark Mountain, Chaval, Dirtyface, and Sloan Creek intrusions (Fig. 2) (Hurlow, 1992; Walker and Brown, 1991). The MSB was emplaced into the Chiwaukum Schist, an interlayered metapelitic and metapsammitic unit, at mid-crustal levels of this crustal section (Fig. 3). Andalusite and cordierite are well-documented in the contact aureole of the batholith (Evans and Berti, 1986; Plummer, 1980). This dynamothermal metamorphism was closely followed by a regional

Barrovian-style loading event that increased pressure to staurolite grade at the southeastern end of the MSB and kyanite grade along the northeastern edge of the MSB (Brown and Walker, 1993; Evans and Berti, 1986; Evans and Davidson, 1999). This increase in pressure has been attributed to crustal shortening (Evans and Davidson, 1999; Whitney et al., 1999) or alternatively, magma loading (Brown and Walker, 1993).

The Tenpeak intrusion was emplaced into the Napeequa Complex (formally known as rocks of the Napeequa River area), a heterogeneous assemblage of amphibolite, quartzite, marble, metaperidotite, and biotite schist (Cater and Crowder, 1967). Garnet amphibolite from this region records peak P-T conditions of 9-11 kbar and 625-675°C (Valley et al., 2003). The exact timing of this high-P metamorphism is not well-constrained; however several independent lines of evidence suggest that the Napeequa Complex was deeply buried before the emplacment of the Tenpeak intrusion. Al-in-hornblende barometry from the 96-84 Ma intrusions in the southern part of the Tenpeak domain (i.e. Tenpeak, Sulphur Mountain, High Pass and Clark Mountain intrusions) yields emplacement pressures of 7-9 kbar, and garnet-biotite-muscovite-plagioclase thermobarometry from the High Pass and Clark Mountain intrusions yields pressures of 7-10 kbar (Dawes, 1993). In addition, the same intrusions contain euhedral, magmatic epidote (Dawes, 1993; Zen and Hammarstrom, 1984), which suggest that these intrusions crystallized at pressures $\geq$6 kbar (Dawes, 1993; Zen and Hammarstrom, 1984). The deep crustal evolution of the Tenpeak intrusion contrasts with the more shallowly-emplaced MSB and forms an important point of comparison for later discussion.

Thermochronologic data from the Mount Stuart domain indicate that cooling from magmatic conditions and peak temperatures occurred relatively rapidly after intrusion emplacement. K-Ar and Ar-Ar hornblende cooling dates from the MSB, and the adjacent Chiwaukum Schist and Nason Ridge Migmatitic Gneiss range from 93 to 83 Ma (Engels and Crowder, 1971; Evans and Davidson, 1999). K-Ar and Ar-Ar biotite cooling dates from the same region fall within nearly the same range of ages from 95 to 82 Ma (Tabor et al., 1987; Tabor et al., 1993; Evans and Davidson, 1999; Chapter 4). Cooling dates from the Tenpeak domain are generally younger than those of the Mount Stuart domain, which is consistent with cooling from the higher P-T conditions achieved in the Tenpeak domain. Hornblende K-Ar cooling ages from the Tenpeak intrusion range from 93-85

Ma and biotite K-Ar and Ar-Ar cooling ages range from 75-68 Ma in the Tenpeak intrusion and 69-58 Ma in the surrounding Napeequa Complex (Engels et al., 1976; Chapter 3).

Mount Stuart Batholith

The MSB is the largest composite intrusion in the Cascades core and comprises mulitple bodies that are predominantly tonalitic in composition (Fig. 4). The largest (~700 km^2) northeastern body is the best-studied geochemically and structurally, and will be the focus of further discussion. Several smaller, satellite bodies are also mapped as part of the MSB with the largest being the heterogeneous, mafic, Big Jim Complex. The distinct shape of the northeastern body makes it easily recognizable on any map of the North Cascades. The southeastern part of this body will be referred to as the "mushroom-shaped" region connected by a sill to a "hook-shaped" northwestern region (Fig. 4).

The MSB ranges in composition from two-pyroxene gabbro (1-2% of the map area) through hornblende gabbro-diorite (5%), quartz diorite-tonalite (77%), trondhjemite (2%), granodiorite (13%) and granite (1%) (Erikson, 1977; Paterson et al., 1994). The mushroom-shaped region consists predominantly of coarse-grained, biotite-hornblende tonalite that grades into biotite granodiorite in the center and encloses two-pyroxene gabbro and hornblende-orthopyroxene gabbro-diorite along the southeastern side (Fig. 4). In the hook region, slightly finer-grained biotite tonalite grades into a central region of granodiorite and minor volumes of peraluminous granite.

Geochemical data from MSB samples indicate that it is a medium-K, calc-alkaline intrusion with geochemical characteristics typical of other Cascades intrusions (Paterson et al., 1994); however, the MSB has unusually high MgO for a given SiO_2 content (6.1-7.6% at 56% SiO_2) (Paterson et al., 1994). In fact, it has one of the highest Mg trends for batholiths in the Cordilleran orogen (Paterson et al., 1994). The MSB is also the only Cascades core intrusion to contain orthopyroxene as a stable phase in tonalite. The high Mg trend is characteristic of all phases of the magmatic system and suggests a common parental magma or source region for these different magmas. Several models have been proposed to explain the origin of the Mount Stuart batholith (Anderson, 1992; Erikson, 1977; Kelemen and Ghiorso, 1986; Miller et al., 2000; Paterson et al., 1994; Pongsapich,

1974). The new U-Pb zircon dates indicate that parts of the batholith that were assumed to be co-magmatic formed at distinctly different times, and cast doubt on models that infer continuous processes to generate the compositional variations observed in the batholith.

Tenpeak Intrusion

The Tenpeak intrusion is elliptical in map view (aspect ratio of ~5:1) with an eastern (White Mountain) lobe (Fig. 5). The outer parts of the intrusion form a discontinuous zone of sheeted and mingled gabbro and tonalite (referred to as mafic complex) (Cater and Crowder, 1967; Tabor et al., 1987). The interior of the intrusion is primarily composed of tonalite, and two of the largest pulses form texturally distinct phases that are informally referred to as the Schaefer Lake and Indian Creek phases (Miller et al., 2000). Both phases are composed of hornblende-biotite tonalite with coarse-grained titanite (0.2-0.8 mm) and euhedral, magmatic epidote; garnet is locally common (Cater, 1982). Biotite is more predominant than hornblende in the medium-grained Schaefer Lake phase. These minerals wrap subhedral and rounded plagioclase, giving the rock a "popcorn" texture. In contrast, hornblende and biotite are coarse-grained and euhedral in the Indian Creek phase (Cater, 1982; Dawes, 1993). The Indian Creek phase truncates an interior sheeted complex of felsic and mafic tonalite (defined by differences in color indices and ratios of biotite to hornblende) and an interlayered unit composed of tonalite with numerous rafts of Napeequa amphibolite host rock. Xenoliths of Napeequa amphibolite and meta-peridotite are also widely scattered outside the sheeted zones and are up to 1 km in width. Contacts between the sheeted zone, mafic complex and Schaefer Lake tonalite are generally gradational. The White Mountain lobe is texturally similar to tonalite of the Schaefer Lake phase, but is separated from this phase by a zone of large Napeequa rafts and deformed tonalite referred to as "flaser gneiss" by Cater and Crowder (1967). This highly-deformed, protomylonitic tonalite gneiss forms a wide zone along the northeast margin of the intrusion. Diorite and biotite-hornblende tonalite form in the northern portion of the intrusion.

Geochemical studies have demonstrated that the mafic rocks represent mantle-derived magmas, whereas tonalites likely formed by mixing of mantle- and crust-derived

melts (Dawes, 1993; DeBari et al., 1998). This geochemical modeling is supported by Nd isotope data as well (Chapter 2). The two modeled end-members have distinct geochemical signatures. The mantle-derived magmas are typically basaltic and crop out as heterogeneous gabbros within the mafic complex and as mafic sheets and enclaves within tonalitic phases (Miller et al., 2000). They contain 49-52 wt.% SiO_2 and 5-8 wt.% MgO, and have flat to slightly light REE-enriched patterns (Miller et al., 2000). The crust-derived end-members are felsic tonalites and trondhjemites which crop out only rarely within the intrusion. In contrast to the mafic end-member, the crust-derived end-member has high SiO_2 (68-72 wt.%) and steep REE patterns and was most likely derived by partial melting of a garnet-bearing lower crust (Miller et al., 2000). The tonalitic to dioritic compositions within the intrusion can be modeled as mixtures between these two end-members (Dawes, 1993; DeBari et al., 1998; Miller et al., 2000).

Each of the distinct textural and compositional phases of both magmatic systems were sampled for U-Pb geochronology. These samples were selected to cover the largest possible areal extent and provide an assessment of the duration and episodicity of construction of each magmatic system.

ANALYTICAL TECHNIQUES

Separation of heavy minerals from all samples was carried out according to standard crushing, heavy liquid, and magnetic separation techniques. Zircon and titanite crystals were picked in ethanol under a binocular microscope and sorted by their morphology, color, clarity, and inclusion characteristics. Representative zircons were selected for image analysis. These grains were mounted in epoxy and polished to approximately half their original thickness. Cathodoluminescence (CL) and backscattered electron (BSE) imaging were carried out on grain mounts on the MIT JEOL 733 Superprobe electron microscope. Image analysis was conducted with a 15 keV accelerating voltage and 10 to 30 nA beam current depending on the intensity of luminescence. In select cases, zircon grains were removed from the mount after CL imaging for U-Pb analysis.

All zircons selected for U-Pb analysis were air-abraded, washed in 3M HNO_3 at 50°C for 3-12 hours, and ultrasonicated for at least 1 hour. Following this cycle of

cleaning, the zircons were ultrasonicated in 3M HNO_3 for an additional hour. Each zircon was photographed to estimate sample weight, pipetted with acetone into 300 μL Teflon FEP capsules, washed again in 3M HNO_3 at 75°C for 1-3 hours, and finally rinsed 3 times with 3M HNO_3. Titanite single- and multi-grain fractions were not air-abraded prior to dissolution. Each titanite fraction was weighed, ultrasonicated in high-purity H_2O for 30 minutes, washed in 3M HNO_3 at 75°C for approximately 10 minutes, rinsed three times with high-purity H_2O and finally pipetted into 500 μL Telfon capsules. Zircon and titanite fractions were dissolved in 120 μL concentrated HF and trace HNO_3 with a mixed ^{205}Pb-^{233}U-^{235}U spike at 220°C for 48-72 hours, dried to salts, and redissolved in 120 μL 6M HCl at 180°C for at least 12 hours. Pb and U were separated from the sample using HCl-based (zircon) and two-stage HBr-HCl-based (titanite) anion exchange procedures modified from Krogh (1973).

Approximately 1-2 mg-sized fractions of hand-picked, optically-clear plagioclase feldspar grains from two samples of the MSB and two samples of the Tenpeak intrusion were progressively leached following methods modified from Housh and Bowring (1991). Leaching was carried out in PFA Teflon beakers on at hotplate at ~50°C. After each leach step, the feldspar grains were rinsed twice with 500 μL of high-purity H_2O, and the H_2O rinse was subsequently added to the leachate. Seven sequential leach steps were performed. The first two steps involved short leaching times of about 5 minutes in 6M HCl and 7M HNO_3 respectively. These short leach steps were followed by three leach steps of 1M HF for 20 minutes each, and then two leach steps of 1M HF for 40 minutes each. Each HF-step leachate was dried down, redissolved in 6M HCl, dried down again, and redissolved in 1.1M HBr for separation of Pb by HBr-HCl based anion exchange chemistry. Total procedural blanks are estimated at <20 pg Pb, which represents a negligible contribution to the sample Pb.

Pb and U were analyzed by conventional thermal ionization mass spectrometry on the MIT VG Sector 54 multicollector mass spectrometer. Both Pb and U samples were loaded onto previously degassed single Re filaments with a silica gel-H_3PO_4 mixture (Gerstenberger and Haase, 1997). Pb isotopes were measured either: (1) for ^{207}Pb ion beams >$5x10^{-14}$ A, in a two-cycle dynamic routine with ^{204}Pb in the axial Daly detector and ^{205}Pb through ^{208}Pb in H1-H4 faraday detectors during the first cycle and ^{205}Pb in the

Daly detector and ^{206}Pb through ^{208}Pb in the H1-H3 faraday detectors during the second cycle, providing real-time Daly gain measurement; or (2) for ^{207}Pb ion beams $<5x10^{-14}$ A, by peak-jumping all ion beams into the axial Daly detector in ion-counting mode. Uranium isotopes were measured as UO_2^+ in static mode with masses 270, 267, and 265 in the axial, L1, and L2 faraday collectors, respectively. Pb isotope fractionation was monitored throughout the study by daily analysis of the NBS-981 common Pb standard whereas U fractionation was monitored and corrected by use of the double spike.

DATA ANALYSIS

Zircon and titanite U-Pb data from the Mount Stuart and Tenpeak intrusions are presented at the 2σ uncertainty level in tables 1 and 2, respectively. In general, these relatively young zircon and titanite grains are characterized by low radiogenic Pb contents (>70% of the analyses have Pb contents <5 ppm), making the $^{206}Pb/^{238}U$ date the most precise. The U-Pb zircon data from these samples typically yield clusters of dates on or near the concordia curve, and are thus amenable to calculation of concordia ages (Ludwig, 1998). For a suite of U-Pb data points, the concordia age method provides the best estimate of age and age uncertainty by determining the probability of concordance as well as equivalence. In this method, a weighted mean age is calculated from all three isotope ratios ($^{206}Pb/^{238}U$, $^{207}Pb/^{235}U$, and $^{207}Pb/^{206}Pb$) and statistical evaluation determines how similar they are to each other (i.e. equivalence) and how closely they overlap concordia (i.e. concordance). This method is preferable to the traditional approach for young samples of using just the weighted mean of the $^{206}Pb/^{238}U$ dates. Table 3 lists the concordia ages calculated for each sample with the corresponding MSWD (mean square of weighted deviates) of concordance and equivalence. The uncertainty on the MSWD (Wendt and Carl, 1991) was also calculated to determine if the MSWD derived for a given concordia age is statistically significant, and in all cases, the MSWD of concordance and equivalence falls within the 2σ uncertainty. The weighted mean of concordant $^{206}Pb/^{238}U$ dates and the corresponding MSWDs are also listed in table 3. For most samples, there is no difference between the weighted mean $^{206}Pb/^{238}U$ date and the concordia age, and in all cases, the two ages agree within uncertainty.

Decay constant uncertainties and spike U/Pb calibration uncertainty are not included in the discussion of the data presented below. It is unnecessary to include these systematic errors when comparing data from the same isotopic system collected within the same lab. However, table 3 also lists the full uncertainty on each concordia age for completeness of the data analysis and future reference.

Unlike zircon analyses, U-Pb ratios from titanite analyses commonly require large corrections to the measured Pb ratios because titanite may incorporate significant amounts of initial common Pb into its crystal structure during crystallization. The isotopic composition of this initial common Pb can be estimated in a variety of ways. The simplest method is that inferred from the two-stage Pb evolution model of Stacey and Kramers (1975). A more direct method involves measuring the Pb isotopic composition of a co-existing, low-U mineral such as feldspar (Housh and Bowring, 1991). Pb isotopic compositions of plagioclase feldspar from both the MSB and Tenpeak intrusions are given at the 2σ uncertainty level in Table 4. These isotopic compositions were measured from the last 4 of 5 HF leach steps (labeled as L2 through L5); however, Pb ion beam intensities from steps L2 and L3 were very small, possibly as a result of suppressed ionization from interfering Ca ions. High measurement errors make the data from most of these steps unusable. Leach steps 4 and 5 yielded more precise data. The data from all leach steps from the four samples agree within error. The average of the four reported leach steps from samples *MS6* and *MS13* is the best estimate of the initial Pb isotopic composition of the MSB. The average of the five reported leach steps from samples *TP20* and *TP-524-1* is the best estimate of the initial Pb isotopic composition of the Tenpeak intrusion.

U-Pb RESULTS FROM THE MOUNT STUART BATHOLITH

Twelve samples from the MSB were analyzed (Fig. 4) including two samples from granodiorite that crops out in the hook and mushroom regions (*MS6* and *MS13* respectively), a sample of tonalite from the hook region (*MS5*), three tonalite samples from the sill region (*MS24*, *MS26*, and *MS37*), a sample of diorite from the Big Jim Complex (*MS17C*), two samples of hornblende gabbro from the mushroom region (*MS2* and *MS4*), two samples of tonalite from the mushroom region (*MS31* and *PC-F*), and one

sample of a tonalite sheet that intrudes the surrounding Ingalls Complex (*JR-1*). The data are presented roughly in order from northwest to southeast, and the results are listed in table 1 and summarized in table 3.

Zircon Data

Ten whole grains and fragments of zircon were analyzed from granodiorite sample *MS6* from the hook region of the batholith. All zircon grains were from a population of euhedral, elongate prisms that are commonly colorless, and inclusion- and crack-free. Cathodoluminescence (CL) images from selected grains revealed brightly luminescent cores with dark rims sometimes surrounded by yet another brightly luminescent rim (Fig. 6). All zircon images displayed oscillatory (magmatic) zoning, and this zoning appears concordant between older cores and younger rims with only rare truncations of the zoning pattern. Analyses of abraded whole zircon grains (z1-z3 and z5-z7) are variably discordant (1.0-7.1%) with the most concordant analysis having a $^{206}Pb/^{238}U$ date of 95.97±0.26 Ma (Fig 7). The discordance of these analyses is most reasonably interpreted as resulting from mixtures of slightly older, inherited magmatic cores with slightly younger, magmatic rims. In order to obtain more concordant analyses, I broke two zircon grains into tip and core fragments (Fig. 6). Analyses of the zircon tips are more concordant than most of the whole zircon analyses, and one tip yielded a concordant analysis with a $^{206}Pb/^{238}U$ date of 95.68±0.05 Ma. A core fragment yielded the most discordant analysis (15.6%) and the highest $^{206}Pb/^{238}U$ date of 97.18±0.05 Ma. The variable degrees of discordance of these analyses make it difficult to obtain a precise crystallization age from this sample. The best estimate of the crystallization age comes from the concordant tip analysis (z9a) at 95.68±0.05 Ma.

Five zircon grains and fragments were analyzed from tonalite sample *MS5*, also from the hook region. Whole grain analyses from this sample yielded discordant results (1.6-6.1%) similar to the nearby granodiorite sample *MS6*. CL images from representative zircon grains (Fig. 6) revealed brightly luminescent cores and dark rims also similar to sample *MS6*. Analysis of one zircon fragment yielded a concordant analysis at 96.03±0.05 Ma (Fig. 7), which is interpreted to represent the crystallization age of this sample.

All zircon grains analyzed from tonalite samples of the sill region (*MS26*, *MS37* and *MS24*) were colorless, euhedral, elongate prisms. Five zircon analyses from *MS26* yielded concordant and equivalent results at 96.42±0.08 Ma (Fig. 8). Five zircon analyses from *MS37* also gave concordant and equivalent results at 92.61±0.17 Ma (Fig. 8). Six zircon analyses from *MS24* gave concordant and equivalent results at 92.78±0.07 Ma (Fig. 8). The relatively straightforward U-Pb systematics of these three samples make me confident that the calculated concordia dates represent the crystallization age of each sample.

Sample *MS17C*, a quartz diorite from the Big Jim Complex on the northeastern margin of the batholith, contains clear, colorless, euhedral zircon prisms with stubby terminations. Eleven whole zircon analyses yielded results that are slightly reversely discordant to slightly normally discordant (-2.1% to 3.7%) although all of the error ellipses overlap concordia (Fig. 7). The concordia age of all analyses is 96.00±0.03 Ma, which I interpret to date the crystallization age of the Big Jim Complex.

Near the mushroom region, sample *JR-1* was collected from a tonalite sheet emplaced as an early phase of the MSB into Ingalls Complex host rocks. These tonalite sheets are deformed in the imbricate zone above the Windy Pass thrust which placed the Ingalls Complex on top of the Chiwaukum Schist (Miller, 1985). Six zircon grains yielded variably discordant results (-5.2% to 10.6%), but all analyses except one overlap concordia (Fig. 8). The concordia age of the five concordant analyses is 94.62±0.12 Ma. The sixth, discordant analysis may have experienced minor Pb loss.

Tonalite sample *PC-F* from within the mushroom region exhibits strong, gently-dipping magmatic foliation typical of the MSB near the Windy Pass thrust (Miller and Paterson, 1992; Paterson and Miller, 1998a; Paterson et al., 1994). Ten zircon analyses yielded variably discordant analyses (-11.0 to 32.9%) with more complicated systematics than the other samples (Fig. 8). Seven analyses are concordant. One analysis (z10) is normally discordant and significantly younger than the other analyses. Another analysis (z2) is 32.9% discordant, most likely because of the presence of an inherited core. A third analysis is 11.0% reversely discordant, but its $^{206}Pb/^{238}U$ date agrees within error of four other analyses. The cause of the reverse discordance of this grain is unclear (c.f. Mattinson, 1996), but it may reflect incomplete dissolution. The concordia age of all

analyses but the two normally discordant analyses discussed above is 94.50±0.22 Ma. There is more scatter among the analyses of this sample than of the other samples, which is reflected in a MSWD of 2.00. The $^{206}Pb/^{238}U$ dates of all analyses included in the concordia age calculation range from 94.20±0.61 Ma to 94.83±0.41 Ma, and this spread of dates suggests that these zircons may not belong to one single age population. However, there is no a priori reason to exclude any of the analyses from this cluster of data, and the concordia date is considered the best estimate of the crystallization age.

Zircon crystals obtained from two samples of MSB gabbro in the mushroom region (*MS2* and *MS4*) form stubby multi-faceted prisms. Eight zircon analyses from sample *MS2* yield results that overlap concordia, except for one analysis (z2) that is 8.0% reversely discordant (Fig. 9). The $^{206}Pb/^{238}U$ date of this reversely discordant analysis overlaps 6 of the 7 other analyses, therefore I consider it valid to use this analysis in our calculation of the crystallization age of the sample. Inclusion of all analyses in a concordia age calculation results in an unreasonably high MSWD (6.9) and a statistically insignificant age. The high MSWD is a result of the inclusion of z9 in the regression, which has a $^{206}Pb/^{238}U$ date that falls outside of the uncertainty of all but two of the least precise analyses and may have experience post-crystallization Pb loss. If z9 is excluded from the regression, a concordia age of 90.91±0.03 (MSWD=1.20) is obtained. This statistically significant date best represents the crystallization age of this sample.

Seven zircon analyses from *MS4* gabbro (mushroom region) overlap concordia except for one analysis (z11) (Fig. 9). The concordia age of all analyses, including the discordant analysis, is 91.02±0.06 Ma. This date is the same within error as the date calculated excluding the discordant analysis. Therefore, the concordia age calculated from all analyses is a reasonable representation of the crystallization age of this sample.

Sample *MS13* is granodiorite collected from the mushroom-shaped region of the MSB. Seven zircon analyses yield results that are -12.7% to 4.4% discordant; however the error ellipses from all but one analysis (z6) overlap concordia (Fig. 9). This reversely discordant analysis also has the lowest ratio of radiogenic Pb to common Pb, and its position with respect to concordia is sensitive to the amount of common Pb that is attributed to laboratory blank Pb. Inclusion of z6 results in an unreasonably high

MSWD. If z6 is disregarded, the concordia age is 90.79±0.10 Ma (MSWD=0.77), and is therefore the best estimate of the crystallization age of this sample.

The final sample studied from southeastern part of the mushroom region (*MS31*) is a medium-to coarse-grained biotite-hornblende tonalite. Of the six zircon analyses obtained from this sample, all overlap concordia except one analysis (z7) (Fig. 9). Inheritance of a slightly older core is the most likely interpretation of this discordant analysis. The concordia age of all the concordant analyses is 90.84±0.04 Ma.

Titanite Data

A subset of samples from the MSB was selected for U-Pb analysis of titanite. Because titanite has a nominal closure temperature for Pb diffusion of ~600-650°C (Hodges, 2003), U-Pb titanite analyses have the potential to constrain the high temperature cooling history of the intrusion. All but one analysis (*MS37* s1) are from small, multigrain fractions consisting of either a population of irregularly-shaped grain fragments with one or more crystal faces or a population of completely anhedral grains (i.e., no clear crystal faces). Both populations are clear, light yellow in color and sometimes contain inclusions of opaque minerals. A given sample typically contains only one of the populations described above. For example, sample *MS2*, *MS31*, *MS37* and *PC-F* all contain irregular fragments with some crystal faces whereas samples *MS5*, *MS6* and *MS24* only contain anhedral grains. This distribution of grain morphology does not appear to be geographically restricted or controlled by rock type.

Most of the titanite analyses have ratios of radiogenic Pb to common Pb (Pb^*/Pb^c) that fall in the range of 0.2 to 2.2, although two analyses (*MS5* s3 and *PC-F* s3) have Pb^*/Pb^c ratios of 4.4 and 8.4 respectively. The generally low Pb^*/Pb^c ratios of these titanite grains requires a significant common Pb correction, and the choice of the of the initial common Pb isotopic composition is particularly important. If a Stacey and Kramers (1975) model Pb isotopic composition is used, then the analyses are all several percent reversely discordant. When the Pb isotopic composition measured from coexisting plagioclase feldspar crystals is used (Table 4), then the analyses plot on concordia (Fig. 10), indicating that the feldspar-derived correction is more appropriate. Eight additional titanite analyses obtained from these samples are not reported in Table 1

because low Pb^*/Pb^c ratios (<0.1) make the analyses too sensitive to the common Pb correction to be reliable.

The titanite analyses exhibit a wide range of $^{206}Pb/^{238}U$ dates from 95.41±0.08 Ma to 86.55±0.31 Ma, but only two of the eighteen analyses are older than 90.52 Ma (Table 1; Fig. 10). These analyses can be discussed in terms of two different groups: 1) five analyses have dates that are the same as, or within 1.5 Myr of, the zircon crystallization age and, 2) thirteen analyses have dates that are several Myr younger than the zircon crystallization age of the sample. The oldest two analyses have $^{206}Pb/^{238}U$ dates that are either the same as the zircon crystallization age within error (*MS37* s1) or, at most, 0.75 Myr younger than the zircon crystallization age (*MS5* s3). Two additional samples (*MS13* and *MS31*) have titanite analyses that are less than 1.5 Myr younger than the zircon crystallization age of the respective sample, but do not overlap the zircon crystallization age within error. In contrast, three samples (*MS6*, *MS24*, and *PC-F*) have titanite analyses that are all several Myr younger than the zircon crystallization age of the sample. Sample *MS6* has the largest difference between titanite dates (86.74 Ma to 88.30 Ma) and the zircon crystallization age (95.68±0.05 Ma). Samples *MS2* and *MS5* each have one analysis that is only slightly younger than the zircon crystallization age but other analyses that are significantly younger than the zircon crystallization age. In the case of *MS5*, the analysis that is similar in age to the zircon crystallization age has higher Th/U and Pb^*/Pb^c ratios than the younger analysis. In the case of *MS2*, however, all three analyses have similar Th/U and Pb^*/Pb^c ratios. In fact, there appears to be no correlation for any of these samples between geochemical indices such as Th/U or Pb^*/Pb^c ratios and the difference between zircon crystallization age and titanite date (Fig. 11).

In summary, several titanite analyses yield dates that are <1.5 Myr younger than the zircon crystallization age of the sample, and therefore require rapid cooling (~100°C/km) of the intrusion. Other titanite analyses are significantly younger than their corresponding zircon crystallization age which may reflect cooling, isotopic resetting or secondary mineral growth. The significance of these analyses is explored within the discussion of the MSB cooling history.

IMPLICATIONS OF THE U-Pb DATA FOR THE INTRUSIVE AND COOLING HISTORIES OF THE MOUNT STUART BATHOLITH

Intrusive History

Our new U-Pb zircon analyses from the MSB indicate that the batholith was emplaced over a ca. 5.6 Myr time period. Previously published U-Pb zircon dates from a sample of the Big Jim Complex (Tabor et al., 1987) and a diorite sample from the sill region (Walker and Brown, 1991) suggested that the most mafic magmas were emplaced earliest and were then followed by an episode of predominantly tonalitic magmatism (Tabor et al., 1987). Samples *MS17C* and *MS24* were collected from nearby the sample localities of the previously published data. The zircon crystallization age of *MS17C* overlaps within error of the ca. 95.5 Ma age reported in Tabor et al. (1987). Sample *MS24* also yielded a crystallization age that closely agrees with a previously reported age of ca. 93 Ma (Walker and Brown, 1991). However, our additional samples indicate that the intrusive history of the MSB is not as simple as emplacement of early mafic magmas followed by voluminous tonalitic magmatism.

The high density of sampling for geochronology makes it possible to divide the intrusion of the MSB into at least four age groups: 1) 96.4-95.7 Ma, 2) 94.6-94.5, 3) 92.8-92.6 Ma, and 3) 91.0-90.8 Ma (Fig. 12). These four age groups follow a general NW to SE trend in the timing of emplacement although this trend is reversed in the southeast end of the sill region (Fig. 4). The oldest phases crop out in the hook region and in the Big Jim Complex along the NE side of the sill region. The oldest age domain is defined by four samples (*MS5*, *MS6*, *MS17C*, and *MS26*), and includes granodiorite, tonalite and the mafic Big Jim Complex (Fig. 4). Samples with intermediate ages (*MS24*, *MS37*, *PC-F*, and *JR-1*) are tonalitic in composition and were collected from the sill and mushroom regions. The youngest ages are confined to the mushroom region, and the four samples that define this age domain (*MS2*, *MS4*, *MS13*, and *MS31*) range in composition from gabbro to tonalite to granodiorite.

Paterson and Miller (1998) infer that the complex shape, petrological variations, internal magmatic contacts, and local magma mingling indicate that magma ascended in variably-sized (hundreds to thousands of cubic meters) and variably-shaped batches that were assembled at the site of emplacement. The new age data, which show gaps in the

range of crystallization ages and a distinct geographic distribution of ages, support this idea of construction of the batholith from multiple batches of magma of varying age, size and composition.

Contacts between different compositional phases within an age domain are gradational, and in the field, internal magmatic contacts between the different compositional phases are difficult to delineate. The gradation from tonalite to granodiorite is defined by a gradual decrease in hornblende content, a concomitant increase in biotite content, and the presence of potassium feldspar. Contacts between tonalite, diorite, and gabbro in the mushroom region are also gradational, although it is common to observe local, feathery, net-veining of tonalite and diorite into gabbro (e.g. Paterson et al., 1994).

Contacts between magma pulses of different age are also difficult to delineate. The bold dashed lines on figure 4 mark the approximate placement of contacts between tonalite of different age domains, but I have not been able to confirm the location of these contacts in the field. The contact between the oldest age domain (hook region) and the intermediate ca. 92.6-92.8 domain is only constrained by two samples (*MS26* and *MS37*) from the sill region, which are ~10 km apart. I infer that the contact is nearer to sample *MS37* at the point where the sill appears to thin at the surface and to the southeast of a small mafic body that may be coeval with the ca. 96 Ma Big Jim Complex. The contact between ca. 92.6-92.8 Ma tonalite and ca. 94.5-94.6 Ma tonalite is inferred to lie between samples *MS24* at the southeast end of the sill region and the Windy Pass thrust for reasons discussed in the next paragraph. A contact between ca. 94.5-94.6 Ma tonalite and ca. 90.8-91.0 Ma tonalite is inferred to lie between tonalite sample *PCF* near the center of the mushroom region and granodiorite sample *MS13* and gabbro sample *MS2*.

The orientation of magmatic fabrics can give insight into the relationships between different phases of the batholith (Paterson and Miller, 1998a; Paterson et al., 1994). The term "magmatic fabric" refers to foliations, mineral lineations, and associated microstructures that formed during crystal alignment in the presence of a melt. These fabrics are preserved late in the crystallization history of the intrusion and record the final increments of strain while ~20-40% melt remains (Paterson et al., 1998). In the MSB, magmatic fabrics are defined by aligned mafic microgranitoid enclaves and euhedral

igneous minerals such as plagioclase, pyroxene, hornblende and biotite (Paterson and Miller, 1998a; Paterson et al., 1994). Magmatic foliation in the mushroom region dips steeply and defines margin-parallel, "onion-skin" patterns (Paterson et al., 1994). This foliation pattern is continuous across phases of different composition in the ca. 90.8-91.0 Ma age domain from granodiorite to tonalite and into diorite and gabbro without an apparent deflection (Fig. 4). This pattern is interrupted by strong, gently-dipping foliation near the Windy Pass thrust, which is semi-continuous with thrust-related ductile fabrics in the Ingalls Complex and Chiwaukum Schist. Miller and Paterson (1992, 1994) inferred that the batholith was deformed by thrusting while melt-dominated, but upon reaching its solidus, locked up displacement on the thrust. The gently-dipping magmatic foliation is preserved in the 94.50±0.22 Ma sample *PC-F*, and appears to continue smoothly into ca. 91 Ma phases of the batholith without deflection. In the sill region, magmatic foliation defines complex patterns of large and small magmatic folds with subhorizontal, NW-SE trending axes (Paterson and Miller, 1998a). Magmatic foliation is similarly folded by decameter- to kilometer-scale folds in the hook region, and the hook shape itself may reflect a large-scale fold (Benn et al., 2001; Paterson and Miller, 1998a). These magmatic fabrics are also continuous with fabric in the host rock and are locally at high angles to the batholith margin. Therefore, the magmatic fabrics are interpreted to reflect regional strain rather than magmatic flow lines during emplacement (Miller and Paterson, 1992; Paterson and Miller, 1998a; Paterson et al., 1994). Once again, the magmatic fabric in the hook region is continuous with the fabric in the adjacent age domain.

The smooth variation of magmatic fabrics and lack of observable contacts between tonalite of different age are problematic. However, several possibilities may explain this apparent lack of distinct contacts. If the strain field that controls the orientation of the magmatic fabric remained constant throughout the emplacement of the MSB, then magmatic fabrics would appear continuous across different pulses of magma even though those pulses locked in their respective magmatic fabrics at different times. There may be distinct, sharp contacts between tonalite pulses of different age, but the differences in composition, texture, and/or fabric orientation are so subtle as to be missed in the field. Alternatively, moderately slow cooling of the batholith (~15°C/Myr) may

allow earlier pulses of magma to stay partially molten until the next pulse of magma intruded. This possibility is considered in the upcoming discussion of the titanite data and the cooling history of the intrusion.

Cooling History

Interpretation of titanite data from the MSB must address the question of whether the ~9 Myr time span represented by the U-Pb titanite dates records cooling ages, isotopic resetting or secondary mineral growth. These three interpretations have distinctly different implications for the evolution of the MSB.

The cryptic contacts between different age domains and the smooth variation of magmatic fabrics across internal magmatic contacts suggest that a slow-cooling model may explain the data. However, if the titanite dates are interpreted as cooling ages, this requires differential cooling between the hook and mushroom regions. More importantly, it requires that the MSB remained above the titanite closure temperature (600-650 °C; Hodges, 2003) for as long as 9 Myr in the hook region and as long as 4 Myr in the mushroom region. These time spans are much longer than cooling times predicted by simple thermal models which suggest that even large intrusion should cool below the solidus in hundreds of thousands of years rather than millions of years (e.g. Jaeger, 1957, 1961; Harrison and Clarke, 1979).

Titanite textures observed in thin section and back-scattered electron imaging make a much stronger case for secondary grain growth. In most thin sections examined from the MSB, titanite grains occur as long, thin crystals along cleavage planes or grain boundaries of biotite and amphibole that have been partially replaced by chlorite (Fig. 13). These textures indicate that titanite growth likely occurred as a result of Ti release during hydration of biotite to chlorite (Ferry, 1979) or breakdown of primary igneous hornblende to ferro-actinolite, titanite and albite (Gibbons and Horak, 1984). These greenschist facies reactions likely took place well below the closure temperature of titanite. The hook region, in particular, appears to have undergone a low-temperature subsolidus alteration of hornblende rims to actinolite as a result of the regional loading event (Ague and Brandon, 1996). In some of the more mafic, orthopyroxene-bearing rocks, titanite growth may have occurred during hydration of pyroxene to hornblende

(Frost et al., 2000). Textures that suggest primary magmatic growth, such as inclusion of titanite in primary plagioclase and potassium feldspar are present (Fig. 13), but not common.

In light of the textural evidence suggesting both primary and widespread secondary titanite growth, the large spread of titanite analyses along concordia is most reasonably interpreted as resulting from mixtures of primary and secondary titanite. Titanite analyses that are <1.5 Myr younger than their corresponding zircon crystallization age most likely date primary titanite and reflect rapid cooling after emplacement. Assuming an emplacement temperature for MSB tonalite of ~800°C (Paterson et al., 1994) and a titanite closure temperature of ~650°C, a cooling rate of ~100°C/Myr is estimated.

Several previous studies have noted that titanite of secondary origin is typically pale yellow in color and has lower U concentrations and lower Th/U ratios than coexisting dark brown, primary titanite (Abraham et al., 1994; Aleinikoff et al., 2002; Corfu and Stone, 1998; Getty and Gromet, 1992; Ketchum et al., 1997; Verts et al., 1996) although some reversals of this trend do occur. There is no discernible difference in color or morphology between primary and secondary titanite in the MSB mineral separates. However, certain samples, such as *MS5*, do exhibit a difference in U content and Th/U ratios between titanite analyses that yield dates that are close in time to the zircon crystallization age and those that are much younger. Samples in which both the biotite and amphibole are extensively chloritized, such as granodiorite sample *MS6*, yield titanite dates that are much younger than the zircon crystallization age and have some of the lowest Th/U ratios of all the analyses. This trend is not present in all MSB samples and may reflect that the overall variation in U content and Th/U ratio is more dependent on the composition of the host rock (Corfu and Stone, 1998).

Potential triggers for the breakdown reaction recorded by the titanite grains include release of fluids from the youngest pulses of magma or from metamorphic reactions occurring in the host rocks during post-emplacement loading of the MSB. The majority of titanite dates from the MSB, however, are several Myr younger than the youngest recognized pulse of MSB magmatism. The timing of loading is not well-established, but Sm-Nd dates of garnet in the Chiwaukum Schist near the hook region

suggest garnet growth during loading at 86-88 Ma (Stowell and Tinkham, 2003). The time period of garnet growth overlaps the youngest MSB titanite dates even though these reactions most likely took place under considerably different metamorphic conditions. Hornblende and biotite K-Ar and Ar-Ar cooling dates also fall within this time period (Fig. 4), and suggest rapid cooling of the region. It is unclear from the titanite textures or the U-Pb data if the secondary titanite growth represents one discrete episode of growth or multiple phases of growth occurring by more than one mechanism. It is also important to note that samples from the mushroom region, which did not experience significant crustal loading, contain evidence for secondary titanite growth.

The available cooling data and titanite textures argue against slow cooling as a mechanism to produce the lack of distinct contacts between tonalite of different age domains. The failure to recognize these cryptic contacts because of the similarities in composition, texture, and/or fabric orientation of tonalite of different ages suggest similar sources and/or processes involved in the generation of tonalite over this ca. 5.6 Myr time period. Mapping of subtle variations in trace element and isotope geochemistry in addition to detailed geochronology may be necessary to fully understand the scale of heterogeneity of this batholith.

U-Pb RESULTS FROM THE TENPEAK INTRUSION

Eight samples from the Tenpeak intrusion were analyzed (Fig. 5) including a sample of felsic tonalite from the sheeted zone (*TP1*), two samples of Schaefer Lake phase tonalite (*TP11* and *TP20*), one sample of Indian Creek tonalite (*TP-524-1*), a tonalite sample from the northernmost part of the intrusion (*TP27*), a sample of diorite from the mafic complex (*TP30*), a sample of tonalite from the White Mountain lobe (*TP31*) and a sample of protomylonitic tonalite gneiss from the northeastern margin of the intrusion (*TP29*). Data from the more voluminous phases are presented first, followed by data from marginal phases and the sheeted zone. The results are given in table 2 and summarized in table 3.

Zircon Data

Sample *TP27* is a medium-grained, biotite-hornblende tonalite collected from the northernmost part of the intrusion. This region had been mapped as part of a large diorite body (Tabor et al., 2002), but diorite was not observed at the northernmost tip of the intrusion. Zircon from this sample comprises colorless, elongate prisms. All except one of seven zircon analyses are concordant (Fig. 14) with a concordia age of 90.72±0.04 Ma interpreted as the crystallization age of this sample. The one discordant analysis has younger $^{206}Pb/^{238}U$ and $^{207}Pb/^{235}U$ dates, which can be interpreted as minor Pb loss.

Five concordant zircon analyses from tonalite sample, *TP-524-1*, yield a concordia age of 89.74±0.09 Ma (Fig. 14) that represents the crystallization age of the Indian Creek phase. In contrast, zircon analyses from tonalite samples of the Schaefer Lake phase yield consistently older ages. Eight concordant and equivalent analyses from *TP20* yield a concordia age of 92.21±0.03 Ma (Fig. 15). Six concordant and equivalent analyses from sample *TP11* yield a concordia age of 92.37±0.06 Ma (Fig. 15).

Four zircon grains were analyzed from sample *TP31*, a tonalite from the White Mountain Lobe of the Tenpeak intrusion. The analyses have low ratios of radiogenic Pb to common Pb and consequently have large uncertainties. Three of the four analyses overlap concordia (Fig. 15), and the concordia age of these three analyses is 92.04±0.73 Ma. The fourth analysis is normally discordant, most likely a result of an inherited zircon core. Sample *TP30* is a diorite collected from the mafic complex that is in contact with tonalite of the White Mountain Lobe. Six zircon analyses overlap concordia (Fig. 15) with a concordia age of 92.15±0.18 Ma (MSWD=0.32). Considering that magmas of the mafic complex (*TP30*) and tonalite of the White Mountain Lobe (*TP31*) were mingled on the outcrop scale, and that both yield zircon analyses within error, the crystallization age of the White Mountain Lobe is best represented by the more precise concordia age of sample *TP30*.

Six zircon analyses from tonalite gneiss sample *TP29* along the northeast margin of the body are concordant (Fig. 14) and yield a concordia age of 91.31±0.13 Ma. Six zircon analyses from sample *TP1* (Fig. 14), a felsic tonalite from the southernmost sheeted zone, yield concordant analyses with a concordia age of 91.87±0.08 Ma.

Titanite Data

U-Pb analyses of titanite fractions from six of the eight Tenpeak samples are presented in table 2. Analyses from a seventh sample (northernmost tonalite sample *TP27*) had Pb^*/Pb^c ratios that were too low to give reliable results. The titanite analyses are a mix of multigrain and single-grain fractions as noted in table 2. The grains are generally clear and vary from dark yellow to brown. All grains form anhedral fragments, but the grains analyzed from samples *TP11* and *TP29* are commonly lentil-shaped and aligned with the fabric.

The Tenpeak titanite analyses generally have higher Pb^*/Pb^c ratios than the titanite analyses from the MSB. Most of the Pb^*/Pb^c ratios fall between 1.6 and 5.3 except for one sample (*TP-524-1*), which has a Pb^*/Pb^c ratios of 0.2-0.6. Even with the higher Pb^*/Pb^c ratios, the analyses are still sensitive to the Pb isotopic composition used for the common Pb correction. Unlike the MSB titanite analyses, however, the Tenpeak analyses are normally discordant from 3% to 72% (except *TP-524-1* s3 which is severely reversely discordant) when the Pb isotopic composition that was determined from plagioclase feldspar is used (Table 4). Rather, the analyses are concordant when the Stacey and Kramers (1975) model Pb isotopic composition at 90 Ma is used for the correction (Fig. 16). Plagioclase feldspar may incorporate minor amounts of U into its crystal structure (Housh and Bowring, 1991; Oversby, 1975), and it is possible that the Pb isotope composition measured from Tenpeak plagioclase feldspar is more radiogenic than the true initial Pb isotopic composition of the magma. Therefore, the Stacey and Kramers (1975) model Pb isotopic composition was used for the common Pb correction of the data in table 2. It is important to note, however, that the common Pb correction has little effect on the $^{206}Pb/^{238}U$ dates of samples in this age range, effectively shifting the analyses along nearly horizontal trajectories on a concordia diagram. For this reason, the $^{206}Pb/^{238}U$ dates of the titanite analyses are likely valid regardless of the common Pb correction used.

Titanite analyses from the Tenpeak intrusion have $^{206}Pb/^{238}U$ dates that range from 88.54±0.19 Ma to 92.27±0.07 Ma (Table 3; Fig. 16). Individual titanite analyses are, at most, 1.1 Myr younger than the respective zircon crystallization age of the samples, and the majority of the analyses (13 of 17) are less than 0.5 Myr younger than

the zircon crystallization age. However, the titanite analyses of individual samples scatter outside the range of ages expected from analytical uncertainties such that a statistically significant weighted mean $^{206}Pb/^{238}U$ age of the titanite analyses cannot be determined from any sample. There is no correlation between the titanite $^{206}Pb/^{238}U$ date and geochemical indices such as Th/U or Pb^{*}/Pb^{c} ratios.

IMPLICATIONS OF THE U-Pb DATA FOR THE INTRUSIVE AND COOLING HISTORIES OF THE TENPEAK INTRUSION

Intrusive History

In contrast to the MSB, emplacement of the Tenpeak intrusion took place on a shorter timescale with an approximately 2.7 Myr difference in age between the youngest and oldest phases of the intrusion. The intrusive history suggests that emplacement of the Tenpeak intrusion was a much more continuous process than emplacement of the MSB (Fig. 12). The oldest phases include the Schaefer Lake phase tonalite in the southeastern portion of the intrusion (*TP11* and *TP20*) dated at 92.37±0.06 Ma and 92.21±0.03 Ma, and the mafic complex (*TP30*) near the White Mountain lobe dated at 92.15±0.18 Ma. The zircon crystallization age of tonalite from the White Mountain lobe (*TP31*) also overlaps in age with the Schaefer Lake and mafic complex samples, but the large uncertainties on the White Mountain age make the timing relationships between these pulses difficult to assess. Field relationships, however, suggest that the White Mountain lobe truncates the Schaefer Lake tonalite. The sheeted complex (*TP1*) intruded at 91.87±0.08 Ma, less than 0.5 Myr after emplacement of the voluminous Schaefer Lake tonalite. These dates are consistent with the observation that the sheeted zone is gradational with the Schaefer Lake tonalite. The protolith of the tonalite gneiss (*TP29*) intruded at 91.31±0.13 Ma, closely after development of the sheeted zone on the opposite side of the intrusion. The gneissic texture may reflect late strain localization developed along the northeast margin of the intrusion. At 90.72±0.04 Ma, approximately 0.6 Myr after the emplacement of the tonalite gneiss protolith, tonalite was emplaced in the northernmost parts of the intrusion (*TP27*). Within a Myr, the youngest phase of the intrusion, the Indian Creek tonalite (*TP-524-1*) was emplaced at 89.74±0.09 Ma. The Indian Creek tonalite truncates both the sheeted and interlayered complexes and the

Schaefer Lake tonalite. This relationship implies that these phases had cooled enough to remain rheologically distinct phases during intrusion of Indian Creek tonalite.

Contacts between magma pulses of differing age are much easier to delineate in the Tenpeak intrusion than in the MSB, in part because each phase is texturally distinct. Discrete mafic bodies are generally restricted to the outer margins of the intrusion, and form some of the earliest phases. A sharp boundary exists between Schaefer Lake tonalite and coarse-grained Indian Creek tonalite. A more gradational contact exists between the sheeted zone and the Schaefer Lake tonalite. These discrete contacts and the distinct textures of different pulses of the Tenpeak intrusion contrast with the evolution of the MSB. The lack of homogenization and mixing of pulses of Tenpeak magma are somewhat surprising given that these magmas were emplaced over a shorter timespan than the MSB with less time (~0.5 Myr) between pulses. In addition, Tenpeak magmas yielded emplacement pressures of 7-9 kbar (Dawes, 1993), and intruded host rock that records peak P-T conditions of 10-11 kbar and 625-675°C (Valley et al., 2003), although it is unclear when the peak temperatures were attained prior to the emplacement of the Tenpeak intrusion. These factors should have promoted slower cooling than the MSB and greater potential for mixing and homogenization. However, the thermochronologic data from the Tenpeak intrusion, as discussed in the next section, indicate that cooling following emplacement was rapid which inhibited mixing between magma pulses.

Cooling History

Both the U-Pb zircon data and field relationships suggest that the earlier phases of the Tenpeak intrusion (Schaefer Lake tonalite, mafic complex, White Mountain lobe, and sheeted complex) cooled enough that they were rheologically distinct phases before intrusion of later pulses of magma (protolith of the tonalite gneiss, northwestern diorite/tonalite body, and Indian Creek tonalite). Titanite U-Pb analyses from these samples place further constraints on the high temperature cooling history of the intrusion.

Titanite analyses from the Tenpeak intrusion display an approximately 3.7 Myr range of dates along concordia, although titanite dates from individual samples generally range from the respective zircon crystallization age to about 0.5 Myr younger (Fig. 16). Titanite occurs as large, euhedral to subhedral crystals contained within plagioclase,

suggesting primary magmatic growth (Fig. 13). Unlike the MSB, textural evidence of secondary titanite growth is lacking. The dispersion of titanite dates along concordia most likely records either cooling ages or the timing of isotopic resetting.

Titanite grains recovered from these samples are irregularly-shaped fragments, and it is unclear if there is a variation between age and grain size that would indicate diffusional Pb loss above the titanite closure temperature (e.g. Dodson, 1973). Alternatively, the dispersion of the titanite dates along concordia may indicate that the titanite grains have been partially reset to varying degrees. All of the samples from the southern, oldest part of the intrusion (*TP11*, *TP20*, *TP31*, *TP1*) have titanite dates that cover a range of ages, but are no younger than 91.3 Ma. It is possible that the thermal pulse associated with intrusion of later pulses of magma were responsible for partially resetting titanite grains throughout the southern part of the intrusion. However, this fails to explain why titanite dates from the youngest phase, the Indian Creek tonalite, are up to 1.1 Myr younger than the respective zircon crystallization age. This tonalite is among the youngest known magmatism in the Wenatchee block.

Regardless of whether the dispersion of titanite data along concordia records cooling ages or the timing of isotopic resetting, the thermochronologic data indicate that a substantial volume of the intrusion had solidified and cooled below the titanite closure temperature by 91.3 Ma, within a Myr of emplacement. These observations are supported by cooling dates recorded by the diffusion of Ar from hornblende (T_C~500-550 °C; Harrison, 1981; McDougall and Harrison, 1988) that are less than one Myr younger than the U-Pb titanite dates (Engels et al., 1976; Chapter 3). The earliest formed pulses of the intrusion (Schaefer lake tonalite, mafic complex, White Mountain lobe tonalite, and sheeted complex) acted as rheologically distinct units and did not mix with or become homogenized with later magmas. These data also suggest that the Napeequa Complex had cooled from its peak thermal conditions of 625-675°C (Valley et al., 2003) to below the closure temperature for Ar diffusion in hornblende before emplacement of the Tenpeak intrusion.

RATES OF MAGMA EMPLACEMENT

Magmatism has long been known to play a key role in the thermal evolution of continental magmatic arcs as an efficient mechanism to transfer heat from the lower to upper crust. The timescales of magma chamber construction dictate the rate at which heat is transferred. The geochronologic data presented here along with estimates of the volumes of these intrusions provide a way to quantify magma emplacement rates through this segment of the continental magmatic arc.

The areas of each compositional phase of the MSB and Tenpeak intrusions were calculated using GIS software. Geophysical data, which would constrain the depth of each intrusion and hence volumes, are lacking; however, the topographic relief in this region is great enough that at least a 2.5 km thick section of the MSB and at least a 2.0 km thick section of the Tenpeak intrusion are exposed. These thicknesses provide minimum constraints on the volume of each pulse of magma (Table 5). Gravity modeling of intrusions in a variety of tectonic settings suggest that most intrusions form relatively thin (<10 km) tabular bodies with gently-dipping roofs and floors (Améglio and Vigneresse, 1999; Améglio et al., 1997; Cruden, 1998; Hodge et al., 1982; McCaffrey and Petford, 1997; Petford et al., 2000; Vigneresse, 1990; Vigneresse et al., 1999). This modeling is at odds, however, with the steep nature of the contacts between the both the MSB and Tenpeak intrusion and host rock (Miller and Paterson, 1999; Paterson and Miller, 1998b). Because of the uncertainty in the depth and geometry of each intrusion, only minimum rates corresponding to the known thicknesses of the MSB and Tenpeak intrusion exposed at the surface are calculated. The minimum volume of each intrusion emplaced over the entire duration of magmatism in each intrusion yields a minimum time-average rate for the MSB of 2.1×10^{-4} km^3/yr and a minimum time-average rate for the Tenpeak intrusion of 1.2×10^{-4} km^3/yr.

The average rates calculated for the MSB and Tenpeak intrusion are comparable to rates estimated from other continental batholiths and batholithic belts (Crisp, 1984; Francis and Rundle, 1976). Average magma emplacement rates determined by Crisp (1984) for outcrop areas between 10^3 to 10^4 km^2 range from $>2.1 \times 10^{-4}$ km^3/yr for the Guichon Creek batholith, B.C. to up to $63(\pm 3) \times 10^{-4}$ km^3/yr for the Boulder batholith. Average rates for outcrop areas at least 10^4 to $>10^5$ km^2 are generally higher and range

from $1.9x10^{-3}$ km^3/yr for the entire Sierra Nevada batholith to $14x10^{-3}$ km^3/yr for the entire Coast Range Plutonic Complex (Crisp, 1984). The average magma emplacement rate determined from the Coastal batholith of Peru is $3.3x10^{-4}$ km^3/yr assuming a tabular shape with a 5 km thickness (Francis and Rundle, 1976). All of Crisp's estimates for continental batholiths are greater than the rates determined for the MSB and Tenpeak intrusion. This is likely due in part to the fact that Crisp (1984) used an arbitrary 10 km thickness for all measured areas when determining intrusion volumes. If I make the same assumption, the rates are comparable. In addition, the durations of magmatism used in both studies are considerably longer than the duration of the MSB or Tenpeak magmatism, which may be an artifact of the less precise geochronologic data that was available prior to these studies. Considering the large uncertainties in estimated volumes, it seems noteworthy that the average magma emplacement rates of the MSB and Tenpeak intrusions are within an order of magnitude of earlier estimates from continental batholiths.

The density of sampling from the MSB makes it possible to estimate the magma emplacement rate through each age domain. Rates from the hook and sill age domains are lower than the estimated rates from the youngest age domain. Volumes of the hook and mushroom age domains are comparable (Table 5); therefore, the difference in rates is dominantly a result of the inferred longer duration of magmatism in the hook region. The uncertainties on these magma emplacement rates are difficult to quantify. The uncertainty of the thickness and geometry of each pulse, as well as the uncertainty in the position of the boundaries between different age domains in the MSB, is unknown. Uncertainty in the time it takes for each magma pulse to be emplaced is also a critical factor. Even with the high density of sampling for geochronology, these rate calculations are based on the assumption that emplacement of magma was continuous for the time period represented by the geochronological data for a given age domain. Geodetic data from the regions above active crustal magma chambers reveal episodic uplift (infilling) and subsidence on timescales from days to years (Dvorak and Dzurisin, 1997) reflecting rates that are orders of magnitude greater than those estimated here. Petford et al. (2000) calculated volumetric intrusion filling rates of 0.01 to 100 m^3/s using reasonable values of magma viscosity, wall rock/magma density differences, and feeder dike morphologies.

These filling rates predict that an intrusion roughly the size of each age domain of the MSB could be emplaced in as little as a few hundred years to up to roughly a Myr. The large range of estimates for the duration of emplacement of any given magma pulse make the value of calculating the magma emplacement rates through a specific age domain uncertain. In contrast, comparisons between long term or average rates of magma addition are probably more valuable to understanding rates of magma generation and heat transfer through the crust than are short period rates from volcanic systems which are influenced by factors such as vent and conduit geometry (Crisp, 1984).

COMPARISON OF THE MOUNT STUART AND TENPEAK INTRUSIONS

Comparison of these two magmatic systems can lead to a better understanding of how processes that control the construction of intrusions change with depth. These systems are similar in terms of their range of compositions, timing of emplacement during regional deformation, and rapid cooling after emplacement. However, significant differences between these systems must be explained. Construction of the Tenpeak intrusion appears to have been a more continuous process yet texturally distinct phases and internal sheeting are well-documented and there does not appear to be significant homogenization of different magma pulses. In contrast, the MSB appears to have been constructed over four discrete time periods yet it shows gradational contacts between magma pulses of differing composition, and similar textures and magmatic fabrics between pulses that are significantly different in age.

The differences between these two systems may be related to the rate at which magma is generated and/or segregated from its source region. At relatively slow rates of intrusion relative to cooling, magmatic systems may consist mostly of mush and relatively evolved melt (Shaw, 1985; Sinton and Detrick, 1992). At higher rates of intrusion, magma recharge may be frequent, which sustains the magma reservoir and may result in appreciable magma mixing (Koyaguchi and Kaneko, 2000; Reid, 2003). The Tenpeak system is more likely examples of a slow rate of intrusion because higher proportions of mush relative to liquid inhibit mixing and result in texturally distinct magma pulses. Less frequent recharge also implies a greater degree of cooling between magma pulses, also encouraging distinct textures. When magma is generated at a slower

rate or cannot be as efficiently separated from its source region, then only small batches of magma are available to periodically ascend through the crust, and the limited thermal energy these magma batches controls their level of emplacement. The rate of intrusion of the MSB may be faster, encouraging homogenization of different magma batches during ascent.

Miller et al. (2000, 2003) and Miller and Paterson (2001a) describe an alternative model in which mid- to lower-crustal intrusions, such as the Tenpeak intrusion, represent a "filtering system" between lower crustal zones of magma generation and mixing, and upper crustal zones of large, relatively homogeneous intrusions, such as the MSB. These deep-level magma reservoirs are dynamic systems with early mafic sheets solidified along the sides and large volumes of magma passing upwards to higher chambers where they may become thoroughly hybridized. The deep-level magma chambers act as conduits to upper crustal sites of magma collection and serve as a snapshot of the ascent of magma through the crust. If such systems are linked, then it is unclear from this model why magma emplacement in the mid- to upper-crustal system (i.e. MSB) shows more punctuated evolution whereas the lower-crustal system (i.e. Tenpeak intrusion) shows more continuous development.

It is clear from the petrologic variations, internal magmatic contacts, and local magma mingling that the MSB and Tenpeak intrusion were constructed from multiple batches of magma. Most, if not all, intrusions from similar tectonic settings can be argued to have been constructed in this fashion. However, the recent assertion that only small volumes of melt are present in a magma chamber at any given time (Coleman et al., 2004; Glazner et al., 2004) is at odds with the U-Pb data from the MSB. The thermochronologic data suggest that the entire MSB never formed a single convecting magma chamber, but in the case of the mushroom-shaped region, at least 520 km^3 of magma was emplaced in 200-400 thousand years, necessitating a magma reservoir (both mush and liquid) of considerable size. This contrasts with the Tenpeak intrusion, in which any magma chamber was smaller in size and potentially more ephemeral in nature.

CONCLUSIONS

The petrologic diversity, internal magmatic contacts and local magma mingling observed from the MSB and Tenpeak intrusion indicate that these intrusions were constructed from multiple batches of magma. For the MSB, construction of the batholith took place over a ca. 5.6 Myr time period with four discrete episodes of magma emplacement. Construction of the Tenpeak intrusion took place over a shorter time span of ca. 2.7 Myr with <0.5 Myr between emplacement of different magma pulses. Different compositional phases of the Tenpeak intrusion cooled and solidified within ~1 Myr after emplacement as evidenced by both field relationships and the U-Pb data. The cooling history of the MSB is comparable. Several titanite dates from the MSB are similar in age to the respective zircon crystallization age of the sample; however, secondary titanite also grew by breakdown reactions of hornblende and biotite, potentially as a response to regional loading of the MSB. The interpretation of the intrusive history of the MSB, and magmatic fabric orientations in particular, are obscured by cryptic contacts between pulses of tonalite of differing age. Smooth variations in magmatic fabric patterns between different age domains require that the strain field was constant during emplacement of the batholith and that deflections of the magmatic fabrics are too subtle to be detected in the field. Average magma emplacement rates calculated from these two intrusions are similar to those calculated from other continental batholithic belts. The magma emplacement rates calculated from the mushroom-shaped region, in particular, suggest that a relatively large volume of melt was present in the middle to upper crust for at least a 400 thousand year time period. Compositional and textural similarities of tonalite from different age domains of the MSB suggest a greater degree of homogenization of tonalitic magma, whereas the diversity of rock types and textures observed from the Tenpeak intrusion show a lack of mixing and homogenization. These textural differences may reflect different rates of magma generation and/or segregation from their source region. Alternatively, the deeper-level Tenpeak system may represent a "filter" between lower crustal zones of magma generation and mixing, and upper crustal zones of large, relatively homogeneous intrusions such as the Mount Stuart batholith.

REFERENCES

Abraham, A. P. G., Davis, D. W., Kamo, S. L., and Spooner, E. T. C., 1994, Geochronological constraints on late Archean magmatism deformation and gold-quartz vein mineralization in the northwestern Anialik River greenstone belt and igneous complex, Slave Province, N.W.T.: Canadian Journal of Earth Sciences, v. 31, p. 1365-1383.

Ague, J. J., and Brandon, M. T., 1996, Regional tilt of the Mount Stuart Batholith, Washington, determined using aluminum-in-hornblende barometry: Implications for northward translation of Baja British Columbia: Geological Society of America Bulletin, v. 108, p. 471-488.

Aleinikoff, J. N., Wintsch, R. P., Fanning, C. M., and Dorais, M. J., 2002, U-Pb geochronology of zircon and polygenetic titanite from the Glastonbury Complex, Connecticut, USA; an integrated SEM, EMPA, TIMS, and SHRIMP study: Chemical Geology, v. 188, p. 125-147.

Améglio, L., and Vigneresse, J. L., 1999, Geophysical imaging of the shape of granitic intrusions at depth: a review, *in* Castro, A., Fernandez, C., and Vigneresse, J. L., eds., Understanding Granites: Integrating New and Classical Techniques: London, Geological Society, p. 39-54.

Améglio, L., Vigneresse, J. L., and Bouchez, J. L., 1997, Granite pluton geometry and emplacement mode inferred from combined fabric and gravity data, *in* Bouchez, J. L., Hutton, D. H. W., and Stephens, W. E., eds., Granite: From Segregation of Melt to Emplacement Fabrics: Dordrecht, Kluwer Academic Publishers, p. 199-214.

Anderson, J. L., 1992, Compositional variation within the high-Mg, tonalitic Mount Stuart Batholith, North Cascades, Washington: Geological Society of America Abstracts with Programs, v. 24, p. 3.

Benn, K., Paterson, S. R., Lund, S. P., Pignotta, G. S., and Kruse, S., 2001, Magmatic fabrics in batholiths as markers of regional strains and plate kinematics: Example of the cretaceous Mt. Stuart Batholith: Physics and Chemistry of the Earth, v. 26, p. 343-354.

Brown, E. H., and Walker, N. W., 1993, A magma-loading model for Barrovian metamorphism in the Southeast Coast Plutonic Complex, British Columbia and Washington: Geological Society of America Bulletin, v. 105, p. 479-500.

Cater, F. W., 1982, Intrusive rocks of the Holden and Lucerne quadrangles, Washington: the relation of depth zones, composition, textures, and emplacement of plutons: U. S. Geological Survey Professional Paper, v. 1220, p. 108.

Cater, F. W., and Crowder, D. F., 1967, Geologic map of the Holden Quadrangle, Snohomish and Chelan counties, Washington: U. S. Geological Survey.

Coleman, D. S., Gray, W., and Glazner, A. F., 2004, Rethinking the emplacement and evolution of zoned plutons: Geochronologic evidence for incremental assembly of the Tuolumne Intrusive Suite, California: Geology, v. 32, p. 433-436.

Corfu, F., and Stone, D., 1998, The significance of titanite and apatite U-Pb ages: Constraints for the post-magmatic thermal-hydrothermal evolution of a batholithic complex, Berens River area, northwestern Superior Province, Canada: Geochimica et Cosmochimica Acta, v. 62, p. 2979-2995.

Crisp, J. A., 1984, Rates of magma emplacement and volcanic output: Journal of Volcanology and Geothermal Research, v. 20, p. 177-211.

Cruden, A. R., 1998, On the emplacement of tabular granites: Journal of the Geological Society of London, v. 155, p. 853-862.

Dawes, R. L., 1993, Mid-crustal, Late Cretaceous plutons of the North Cascades: petrogenesis and implications for the growth of continental crust [PhD thesis]: University of Washington, Seattle, 272 p.

DeBari, S. M., Miller, R. B., and Paterson, S. R., 1998, Genesis of tonalitic plutons in the Cretaceous magmatic arc of the North Cascades: mixing of mantle-derived mafic magmas and melts of a garnet-bearing lower crust: Geological Society of America Abstracts with Programs, v. 30, p. 257-258.

Dodson, M. H., 1973, Closure temperature in cooling geochronological and petrological systems: Contributions to Mineralogy and Petrology, v. 40, p. 259-274.

Dragovich, J. D., and Norman, D. K., 1995, Geologic map of the west half of the Twisp 1:100,000 Quadrangle, Washington, scale 1:100,000.

Dvorak, J. J., and Dzurisin, D., 1997, Volcano geodesy: the search for magma reservoirs and the formation of eruptive vents: Reviews of Geophysics, v. 35, p. 343-384.

Engels, J. C., and Crowder, D. F., 1971, Late Cretaceous fission-track and potassium-argon ages of the Mount Stuart granodiorite and Beckler Peak stock, North Cascades, Washington: U.S. Geological Survey Professional Paper, v. 750-D, p. D39-D43.

Erikson, E. H., 1977, Petrology and petrogenesis of the Mount Stuart batholith: Plutonic equivalent of high-alumina basalt association?: Contributions to Mineralogy and Petrology, v. 60, p. 183-207.

Evans, B. W., and Berti, J. W., 1986, Revised metamorphic history for the Chiwaukum Schist, North Cascades, Washington: Geology, v. 14, p. 695-698.

Evans, B. W., and Davidson, G. F., 1999, Kinetic control of metamorphic imprint during synplutonic loading of batholiths: An example from Mount Stuart, Washington: Geology, v. 27, p. 415-418.

Ferry, J. M., 1979, Reaction mechanisms, physical conditions, and mass transfer during hydrothermal alteration of mica and feldspar in granitic rocks from south-central Maine, USA: Contributions to Mineralogy and Petrology, v. 68, p. 125-139.

Francis, P., and Rundle, C. C., 1976, Rates of production of the main magma types in the central Andes: Geological Society of America Bulletin, v. 87, p. 474-480.

Friedman, R. M., and Armstrong, R. L., 1995, Jurassic and Cretaceous geochronology of the southern Coast Belt, British Columbia, 49° to 51°N, *in* Miller, D. M., and Busby, C., eds., Jurassic magmatism and tectonics of the North American Cordillera: Boulder, Geological Society of America, p. 95-139.

Friedman, R. M., Mahoney, J. B., and Cui, Y., 1995, Magmatic evolution of the southern Coast Belt: constraints from Nd-Sr isotopic systematics and geochronology of the southern Coast Plutonic Complex: Canadian Journal of Earth Sciences, v. 32, p. 1681-1698.

Frost, B. R., Chamberlain, K. R., and Schumacher, J. C., 2000, Sphene (titanite): phase relations and role as a geochronometer: Chemical Geology, v. 172, p. 131-148.

Gerstenberger, H., and Haase, G., 1997, A highly effective emitter substance for mass spectrometric Pb isotope ratio determinations: Chemical Geology, v. 136, p. 309-312.

Getty, S. R., and Gromet, L. P., 1992, Geochronological constraints on ductile deformation, crustal extension, and doming about a basement-cover boundary, New England Appalachians: American Journal of Science, v. 292, p. 359-397.

Gibbons, W., and Horak, J., 1984, Alpine metamorphism of Hercynian hornblende granodiorite beneath the blueschist facies *schistes lustrés* nappe of NE Corsica: Journal of Metamorphic Geology, v. 2, p. 95-113.

Glazner, A. F., Bartley, J. M., Coleman, D. S., Gray, W., and Taylor, R. Z., 2004, Are plutons assembled over millions of years by amalgamation from small magma chambers?: GSA Today, v. 14, p. 4-11.

Harrison, T. M., 1981, Diffusion of ^{40}Ar in hornblende: Contributions to Mineralogy and Petrology, v. 78, p. 324-331.

Harrison, T. M., and Clarke, G. K. C., 1979, A model of the thermal effects of igneous intrusion and uplift as applied to Quottoon Pluton, British Columbia: Canadian Journal of Earth Sciences, v. 16, p. 411-420.

Hodge, D. S., Abbey, D. A., Harbin, M. A., Patterson, J. L., Ring, M. J., and Sweeney, J. F., 1982, Gravity studies of subsurface mass distributions of granitic rocks in Maine and New Hampshire: American Journal of Science, v. 282, p. 1289-1234.

Hodges, K. V., 2003, Geochronology and thermochronology in orogenic systems, *in* Rudnick, R. L., ed., Treatise on Geochemistry: Amsterdam, Elsevier, p. 263-292.

Housh, T. B., and Bowring, S. A., 1991, Lead isotopic heterogeneities within alkali feldspars: implications for the determination of initial lead isotopic compositions: Geochimica et Cosmochimica Acta, v. 55, p. 2309-2316.

Hurlow, H. A., 1992, Structural and U/Pb geochronologic studies of the Pasayten Fault, Okanogan Range Batholith, and southeastern Cascades crystalline core, Washington [PhD thesis]: University of Washington, Seattle, 180 p.

Jaeger, J. C., 1957, The temperature in the neighborhood of a cooling intrusive sheet: American Journal of Science, v. 255, p. 306-318.

Jaeger, J. C., 1961, The cooling of irregularly shaped igneous bodies: American Journal of Science, v. 259, p. 721-734.

Jaffey, A. H., Flynn, K. F., Glendenin, L. E., Bentley, W. C., and Essling, A. M., 1971, Precision measurements of half-lives and specific activities of ^{235}U and ^{238}U: Physics Review, v. C4, p. 1889-1906.

Kelemen, P. B., and Ghiorso, M. S., 1986, Assimilation of peridotite in zoned calc-alkaline plutonic complexes: Evidence from the Big Jim Complex, Washington Cascades: Contributions to Mineralogy and Petrology, v. 94, p. 12-28.

Ketchum, J. W. F., Culshaw, N. G., and Dunning, G. R., 1997, U-Pb geochronologic constraints on Paleoproterozoic orogenesis in the northwestern Makkovik Province, Labrador, Canada: Canadian Journal of Earth Sciences, v. 34, p. 1072-1088.

Koyaguchi, T., and Kaneko, K., 2000, Thermal evolution of silicic magma chambers after basalt replenishments: Transactions of the Royal Society of Edinburgh: Earth Sciences, v. 91, p. 46-60.

Krogh, T. E., 1973, A low contamination method for hydrothermal decomposition of zircon and extraction of U and Pb for isotopic age determination: Geochimica et Cosmochimica Acta, v. 37, p. 485-494.

Ludwig, K. R., 1998, On the treatment of concordant uranium-lead ages: Geochimica et Cosmochimica Acta, v. 62, p. 665-676.

Magloughlin, J. F., 1993, A Nason Terrane trilogy: I, Nature and significance of pseudotachylyte: II, Summary of the structural and tectonic history: III, Major and trace element geochemistry and strontium and neodymium isotope geochemistry of the Chiwaukum Schist, amphibolite, and meta-tonalite gneiss of the Nason Terrane [PhD thesis]: University of Minnesota, Minneapolis, 325 p.

McCaffrey, K. J. W., and Petford, N., 1997, Are granitic intrusions scale invariant?: Journal of the Geological Society of London, v. 154, p. 1-4.

McDougall, I., and Harrison, T. M., 1988, Geochronology and thermochronology by the $^{40}Ar/^{39}Ar$ method, Oxford Monographs on Geology and Geophysics, 212 p.

Miller, R. B., 1985, The Ophiolitic Ingalls Complex, North Central Cascade Mountains, Washington: Geological Society of America Bulletin, v. 96, p. 27-42.

Miller, R. B., Brown, E. H., McShane, D. P., and Whitney, D. L., 1993, Intra-arc crustal loading and its tectonic implications, North Cascades crystalline core, Washington and British Columbia: Geology, v. 21, p. 255-258.

Miller, R. B., and Paterson, S. R., 1992, Tectonic implications of syn-emplacement and postemplacement deformation of the Mount Stuart batholith for mid-Cretaceous orogenesis in the North Cascades: Canadian Journal of Earth Sciences, v. 29, p. 479-485.

Miller, R. B., and Paterson, S. R., 1999, In defense of magmatic diapirs: Journal of Structural Geology, v. 21, p. 1161-1173.

Miller, R. B., and Paterson, S. R., 2001a, Construction of mid-crustal sheeted plutons: Examples from the north Cascades, Washington: Geological Society of America Bulletin, v. 113, p. 1423-1442.

Miller, R. B., and Paterson, S. R., 2001b, Influence of lithological heterogeneity, mechanical anisotropy, and magmatism on the rheology of an arc, North Cascades, Washington: Tectonophysics, v. 342, p. 351-370.

Miller, R. B., Paterson, S. R., DeBari, S. M., and Whitney, D. L., 2000, North Cascades Cretaceous crustal section: changing kinematics, rheology, metamorphism, pluton emplacement and petrogenesis from 0 to 40 km depth, *in* Woodsworth, G. J., Jackson, J. L. E., Nelson, J. L., and Ward, B. C., eds., Guidebook for geological field trips in southwestern British Columbia and northern Washington: Vancouver, Geological Association of Canada, p. 229-278.

Monger, J. W. H., Price, R. A., and Tempelman-Kluit, D. J., 1982, Tectonic accretion and the origin of the two major metamorphic and plutonic welts in the Canadian Cordillera: Geology, v. 10, p. 70-75.

Oversby, V. M., 1975, Lead isotopic systematics and ages of Archaean acid intrusives in the Kalgoorlie-Norseman area, Western Australia: Geochimica et Cosmochimica Acta, v. 39, p. 1107-1125.

Paterson, S. R., Fowler, T. K., Jr., Schmidt, K. L., Yoshinobu, A. S., Yuan, E. S., and Miller, R. B., 1998, Interpreting magmatic fabric patterns in plutons: Lithos, v. 44, p. 53-82.

Paterson, S. R., and Miller, R. B., 1998a, Magma emplacement during arc-perpendicular shortening: An example from the Cascades crystalline core, Washington: Tectonics, v. 17, p. 571-586.

Paterson, S. R., and Miller, R. B., 1998b, Stoped blocks in plutons: paleo-plumb bobs, viscometers, or chronometers?: Journal of Structural Geology, v. 20, p. 1261-1272.

Paterson, S. R., Miller, R. B., Anderson, J. L., Lund, S. P., Bendixen, J., Taylor, N., and Fink, T., 1994, Emplacement and evolution of the Mt. Stuart batholith, *in* Swanson, D. A., and Haugerud, R. A.,

eds., Geologic field trips in the Pacific Northwest: 1994 Geological Society of American Annual Meeting, Geological Society of America, p. 2F1-2F47.
Petford, N., Cruden, A. R., McCaffrey, K. J. W., and Vigneresse, J. L., 2000, Granite magma formation, transport and emplacement in the Earth's crust: Nature, v. 408, p. 669-673.
Plummer, C. C., 1980, Dynamothermal contact metamorphism superposed on regional metamorphism in the pelitic rocks of the Chiwaukum Mountains area, Washington Cascades: Geological Society of America Bulletin, v. 91, p. 386-388.
Pongsapich, W., 1974, The geology of the eastern part of the Mount Stuart Batholith, central Cascades, Washington [PhD thesis]: University of Washington, Seattle, 170 p.
Reid, M. R., 2003, Timescales of magma transfer and storage in the crust, *in* Rudnick, R. L., ed., Treatise on Geochemistry: Amsterdam, Elsevier, p. 263-292.
Shaw, H. R., 1985, Links between magma-tectonic rate balances, plutonism, and volcanism: Journal of Geophysical Research, v. 90, p. 11,275-11,288.
Sinton, J. M., and Detrick, R. S., 1992, Mid-ocean ridge magma chambers: Journal of Geophysical Research, v. 97, p. 197-216.
Stacey, J. C., and Kramers, J. D., 1975, Approximation of terrestrial lead isotope evolution by a two-stage model: Earth and Planetary Science Letters, v. 26, p. 207-221.
Stowell, H. H., and Tinkham, D. K., 2003, Integration of phase equilibria modelling and garnet Sm-Nd chronology for construction of P-T-t paths: Examples from the Cordilleran Coast Plutonic Complex, USA, *in* Vance, D., Muller, W., and Villa, I., eds., Geochronology: Linking the Isotopic Record with Petrology and Textures, Geological Society of London, p. 119-145.
Tabor, R. W., Booth, D. B., Vance, J. A., and Ford, A. B., 2002, Geologic map of the Sauk River 30- by 60-minute quadrangle, Washington: U.S. Geological Survey, scale 1:100000.
Tabor, R. W., Frizzell, V. A., Jr., Booth, D. B., Waitt, R. B., Whetten, J. T., and Zartman, R. E., 1993, Geologic map of the Skykomish River 30- by 60-minute Quadrangle, Washington: U. S. Geological Survey, scale 1:100,000.
Tabor, R. W., Frizzell, V. A., Jr., Whetten, J. T., Waitt, R. B., Jr., Swanson, D. A., Byerly, G. R., Booth, D. B., Hetherington, M. J., and Zartman, R. E., 1987, Geologic map of the Chelan 30' by 60' Quadrangle, Washington: U. S. Geological Survey, scale 1:100,000.
Valley, P. M., Whitney, D. L., Paterson, S. R., Miller, R. B., and Alsleben, H., 2003, Metamorphism of the deepest exposed arc rocks in the Cretaceous to Paleogene Cascades belt, Washington: evidence for large- scale vertical motion in a continental arc: Journal of Metamorphic Geology, v. 21, p. 203-220.
van der Heyden, P., 1992, A Middle Jurassic to early Tertiary Andean-Sierran arc model for the Coast Belt of British Columbia: Tectonics, v. 11, p. 82-97.
Van der Heyden, P. A. H., 1989, U-Pb and K-Ar geochronometry of the Coast plutonic complex, 53°N to 54°N, British Columbia, and implications for the Insular-Intermontane superterrane boundary [PhD thesis]: The University of British Columbia, Vancouver.
Van Diver, B. B., 1967, Contemporaneous faulting-metamorphism in Wenatchee Ridge area, Northern Cascades, Washington: American Journal of Science, v. 265, p. 132-150.
Verts, L. A., Chamberlain, K. R., and Frost, C. D., 1996, U-Pb sphene dating of metamorphism: The importance of sphene growth in the contact aureole of the Red Mountain Pluton, Laramie Mountains, Wyoming: Contributions to Mineralogy and Petrology, v. 125, p. 186-199.
Vigneresse, J. L., 1990, Use and misuse of geophysical data to determine the shape at depth of granitic intrusions: Geological Journal, v. 25, p. 249-260.
Vigneresse, J.-L., Tikoff, B., and Améglio, L., 1999, Modification of the regional stress field by magma intrusion and formation of tabular granitic plutons: Tectonophysics, v. 302, p. 203-224.
Walker, N. W., and Brown, E. H., 1991, Is the southeast Coast Plutonic Complex the consequence of accretion of the Insular Superterrane: Evidence from U-Pb zircon geochronometry in the Northern Washington Cascades: Geology, v. 19, p. 714-717.
Wendt, I., and Carl, C., 1991, The statistical distribution of the mean squared weighted deviation: Chemical Geology, v. 86, p. 275-285.
Whitney, D. L., Miller, R. B., and Paterson, S. R., 1999, P-T-t evidence for mechanisms of vertical tectonic motion in a contractional orogen: north-western US and Canadian Cordillera: Journal of Metamorphic Geology, v. 17, p. 75-90.

Woodsworth, G. W., Anderson, R. G., and Armstrong, R. L., 1991, Plutonic regimes, *in* Gabrielse, H., and Yorath, C. J., eds., Geology of the Cordilleran Orogen in Canada, Geological Survey of Canada, p. 491-531.

Zen, E.-a., and Hammarstrom, J. M., 1984, Magmatic epidote and its petrologic significance: Geology, v. 12, p. 515-518.

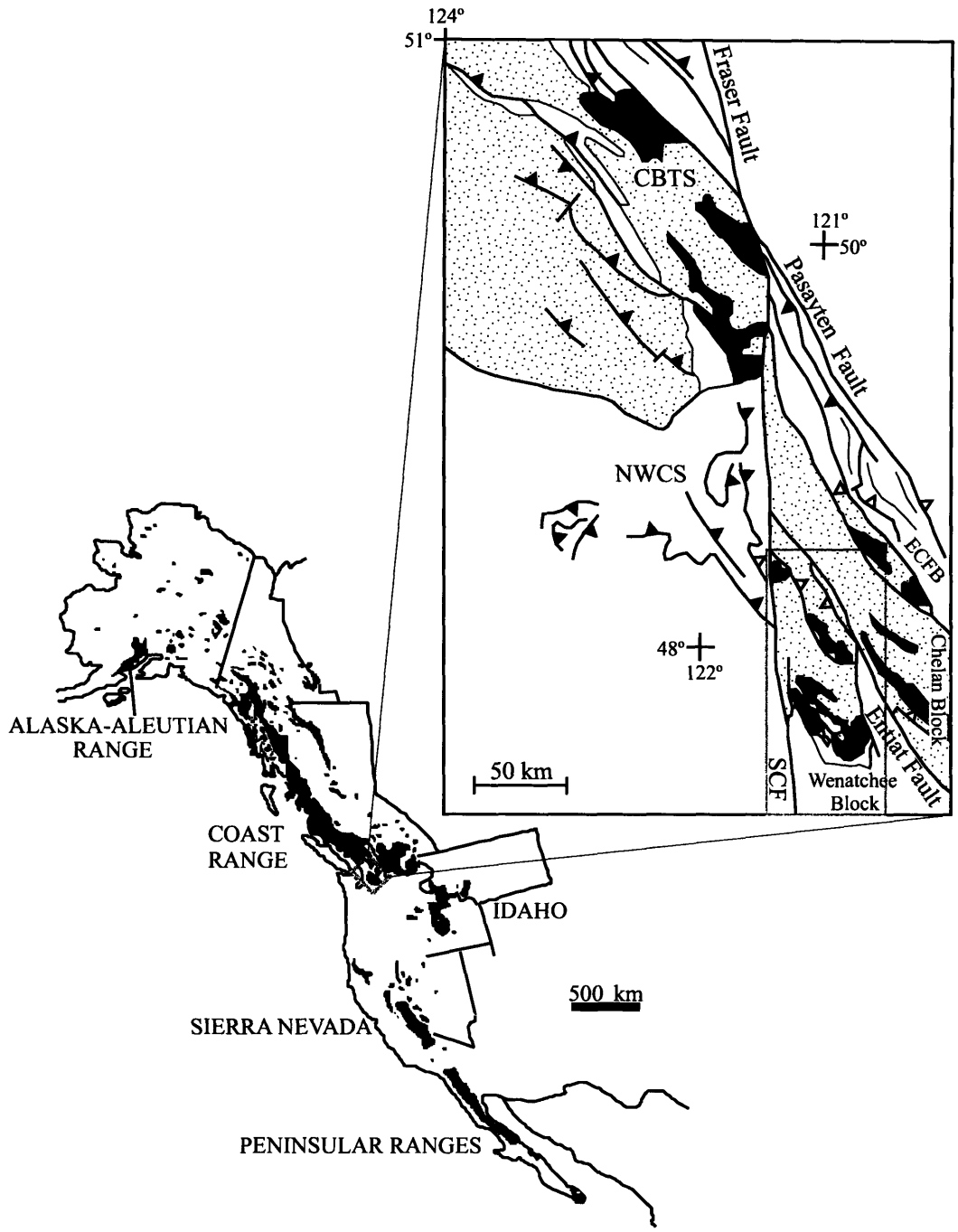

Figure 1. Sketch map of Mesozoic and Paleogene arc plutons in the western North American Cordillera (after Miller et al., 2000). Inset emphasizes distribution of metamorphic rocks (speckled pattern) and plutons (dark grey). Also shown are the Coast Belt thrust system (CBTS), lower-grade rocks of the Eastern Cascades fold belt (ECFB), and Northwest Cascades fault system (NWCS). The dextral Fraser-Straight Creek (SCF) fault offsets the Cascades core from the main part of the Coast Belt. The Entiat fault is a Tertiary, high-angle fault that divides that Cascades core into the Wenatchee and Chelan blocks. Light grey box in inset outlines the area of figure 2.

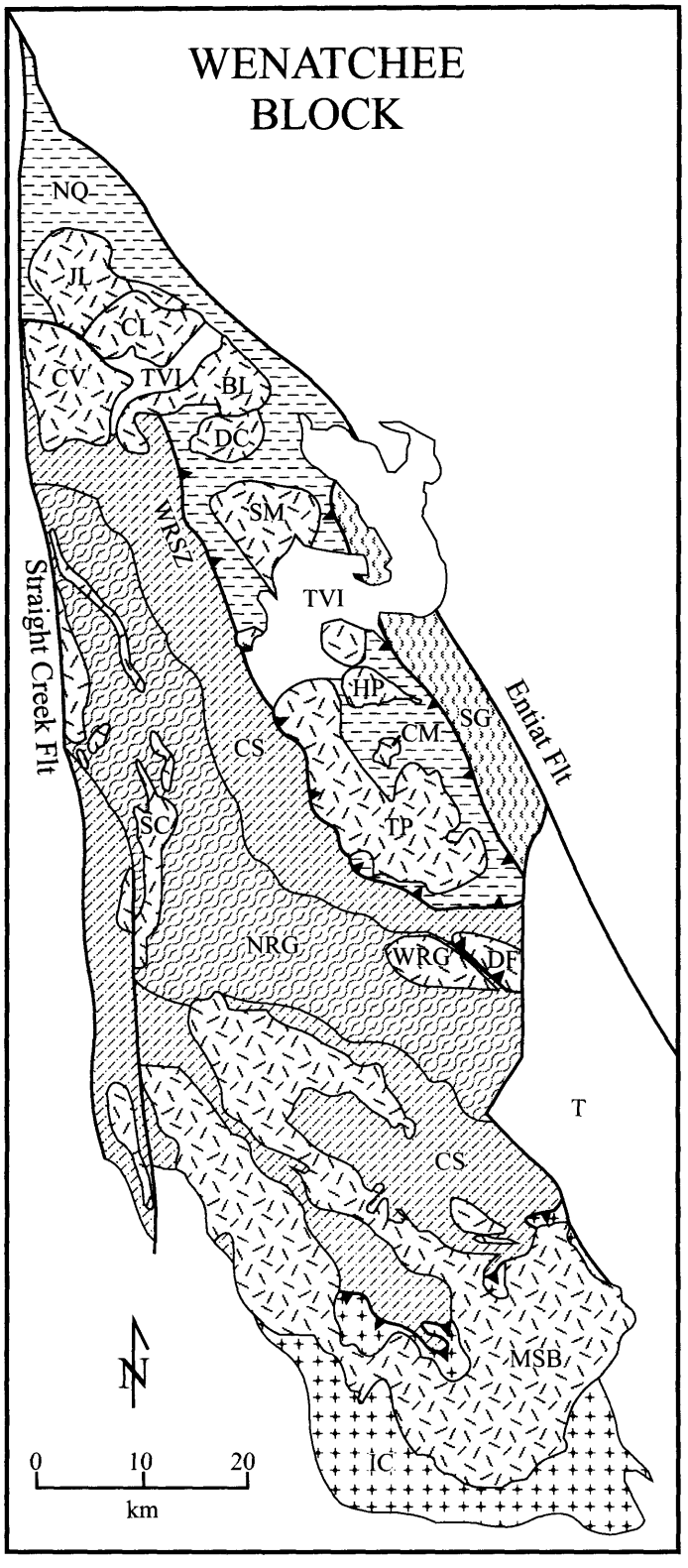

Figure 2. Geologic map of the Wenatchee Block. Plutons shown in a light grey random dash pattern. Abbreviations are as follows: BL, Bench Lake; CL, Cyclone Lake; CM, Clark Mountain; CS, Chiwaukum Schist; CV, Chaval; DC, Downey Creek; DF, Dirtyface; HP, High Pass; IC, Ingalls Complex; JL, Jordan Lakes; MSB, Mount Stuart; NRG, Nason Ridge Migmatitic Gneiss; NQ, Napeequa Complex; SC, Sloan Creek; SG, Swakane Gneiss; SM, Sulphur Mountain; T, Tertiary sediments; TP, Tenpeak; TVI, Tertiary volcanics and intrusives; WRG, Wenatchee Ridge Gneiss.

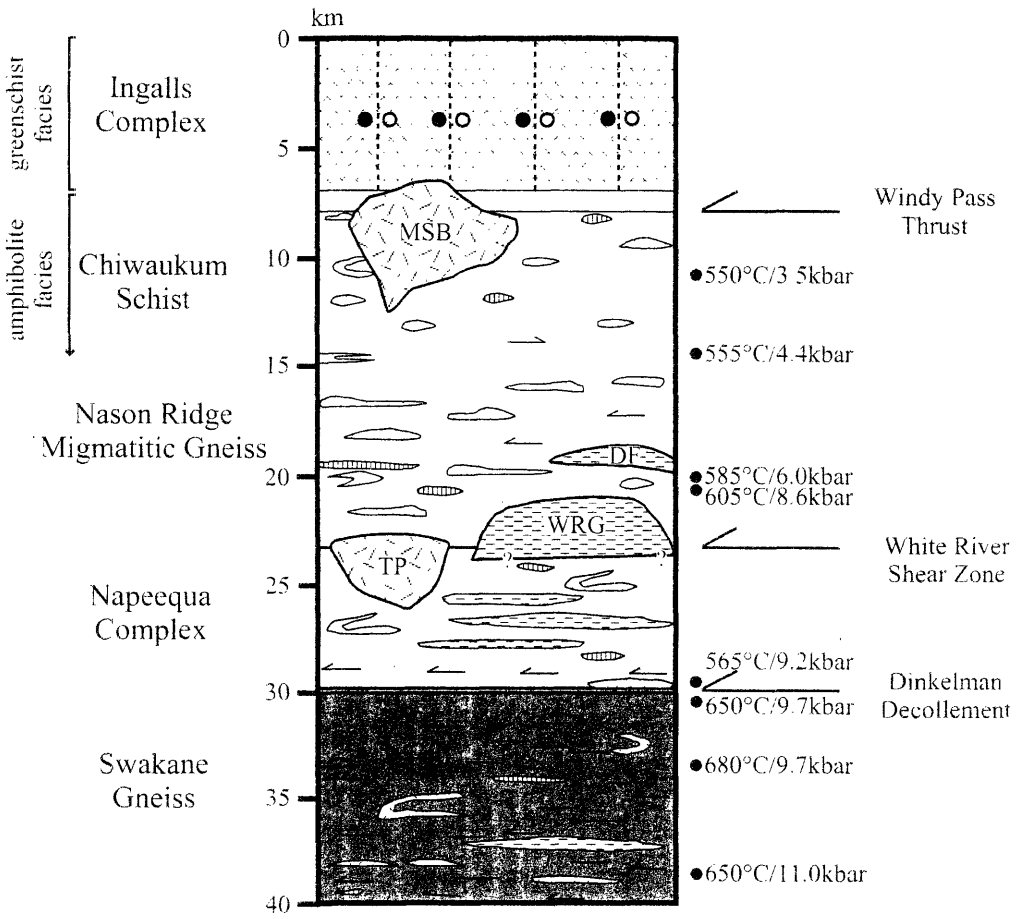

Figure 3. Schematic diagram of the North Cascades crustal section modified from Miller and Paterson (2001b). Random dashes denote plutons with mostly magmatic fabrics, whereas bold horizontal dashes denote intrusive rocks with strongly developed solid-state deformation and/or intense magmatic foliation. Other lenses in the Chiwaukum and Napeequa units are amphibolite, metaperidotite and minor marble, and half-arrows show areas with non-coaxial shear. Vertical dashed lines are faults in the Ingalls Complex. Numbers on right side of diagram list representative temperatures (°C) and pressures (kbar) summarized in Miller and Paterson (2001b). Abbreviations are the same as in figure 2.

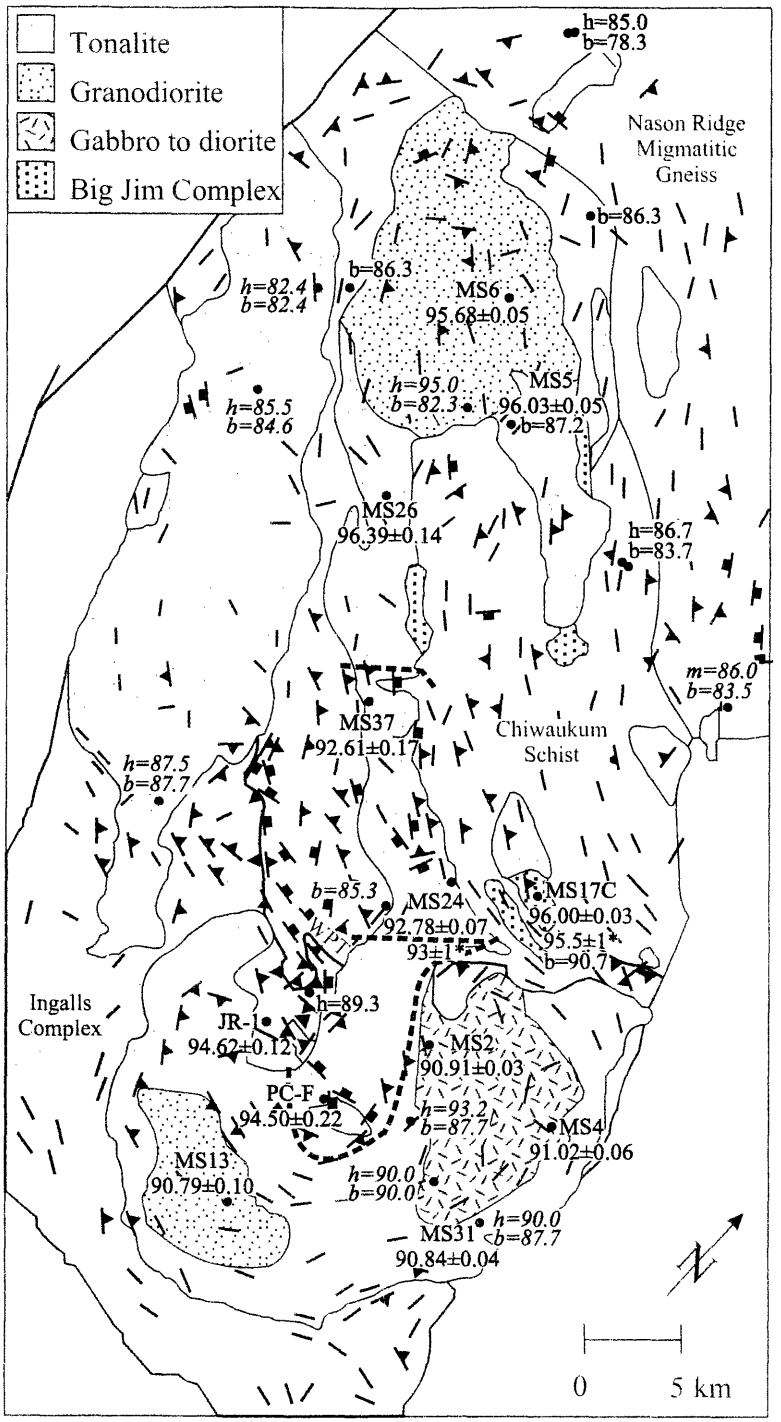

Figure 4. Map of the Mount Stuart batholith showing internal petrologic variations, regional foliation patterns and geochronologic data (after Paterson et al., 1994). Dates with an asterisk are U-Pb zircon dates from previously published studies (Tabor et al., 1987; Walker and Brown, 1991). K-Ar and ^{40}Ar-^{39}Ar dates (Chapter 3; Evans and Davidson, 1999; Tabor et al., 1987; Tabor et al., 1993) are denoted with a "h" for hornblende, a "m" for muscovite and "b" for (biotite). K-Ar dates are in italics. Foliation measurements are depicted by a strike line with filled square (dip=0-29°), with filled triangle (dip=30-59°) or without dip symbol (dip=60-90°). Foliation symbols in the host rock represent average orientations of the most pervasive foliation in the region. Heavy dashed lines approximate the boundaries of different age domains. The Windy Pass thrust is labeled as WPT.

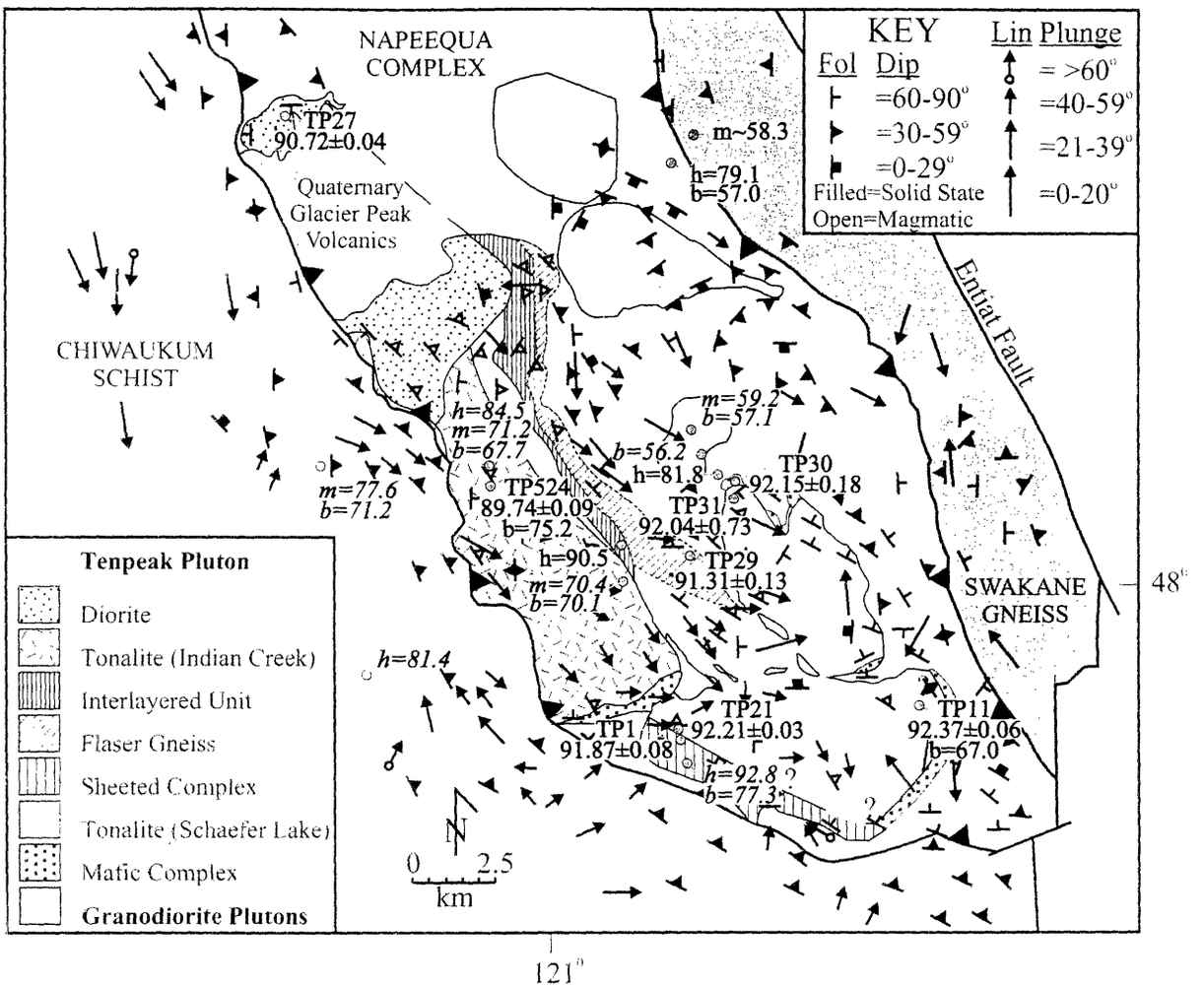

Figure 5. Map of the Tenpeak pluton showing internal petrologic variations, regional foliation patterns and geochronologic data. U-Pb zircon dates labeled with sample numbers. K-Ar dates (in italics) and ^{40}Ar-^{39}Ar dates are denoted with a "h" for hornblende, "m" for muscovite and "b" for biotite (Chapter 3; Dragovich and Norman, 1995; Tabor et al., 1987; Tabor et al., 1993; Tabor et al., 2002).

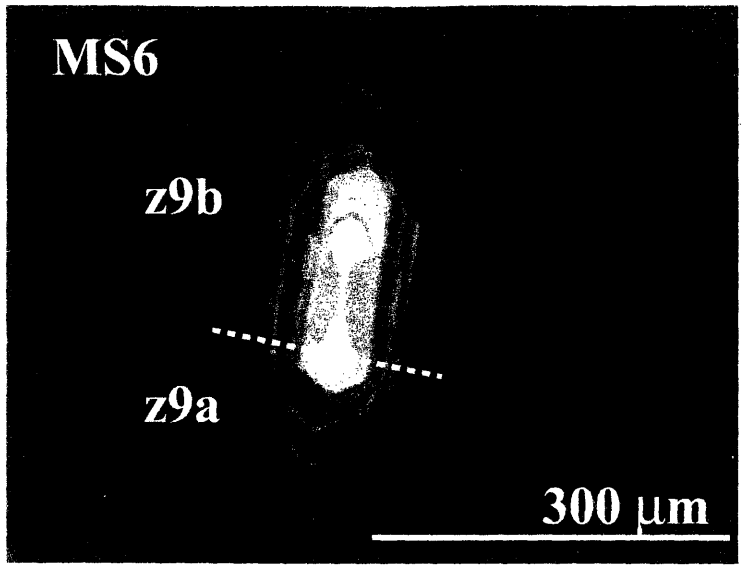

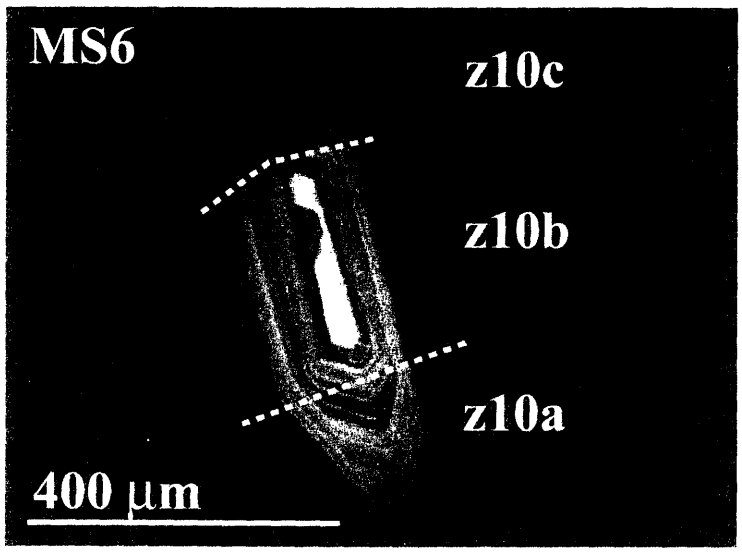

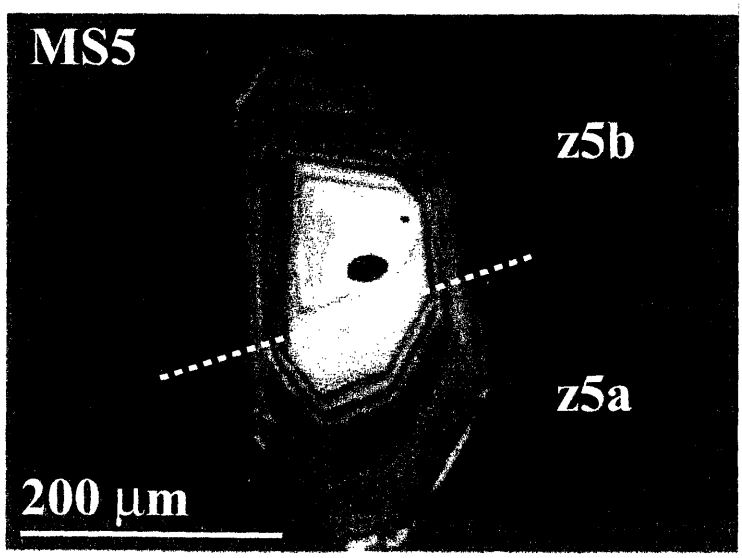

Figure 6. Cathodoluminescence images of zircons from samples MS5 and MS6. Dashed red line approximates where each grain was broken into fragments for U-Pb analysis.

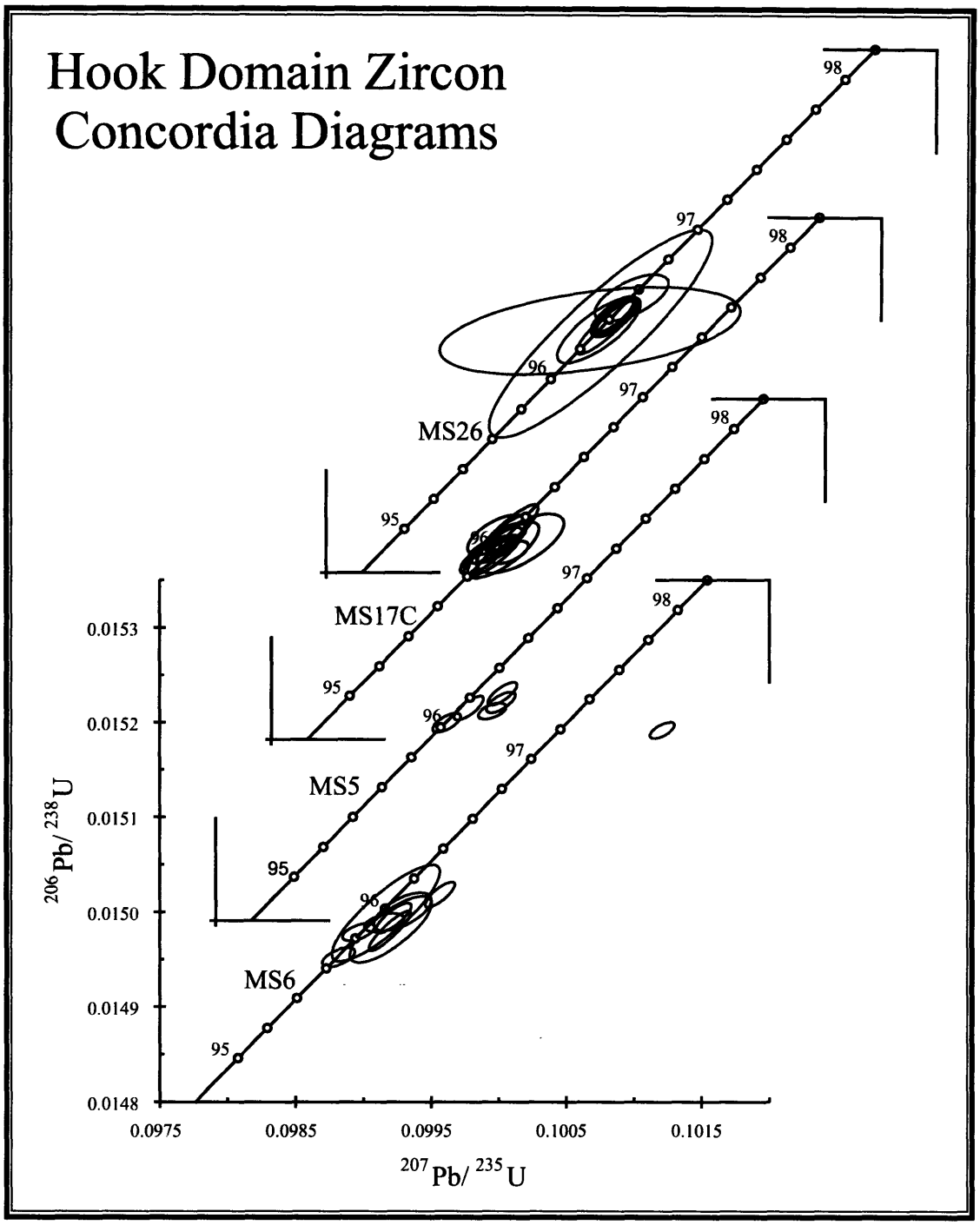

Figure 7. U-Pb zircon concordia diagrams for samples from the hook-shaped region of the MSB. All samples are plotted at the same scale and the axes of each diagram step up and to the right. Concordia ellipses are represented by heavy black lines.

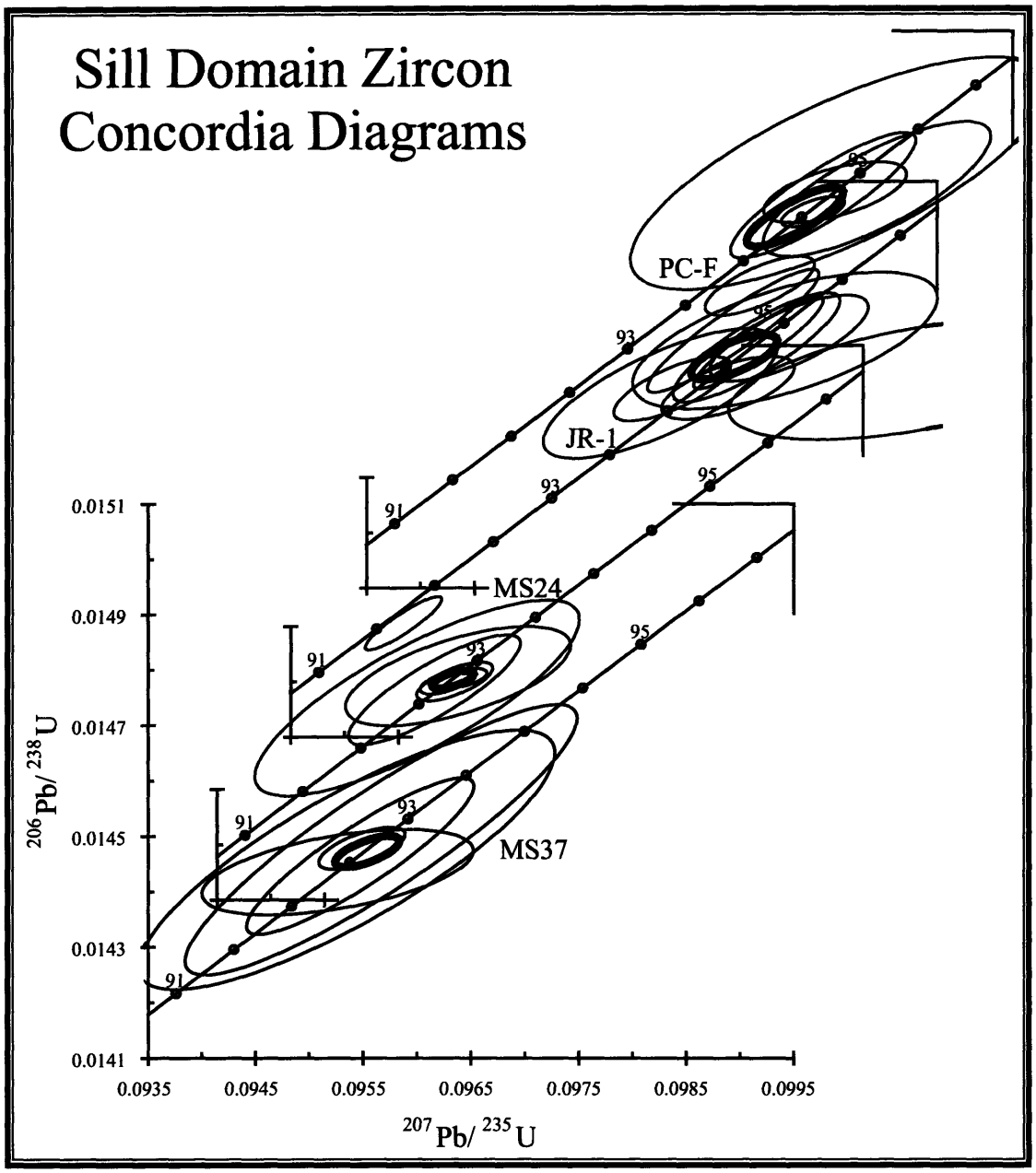

Figure 8. U-Pb zircon concordia diagrams for samples from the intermediate age groups of the MSB. All samples are plotted at the same scale and the axes of each diagram step and to the right. Concordia ellipses are represented by heavy black lines.

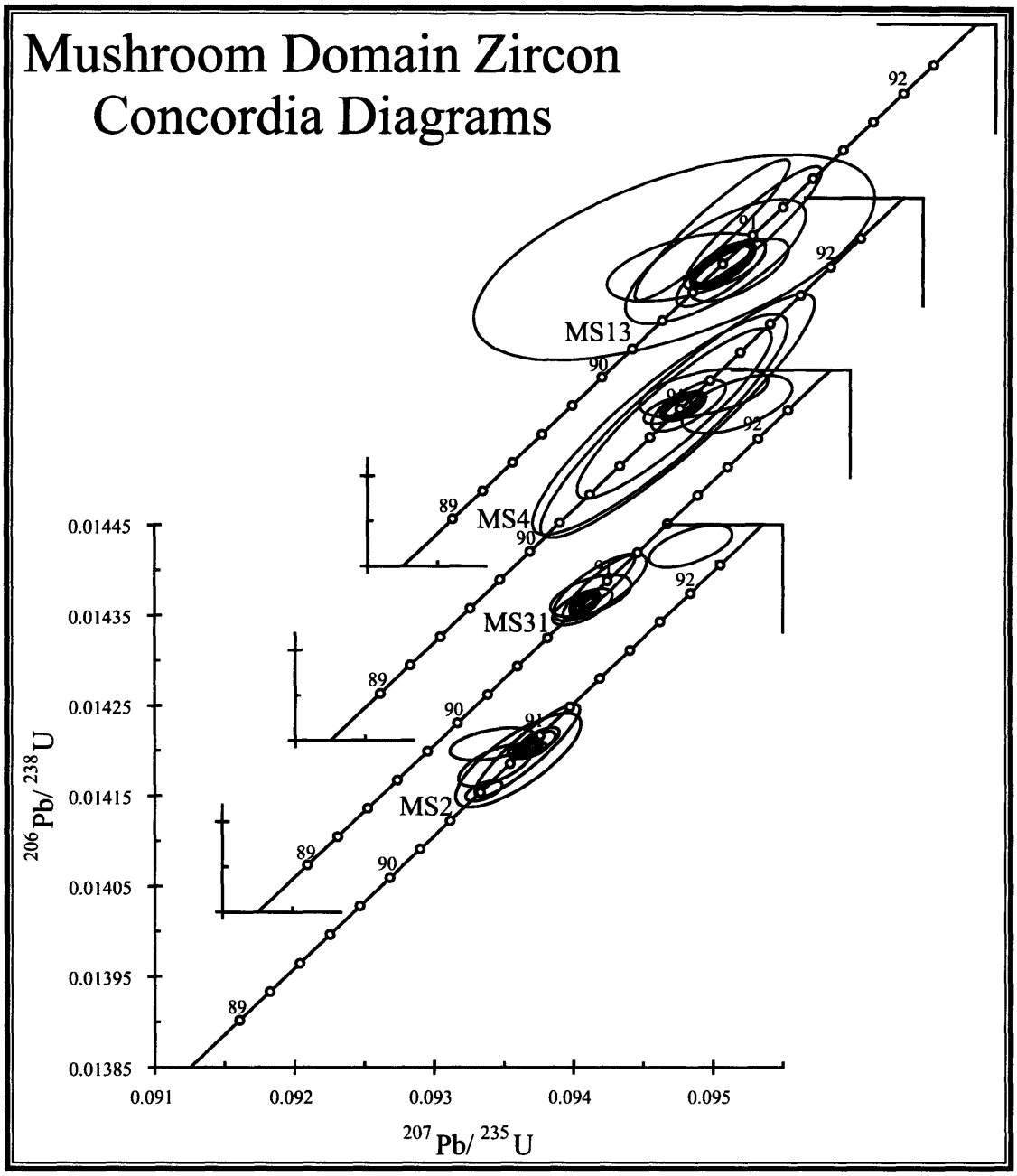

Figure 9. U-Pb zircon concordia diagrams from samples from the mushroom-shaped region of the MSB. All samples are plotted at the same scale and the axes of each diagram step and to the right. Concordia ellipses are represented by heavy black lines.

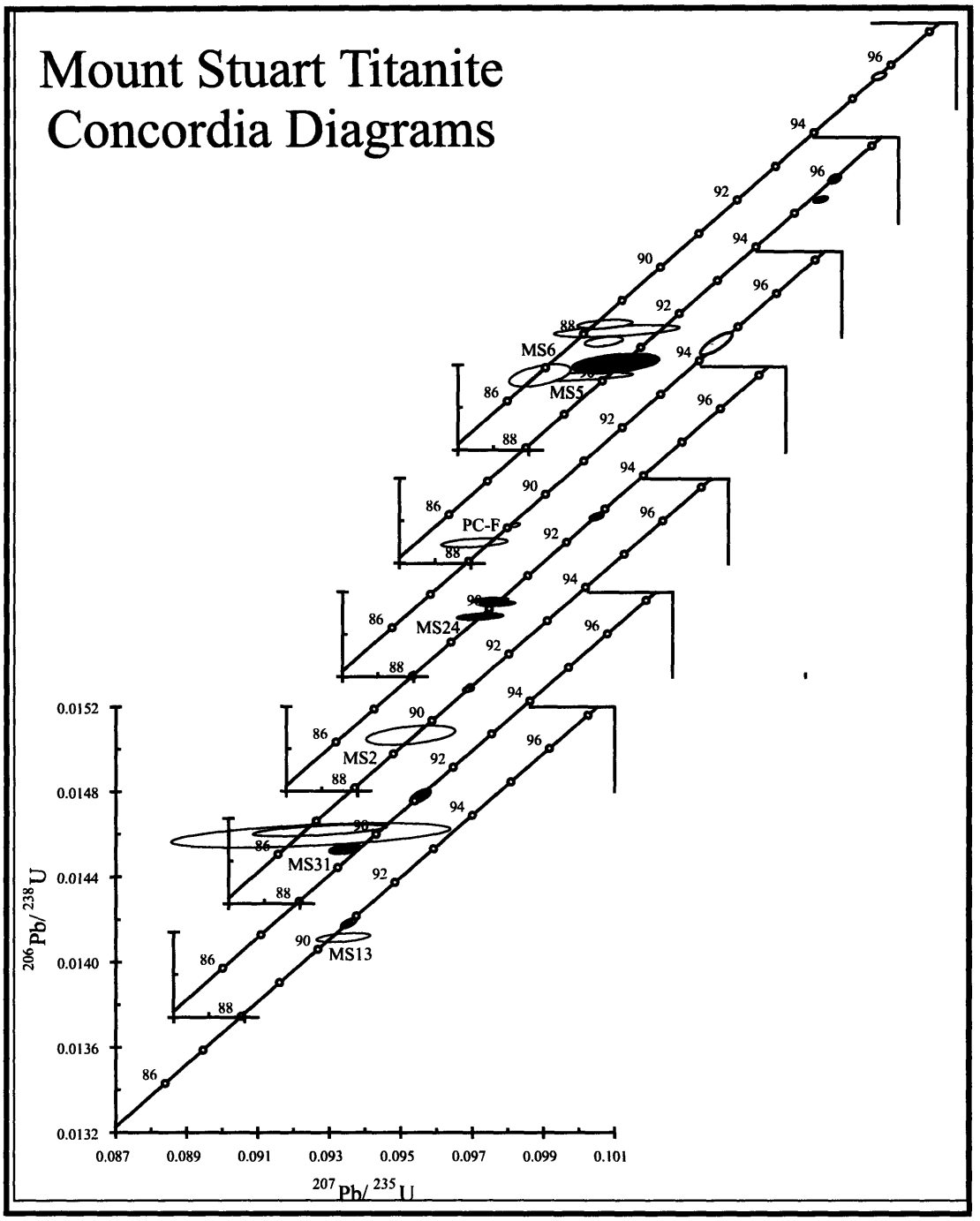

Figure 10. U-Pb titanite concordia diagrams for MSB samples. Ellipses for a given sample have the same fill color. The fill color alternates in color between samples so that each sample is distinguishable from the next. For comparison, zircon concordia ellipses or the most concordant zircon analysis (for *MS5* and *MS6*) are outlined in red.

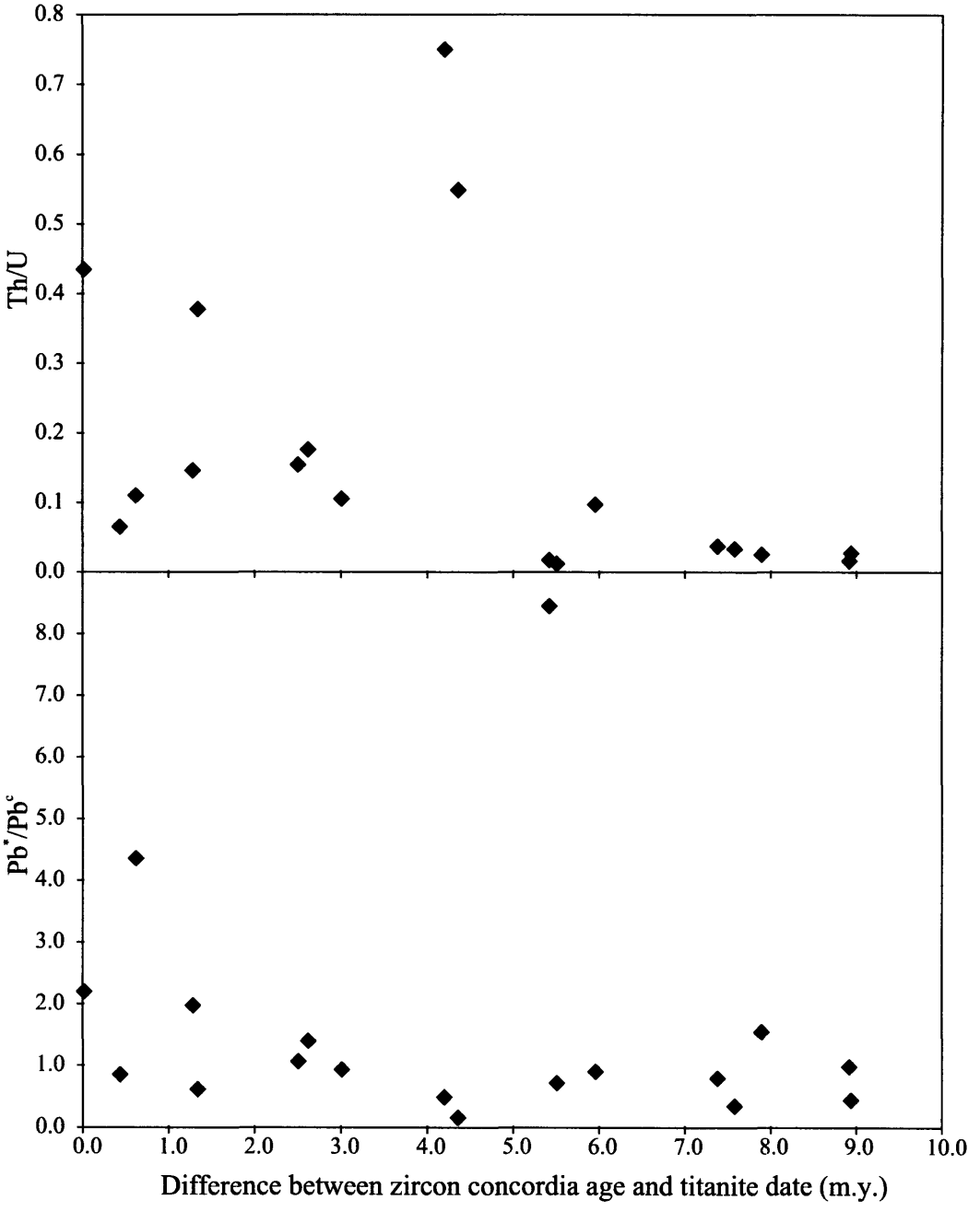

Figure 11. Variations in Th/U and Pb^*/Pb^c ratios of titanite grains versus difference in zircon crystallization ages and titanite dates.

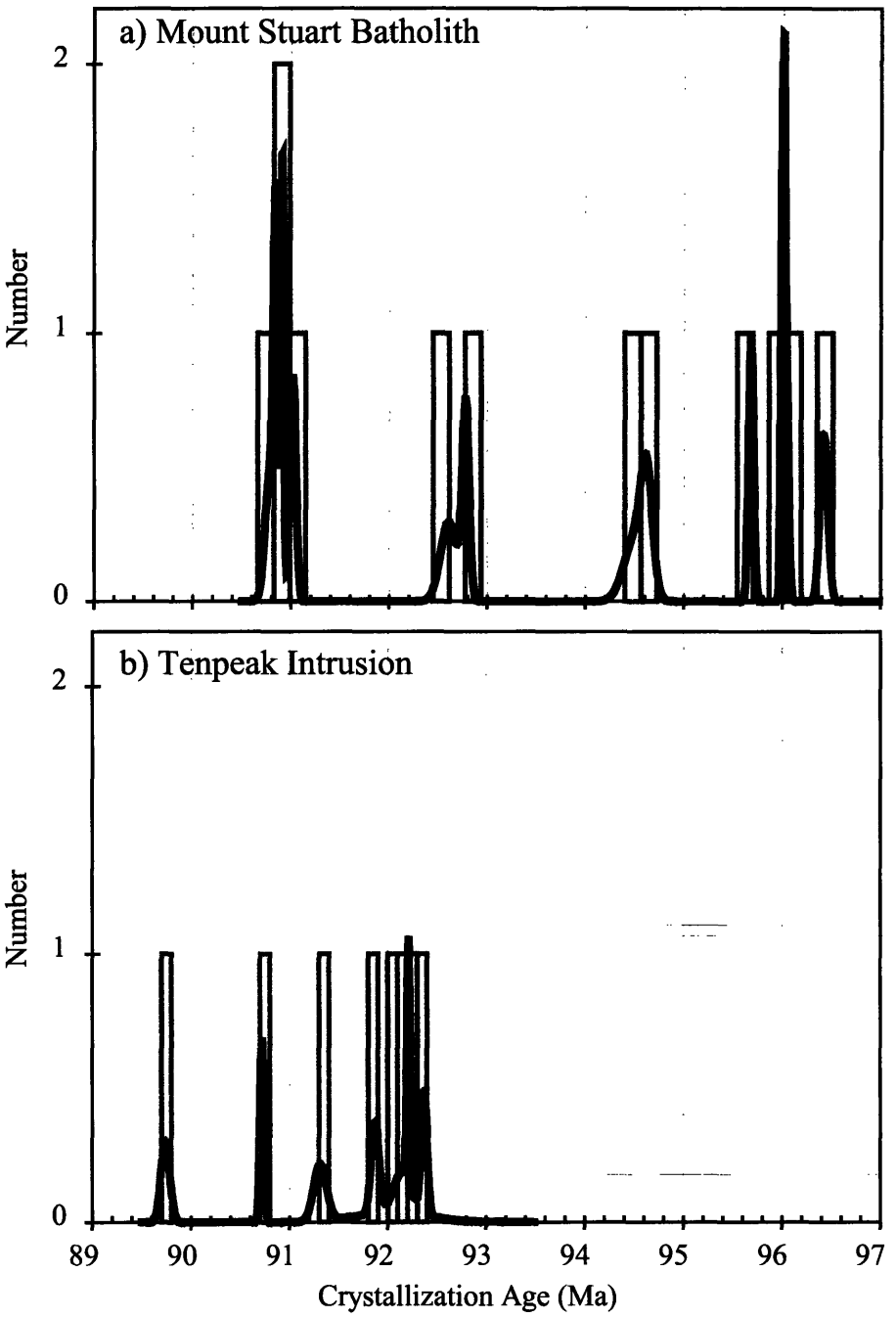

Figure 12. Histograms (heavy gray lines) and probability density functions (heavy black lines) of zircon U-Pb concordia ages from the a) Mount Stuart batholith and b) Tenpeak intrusion. Probability density functions are constructed by summing the probability distribution of each datum with normally distributed errors.

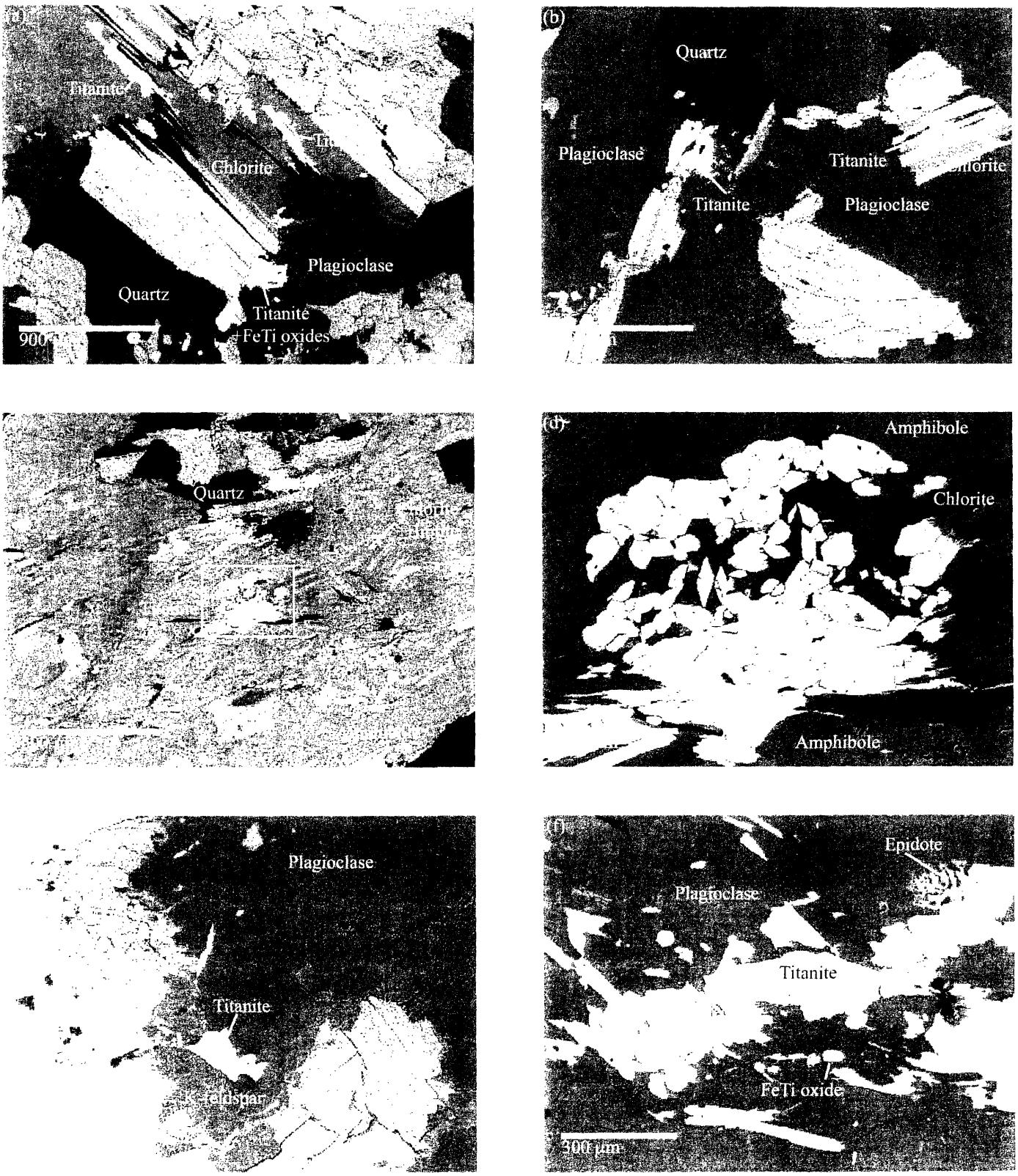

Figure 13. Back-scattered electron images of titanite grains from the MSB (a-e) and Tenpeak pluton (f). Image (d) is a close up of the area outlined in the box in image (c).

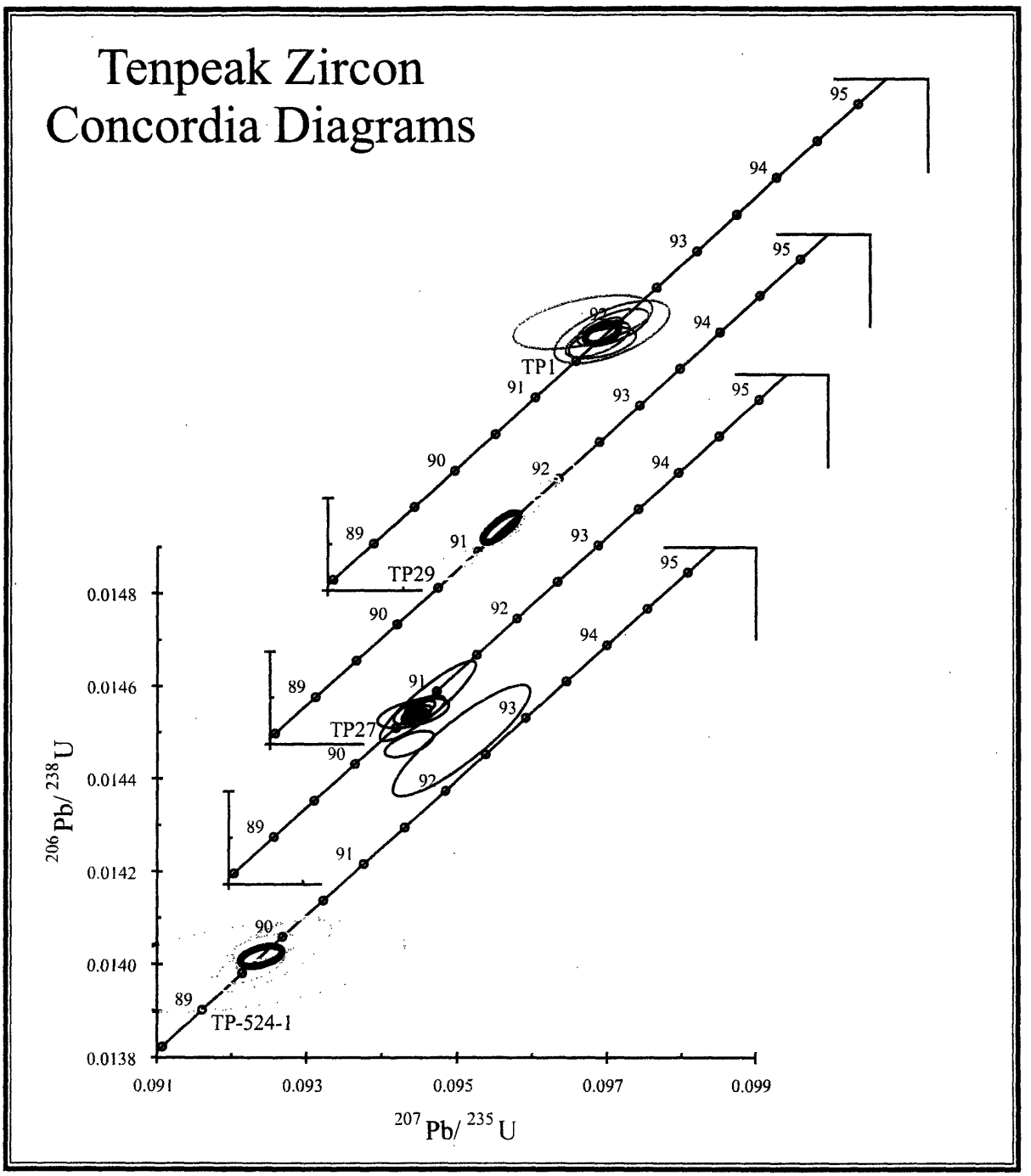

Figure 14. U-Pb zircon concordia diagrams from the youngest four Tenpeak samples. Concordia ellipses are represented by heavy black lines.

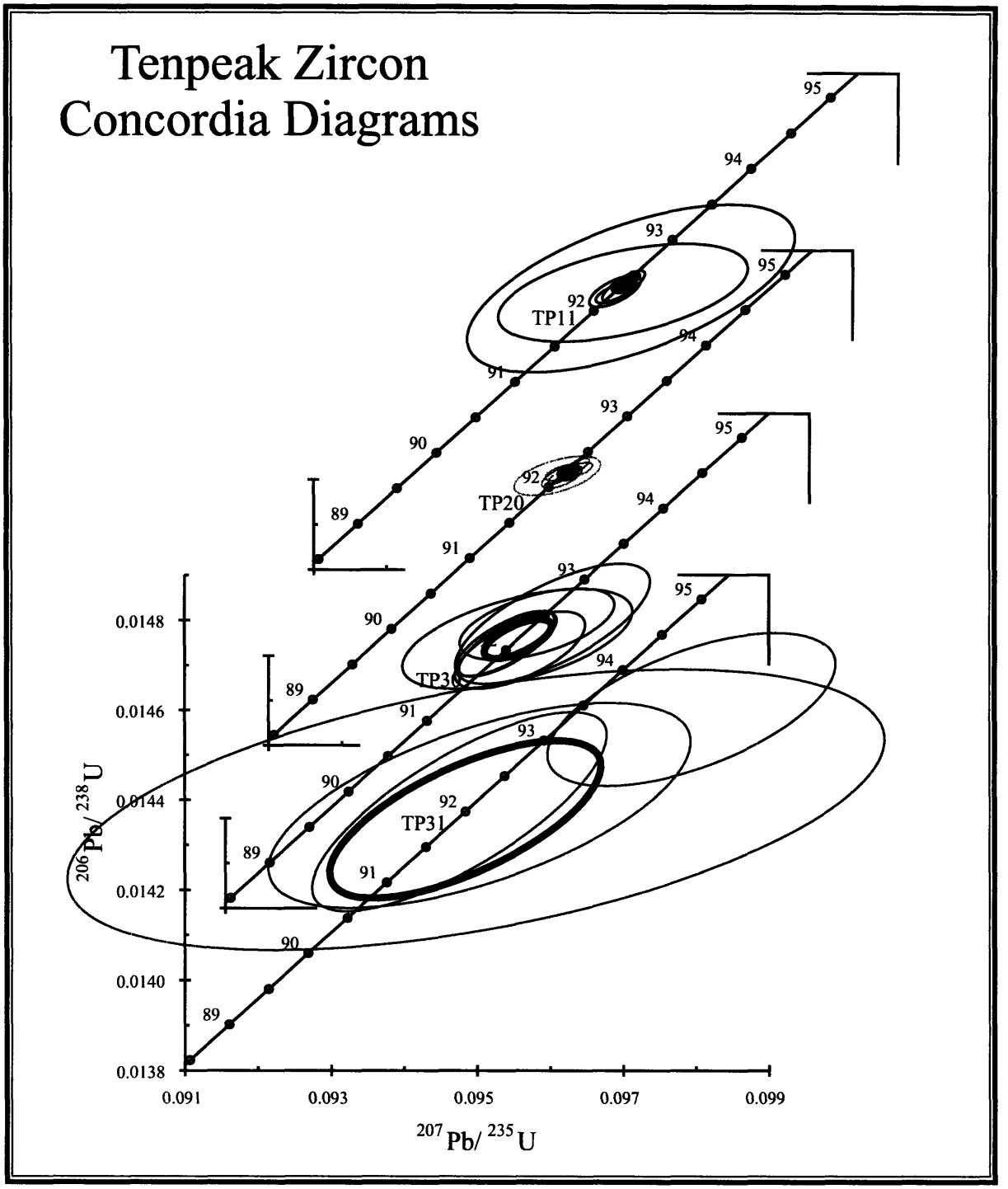

Figure 15. U-Pb zircon concordia diagrams from the oldest four Tenpeak samples. Concordia ellipses are represented by heavy black lines.

Table 1. U-Pb analyses from the Mount Stuart batholith.

	Composition						Isotopic Ratios								Dates (Ma)				
Frac[a]	Wt (μg)[b]	U (ppm)	Pb (ppm)	Th[c] / U	Pb*[d] / Pbc	Pbc[d] (pg)	$^{206}Pb/^{204}Pb$[e]	$^{208}Pb/^{206}Pb$[f]	$^{206}Pb/^{238}U$[f]	% err[g]	$^{207}Pb/^{235}U$[f]	% err[g]	$^{207}Pb/^{206}Pb$[f]	% err[g]	$^{206}Pb/^{238}U$[h]	$^{207}Pb/^{235}U$[h]	$^{207}Pb/^{206}Pb$[h]	corr. coef.	Discord-ance
MS2: GABBRO																			
z2	88.6	70.0	1.0	0.347	58.4	1.5	3790	0.111	0.014207	(.10)	0.09342	(.27)	0.047692	(.24)	90.94	90.69	84.0	0.443	-8.4
z3	64.1	75.9	1.1	0.296	114.5	0.6	7523	0.095	0.014201	(.05)	0.09367	(.12)	0.047838	(.11)	90.90	90.91	91.3	0.465	0.4
z4	38.6	65.3	0.9	0.349	47.0	0.8	3053	0.112	0.014211	(.09)	0.09375	(.13)	0.047848	(.10)	90.96	90.99	91.8	0.671	0.9
z5	93.6	40.2	0.6	0.332	44.5	1.2	2902	0.106	0.014206	(.09)	0.09373	(.12)	0.047851	(.09)	90.93	90.97	91.9	0.705	1.1
z6	49.3	73.1	1.0	0.317	24.7	2.0	1627	0.101	0.014200	(.29)	0.09367	(.33)	0.047842	(.14)	90.89	90.92	91.4	0.902	0.6
z7	93.6	53.5	0.8	0.334	15.8	4.5	1035	0.107	0.014189	(.30)	0.09360	(.39)	0.047845	(.25)	90.83	90.85	91.6	0.777	0.8
z8	47.1	79.9	1.1	0.251	26.7	1.9	1793	0.080	0.014183	(.13)	0.09344	(.23)	0.047779	(.18)	90.79	90.70	88.3	0.625	-2.8
z9	54.2	163.6	2.2	0.242	63.8	1.9	4261	0.077	0.014155	(.07)	0.09336	(.11)	0.047832	(.09)	90.61	90.62	91.0	0.594	0.4
t1	250.6	30.3	1.4	0.750	0.5	234.1	46.8	0.241	0.013542	(.15)	0.08956	(1.71)	0.047966	(1.62)	86.71	87.10	97.6	0.620	11.2
t2	177.8	10.3	1.1	0.549	0.2	163.0	28.5	0.176	0.013517	(.36)	0.08901	(3.83)	0.047760	(3.63)	86.55	86.58	87.4	0.579	1.0
t3	97.0	29.7	1.1	0.378	0.6	66.3	57.6	0.121	0.013992	(.27)	0.09210	(1.09)	0.047740	(1.01)	89.57	89.46	86.5	0.414	-3.6
MS4: GABBRO																			
z2	25.0	155.4	2.2	0.380	43.5	1.3	2804	0.121	0.014215	(.09)	0.09367	(.15)	0.047792	(.12)	90.99	90.92	88.9	0.607	-2.3
z3	49.0	59.9	0.9	0.361	28.7	1.5	1865	0.116	0.014234	(.16)	0.09393	(.40)	0.047859	(.35)	91.11	91.16	92.3	0.494	1.3
z6	27.2	47.7	0.8	0.355	3.8	4.8	262	0.113	0.014209	(.78)	0.09374	(.85)	0.047847	(.34)	90.95	90.98	91.8	0.919	0.9
z7	38.3	49.7	0.8	0.382	6.6	4.1	440	0.122	0.014212	(.54)	0.09372	(.61)	0.047827	(.26)	90.97	90.96	90.7	0.904	-0.3
z11	46.6	36.3	0.5	0.345	16.8	1.4	1105	0.111	0.014222	(.18)	0.09417	(.34)	0.048022	(.28)	91.04	91.38	100.3	0.563	9.3
z12	44.8	40.8	0.6	0.378	19.5	1.3	1265	0.121	0.014220	(.16)	0.09382	(.23)	0.047851	(.16)	91.02	91.06	91.9	0.726	1.0
z13	34.7	41.7	0.7	0.384	4.5	4.6	303	0.123	0.014200	(.70)	0.09362	(.80)	0.047815	(.36)	90.89	90.87	90.1	0.895	-0.9
MS5:TONALITE																			
z1	39.2	785.7	11.3	0.202	119.2	3.7	7995	0.065	0.015030	(.06)	0.09960	(.09)	0.048064	(.06)	96.17	96.41	102.4	0.694	6.1
z2	34.6	964.7	13.8	0.182	327.0	1.5	22147	0.058	0.015039	(.07)	0.09962	(.09)	0.048040	(.06)	96.23	96.42	101.3	0.766	5.0
z3	30.6	1121.4	16.0	0.167	234.2	2.1	15931	0.053	0.015024	(.07)	0.09937	(.09)	0.047968	(.06)	96.13	96.19	97.7	0.758	1.6
z5a	18.5	669.4	9.4	0.144	134.3	1.3	9210	0.046	0.015008	(.05)	0.09920	(.08)	0.047939	(.06)	96.03	96.04	96.3	0.660	0.2
z5b	21.9	658.0	9.2	0.119	170.9	1.2	11799	0.038	0.015021	(.05)	0.09954	(.08)	0.048062	(.07)	96.11	96.35	102.3	0.545	6.1
t3	51.6	628.3	10.7	0.110	4.4	103.3	317.0	0.035	0.014911	(.08)	0.09880	(.17)	0.048058	(.14)	95.41	95.67	102.1	0.537	6.6
t4	27.9	107.3	3.2	0.012	0.7	53.4	69.3	0.004	0.014142	(.27)	0.09305	(1.07)	0.047722	(.99)	90.52	90.34	85.5	0.412	-5.9
MS6:GRANODIORITE																			
z1	22.0	1016.4	14.5	0.162	131.8	2.4	8969	0.052	0.015018	(.07)	0.09957	(.09)	0.048083	(.05)	96.09	96.38	103.4	0.799	7.1
z2	18.0	1113.4	15.6	0.117	132.7	2.1	9165	0.038	0.014994	(.09)	0.09922	(.11)	0.047995	(.06)	95.94	96.06	99.1	0.800	3.2
z3	25.0	1179.8	16.6	0.146	478.4	0.9	32737	0.047	0.014980	(.11)	0.09919	(.13)	0.048025	(.06)	95.85	96.03	100.5	0.898	4.7
z5	20.2	787.6	11.1	0.148	101.5	2.2	6951	0.047	0.015000	(.11)	0.09929	(.17)	0.048007	(.13)	95.98	96.12	99.6	0.636	3.7
z6	10.3	1752.9	25.3	0.124	24.9	10.1	1717	0.040	0.014982	(.19)	0.09920	(.25)	0.048023	(.16)	95.86	96.04	100.4	0.778	4.6
z7	19.1	189.8	2.8	0.197	15.3	3.4	1044	0.063	0.014999	(.28)	0.09917	(.33)	0.047952	(.17)	95.97	96.01	96.9	0.854	1.0
z9a	10.4	1082.3	15.2	0.150	167.2	1.0	11438	0.048	0.014952	(.05)	0.09882	(.10)	0.047931	(.08)	95.67	95.68	95.9	0.565	0.2
z10a	13.7	985.4	13.9	0.145	180.4	1.1	12360	0.046	0.014979	(.05)	0.09896	(.10)	0.047918	(.08)	95.84	95.82	95.2	0.561	-0.7
z10b	16.7	1231.7	17.7	0.157	255.3	1.2	17408	0.051	0.015192	(.05)	0.10121	(.07)	0.048319	(.06)	97.19	97.89	115.0	0.640	15.6
z10c	11.4	800.8	11.2	0.131	109.5	1.2	7539	0.042	0.014989	(.05)	0.09915	(.12)	0.047977	(.11)	95.91	95.99	98.1	0.445	2.3

Table 1 (cont.). U-Pb analyses from the Mount Stuart batholith.

	Composition						Isotopic Ratios								Dates (Ma)				
Frac[a]	Wt (μg)[b]	U (ppm)	Pb (ppm)	Th[c] / U	Pb*[d] / Pbc	Pbc[d] (pg)	^{206}Pb[e] / ^{204}Pb	^{208}Pb[f] / ^{206}Pb	^{206}Pb[f] / ^{238}U	% err[g]	^{207}Pb[f] / ^{235}U	% err[g]	^{207}Pb[f] / ^{206}Pb	% err[g]	^{206}Pb[h] / ^{238}U	^{207}Pb[h] / ^{235}U	^{207}Pb[h] / ^{206}Pb	corr. coef.	Discord-ance
MS6:GRANODIORITE (cont.)																			
t1	54.4	90.9	4.4	0.034	0.3	179.2	43.0	0.011	0.013761	(.16)	0.09147	(1.54)	0.048208	(1.47)	88.10	88.87	109.5	0.527	19.7
t2	34.2	81.5	2.0	0.016	1.0	34.8	88.1	0.005	0.013550	(.32)	0.08930	(.79)	0.047796	(.69)	86.76	86.85	89.2	0.504	2.7
t3	41.7	280.4	11.2	0.028	0.4	325.9	49.8	0.009	0.013547	(.12)	0.09040	(1.36)	0.048396	(1.29)	86.74	87.87	118.7	0.575	27.1
t4	42.3	177.1	5.0	0.037	0.8	118.2	74.6	0.012	0.013792	(.12)	0.09112	(.69)	0.047914	(.65)	88.30	88.54	95.0	0.401	7.1
t5	24.2	333.7	6.8	0.025	1.5	65.0	127.5	0.008	0.013711	(.13)	0.09110	(.48)	0.048189	(.44)	87.79	88.53	108.5	0.409	19.2
MS13:GRANODIORITE																			
z1	11.8	225.1	3.3	0.344	12.2	3.1	805	0.110	0.014188	(.40)	0.09349	(.56)	0.047793	(.38)	90.82	90.75	89.0	0.739	-2.0
z2	18.7	95.4	1.3	0.310	15.6	1.6	1036	0.099	0.014178	(.20)	0.09366	(.31)	0.047912	(.22)	90.76	90.91	94.9	0.681	4.4
z3	5.5	81.2	1.2	0.404	4.6	1.4	314	0.129	0.014192	(.66)	0.09319	(1.26)	0.047626	(1.02)	90.84	90.47	80.7	0.587	-12.7
z4	19.6	137.8	2.0	0.354	13.3	2.9	872	0.113	0.014225	(.39)	0.09376	(.43)	0.047802	(.17)	91.06	91.00	89.5	0.917	-1.8
z5	7.2	129.8	1.8	0.328	14.1	0.9	932	0.105	0.014181	(.22)	0.09328	(.50)	0.047707	(.42)	90.78	90.56	84.7	0.524	-7.2
z6	10.7	219.8	3.4	0.614	14.2	2.5	870	0.196	0.014223	(.45)	0.09347	(.48)	0.047662	(.17)	91.04	90.73	82.5	0.934	-10.4
z7	5.9	236.1	3.3	0.313	14.2	1.4	944	0.100	0.014175	(.21)	0.09353	(.28)	0.047855	(.17)	90.74	90.79	92.1	0.785	1.4
t1	71.7	105.3	2.9	0.065	0.9	115.0	77.8	0.021	0.014115	(.12)	0.09340	(.65)	0.047988	(.61)	90.36	90.66	98.7	0.410	8.5
MS17C:DIORITE OF THE BIG JIM COMPLEX																			
z1	38.2	272.9	4.2	0.493	132.4	1.2	8235	0.158	0.015005	(.06)	0.09922	(.09)	0.047958	(.07)	96.01	96.06	97.2	0.660	1.2
z2	30.8	205.4	3.3	0.470	14.5	6.7	918	0.150	0.015000	(.16)	0.09921	(.22)	0.047969	(.14)	95.98	96.05	97.7	0.761	1.8
z3	28.0	150.1	2.3	0.457	46.6	1.4	2941	0.146	0.014991	(.09)	0.09904	(.13)	0.047919	(.09)	95.92	95.89	95.3	0.712	-0.7
z4	26.2	210.6	3.2	0.454	72.2	1.2	4545	0.145	0.014998	(.06)	0.09926	(.11)	0.048000	(.09)	95.96	96.09	99.2	0.601	3.3
z5	41.8	177.7	2.8	0.474	33.7	3.4	2113	0.151	0.014998	(.14)	0.09913	(.18)	0.047938	(.11)	95.97	95.98	96.2	0.804	0.2
z6	60.7	243.7	3.8	0.440	30.7	7.4	1936	0.141	0.015013	(.08)	0.09923	(.12)	0.047936	(.09)	96.06	96.06	96.1	0.674	0.1
z7	35.4	181.1	2.8	0.515	65.9	1.5	4085	0.165	0.014999	(.07)	0.09911	(.13)	0.047922	(.10)	95.97	95.95	95.4	0.589	-0.6
z8	23.6	263.0	4.2	0.482	23.5	4.1	1471	0.154	0.015007	(.17)	0.09934	(.26)	0.048008	(.19)	96.02	96.16	99.7	0.678	3.7
z9	35.9	324.4	5.1	0.496	41.5	4.4	2579	0.158	0.015016	(.11)	0.09916	(.18)	0.047895	(.13)	96.08	96.00	94.1	0.654	-2.1
z10	36.1	290.2	4.6	0.516	68.1	2.4	4213	0.165	0.015018	(.10)	0.09925	(.14)	0.047931	(.08)	96.09	96.08	95.8	0.779	-0.3
z11	26.7	235.3	3.7	0.488	48.2	2.0	3012	0.156	0.015018	(.16)	0.09924	(.19)	0.047928	(.09)	96.09	96.08	95.7	0.883	-0.4
MS24:TONALITE																			
z1	44.3	95.6	1.4	0.378	50.3	1.2	3241	0.121	0.014500	(.10)	0.09574	(.23)	0.047888	(.20)	92.80	92.83	93.8	0.499	1.0
z2	11.4	182.6	2.7	0.243	9.6	3.0	655	0.078	0.014503	(.50)	0.09574	(.89)	0.047876	(.70)	92.82	92.84	93.2	0.618	0.4
z3	13.7	133.1	2.0	0.216	7.4	3.4	510	0.069	0.014479	(.56)	0.09552	(.68)	0.047846	(.37)	92.67	92.63	91.7	0.843	-1.1
z4	47.3	116.3	1.7	0.250	19.4	4.0	1301	0.080	0.014494	(.20)	0.09571	(.30)	0.047893	(.22)	92.76	92.81	94.0	0.693	1.3
z5	6.3	185.9	2.6	0.267	24.7	0.7	1652	0.085	0.014493	(.13)	0.09564	(.21)	0.047859	(.17)	92.76	92.74	92.3	0.613	-0.5
z9	5.0	205.9	3.0	0.221	5.6	2.5	396	0.071	0.014464	(1.00)	0.09536	(1.29)	0.047815	(.77)	92.57	92.48	90.1	0.802	-2.7
t1	133.7	216.4	4.9	0.176	1.4	276.8	112.7	0.056	0.014084	(.07)	0.09290	(.43)	0.047839	(.41)	90.16	90.20	91.3	0.412	1.2
t2	108.4	307.7	8.3	0.106	0.9	465.8	82.8	0.034	0.014023	(.08)	0.09242	(.57)	0.047797	(.54)	89.77	89.75	89.3	0.447	-0.6
t3	84.5	262.5	6.7	0.155	1.1	277.3	90.7	0.049	0.014102	(.06)	0.09268	(.46)	0.047666	(.44)	90.27	90.00	82.7	0.431	-9.2

Table 1 (cont.). U-Pb analyses from the Mount Stuart batholith.

	Composition						Isotopic Ratios								Dates (Ma)				
Frac[a]	Wt (μg)[b]	U (ppm)	Pb (ppm)	Th[c]/U	Pb*[d]/Pbc	Pbc[d] (pg)	$^{206}Pb/^{204}Pb$[e]	$^{208}Pb/^{206}Pb$[f]	$^{206}Pb/^{238}U$[f]	% err[g]	$^{207}Pb/^{235}U$[f]	% err[g]	$^{207}Pb/^{206}Pb$[f]	% err[g]	$^{206}Pb/^{238}U$[h]	$^{207}Pb/^{235}U$[h]	$^{207}Pb/^{206}Pb$[h]	corr. coef.	Discord-ance
MS26:TONALITE																			
z1	22.0	297.6	4.3	0.174	43.3	2.2	2953	0.056	0.015059	(.16)	0.09957	(.18)	0.047954	(.08)	96.35	96.38	97.0	0.888	0.7
z2	10.9	175.2	2.5	0.168	15.8	1.7	1096	0.054	0.015055	(.19)	0.09951	(.25)	0.047939	(.16)	96.33	96.33	96.3	0.772	-0.1
z3	9.1	181.9	2.7	0.173	7.7	3.1	540	0.055	0.015052	(.59)	0.09952	(.68)	0.047956	(.30)	96.31	96.34	97.0	0.894	0.8
z4	8.6	142.1	2.0	0.159	22.6	0.8	1561	0.051	0.015089	(.13)	0.09975	(.22)	0.047947	(.17)	96.55	96.55	96.7	0.628	0.1
z5	7.9	76.6	1.1	0.191	12.7	0.7	877	0.061	0.015054	(.25)	0.09945	(.91)	0.047910	(.83)	96.32	96.26	94.8	0.448	-1.6
MS31:TONALITE																			
z1	56.8	91.0	1.3	0.306	29.0	2.5	1908	0.098	0.014210	(.21)	0.09371	(.29)	0.047829	(.19)	90.96	90.95	90.8	0.757	-0.2
z2	78.8	210.9	2.9	0.168	36.0	6.2	2443	0.054	0.014188	(.12)	0.09358	(.19)	0.047838	(.14)	90.82	90.83	91.3	0.640	0.5
z4	33.3	85.1	1.2	0.361	55.3	0.7	3577	0.116	0.014200	(.13)	0.09364	(.25)	0.047827	(.21)	90.90	90.89	90.7	0.551	-0.2
z5	65.2	81.4	1.2	0.342	20.8	3.6	1354	0.109	0.014210	(.20)	0.09370	(.23)	0.047822	(.10)	90.96	90.94	90.5	0.898	-0.5
z6	75.3	139.8	1.9	0.180	140.2	1.0	9511	0.057	0.014188	(.05)	0.09359	(.08)	0.047840	(.06)	90.82	90.84	91.4	0.658	0.6
z7	37.8	41.1	0.6	0.403	25.3	0.9	1624	0.129	0.014255	(.13)	0.09436	(.26)	0.048007	(.21)	91.24	91.55	99.6	0.582	8.5
t1	39.3	202.8	4.0	0.147	2.0	53.0	152.7	0.047	0.013989	(.13)	0.09181	(.38)	0.047597	(.35)	89.56	89.19	79.3	0.448	-13.0
MS37:TONALITE																			
z1	5.8	308.5	4.2	0.170	13.6	1.8	944	0.054	0.014478	(.21)	0.09549	(.34)	0.047833	(.26)	92.66	92.60	91.1	0.666	-1.8
z2	1.9	671.3	9.5	0.160	6.8	2.6	479	0.051	0.014464	(.80)	0.09547	(.90)	0.047872	(.40)	92.57	92.59	92.9	0.896	0.4
z3	2.7	288.5	4.1	0.258	5.0	2.2	352	0.082	0.014458	(1.32)	0.09534	(1.66)	0.047829	(.93)	92.53	92.47	90.8	0.826	-1.9
z4	1.5	485.1	7.6	0.138	2.8	3.5	208	0.044	0.014494	(1.37)	0.09566	(1.55)	0.047870	(.68)	92.76	92.76	92.8	0.899	0.1
z5	1.2	482.6	6.6	0.166	6.6	1.2	465	0.053	0.014435	(.44)	0.09526	(1.08)	0.047860	(.94)	92.39	92.39	92.4	0.505	0.0
t1	41.0	435.9	9.3	0.435	2.2	120.4	155.7	0.140	0.014467	(.07)	0.09584	(.31)	0.048046	(.29)	92.59	92.93	101.6	0.399	8.9
JR1:TONALITE																			
z1	15.9	443.8	7.0	0.243	7.9	12.8	538	0.078	0.014777	(.15)	0.09764	(.24)	0.047922	(.19)	94.56	94.59	95.5	0.647	1.0
z2	5.2	659.7	10.1	0.259	9.0	5.4	608	0.083	0.014644	(.30)	0.09714	(.43)	0.048112	(.30)	93.72	94.14	104.8	0.724	10.6
z3	3.8	395.5	5.9	0.275	8.2	2.7	555	0.088	0.014818	(.67)	0.09824	(.88)	0.048082	(.55)	94.82	95.15	103.3	0.784	8.3
z4	5.4	162.6	2.6	0.298	4.2	3.1	292	0.095	0.014846	(1.14)	0.09788	(1.62)	0.047819	(1.09)	95.00	94.82	90.4	0.742	-5.2
z7	4.4	361.6	5.4	0.249	7.6	3.0	522	0.080	0.014806	(.62)	0.09773	(.72)	0.047873	(.35)	94.75	94.68	93.0	0.878	-1.9
z9	0.9	826.7	11.8	0.238	9.9	1.1	681	0.076	0.014812	(.30)	0.09784	(.55)	0.047909	(.45)	94.78	94.78	94.8	0.598	0.0
PCF:TONALITE																			
z2	9.4	179.2	2.9	0.321	5.4	4.6	367	0.105	0.014745	(.60)	0.09930	(1.43)	0.048842	(1.23)	94.36	96.13	140.2	0.517	32.9
z3	8.3	224.6	3.4	0.250	8.2	3.3	562	0.080	0.014803	(.54)	0.09782	(.65)	0.047926	(.34)	94.73	94.76	95.6	0.853	1.0
z4	7.4	192.1	3.4	0.316	3.2	6.5	226	0.101	0.014815	(.68)	0.09808	(1.18)	0.048016	(.92)	94.80	95.01	100.1	0.625	5.3
z5	24.5	130.1	2.2	0.342	4.6	10.2	311	0.109	0.014729	(.32)	0.09704	(.46)	0.047783	(.31)	94.25	94.04	88.5	0.731	-6.6
z6	15.4	184.0	2.8	0.430	14.4	3.0	922	0.138	0.014820	(.43)	0.09812	(.61)	0.048021	(.42)	94.83	95.04	100.3	0.729	5.5
z8	18.1	90.7	1.3	0.234	10.0	2.4	684	0.075	0.014833	(.61)	0.09760	(.67)	0.047724	(.26)	94.92	94.56	85.6	0.922	-11.0
z9	14.8	148.9	2.2	0.229	11.4	2.8	779	0.073	0.014811	(.46)	0.09784	(.50)	0.047908	(.20)	94.78	94.78	94.7	0.915	-0.1
z10	38.5	100.2	1.3	0.108	23.9	2.1	1670	0.035	0.014305	(.27)	0.09454	(.31)	0.047933	(.13)	91.56	91.73	96.0	0.903	4.6
z11	14.7	82.0	1.1	0.093	9.0	1.8	643	0.030	0.014730	(.31)	0.09756	(.52)	0.048033	(.39)	94.26	94.52	100.9	0.651	6.6
z12	7.5	76.2	1.1	0.138	4.3	1.8	316	0.044	0.014720	(.65)	0.09693	(.92)	0.047758	(.62)	94.20	93.94	87.2	0.738	-8.0

Table 1 (cont.). U-Pb analyses from the Mount Stuart batholith.

	Composition						Isotopic Ratios								Dates (Ma)				
Frac[a]	Wt (μg)[b]	U (ppm)	Pb (ppm)	Th[c] / U	Pb*[d] / Pbc	Pbc[d] (pg)	^{206}Pb[e] / ^{204}Pb	^{208}Pb[f] / ^{206}Pb	^{206}Pb[f] / ^{238}U	% err[g]	^{207}Pb[f] / ^{235}U	% err[g]	^{207}Pb[f] / ^{206}Pb	% err[g]	^{206}Pb[h] / ^{238}U	^{207}Pb[h] / ^{235}U	^{207}Pb[h] / ^{206}Pb	corr. coef.	Discord-ance
t2	80.0	100.0	2.7	0.097	0.9	113.5	80.9	0.031	0.013830	(.12)	0.09068	(.83)	0.047553	(.78)	88.54	88.13	77.1	0.465	-14.9
t3	57.3	1488.6	20.9	0.017	8.4	127.2	613.6	0.006	0.013914	(.05)	0.09184	(.10)	0.047870	(.09)	89.08	89.22	92.8	0.545	4.1

[a] All zircon fractions (i.e. z1) are composed of single grains or fragments. Titanite analyses (i.e. t1) are either small multi-grain fractions (*) or single grains.

[b] Sample weights were estimated to within 40% using measured grain dimensions and a nominal density of 4.5 g/cm^3 for zircon and 3.5g/cm^3 for titanite.

[c] Th contents calculated from radiogenic ^{208}Pb and the $^{207}Pb/^{206}Pb$ date of the sample, assuming concordance between U-Th-Pb systems.

[d] Pb* and Pbc represent radiogenic Pb and common Pb respectively.

[e] Measured ratio corrected for fractionation and spike; Pb fractionation was 0.12 ±0.04%/a.m.u. for Faraday detector or 0.20 ± 0.04%/a.m.u.for Daly detector analysis, based on daily analysis of NBS-981.

[f] Measured ratios corrected for fractionation, spike, blank, and initial common Pb; nominal U blank = 0.1 pg ± 50% (2 σ); nominal Pb blank = 2.0 pg ± 50% (2s) or where lower, the total common Pb of the analysis±10% (2σ); measured laboratory Pb composition: $^{206}Pb/^{204}Pb$ = 19.10, $^{207}Pb/^{204}Pb$ = 15.72, $^{208}Pb/^{204}Pb$ = 38.65 ± 0.05 (2σ); initial Pb composition of zircon from model of Stacey and Kramers (1975) at the nominal age of the fraction (i.e. 0.1 Ga), and initial Pb composition of titanite from measured Pb isotopi composition of coexisting plagioclase feldspar.

[g] Numbers in parentheses are the % errors reported at the 2 σ confidence interval, propagated using the algorithms of Ludwig (1980).

[h] Isotopic ages calculated using the decay constants of Jaffey et al. (1971): $\lambda(^{235}U) = 9.8485 \times 10^{-10}$ yr^{-1} and $\lambda(^{238}U) = 1.55125 \times 10^{-10}$ yr^{-1}; error in $^{207}Pb/^{206}Pb$ date reported at the 2σ confidence interval.

Table 2. U-Pb analyses from the Tenpeak pluton.

	Composition						Isotopic Ratios								Dates (Ma)				
Frac[a]	Wt (μg)[b]	U (ppm)	Pb (ppm)	Th[c] / U	Pb*[d] / Pbc	Pbc[d] (pg)	^{206}Pb[e] / ^{204}Pb	^{208}Pb[f] / ^{206}Pb	^{206}Pb[f] / ^{238}U	% err[g]	^{207}Pb[f] / ^{235}U	% err[g]	^{207}Pb[f] / ^{206}Pb	% err[g]	^{206}Pb[h] / ^{238}U	^{207}Pb[h] / ^{235}U	^{207}Pb[h] / ^{206}Pb	corr. coef.	Discord-ance
TP1:TONALITE/SHEETED ZONE																			
z1	9.4	210.8	3.0	0.379	19.9	1.4	1295	0.121	0.014362	(.16)	0.09465	(.23)	0.047800	(.16)	91.92	91.83	89.4	0.718	-2.8
z2	2.9	432.0	6.1	0.303	13.4	1.3	894	0.097	0.014367	(.23)	0.09479	(.41)	0.047850	(.33)	91.96	91.95	91.8	0.609	-0.1
z8	3.3	306.0	4.4	0.341	9.9	1.4	663	0.109	0.014378	(.33)	0.09439	(.80)	0.047610	(.70)	92.03	91.58	79.9	0.507	-15.3
z10	9.9	90.1	1.2	0.213	14.0	0.9	957	0.068	0.014341	(.21)	0.09459	(.37)	0.047836	(.29)	91.79	91.77	91.2	0.617	-0.6
z11	10.6	74.0	1.1	0.340	17.1	0.6	1122	0.109	0.014334	(.19)	0.09465	(.39)	0.047891	(.34)	91.75	91.82	93.9	0.524	2.3
z12	6.1	65.8	1.0	0.429	8.1	0.7	530	0.137	0.014358	(.38)	0.09478	(.66)	0.047880	(.52)	91.90	91.95	93.3	0.631	1.5
t1	177.6	200.3	5.3	1.254	2.1	300.4	126.7	0.400	0.014335	(.06)	0.09449	(.37)	0.047805	(.35)	91.75	91.68	89.7	0.422	-2.3
t4	83.1	141.7	3.6	1.100	2.1	95.9	130.5	0.351	0.014315	(.10)	0.09417	(.48)	0.047708	(.45)	91.63	91.38	84.8	0.423	-8.1
TP11: TONALITE																			
z1	15.3	139.1	1.9	0.155	15.0	1.9	1041	0.050	0.014429	(.20)	0.09524	(.25)	0.047872	(.15)	92.35	92.38	93.0	0.791	0.7
z4	17.0	187.4	2.6	0.217	42.7	1.0	2881	0.069	0.014444	(.08)	0.09533	(.12)	0.047868	(.08)	92.44	92.46	92.8	0.696	0.3
z5	3.8	396.1	5.3	0.118	14.2	1.4	1000	0.038	0.014418	(.20)	0.09512	(.30)	0.047851	(.21)	92.28	92.26	91.9	0.710	-0.4
z6	17.6	60.3	0.8	0.068	24.9	0.6	1763	0.022	0.014412	(.12)	0.09510	(.20)	0.047858	(.16)	92.24	92.24	92.2	0.615	0.0
z7	2.6	46.9	0.7	0.211	2.7	0.6	202	0.067	0.014425	(1.05)	0.09536	(1.93)	0.047944	(1.53)	92.33	92.48	96.5	0.609	4.4
z8	3.2	68.0	0.9	0.090	4.7	0.6	343	0.029	0.014416	(.61)	0.09524	(1.47)	0.047916	(1.26)	92.27	92.37	95.1	0.519	3.0
t2	290.5	134.1	3.0	0.661	2.2	275.8	148.1	0.211	0.014406	(.22)	0.09506	(.34)	0.047857	(.25)	92.21	92.21	92.2	0.679	0.0
t3	57.8	124.5	3.1	0.710	1.7	67.2	116.1	0.227	0.014287	(.13)	0.09423	(.45)	0.047835	(.41)	91.45	91.44	91.1	0.421	-0.4
t4	9.6	1372.6	32.7	0.809	2.0	103.9	134.4	0.258	0.014342	(.09)	0.09456	(.59)	0.047817	(.55)	91.80	91.74	90.2	0.455	-1.8
TP20: TONALITE																			
z1	15.6	334.0	4.7	0.242	44.9	1.6	3005	0.077	0.014395	(.08)	0.09496	(.12)	0.047847	(.09)	92.13	92.12	91.8	0.692	-0.4
z2	11.7	548.5	7.9	0.346	98.7	0.9	6391	0.111	0.014402	(.06)	0.09512	(.10)	0.047902	(.08)	92.18	92.27	94.5	0.635	2.4
z3	10.8	298.0	4.2	0.264	48.3	0.9	3212	0.084	0.014413	(.09)	0.09524	(.17)	0.047923	(.14)	92.25	92.37	95.5	0.595	3.4
z4	7.4	277.8	4.0	0.315	35.4	0.8	2327	0.101	0.014422	(.10)	0.09522	(.14)	0.047887	(.10)	92.31	92.36	93.7	0.699	1.5
z5	5.7	807.8	11.2	0.228	73.4	0.9	4919	0.073	0.014413	(.06)	0.09510	(.10)	0.047853	(.07)	92.25	92.24	92.0	0.680	-0.3
z6	8.7	220.2	3.1	0.236	22.2	1.2	1501	0.076	0.014397	(.15)	0.09501	(.24)	0.047861	(.18)	92.15	92.16	92.5	0.660	0.3
z7	6.9	373.4	5.2	0.240	41.0	0.9	2747	0.077	0.014406	(.10)	0.09502	(.20)	0.047837	(.17)	92.20	92.17	91.2	0.561	-1.1
z11	2.0	482.7	6.8	0.275	12.3	1.1	828	0.088	0.014399	(.25)	0.09495	(.51)	0.047825	(.42)	92.16	92.11	90.7	0.560	-1.7
t1	202.5	118.8	3.5	1.257	1.6	276.6	98.1	0.402	0.014370	(.20)	0.09484	(.83)	0.047864	(.76)	91.98	92.00	92.5	0.422	0.6
t3	159.2	138.4	4.0	1.856	2.3	194.4	122.5	0.595	0.014416	(.08)	0.09538	(.37)	0.047985	(.35)	92.27	92.50	98.5	0.388	6.4
t4	185.0	107.5	2.8	1.244	2.1	165.9	127.7	0.398	0.014302	(.09)	0.09442	(.43)	0.047881	(.40)	91.54	91.61	93.4	0.410	2.1
TP27: TONALITE																			
z1	15.6	111.9	1.5	0.215	18.6	1.3	1265	0.069	0.014103	(.17)	0.09340	(.28)	0.048031	(.22)	90.28	90.66	100.7	0.622	10.5
z2	10.2	116.8	1.6	0.258	17.3	0.9	1163	0.082	0.014169	(.19)	0.09345	(.41)	0.047834	(.35)	90.70	90.71	91.1	0.524	0.4
z3	12.2	240.3	3.2	0.160	48.9	0.8	3348	0.051	0.014169	(.10)	0.09349	(.17)	0.047858	(.14)	90.70	90.75	92.2	0.611	1.7
z4	21.5	97.2	1.3	0.193	11.3	2.5	780	0.062	0.014195	(.50)	0.09365	(.56)	0.047846	(.23)	90.86	90.89	91.7	0.912	0.9
z5	19.2	68.2	0.9	0.284	17.4	1.0	1162	0.091	0.014176	(.18)	0.09353	(.30)	0.047850	(.23)	90.74	90.78	91.9	0.637	1.3
z6	14.8	173.4	2.3	0.156	36.8	0.9	2530	0.050	0.014180	(.09)	0.09354	(.17)	0.047842	(.14)	90.77	90.80	91.4	0.576	0.7
z7	9.5	532.5	7.0	0.084	53.7	1.2	3759	0.027	0.014168	(.07)	0.09346	(.11)	0.047842	(.08)	90.69	90.72	91.4	0.669	0.8

Table 2 continued. U-Pb analyses from the Tenpeak pluton.

	Composition						Isotopic Ratios								Dates (Ma)				
Frac[a]	Wt (μg)[b]	U (ppm)	Pb (ppm)	Th[c] / U	Pb* / Pbc[d]	Pbc[d] (pg)	^{206}Pb / ^{204}Pb[e]	^{208}Pb / ^{206}Pb[f]	^{206}Pb / ^{238}U[f]	% err[g]	^{207}Pb / ^{235}U[f]	% err[g]	^{207}Pb / ^{206}Pb[f]	% err[g]	^{206}Pb / ^{238}U[h]	^{207}Pb / ^{235}U[h]	^{207}Pb / ^{206}Pb[h]	corr. coef.	Discord-ance
TP29: FLASER GNEISS																			
z1	8.1	385.0	5.3	0.140	15.1	2.7	1051	0.045	0.014269	(.34)	0.09410	(.37)	0.047831	(.15)	91.33	91.32	91.0	0.918	-0.4
z2	9.5	204.0	2.8	0.175	12.4	2.1	862	0.056	0.014285	(.54)	0.09417	(.57)	0.047813	(.19)	91.44	91.39	90.0	0.942	-1.6
z3	4.2	478.5	6.9	0.154	7.2	3.7	507	0.049	0.014280	(.52)	0.09417	(.65)	0.047827	(.38)	91.40	91.38	90.7	0.813	-0.7
z4	3.5	404.9	6.1	0.184	4.6	4.2	331	0.059	0.014281	(.71)	0.09412	(.80)	0.047801	(.35)	91.41	91.34	89.4	0.901	-2.2
z6	4.4	445.3	6.0	0.140	14.9	1.8	1039	0.045	0.014261	(.19)	0.09396	(.26)	0.047787	(.17)	91.28	91.19	88.7	0.770	-2.9
z7	1.5	1601.6	21.9	0.112	10.6	3.0	751	0.036	0.014261	(.44)	0.09412	(.51)	0.047864	(.25)	91.28	91.33	92.5	0.874	1.4
t2	382.6	353.8	6.1	0.228	4.0	461.3	284.5	0.073	0.014236	(.06)	0.09387	(.15)	0.047823	(.13)	91.12	91.10	90.5	0.467	-0.7
t4	91.8	605.0	9.9	0.173	4.5	167.7	317.8	0.055	0.014195	(.05)	0.09353	(.14)	0.047786	(.13)	90.86	90.78	88.7	0.425	-2.5
TP30: DIORITE IN MAFIC COMPLEX																			
z1	8.9	281.7	4.3	0.264	7.2	4.9	490	0.084	0.014387	(.41)	0.09486	(.58)	0.04782	(.39)	92.08	92.02	90.5	0.737	-1.8
z2	3.5	282.0	3.9	0.239	7.2	1.9	496	0.076	0.014388	(.41)	0.09482	(.58)	0.04780	(.40)	92.09	91.99	89.3	0.730	-3.2
z6	3.2	174.3	2.4	0.158	5.8	1.3	417	0.051	0.014375	(.49)	0.09503	(.77)	0.04795	(.57)	92.00	92.18	96.7	0.681	4.9
z7	2.4	158.1	2.2	0.233	4.8	1.1	338	0.075	0.014400	(.63)	0.09499	(1.37)	0.04784	(1.15)	92.16	92.14	91.6	0.544	-0.6
z8	1.7	271.5	3.9	0.301	6.7	1.0	460	0.096	0.014432	(.44)	0.09527	(.91)	0.047876	(.76)	92.37	92.40	93.2	0.554	0.8
z9	1.9	134.1	1.9	0.308	3.9	0.9	275	0.099	0.014433	(.76)	0.09548	(1.15)	0.047977	(.83)	92.38	92.59	98.1	0.697	5.9
TP31: TONALITE (WHITE MOUNTAIN LOBE)																			
z3	2.4	117.6	1.8	0.494	2.4	1.7	171.0	0.158	0.014375	(1.26)	0.09475	(1.75)	0.047804	(1.14)	92.01	91.92	89.6	0.761	-2.7
z4	1.3	75.9	1.1	0.407	2.4	0.6	170.6	0.130	0.014388	(1.29)	0.09502	(2.47)	0.047900	(1.99)	92.09	92.17	94.3	0.596	2.4
z6	1.7	95.4	1.4	0.329	3.1	0.8	221.0	0.107	0.014602	(.96)	0.09796	(1.69)	0.048654	(1.33)	93.45	94.89	131.2	0.616	29.0
z9	3.0	32.3	0.5	0.395	1.7	0.8	130.2	0.126	0.014378	(1.74)	0.09495	(4.74)	0.047895	(4.17)	92.02	92.10	94.1	0.494	2.2
t1	106.9	489.3	8.0	0.162	4.7	151.1	335.2	0.052	0.014374	(.05)	0.09478	(.14)	0.047824	(.12)	92.00	91.95	90.6	0.454	-1.6
t2	64.9	568.6	9.2	0.169	5.3	95.1	373.3	0.054	0.014358	(.06)	0.09476	(.14)	0.047863	(.12)	91.90	91.92	92.5	0.480	0.7
t3	148.3	379.2	6.5	0.188	3.8	201.8	272.6	0.060	0.014319	(.06)	0.09442	(.18)	0.047825	(.16)	91.65	91.61	90.6	0.436	-1.2
t4	91.8	405.3	6.7	0.096	4.0	125.0	291.1	0.031	0.014380	(.05)	0.09492	(.15)	0.047873	(.14)	92.04	92.07	93.0	0.431	1.0
TP-524-1: TONALITE																			
z1	11.3	124.9	1.7	0.236	20.3	0.9	1368	0.076	0.014012	(.15)	0.09238	(.29)	0.047815	(.24)	89.70	89.72	90.1	0.571	0.5
z2	6.8	104.3	1.4	0.272	14.5	0.7	976	0.087	0.013996	(.22)	0.09226	(.40)	0.047810	(.32)	89.60	89.61	89.9	0.602	0.3
z7	6.5	73.9	1.0	0.261	6.2	1.1	431	0.084	0.014023	(.47)	0.09253	(.71)	0.047857	(.50)	89.77	89.86	92.2	0.702	2.7
z13	9.5	91.7	1.3	0.284	20.4	0.6	1357	0.091	0.014037	(.17)	0.09245	(.39)	0.047767	(.34)	89.86	89.78	87.7	0.500	-2.5
z14	6.7	26.0	0.4	0.336	5.2	0.5	356	0.107	0.013997	(.58)	0.09220	(1.86)	0.047776	(1.67)	89.60	89.55	88.2	0.463	-1.6
t2	142.8	9.2	0.8	0.030	0.2	101.5	30.1	0.010	0.013967	(.37)	0.09271	(3.70)	0.048138	(3.51)	89.42	90.02	106.0	0.529	15.8
t3	146.9	21.9	1.0	0.015	0.3	115.5	43.1	0.005	0.013829	(.22)	0.08522	(1.98)	0.044693	(1.88)	88.54	83.04	-72.3	0.500	-224
t4	37.5	43.1	1.4	0.010	0.6	33.7	61.0	0.003	0.013891	(.48)	0.08991	(1.14)	0.046943	(.99)	88.93	87.42	46.4	0.499	-92.5

[a] All zircon fractions (i.e. z1, z2) are composed of single zircons. Titanite analyses (i.e. t1) are either small multi-grain fractions(*) or single grains.

[b] Sample weights were estimated to within 40% using measured grain dimensions and a nominal density of 4.5 g/cm ^{3} for zircon and 3.5g/cm^3 for titanite.

[c] Th contents calculated from radiogenic ^{208}Pb and the $^{207}Pb/^{206}Pb$ date of the sample, assuming concordance between U-Th-Pb systems.

[d] Pb* and Pbc represent radiogenic Pb and common Pb respectively.

Table 2 continued. U-Pb analyses from the Tenpeak pluton.

[f] Measured ratios corrected for fractionation, spike, blank, and initial common Pb; nominal U blank = 0.1 pg ± 50% (2 σ); nominal Pb blank = 2.0 pg ± 50% (2s) or where lower, the total common Pb of the analysis±10% (2σ); measured laboratory Pb composition: $^{206}Pb/^{204}Pb$ = 19.10, $^{207}Pb/^{204}Pb$ = 15.72, $^{208}Pb/^{204}Pb$ = 38.65 ± 0.05 (2σ); initial Pb composition of zircon from model of Stacey and Kramers (1975) at the nominal age of the fraction (i.e. 0.1 Ga), and initial Pb composition of titanite from measured Pb isotopic composition of coexisting plagioclase feldspar.

[g] Numbers in parentheses are the % errors reported at the 2 σ confidence interval, propagated using the algorithms of Ludwig (1980).

[h] Isotopic ages calculated using the decay constants of Jaffey et al. (1971): $\lambda(^{235}U) = 9.8485 \times 10^{-10}$ yr^{-1} and $\lambda(^{238}U) = 1.55125 \times 10^{-10}$ yr^{-1}; error in $^{207}Pb/^{206}Pb$ date reported at the 2σ confidence interval.

Table 3. Weighted mean $^{206}Pb/^{238}U$ and concordia zircon ages (with and without decay constant errors) from MSB and Tenpeak samples

Sample	$^{206}Pb/^{238}U$ Age (Ma)	MSWD	Concordia Age (Ma)†	MSWD	Concordia Age (Ma)‡	MSWD	$2\sigma_{MSWD}$"	Fractions	n
MS26	96.39±0.14	1.63	96.42±0.08	0.78	96.43±0.12	0.66	1.63	z1-z5	5
MS5	96.03±0.05	-	-	-	-	-	-	z5a	1
MS17C	96.01±0.04	1.55	96.00±0.03	1.60	96.01±0.09	1.50	0.94	z1-z11	11
MS6	95.68±0.05	-	-	-	-	-	-	z9a	1
JR-1	94.62±0.12	0.77	94.62±0.12	0.59	94.63±0.15	0.58	1.63	z1,z3,z4,z7,z9	5
PC-F	94.59±0.27	2.05	94.50±0.22	2.00	94.48±0.25	1.90	1.15	z3-z6,z8,z9,z11,z12	8
MS24	92.78±0.03	0.15	92.78±0.07	0.12	92.78±0.11	1.00	1.41	z1-z5,z9	6
MS37	92.61±0.17	0.39	92.61±0.17	0.22	92.60±0.19	0.21	1.63	z1-z5	5
MS4	91.02±0.06	0.43	91.02±0.06	0.98	91.02±0.10	0.98	1.26	z2,z3,z6,z7,z11-z13	7
MS2	90.90±0.06	1.18	90.91±0.03	1.20	90.92±0.08	1.20	1.26	z2-z8	7
MS31	90.88±0.08	1.20	90.84±0.04	0.62	90.84±0.09	0.60	1.63	z1,z2,z4-z6	5
MS13	90.80±0.10	0.70	90.79±0.10	0.77	90.79±0.13	0.77	1.26	z1-z7*	7
TP11	92.33±0.10	2.13	92.37±0.06	1.01	92.37±0.10	1.00	1.41	z1,z4-z8	6
TP20	92.21±0.05	1.95	92.21±0.03	1.70	92.22±0.08	1.50	1.15	z1-z7,z11	8
TP30	92.16±0.15	0.44	92.15±0.18	0.32	92.15±0.20	0.32	1.41	z1,z2,z6-z9	6
TP31	92.04±0.72	0.01	92.04±0.73	0.01	92.04±0.74	0.01	2.83	z3,z4,z9	3
TP1	91.88±0.12	1.01	91.87±0.08	0.89	91.86±0.12	0.82	1.41	z1,z2,z8,z10-z12	6
TP29	91.32±0.06	0.13	91.31±0.13	0.29	91.30±0.15	0.20	1.41	z1-z4,z6,z7	6
TP27	90.72±0.04	0.58	90.72±0.04	0.45	90.73±0.09	0.30	1.41	z2-z7	6
TP-524-1	89.72±0.15	1.29	89.74±0.09	0.65	89.73±0.12	0.65	1.63	z1,z2,z7,z13,z14	5

†without decay constant errors

‡with decay constant errors

"2σ uncertainty about an MSWD of 1

*z6 not included in concordia age calculation

Table 4. Pb isotopic composition of plagioclase feldspar from the MSB and Tenpeak pluton.

Sample Name		$^{206}Pb/^{204}Pb$	%SE	$^{207}Pb/^{204}Pb$	%SE	$^{208}Pb/^{204}Pb$	%SE
MS6	L3	18.778	0.084	15.579	0.085	38.396	0.079
	L4	18.828	0.010	15.621	0.011	38.491	0.012
MS13	L4	18.745	0.034	15.579	0.027	38.342	0.027
	L5	18.742	0.019	15.584	0.019	38.339	0.019
TP20	L3	18.720	0.137	15.561	0.139	38.348	0.142
	L4	18.769	0.026	15.613	0.027	38.454	0.028
	L5	18.714	0.034	15.575	0.036	38.332	0.035
TP-524-1	L4	18.745	0.041	15.582	0.043	38.391	0.042
	L5	18.717	0.021	15.560	0.021	38.329	0.022
MSB Ave		**18.773**		**15.591**		**38.392**	
Tenpeak Ave		**18.733**		**15.578**		**38.371**	

Table 5. Volumes and magma emplacement rates of different pulses of the MSB and Tenpeak pluton.

"Pulse"	Estimated Volume (km^3)	Emplacement Rate (km^3/yr)
Total MSB NE Body	1200	$2.1x10^{-4}$
Hook Domain	485	$6.8x10^{-4}$
ca. 96 Ma granodiorite	270	
ca. 96 Ma tonalite	180	
Big Jim Complex	35	
Intermediate Domains	195	
Mushroom Domain	520	$2.4x10^{-3}$
ca. 91 Ma granodiorite	80	
ca. 91 Ma tonalite	290	
ca. 91 Ma gabbro	150	
Total Tenpeak pluton	394	$1.2x10^{-4}$
Schaefer Lake tonalite	110	
White Mountain Lobe	45	
Mafic Complex	7	
Sheeted Complex	20	
Interlayered Unit	13	
Flaser Gneiss	14	
NW Body	95	
Indian Creek tonalite	90	

Chapter 5

TEMPORAL EVOLUTION OF MID-CRUSTAL SHEETED INTRUSIONS: EVIDENCE FROM U-Pb GEOCHRONOLOGY OF THE ENTIAT AND SEVEN-FINGERED JACK INTRUSIVE SUITES, NORTH CASCADES, WA

ABSTRACT

The Seven-Fingered Jack and Entiat intrusive suites (North Cascades, Washington) provide a natural laboratory for study of the construction of mid-crustal sheeted intrusions. Prior to this study, these intrusive suites were assumed to be coeval. Models for their construction involved emplacement of thin magmatic sheets at the northwestern end of the intrusion which then formed "preheated pathways" for the development of a more homogeneous magma chamber. U-Pb zircon grains from thin tonalite and diorite sheets at the northwestern tip yield ca. 90-92 Ma dates and belong to the Seven-Fingered Jack suite. In contrast, coarse-grained tonalite and fine-grained diorite from the southeastern end of the body yield ca. 71-73 Ma dates and belong to the Entiat intrusive suite. The contact between these suites is not well-mapped but probably extends southeast of sheeted, biotite granodiorite that forms the center of the body. These geochronologic data indicate that the Seven-Fingered Jack sheets could not have formed preheated pathways for the more homogenous tonalite of the Entiat intrusion because of an approximately 20 Myr time lag between the emplacement of each intrusion. Zircon inheritance in nearly all samples indicates that sheets incorporated host rock near the level of emplacement and that early-formed sheets were intruded by, and partially mixed with, slightly younger sheets. These zircon inheritance patterns suggest that the Seven-Fingered Jack and Entiat suites were each constructed over a ca. 2-3 Myr time period. This timespan is much longer than predicted by dike emplacement models, but is shorter than predicted by proposed models of incremental pluton growth. Well-developed folds of magmatic foliation indicate that both suites formed during regional NE-SW, arc-perpendicular contraction. The orientation of the regional strain field was remarkably constant between these two time periods. This regional strain field may be responsible, in part, for the consistent orientation of sheeted bodies in the North Cascades during the Late Cretaceous. In addition, the structural anisotropy generated by the Seven-Fingered Jack sheets may have focused flow during the emplacment of the Entiat suite.

INTRODUCTION

Zones of highly elongate plutons are a common feature of some continental magmatic arcs (i.e., Caledonides, Hercynian, Lachlan, Coast Plutonic Complex). These internally-sheeted bodies intrude varying levels of the crust and are constructed by injection of multiple "dike-like" sheets of magma (Hutton, 1992; Ingram and Hutton, 1994; Pitcher and Berger, 1972). The tectonic significance of these zones is unclear. For example, is this distinctive intrusive style controlled by the regional stress field, pre-existing structural anisotropy or ascent along fault zones (i.e. Hutton, 1992; Paterson and Schmidt, 1999)? Furthermore, the timescales over which such systems form is debated. Dike emplacement models predict rapid pluton filling rates (median rate of ~1m^3/s) (Petford et al., 2000). At this rate, the ages of multiple magmatic sheets determined by even the most precise geochronological techniques should overlap within uncertainty. In contrast, geochronological evidence from the Tuolumne Intrusive Suite in the Sierra Nevada has been interpreted to reflect incremental assembly over a period of ~10 Myr (Coleman et al., 2004; Glazner et al., 2004). Thermal models of incremental pluton growth predict an initial stage of emplacement of multiple, thin magmatic sheets. Once "preheated pathways" are established, a central, more homogeneous, steady-state magma chamber develops (Hanson and Glazner, 1995; Yoshinobu et al., 1998). These models have yet to be thoroughly tested with precise geochronologic data from natural systems. Chemical, textural or compositional homogeneity are proposed to be inherited from the source region because little time is available in these models for chemical evolution during ascent or mixing at the level of emplacement (Coleman et al., 2004; Glazner et al., 2004; Petford et al., 2000).

The Coast Plutonic Complex and its southeastern extension, the crystalline core of the North Cascades (Fig. 1), contain numerous, highly elongate plutons constructed from multiple magmatic sheets. Within the Chelan structural block of the North Cascades, this intrusive style is particularly well-developed in a 20-25 km wide zone (Fig. 2). Mid-crustal magmatic sheets mapped as the Entiat and Seven-Fingered Jack plutons (Cater and Crowder, 1967; Cater and Wright, 1967; Tabor et al., 1987a) are the focus of this study. These sheeted complexes provide a natural laboratory for examining an intrusion constructed by multiple pulses of magma and provide a direct test of the models proposed

based on field relationships and thermal modeling. Samples for U-Pb dating were collected in several transects across multiple sheet contacts that parallel the NW-SE strike of the body. Dates from these samples can be used to constrain the duration over which this system was active. These dates also make it possible to test the prediction of thermal models that thin sheets along the margins are the oldest and grade inward to a younger, more homogeneous central sheet. The new geochronological data indicate, however, that the Entiat pluton as mapped is not one simple system. Rather, the intrusive sheets can be separated into at least three temporally distinct suites. The oldest sheets are contemporaneous with the elongate Triassic Dumbell plutons which form the host rock for later sheets. The second suite predominates at the northwestern and central portions of the intrusion and is referred to as the Seven-Fingered Jack suite. The third suite forms the southeast end of the intrusion and is referred to as the Entiat intrusive suite. High-precision, U-Pb geochronology data demonstrates the problems inherent in delineating sheeted complexes and the need for precise geochronology in interpreting their structural and chemical evolution. Consideration of the timescales over which such systems are active can give insight into the mechanisms by which magma is transported through the crust.

REGIONAL SETTING

The crystalline core of the North Cascades records the Cretaceous to Paleogene history of magmatism, deformation and crustal growth along a segment of the North American margin (e.g., Monger et al., 1982; Tabor et al., 1989). The core is composed of a series of Paleozoic to Mesozoic oceanic and island-arc terranes that were accreted prior to the intrusion of arc-related plutons starting at ca. 96 Ma (Misch, 1966; Tabor et al., 1989; Tabor et al., 1987b). The Entiat and Seven-Fingered Jack intrusions are part of a zone of ca. 92-46 Ma elongate plutons that intrude the Chelan structural block of the Cascades core (Fig. 2). The Chelan block is bound on the west by the high-angle, Tertiary Entiat fault and on the east by the Ross Lake fault zone.

Two tectonostratigraphic terranes, the Swakane and Chelan Mountains terranes, make up the Chelan block (Tabor et al., 1989; Tabor et al., 1987b). The Swakane terrane is composed almost entirely of biotite gneiss (Tabor et al., 1989; Waters, 1932). It is a

metasupracrustal unit that was rapidly underthrust beneath the Napeequa Complex of the Chelan Mountains terrane from ca. 73-68 Ma (Chapter 1). The Napeequa Complex, which is intruded by both the Entiat and Seven-Fingered Jack intrusions along their western margins, is an oceanic unit comprising amphibolite, quartzite (metachert), hornblende-biotite schist and minor calc-silicate, metaperidotite, leucocratic gneiss and biotite schist (Cater and Crowder, 1967; Tabor et al., 1987a; Tabor et al., 1989). The other major supracrustal units of the Chelan Mountains terrane include the Cascade River unit and a correlative unit, the Holden assemblage, which are part of a Triassic arc sequence (Tabor et al., 1989). At the northwestern end of the zone of elongate intrusions, the Cascade River unit and Holden assemblage are intruded by the tonalitic, strongly deformed, Triassic Dumbell plutons, which form the roots of the Holden-Cascade River arc (Miller et al., 1994; Tabor et al., 1989). At the southeastern end of the zone of elongate magmatism, the Holden assemblage is injected by numerous dikes and grades into the orthogneiss dominated Chelan Complex (Hopson and Mattinson, 1994; Tabor et al., 1987a). Tonalitic sheets intrude the Chelan Complex along the southeastern margin of the Entiat intrusion, whereas the tonalitic to dioritic sheets intrude the Holden assemblage and the gneissic Dumbell plutons along the northeastern margin of the Seven-Fingered Jack intrusion. Also along the eastern margin of the intrusions, the Entiat and the Seven-Fingered Jack bodies are intruded by the ca. 46 Ma Duncan Hill pluton (Fig. 2) (Dellinger, 1996; Tabor et al., 1987a).

Peak metamorphic conditions of the Napeequa Complex in the Chelan block reached 10-11 kbar and 640-740°C (Valley et al., 2003). One metapelitic Napeequa schist adjacent to the Seven-Fingered Jack intrusive suite, however, yielded a pressure of 7 kbar (GASP) at 650°C (Valley et al., 2003). This pressure estimate is consistent with Al-in-hornblende pressures of 6-7 kbar determined from several localities in both the Entiat and Seven-Fingered Jack suites (Dawes, 1993), and suggests that the Napeequa Complex had experienced ~3-5 kbar of unroofing before emplacement of the Seven-Fingered Jack sheets.

ENTIAT AND SEVEN-FINGERED JACK INTRUSIVE SUITES

The Entiat and Seven-Fingered Jack intrusive suites form a single elongate body that is ~80 km in length and ~8 km wide at its widest point (Fig. 3). The southeastern end of this body is obscured by the Miocene Columbia River basalts. It narrows to the northwest where steep sheets are abundant, and ends in several narrow, steep, overlapping bodies (Figs. 3-5) (Cater and Crowder, 1967; Cater and Wright, 1967; Miller and Paterson, 2001a; Paterson and Miller, 1998b). Typical sheet thicknesses at the northwestern end of the body range from ~1-2 m thick but are locally 10s of m thick. These meter-scale sheets coalesce to form composite sheets that are ~1-2 km in width.

Cater and Crowder (1967) and Cater and Wright (1967) mapped the northwestern end of the body on a 1:62,500 scale. Hornblende quartz diorite gneiss sheets and hornblende diorite and gabbro sheets were described as the Seven-Fingered Jack plutons, whereas the term Entiat pluton was restricted to hornblende-biotite tonalite sheets (Fig. 4). This distinction between different plutons was abandoned during later 1:100,000 scale mapping because these distinctions were unclear to the southeast (Dragovich and Norman, 1995; Tabor et al., 1987a). The new U-Pb geochronology presented below indicates a distinct difference in age between the northwestern and southeastern sheets. I propose a return to the term Seven-Fingered Jack intrusive suite to describe the northwestern sheets and retain the use of the term Entiat intrusive suite for only the southeastern end of the body. The boundary between these two intrusive suites is discussed below.

Both the Entiat and Seven-Fingered Jack intrusive suites are predominantly tonalitic in composition (Fig. 3). The typical mineralogy is hornblende + biotite + plagioclase (An_{38-35}) + quartz + titanite + epidote + K-feldspar (Cater, 1982; Dawes, 1993). Tonalitic sheets throughout the Seven-Fingered Jack are typically medium-grained. Tonalite of the Entiat suite is typically much coarser grained with hornblende crystals up to one cm in length.

The Entiat and Seven-Fingered Jack suites exhibit a general trend from mafic to felsic from the margins of each intrusion to the interior and from the northwest to southeast (Cater, 1982; Dawes, 1993; Miller and Paterson, 2001a). Mafic rock (i.e., hornblendite, gabbro and diorite) is particularly abundant in the northwestern, intensely-

sheeted end of the Seven-Fingered Jack where mafic sheets are not restricted to the margins of the intrusion (Fig. 4). Heterogeneous sheets of leucocratic biotite granodiorite form the southeastern extent of the Seven-Fingered Jack suite (Dawes, 1993; Tabor et al., 1987a).

Heterogeneous mafic "contact" complexes are developed along the margins and between sheets at the northwestern tip of the Seven-Fingered Jack intrusion (Cater and Crowder, 1967; Cater and Wright, 1967; Dawes, 1993; Miller and Paterson, 2001a). Textures vary from fine-grained to pegmatitic. Hornblende gabbro and diorite are the most abundant rock types, but hornblendite, quartz diorite, tonalite, trondhjemite, granodiorite and widespread host-rock inclusions are also present. Within the contact complexes, mafic rock generally formed first and then was mixed with or brecciated by later tonalitic to trondhjemitic magma (Fig. 6) (Cater and Crowder, 1967; Cater and Wright, 1967; Dawes, 1993; Miller and Paterson, 2001a). In contrast, diffuse, swirled and locally crenulate contacts indicate mingling of mafic and tonalitic magmas (Dawes, 1993; Miller and Paterson, 2001a). A body of two-pyroxene gabbro and diorite forms along the eastern margin of the Entiat intrusion. This body is finer-grained and distinct sheets are not well-defined. It grades into the central tonalite sheets (Tabor et al., 1987a).

Prior to this study, most of the available U-Pb dates were from tonalite from the southeastern end of the Entiat intrusion. Discordant, multi-grain, zircon fractions from two tonalite samples displayed a range of possible U-Pb crystallization dates from 75-85 Ma (Tabor et al., 1987a). More recent U-Pb zircon data is also discordant, but an estimate of the crystallization age of the tonalite sheet can be made from the $^{206}Pb/^{238}U$ date of the oldest concordant fraction at 73.2±0.4 Ma (Paterson et al., 2004).

Tonalite sheets of the Seven-Fingered Jack intrusion are texturally and petrologically more homogeneous than the mafic complex. Tonalite sheets from the Entiat intrusion are thicker than the Seven-Fingered Jack sheets, with most being >50 m thick, and sheet contacts are more difficult to define (Miller and Paterson, 2001a). In both intrusions, trails of host rock inclusions sometimes mark internal contacts between sheets with slightly different composition and texture. In some localities, tonalite sheets are separated by host rock, but then coalesce along strike. The existence of sheets with diffuse, cryptic contacts is suggested by widespread zones of schlieren, narrow (<5 m

wide) zones of finer-grained tonalite, and subtle changes in orientation of magmatic foliation across planar boundaries (Miller and Paterson, 2001a).

Several types of internal structures are displayed in the both intrusive suites. Sheets and layers are defined by the ratios of felsic to mafic minerals, and are the earliest structures. The sheets and layers dip steeply in the northwestern tip and gently southward in the wider southeastern end (Fig. 5). Foliation and compositional layering in the Napeequa Complex mostly dip <50° away from the sheets, but steepen and bend downward into subparallelism with the moderately northeast-dipping margin in a ~500 m wide aureole (Fig. 5) (Miller and Paterson, 2001a). At the northwestern tip of the Seven-Fingered Jack, sheets intrude parallel to the axial planes of upright, northwest-trending, gently-plunging folds, cutting the folded host rock foliation (Fig. 5) (Paterson and Miller, 1998b).

Magmatic foliation is well-developed throughout the sheets of both suites and is in most cases stronger than subsolidus foliation. In some cases, magmatic foliation is parallel to layers and sheets, but in many other places, it cuts these structures at small to moderate and locally high angles (Miller and Paterson, 2001a). Magmatic foliation, layering, and sheets are folded by both small scale folds (wavelengths of 5 cm to 3 m) and map-scale folds (Miller and Paterson, 2001a). An axial planar magmatic foliation is also formed locally, and fold axes are generally subparallel to magmatic lineations and the length of the intrusion (Miller and Paterson, 2001a; Paterson and Miller, 1998b). Miller and Paterson (2001) argue that these folds developed during emplacement of the intrusion because the folds are accompanied by only minor subsolidus deformation, have an axial planar magmatic foliation and axes that are parallel to magmatic lineation, and because folded host-rock foliation is continuous with magmatic foliation.

U-Pb RESULTS

Thirteen samples were selected for U-Pb analysis. Eight of these samples were collected from the northwestern sheets that cover the entire compositional range observed in the Seven-Fingered Jack intrusion. The remaining five samples were collected from widely-spaced localities that represent the variety of compositions present in the central and southern sheets. Sample localities are plotted on figure 3, and the results are given in

Table 1 at the 2σ uncertainty level. If a statistically significant concordia age can be determined (Ludwig, 1998; Wendt and Carl, 1991), then the age is shown on the concordia diagram. Analytical techniques are the same as described in Chapter 4. Zircon analyses are of single grains, whereas titanite analyses are small multi-grain fractions. In the following paragraphs, the data are presented from northwest to southeast.

The first sample (*Ho-52-1*) was collected from the northwestern-most body mapped as one of the Seven-Fingered Jack plutons by Cater and Crowder (1967). This sample comprises hornblende quartz diorite with a strong magmatic foliation. Two zircon U-Pb analyses overlap within uncertainty and yield a concordia age of 91.45±0.08 Ma (MSWD=1.16) interpreted as the crystallization age of this sheet (Fig. 7a). A third analysis has a $^{207}Pb/^{206}Pb$ date of 189.1±2.2 Ma. This body intrudes the ca. 220 Ma Dumbell Gneiss, and the third zircon analysis most likely reflects inheritance from the gneiss.

Moving to the southeast, the next five samples comprise a northeast to southwest transect across most of the major sheets mapped at the northwestern end of the intrusion. Sample *EN41* is hornblende gabbro collected from a sheet emplaced near the northeastern margin of the intrusion. Three concordant zircon analyses yield a concordia age of 79.05±0.23 Ma (MSWD=1.40) (Fig. 7b). This date is interpreted as the crystallization age of the sheet, and is the youngest age obtained from the northwestern end of the intrusion. The age of this sheet is distinctly different than other sheets of the Seven-Fingered Jack or Entiat intrusive suites and should be viewed as a separate body.

Sample *EN42* was collected from a hornblende-biotite tonalite sheet that is separated from the previous sample by a ~0.6 km wide zone of mafic complex. This tonalite sheet was originally referred to as part of the Entiat intrusion (Cater and Crowder, 1967). Four zircon analyses from this sample yield an array of concordant and near-concordant results with $^{206}Pb/^{238}U$ dates from 90.48±0.06 Ma to 92.34±1.20 Ma (Fig 7c). The crystallization age of this sample is probably best represented by the youngest concordant analysis, and older analyses most likely represent inheritance of zircon from earlier formed sheets. These dates suggest that this tonalite sheet is contemporaneous with the northern quartz diorite body (*Ho-52-1*) and should be considered part of the Seven-Fingered Jack suite. A distinct intrusive contact should be present between the ca.

79.0 Ma hornblende gabbro sheet and the nearby ca. 90.5 tonalite sheet, but this contact is difficult to recognize because of the heterogeneity of the intervening mafic complex.

To the southwest, samples *EN28* and *E-281* were also collected from the same hornblende-biotite tonalite body as sample *EN42*. Six zircon analyses from *EN28* yield concordant and equivalent results with a concordia age of 91.69±0.06 Ma (MSWD=1.41) interpreted as the crystallization age of this sample (Fig. 7d). A seventh analysis is slightly younger than the others outside of uncertainty which is more difficult to interpret. This zircon may have been disturbed by Pb loss.

Five zircon analyses from *E-281* yield concordant results that overlap within uncertainty (Fig. 7e); however a statistically significant concordia age cannot be determined because the analyses spread out along concordia. The crystallization age of this sample is probably best represented by the youngest analysis at 90.99±0.09 Ma, and the other analyses may represent inheritance of earlier formed sheets.

The last sample in the transect was collected from a hornblende quartz diorite gneiss sheet along the western margin of the intrusion. This sheet differs from the previously described sheets in that it displays a strong subsolidus fabric. Five zircon U-Pb analyses display a range of Triassic $^{206}Pb/^{238}U$ dates from 206.44±0.13 Ma to 221.52±0.16 Ma (Fig. 7f). Three analyses are concordant. If the youngest concordant analysis (z2) is not included, the other four analyses define a discordia line (MSWD=1.73) with an upper intercept of 222.8±2.4 Ma and a poorly constrained lower intercept of 114.8±28.0 Ma. This discordia line is consistent with the interpretation that this sheet is actually part of the ca. 220 Ma Dumbell Gneiss not the Seven-Fingered Jack plutons as mapped by Cater and Crowder (1967) and Cater and Wright (1967). The crystallization age of the sheet is probably best represented by the age of the oldest concordant analysis (z3). The other analyses most likely reflect the presence of mid-Cretaceous or Late Triassic overgrowths. Overgrowths of varying thickness are observable in cathodoluminescence (CL) images of representative grains (Fig. 8).

Southeast of the transect, sample *E-498* was collected from a ductilely-deformed dike that cuts across a diorite sheet. Five concordant and equivalent zircon analyses from this sample yield a concordia age of 46.39±0.06 Ma (MSWD=0.64) (Fig. 7g). This age is interpreted as the crystallization age of the dike, and it overlaps within uncertainty the

crystallization age of the Duncan Hill pluton (Tabor et al., 1987a). Strain is strongly partitioned into the dike and indicates that ductile deformation was ongoing in this region until the Eocene.

Farther southeast, sample *E-436* is hornblende-biotite tonalite collected from an outcrop that displays well-developed magmatic folds (Paterson et al., 1998). Four zircon analyses display a wide range of $^{206}Pb/^{238}U$ dates from 90.75±0.05 Ma to 216.25±0.29 Ma (Fig. 7h). The crystallization age of this sheet is probably best represented by the age of the youngest concordant analysis at 90.75±0.05 Ma. The other zircons analyzed likely contain Triassic grains overgrown to varying degrees by ca. 91 Ma magmatic overgrowths. Again, overgrowths of varying thickness are observable in CL images (Fig. 8).

Sample *EN65* is a medium-grained hornblende-biotite tonalite collected ~12 km to the southeast along strike from sample *E-436*. This sample is near the mid-point of the presently exposed length of the two intrusive suites. Five concordant zircon analyses form a nearly bimodal distribution with $^{206}Pb/^{238}U$ dates from 89.85±0.07 Ma to 92.01±0.08 Ma (Fig. 7i). CL images show fine-scale oscillatory zoning and lack obvious overgrowths (Fig. 8). The youngest analysis most likely represents the crystallization age of this sheet, whereas the three older analyses probably represent a disaggregated, ca. 92 Ma sheet.

Six zircon analyses from the southeastern extent of the central biotite granodiorite body (*EN3*) spread out along concordia from 103.80±0.73 Ma to 162.50±0.35 Ma (Fig. 7j). Magmatic fabrics in the granodiorite body are continuous with magmatic fabrics in the host tonalite sheets and locally cut the contact at a high angle, implying that the tonalite and granodiorite are co-magmatic and that the magmatic fabric reflects regional strain (Payne, 2001). I infer that the tonalite adjacent to the granodiorite tip was emplaced at ca. 90 Ma based on the previously described sample. Therefore, it seems unlikely that any of the analyses from *EN3* represent the crystallization age of the granodiorite body. The fact that all the analyses overlap concordia suggest these grains do not represent mixtures of Late Cretaceous and Triassic zircon as analyses from samples *Ho-52-1* and *E-436* are interpreted. Early Cretaceous dates such as those obtained from *EN3* are relatively uncommon in the Cascades core. The only other region

in the Cascades core where Early Cretaceous ages have been obtained is in the Chelan Complex (Mattinson, 1972), which the Entiat intrudes along its southeastern margin. A reasonable interpretation of these zircon analyses is that they represent zircon inherited from the Chelan Complex.

Sample *EN16* is a fine-grained tonalite that displays a gradational contact with the fine-grained two-pyroxene diorite body along the eastern-central margin of the intrusion. Three concordant and equivalent zircon analyses yield a concordia age of 72.57±0.03 Ma (MSWD=0.97) (Fig. 7k). This age is interpreted to represent the crystallization age of this sample and the relatively homogeneous diorite body as a whole.

Sample *EN11* represents the coarse-grained, more homogeneous, hornblende-biotite tonalite sheets typical of the southeastern end of the intrusion. Eight zircon U-Pb analyses define an array with concordant analyses as old as 72.91±0.13 Ma and discordant analyses with $^{206}Pb/^{238}U$ dates as young as 71.21±0.07 Ma (Fig. 7l). Six of the eight analyses form a concordant cluster; however there is enough dispersion in the analyses that a statistically significant concordia age cannot be defined. Again, I interpret the youngest concordant analysis at 72.51±0.10 Ma as the best estimate of the crystallization age of the sheet and the slightly older analyses as zircon crystallized in slightly older sheets. The two discordant analyses may reflect post-crystallization Pb loss. Four titanite multi-grain fractions define a concordant cluster that yields a concordia age of 66.47±0.08 Ma (MSWD=1.3) (Fig. 7m). This concordia age is interpreted as the time of cooling through the titanite closure temperature for Pb (600-650°C; Hodges, 2003) and reflects moderate cooling (~15-30°C/Myr) after emplacement of this tonalite sheet.

The final sample analyzed (*E-25*) was collected from the mylonitized southwest margin of the Entiat intrusion. Three concordant and equivalent zircon analyses yield a concordia age of 71.42±0.12 Ma (MSWD=0.09) interpreted as the crystallization age of the sample (Fig. 7n).

DISCUSSION

Temporal History of Sheet Emplacement

The new geochronologic data from this study indicate that magmatic sheets mapped as the Entiat and Seven-Fingered Jack intrusions actually represent at least three different episodes of magma emplacement. The earliest sheets are Triassic in age and contemporaneous with the ca. 220 Ma Dumbell plutons at the roots of the Cascade River-Holden arc. Hurlow (1992) also obtained two discordant zircon fractions with $^{207}Pb/^{206}Pb$ dates of 215-218 Ma from a mylonitic biotite-hornblende quartz diorite sheet mapped as part of the northwestern tip of the Seven-Fingered Jack intrusion by Cater and Crowder (1967). Based on the available data, the Triassic sheets appear restricted to the northwestern end of the Seven-Fingered Jack intrusion and can be distinguished from adjacent sheets by their strong subsolidus fabric and gneissic texture.

The next phase of magmatism forms the Seven-Fingered Jack intrusive suite and is represented by ca. 90-92 Ma sheets. These sheets range in composition from quartz diorite to hornblende-biotite tonalite. Mafic contact complexes developed in between ca. 90-92 Ma sheets. Tabor et al. (1987a) also mapped banded migmatitic tonalite gneiss and mafic amphibolite along the northeastern margin which they describe as equivalent to the mafic complexes of Cater and Crowder (1967) and Cater and Wright (1967). These rocks are tentatively included in the Seven-Fingered Jack suite although it may actually be part of the Chelan Complex host rock instead. Textures within the contact complexes suggest that hornblendite and hornblende gabbro were emplaced first and then disaggregated by later tonalitic to trondhjemitic magmas. Angular blocks of tonalite or hornblende quartz diorite similar to adjacent sheets were not identified. This observation suggests that the contact complexes do not significantly post-date the adjacent sheets and are more likely co-magmatic with the ca. 90-92 Ma sheets.

The final phase of magmatism is termed the Entiat intrusive suite and is represented by ca. 71-73 Ma coarse-grained tonalite sheets at the southeastern end of the body, mylonitized sheets along the southwestern margin, and diorite along the eastern-central margin (Fig. 3). Internal sheet contacts are less distinctive within this suite, and coarse-grained tonalite is much more volumetrically significant than other rock types. The ca. 73 Ma diorite body that crops out along the eastern-central margin is distinct

from the earlier contact complexes because of its relative homogeneity. The ca. 79 Ma hornblende gabbro sheet within the northwest tip region is not considered part of the Entiat suite because it is at least 6 Myr older than the southeastern Entiat sheets and because it is more similar in age to the nearby ca. 77 Ma Riddle Peaks gabbro (Fig. 2) (McPeek et al., 2002).

The contact complexes, quartz diorite, and tonalite sheets present in the northwestern tip of the Seven-Fingered Jack intrusion cover a much wider compositional range than the later, more homogeneous southeastern Entiat tonalite sheets. In general, the ca. 71-73 Ma sheets are also coarser grained than earlier sheets. These characteristics are used to infer the approximate location of the contact between the Seven-Fingered Jack and Entiat suites. However, the location of this contact is insufficiently mapped because of a lack of field observations and geochronological data through the center of the body. The discussion about the location of a contact between the Seven-Fingered Jack and Entiat suites is focused on textural differences from southeast to northwest implying a NE-SW trending contact, but the contact in all likelihood may parallel sheet margins in a NW-SE trend. The presence of a distinct ca. 79 Ma hornblende gabbro sheet within the northwest tip also highlights the possibility that previously unrecognized "Entiat-aged" sheets may discontinuously intrude the Seven-Fingered Jack intrusion along its length, making a clear geographic distinction between the intrusions difficult.

Withstanding the stated uncertainties of the location of a contact, I would place an approximate contact with a roughly N-S trend to the west of the two pyroxene diorite body (Fig. 3). Coarse-grained tonalite typical of the Entiat intrusive suite crops out at the farthest southeastern extent of the body and as far north as the ca. 73 Ma diorite body. At least one coarse-grained tonalite locality (marked by an x on figure 3) contains angular blocks of medium-grained tonalite which are interpreted as xenoliths of ca. 90-92 Ma sheets. Medium-grained tonalite more typical of the northwestern ca. 90-92 Ma sheets crops out at least as far southeast as the ca. 90 Ma sample *EN65*. Observations that magmatic foliation within the granodiorite body is continuous with magmatic foliation in the surrounding tonalite (Payne, 2001) suggests that ca. 90 Ma tonalite is present at least as far southeast as the southeast tip of the granodiorite body. More fieldwork and geochronological data are necessary to better define this boundary.

Thermal models of the construction of sheeted intrusions predict an initial stage dominated by the emplacement of thin magmatic sheets, followed by the development of a central, more homogeneous, steady-state magma chamber (Hanson and Glazner, 1995; Yoshinobu et al., 1998). Miller and Paterson (2001a) proposed a similar scenario for the construction of the Entiat intrusion without the benefit of high-precision geochronology. (Note that Miller and Paterson also included the Seven-Fingered Jack sheets as part of the Entiat intrusion.) This scenario involved initial emplacement of thin mafic sheets, followed by emplacement of early tonalite sheets at the northwestern end of the intrusion. These early sheets were proposed to have served as a planar anisotropy which controlled the ascent of subsequent bodies and acted as preheated pathways for larger, more felsic, "diapir-like" batches of magma at the southeastern end. This geochronologic study indicates, however, that the Seven-Fingered Jack sheets are unlikely to have formed "preheated pathways" for the emplacement of more homogeneous tonalite of the Entiat intrusion because of the ~20 Myr time lag between emplacement of each intrusion. Their proposed model may explain the transition from multiple, thin, compositionally-diverse sheets at the northwestern tip of the Seven-Fingered Jack intrusion to the thicker tonalite sheets near the center of the body. Zircon U-Pb dates from the widely-spaced Seven-Fingered Jack samples suggest, however, are not sufficiently precise to discern an age difference between the thin northwestern sheets and thicker tonalite sheets that make up the center of the body.

If the differences in sheet characteristics between the northwestern and southeastern ends are not a result of an evolving thermal regime, then some other mechanism must be responsible. Although the dimensions of the sheets within the southeastern end of the body are not well-defined because sheet contacts are not easily recognized, the sheets at the southeastern end are generally thicker and have lower aspect ratios than the Seven-Fingered Jack sheets (Miller and Paterson, 2001a). The final aspect ratio and internal sheet characteristics of each body may reflect an interplay between regional deformation and ascent mechanisms that are transitional between elastic dikes and "visco-elastic" diapirs (Paterson and Miller, 1998b). The possibility that ascent of the Entiat and Seven-Fingered Jack sheets was controlled by faults was considered by Paterson and Miller (1998b) and Miller and Paterson (2001a), but both studies indicated

that there is no evidence of faulting associated with sheet emplacement. Alternatively, the crustal anisotropy developed by the Seven-Fingered Jack sheets may have formed vertical walls that potentially focused later rise of magma and influenced the sheet characteristics of the Entiat suite (Paterson and Miller, 1998b).

Implications of Zircon Inheritance for the Construction of Sheeted Intrusions

Unlike other intrusions in the Cascades core (including the Mount Stuart batholith and Tenpeak intrusions; Chapter 4), nearly all samples from the Seven-Fingered Jack and Entiat intrusions show evidence of zircon inheritance. This inheritance is most easily recognized when analyses fall on a discordia line that points to a ca. 220 Ma upper intercept. Several discordant analyses from samples from the northwestern tip of the Seven-Fingered Jack intrusion can be interpreted in this way and indicate that the Dumbell Gneiss was incorporated into these sheets during emplacement. The vertical extent of the Dumbell Gneiss in the crustal column is not well-constrained; however, the Cascades core is generally viewed as a stack of relatively shallowly-dipping thrust sheets (McGroder, 1991; Miller and Paterson, 2001b) and the Dumbell Gneiss is not thought to extend into the source region of the Seven-Fingered Jack and Entiat sheets. This implies that the Dumbell Gneiss was partially assimilated by the Seven-Fingered Jack sheets near the level of emplacement.

Evidence of zircon inheritance in other tonalite and quartz diorite sheets is more subtle, and would be entirely missed by lower precision geochronologic techniques. More detailed work on zircon grains imaged by cathodoluminescence is necessary to test this hypothesis. These sheets yielded zircon analyses that span 2-3 Myr along concordia. The scatter in the dates is too great to be attributed to analytical error and suggests that it has real geologic significance. This type of inheritance pattern could result from the following scenario: 1) a magmatic sheet is emplaced and begins to cool and crystallize zircon, 2) while the sheet is still partially molten, it is intruded and partially disaggregated by the next sheet emplaced along the same magma pathway, 3) the sheets mix and become either partially or completely homogenized, 4) the hybridized sheet begins to cool and crystallize zircon, 5) steps 2-4 may be repeated, and 6) final crystallization locks in the most recent magmatic fabric.

This process has the potential to result in significant chemical evolution of the system during ascent and emplacement, and the timescale of this evolution is recorded episodically in the zircon systematics. Other samples which do not record a similar inheritance pattern may represent rapidly cooled sheets that were not disturbed by later sheet emplacement, or mixing between sheets on a short enough timescale that different age populations are not resolvable. The heterogeneous contact complexes likely represent the situation when the first sheets emplaced are very different compositionally from later sheets and mixing is difficult because of viscosity contrasts (Sparks and Marshall, 1986). The presence of angular mafic blocks in the contact complexes reflects the fact that the earliest sheets emplaced in the mafic complexes were hornblendite and hornblende gabbro.

The zircon inheritance patterns place important constraints on the evolution of these magmatic systems. Coleman et al. (2004) and Glazner et al. (2004) argue that large magma chambers (comparable to the size of the Entiat and Seven-Fingered Jack intrusions) rarely, if ever, exist, and that the chemical and textural variations observed in many intrusions must be inherited from the source region because little opportunity exists for mixing at the site of emplacement. I agree with Coleman et al. (2004) and Glazner et al. (2004) that a single, large, convecting magma chamber did not existed during the construction of the Seven-Fingered Jack or Entiat intrusions. However, I disagree with their proposal that chemical and textural variations are derived from the magma source region. The patterns of zircon inheritance in the Entiat and Seven-Fingered Jack samples imply that mixing between early-formed, partially-solidified sheets and later sheets was an important process in the evolution of these systems. Incorportation of host rock near the site of emplacement also resulted in zircon inheritance and presumably chemical modification of the sheets.

The evolution of both the Seven-Fingered Jack and Entiat intrusions appears to have taken place over an approximately 2-3 Myr time period as indicated by the dispersion of dates within a given sheet. This timespan is much longer than predicted by dike emplacment models (e.g. Petford et al., 2000). The length of time that each system was active may be controlled by the rate of magma generation at the site of melting and/or the rate that space can be made for the growing intrusion.

Interpretation of Magmatic Fabric Patterns

The recognition that magmatic fabrics attributed to the formation of a single Entiat "pluton" (Miller and Paterson, 2001a) actually formed over two discrete time periods ~20 Myr apart requires a re-evaluation of conclusions drawn from the magmatic fabric patterns. Miller and Paterson (2001a) note that magmatic foliation is well-developed throughout the entire body (i.e., both Seven-Fingered Jack and Entiat suites), and is subparallel to moderate- to high-temperature subsolidus foliation and/or lineation. The magmatic foliation is also commonly discordant to sheet contacts, reflecting the fact that the foliation records the orientation of strain late in the crystallization history of the sheet rather than magmatic flow fabrics during emplacement. At the northwestern end, foliation dips moderately to steeply northeast, whereas foliation dips are generally shallower at the southeastern end (Fig. 5) (Miller and Paterson, 2001a).

Magmatic folds of foliation, layering, and sheets are also well-developed throughout the body (Miller and Paterson, 2001a; Paterson and Miller, 1998b). At the northwestern tips of certain Seven-Fingered Jack sheets, magmatic foliation defines well-developed, upright, gently-plunging folds that mimic the orientation and style of folds in the surrounding host rock (Paterson and Miller, 1998b). Locally, the sheet margins are subparallel to the axial plane of host rock folds, whereas host rock foliation dips more gently than the sheet margins in other locations (Paterson and Miller, 1998b). At the southeastern end in the Entiat intrusion, map-scale folds at the scale of intrusion define a broad, asymmetric, southwest-vergent antiform and macroscopic folds lie on the limbs of the large antiform (Miller and Paterson, 2001a). Gently-plunging, fold axes throughout the body have northwest trending axial traces that are subparallel to the length of the intrusion (Miller and Paterson, 2001a).

Miller and Paterson (2001a) argue that several relationships indicate that folding occurred during emplacement. 1) Folds deform magmatic foliation in domains with only minor subsolidus deformation. 2) Locally, magmatic folds defined by aligned hornblende and plagioclase are overgrown by igneous hornblende oriented parallel to the axial plane of the fold (Paterson and Miller, 1998b). 3) Fold axes are subparallel to

magmatic lineation. 4) Folds within the intrusion have similar styles and orientations to host-rock folds, and folded host-rock foliation is continuous with magmatic foliation.

The fact that these magmatic folds developed in both the Seven-Fingered Jack and Entiat suites has important implications for the regional tectonic history. Folding of the Seven-Fingered Jack sheets was coincident with folding of other mid-Cretaceous intrusions within the Cascades core (e.g., Miller and Paterson, 1992; Paterson and Miller, 1998a). This folding is part of larger-scale, core-wide NE-SW contraction, vertical thickening and arc-parallel, sub-horizontal extension (Miller and Paterson, 1992; Paterson and Miller, 1998a). The presence of similarly oriented folds in the Entiat intrusion and the nearby ca. 76 Ma Cardinal Peak intrusion indicate that regional NE-SW contraction continued into the latest Cretaceous. The orientation of the strain field was remarkably constant over these two time periods. The coincidence of the orientation of magmatic fabrics has sometimes been used to argue that two phases of an intrusion are co-magmatic; however, this case clearly shows that foliation patterns cannot be interpreted without caution.

CONCLUSIONS

U-Pb dates from several sheets of what has previously been described as the Entiat pluton indicate that this "pluton" is composed of at least three distinct intrusive suites. Use of the term "pluton" implies that these sheets are co-magmatic or closely spaced in time, and therefore, should no longer be used to describe these systems. The oldest intrusive suite is coeval with the emplacement of the Dumbell Gniess and should be considered a member of that suite. Sheets with ca. 90-92 Ma crystallization ages form the Seven-Fingered Jack suite whereas sheets with ca. 71-73 Ma crystallization ages comprise the Entiat intrusive suite.

The recognition of an approximately 20 Myr time lag between emplacement of the Seven-Fingered Jack and Entiat suites indicates that the multiple thin sheets that form the northwestern end of the body could not have formed preheated pathways for the emplacement of later, more homogeneous sheets. The geochronologic data are not precise enough to evaluate the predictions of thermal models (i.e., Hanson and Glazner, 1995; Yoshinobu et al., 1998) that sheets should decrease in age from the margins to the

center of the intrusion. The sheeting characteristics of each intrusion may be controlled more by regional deformation or variations in ascent mechanism rather than an evolving thermal regime.

The presence of inherited zircon in several of the Entiat and Seven-Fingered Jack samples suggests that the formation of these magmatic sheets involved multiple intrusion and partial homogenization of sheets at the level of emplacement. Seven-Fingered Jack sheets also incorporated zircon from the Dumbell Gneiss and potentially the Chelan Complex. This model for the growth of sheeted intrusions conflicts with other proposals that chemical and textural homogeneity in sheeted intrusions must be inherited from the source region rather than evolve during ascent and emplacement (i.e., Coleman et al., 2004; Glazner et al., 2004). The dispersion of dates within a given sheets suggests the emplacement of both the Seven-Fingered Jack and Entiat suites took place over a 2-3 Myr time period. This timespan is much longer than predicted by dike emplacement models in which an entire intrusion could be constructed in much less than one Myr. The 2-3 Myr timespan, however, is shorter than predicted from the incremental assembly model described by Coleman et al. (2004) and Glazner et al. (2004). Documentation of the timescales of the construction of sheeted intrusions is important for constraining potential ascent mechanisms and/or rates of deformation of host rocks to accommodate the growth of the intrusion.

Magmatic fabric patterns in the Seven-Fingered Jack and Entiat suites suggest that both suites were emplaced during regional NE-SW, arc-perpendicular contraction that was active throughout the Late Cretaceous. The presence of a 46.4 Ma mylonitic dike (*E-498*) that cuts a Seven-Fingered Jack sheet also indicates that ductile deformation continued until at least ca. 46 Ma. The orientation of magmatic structures indicates that the strain field was remarkably constant during this time period. These dates also caution against concluding that sheets are coeval simply based on the similarity in orientation of their respective magmatic fabrics.

The application of high-precision U-Pb geochronology to sheeted magmatic systems indicates such systems are more complicated in both space and time than previously recognized. Useful avenues of future research include documenting the chemical and isotopic evolution of sheeted magmatic systems, constraining the

fundamental control on the initiation of a sheeted system, and understanding why sheeted magmatism persisted through this zone of the Cascades core from ca. 92-46 Ma.

REFERENCES

Cater, F. W., 1982, Intrusive rocks of the Holden and Lucerne quadrangles, Washington: the relation of depth zones, composition, textures, and emplacement of plutons: U. S. Geological Survey Professional Paper, v. 1220, p. 108.

Cater, F. W., and Crowder, D. F., 1967, Geologic map of the Holden Quadrangle, Snohomish and Chelan counties, Washington: U. S. Geological Survey.

Cater, F. W., and Wright, T. L., 1967, Geologic map of the Lucerne Quadrangle, Chelan County, Washington: U.S. Geological Survey.

Coleman, D. S., Gray, W., and Glazner, A. F., 2004, Rethinking the emplacement and evolution of zoned plutons: Geochronologic evidence for incremental assembly of the Tuolumne Intrusive Suite, California: Geology, v. 32, p. 433-436.

Dawes, R. L., 1993, Mid-crustal, Late Cretaceous plutons of the North Cascades: petrogenesis and implications for the growth of continental crust [PhD thesis]: University of Washington, Seattle, 272 p.

Dellinger, D. A., 1996, The geology, petrology, geochemistry, mineralogy, and diapiric emplacement of the Duncan Hill pluton, North Cascades, Washington [PhD thesis]: University of California, Santa Barbara, 536 p.

Dragovich, J. D., and Norman, D. K., 1995, Geologic map of the west half of the Twisp 1:100,000 Quadrangle, Washington, scale 1:100,000.

Glazner, A. F., Bartley, J. M., Coleman, D. S., Gray, W., and Taylor, R. Z., 2004, Are plutons assembled over millions of years by amalgamation from small magma chambers?: GSA Today, v. 14, p. 4-11.

Hanson, R. B., and Glazner, A. F., 1995, Thermal requirements for extensional emplacement of granitoids: Geology, v. 23, p. 213-216.

Hodges, K. V., 2003, Geochronology and thermochronology in orogenic systems, *in* Rudnick, R. L., ed., Treatise on Geochemistry: Amsterdam, Elsevier, p. 263-292.

Hopson, C. A., and Mattinson, J. M., 1994, Chelan Migmatite Complex, Washington: Field evidence for mafic magmatism, crustal anatexis, mixing and protodiapiric emplacment, *in* Swanson, D. A., and Haugerud, R. A., eds., Geologic Field Trips in the Pacific Northwest: Boulder, Geological Society of America, p. 2K-1 - 2K-21.

Hurlow, H. A., 1992, Structural and U/Pb geochronologic studies of the Pasayten Fault, Okanogan Range Batholith, and southeastern Cascades crystalline core, Washington [PhD thesis]: University of Washington, Seattle, 180 p.

Hutton, D. H., 1992, Granite sheeted complexes: evidence for the dyking ascent mechanism: Transactions of the Royal Society of Edinburgh: Earth Sciences, v. 83, p. 377-382.

Ingram, G. M., and Hutton, D. H. W., 1994, The Great Tonalite Sill: Emplacement into a contractional shear zone and implications for Late Cretaceous to early Eocene tectonics in Southeastern Alaska and British Columbia: Geological Society of America Bulletin, v. 106, p. 715-728.

Ludwig, K. R., 1998, On the treatment of concordant uranium-lead ages: Geochimica et Cosmochimica Acta, v. 62, p. 665-676.

Mattinson, J. M., 1972, Ages of zircons from the Northern Cascade Mountains, Washington: Geological Society of America Bulletin, v. 83, p. 3769-3783.

McGroder, M. F., 1991, Reconciliation of two-sided thrusting, burial metamorphism, and diachronous uplift in the Cascades of Washington and British Columbia: Geological Society of America Bulletin, v. 103, p. 189-209.

McPeek, S. L., Miller, R. B., Miller, J. S., and Matzel, J. P., 2002, Significance of fabric development in the gabbroic Riddle Peaks Pluton, North Cascades, Washington: Geological Society of America Abstracts with Programs, v. 34, p. 96.

Miller, R. B., Haugerud, R. A., Murphy, F., and Nicholson, L. S., 1994, Tectonostratigraphic framework of the northeastern Cascades: Washington Division of Geology and Earth Resources Bulletin, v. 80, p. 73-92.

Miller, R. B., and Paterson, S. R., 1992, Tectonic implications of syn-emplacement and postemplacement deformation of the Mount Stuart batholith for mid-Cretaceous orogenesis in the North Cascades: Canadian Journal of Earth Sciences, v. 29, p. 479-485.

Miller, R. B., and Paterson, S. R., 2001a, Construction of mid-crustal sheeted plutons: Examples from the north Cascades, Washington: Geological Society of America Bulletin, v. 113, p. 1423-1442.

Miller, R. B., and Paterson, S. R., 2001b, Influence of lithological heterogeneity, mechanical anisotropy, and magmatism on the rheology of an arc, North Cascades, Washington: Tectonophysics, v. 342, p. 351-370.

Misch, P., 1966, Tectonic evolution of the Northern Cascades of Washington State: a west-cordilleran case history: Canadian Institute of Mining and Metallurgy, v. Special volume 8, p. 101-148.

Monger, J. W. H., Price, R. A., and Tempelman-Kluit, D. J., 1982, Tectonic accretion and the origin of the two major metamorphic and plutonic welts in the Canadian Cordillera: Geology, v. 10, p. 70-75.

Paterson, S. R., Fowler, T. K., Jr., Schmidt, K. L., Yoshinobu, A. S., Yuan, E. S., and Miller, R. B., 1998, Interpreting magmatic fabric patterns in plutons: Lithos, v. 44, p. 53-82.

Paterson, S. R., and Miller, R. B., 1998a, Magma emplacement during arc-perpendicular shortening: An example from the Cascades crystalline core, Washington: Tectonics, v. 17, p. 571-586.

Paterson, S. R., and Miller, R. B., 1998b, Mid-crustal magmatic sheets in the Cascades Mountains, Washington: implications for magma ascent: Journal of Structural Geology, v. 20, p. 1345-1363.

Paterson, S. R., Miller, R. B., Alsleben, H., Whitney, D. L., Valley, P. M., and Hurlow, H., 2004, Driving mechanisms for >40 km of exhumation during contraction and extension in a continental arc, Cascades core, Washington: Tectonics, v. 23, p. 10.1029/2002TC001440.

Paterson, S. R., and Schmidt, K. L., 1999, Is there a close spatial relationship between faults and plutons?: Journal of Structural Geology, v. 21, p. 1131-1142.

Payne, S. J., 2001, Mechanisms of magma ascent: Implications of sheet tips in the Entiat Pluton, Cascades crystalline core, Washington: Geological Society of America Abstracts with Programs, v. 33, p. 38.

Petford, N., Cruden, A. R., McCaffrey, K. J. W., and Vigneresse, J. L., 2000, Granite magma formation, transport and emplacement in the Earth's crust: Nature, v. 408, p. 669-673.

Pitcher, W. S., and Berger, A. R., 1972, The Geology of Donegal: A Study of Granite Emplacement and Unroofing: New York, Wiley, 435 p.

Sparks, R. S. J., and Marshall, L. A., 1986, Thermal and mechanical constraints on mixing between mafic and silicic magmas: Journal of Volcanology and Geothermal Research, v. 29, p. 99-124.

Tabor, R. W., Frizzell, V. A., Jr., Whetten, J. T., Waitt, R. B., Jr., Swanson, D. A., Byerly, G. R., Booth, D. B., Hetherington, M. J., and Zartman, R. E., 1987a, Geologic map of the Chelan 30' by 60' Quadrangle, Washington: U. S. Geological Survey, scale 1:100,000.

Tabor, R. W., Haugerud, R. A., Brown, E. H., Babcock, R. S., and Miller, R. B., 1989, Accreted Terranes of the North Cascades Range, Washington, International Geologic Congress Trip T307: Washington, D.C., American Geophysical Union, 62 p.

Tabor, R. W., Zartman, R. E., and Frizzell, V. A., Jr., 1987b, Possible tectonostratigraphic terranes in the North Cascades crystalline core, Washington, *in* Schuster, J. E., ed., Selected Papers on the Geology of Washington: Anaheim, CA, United States, Washington Division of Geology and Earth Resources, p. 107-127.

Valley, P. M., Whitney, D. L., Paterson, S. R., Miller, R. B., and Alsleben, H., 2003, Metamorphism of the deepest exposed arc rocks in the Cretaceous to Paleogene Cascades belt, Washington: evidence for large- scale vertical motion in a continental arc: Journal of Metamorphic Geology, v. 21, p. 203-220.

Waters, A. C., 1932, A petrologic and structural study of the Swakane Gneiss, Entiat Mountains, Washington: Journal of Geology, v. 40, p. 604-633.

Wendt, I., and Carl, C., 1991, The statistical distribution of the mean squared weighted deviation: Chemical Geology, v. 86, p. 275-285.

Yoshinobu, A. S., Okaya, D. A., and Paterson, S. R., 1998, Modeling the thermal evolution of fault-controlled magma emplacement models: Implications for the solidification of granitoid plutons: Journal of Structural Geology, v. 20, p. 1205-1218.

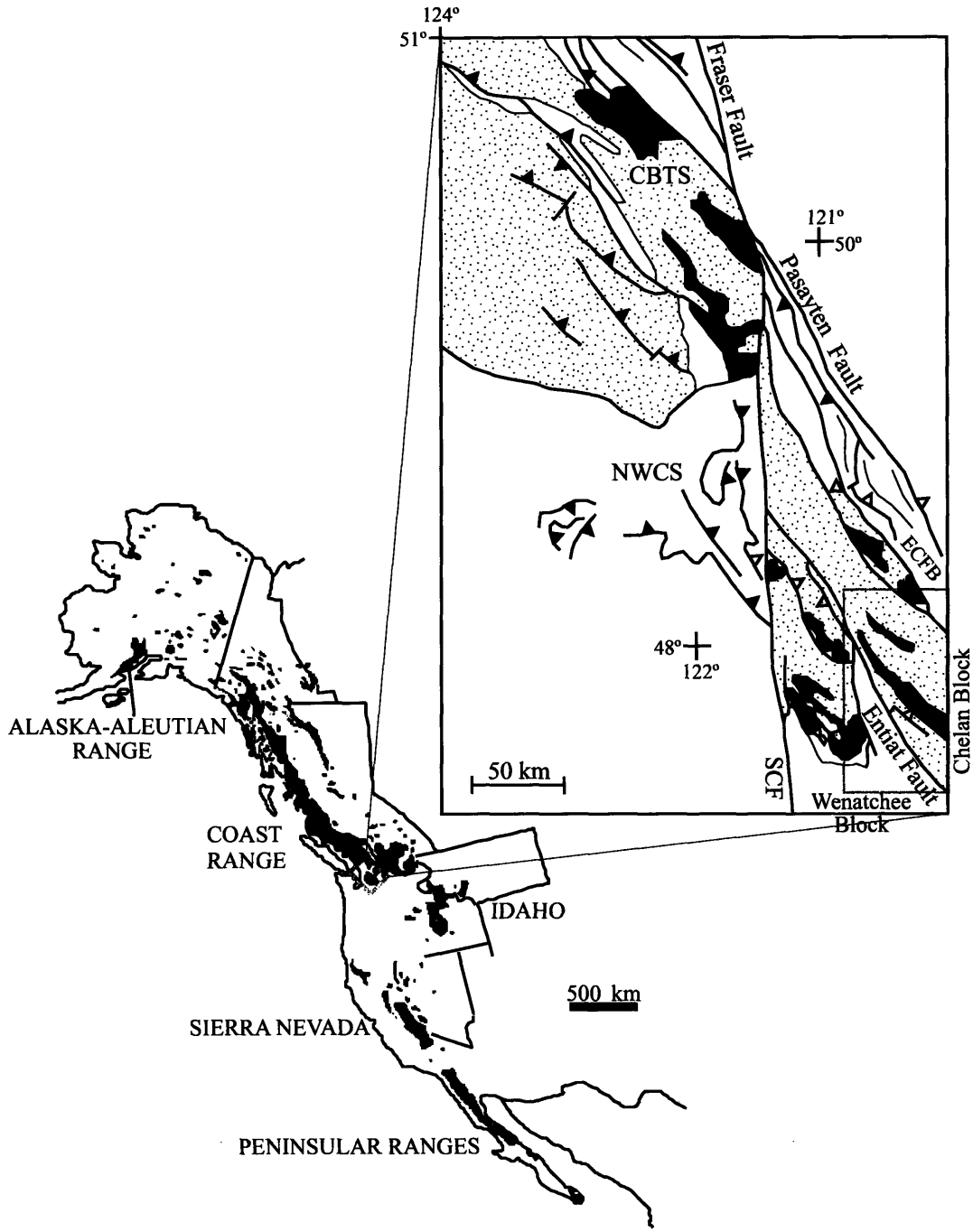

Figure 1. Sketch map of Mesozoic and Paleogene arc plutons in the western North American Cordillera (after Miller et al., 2000). Inset emphasizes distribution of metamorphic rocks (speckled pattern) and plutons (dark grey). Also shown are the Coast Belt thrust system (CBTS), lower-grade rocks of the Eastern Cascades fold belt (ECFB), and Northwest Cascades fault system (NWCS). The dextral Fraser-Straight Creek (SCF) fault offsets the Cascades core from the main part of the Coast Belt. The Entiat fault is a Tertiary, high-angle fault that divides that Cascades core into the Wenatchee and Chelan blocks. Light grey box in inset outlines the area of figure 2.

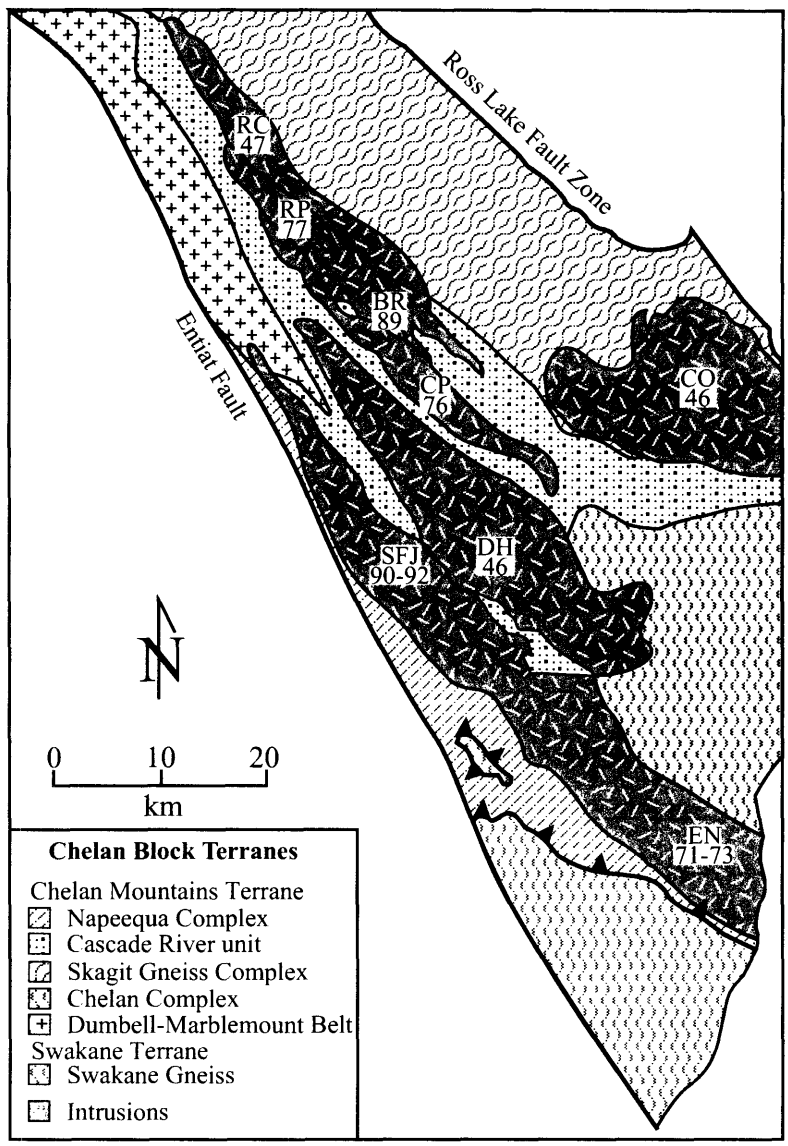

Figure 2. Geologic map of the southwestern Chelan block emphasizing the zone of elongate sheeted intrusions. Abbreviations are as follows: BR, Bearcat Ridge; CO, Cooper Mountain; CP, Cardinal Peak; DH, Duncan Hill; EN, Entiat; RC, Railroad Creek; RLFZ, Ross Lake fault zone; RP, Riddle Peaks; and SFJ, Seven-Fingered Jack. Numbers below the abbreviated pluton names are approximate crystallization ages of each intrusion (McPeek et al., 2002; Tabor et al., 1987b; this study).

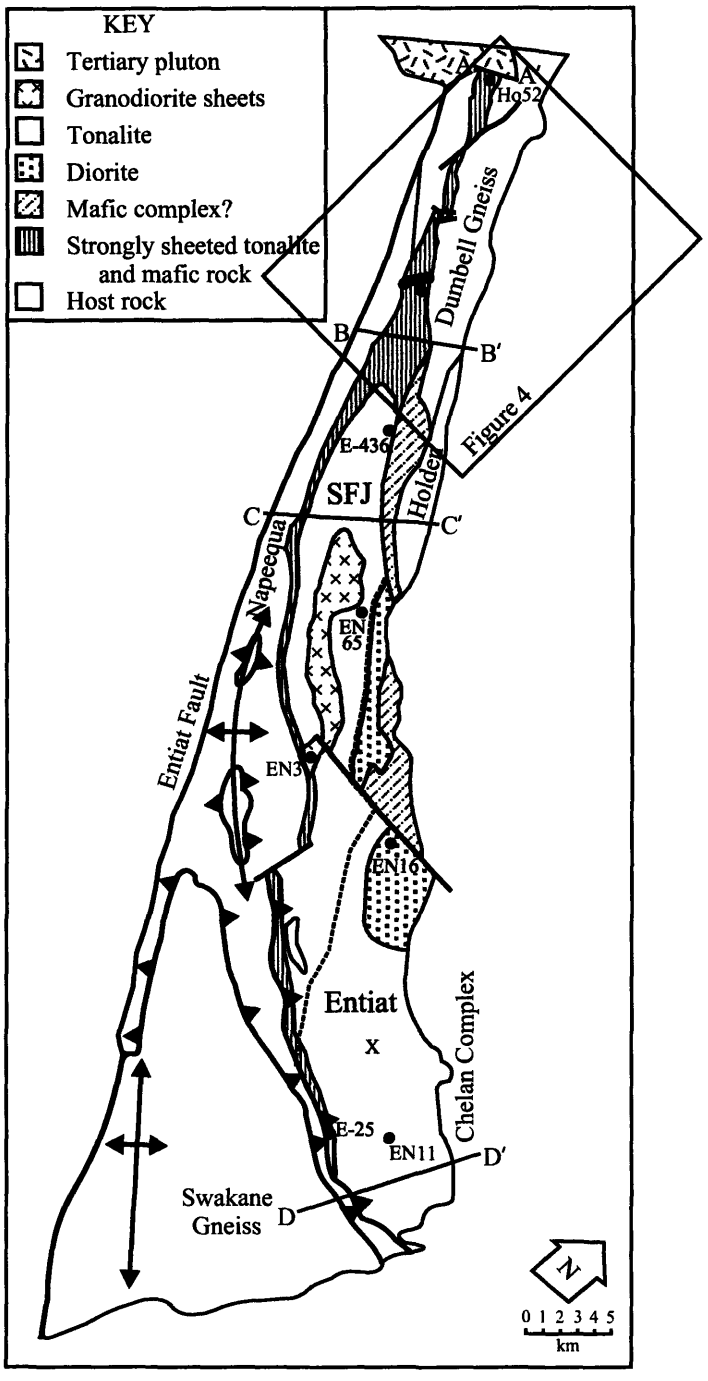

Figure 3. Map of the compositional variation and sheet characteristics of the Seven-Fingered Jack (SFJ) and Entiat intrusions after Miller and Paterson (2001a). Note that the north arrow points at an angle off to the right. Red dots mark geochronology sample localities. Dashed line marks approximate location of contact between the Seven-Fingered Jack and Entiat suites. Box surrounding the northwestern tip region marks the outline of figure 4. Lines of cross-section are shown in figure 5.

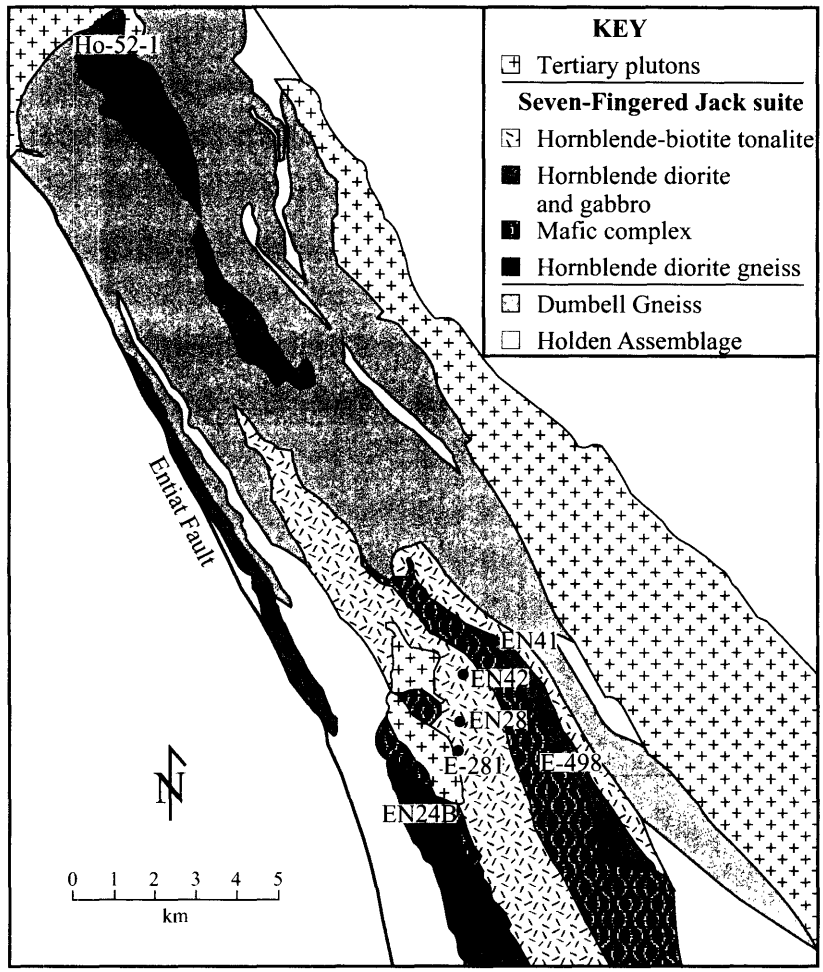

Figure 4. Map of sheets that comprise the northwestern tip of the Seven-Fingered Jack intrusion after Cater and Crowder (1967) and Cater and Wright (1967). Red dots mark geochronology sample localities. U-Pb zircon dates from samples EN24B and EN41 indicate that these sheets should no longer be considered part of the Seven-Fingered Jack suite. Red star marks geochronology sample locality of Triassic sheet dated by Hurlow (1992).

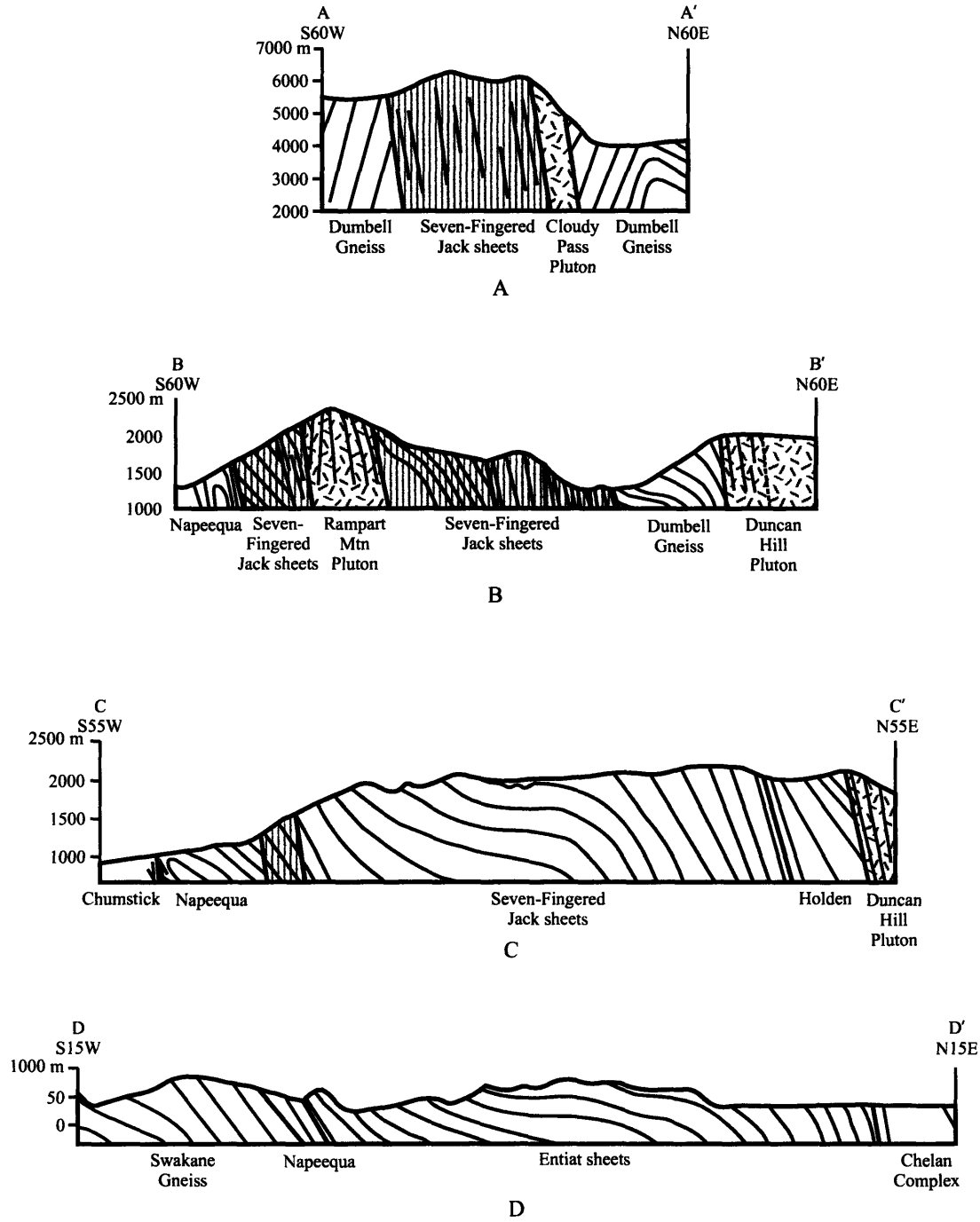

Figure 5. Cross-sections through the Seven-Fingered Jack and Entiat intrusions after Miller and Paterson (2001a). Thin lines within units mark interpreted foliation patterns based on numerous foliation measurements. Thick lines mark contacts between lithologic units. Shaded regions with light vertical lines mark parts of the intrusions that are composed of multiple, thin sheets. Random dash pattern marks Tertiary intrusions that post-date the Seven-Fingered Jack and Entiat intrusions.

a)

b)

c)

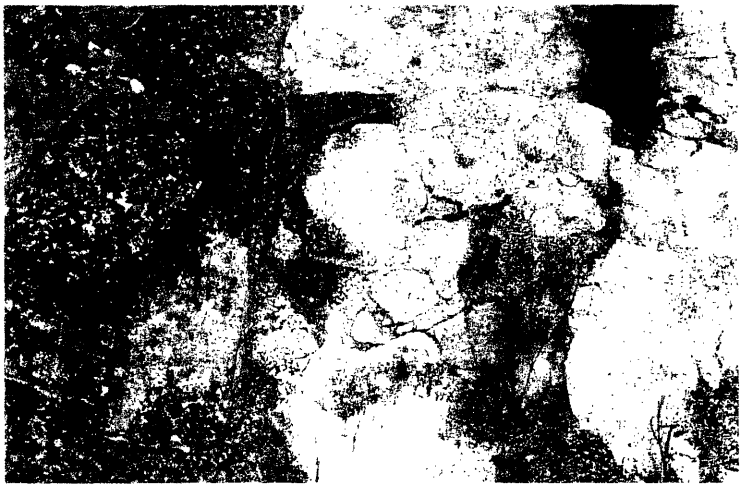

Figure 6. Photographs of textures from mafic complex outcrops. Angular blocks of gabbro (a and b) are contained within a leucocratic, fine-grained matrix. More diffuse contacts (c) indicate mingling between mafic and tonalitic magmas.

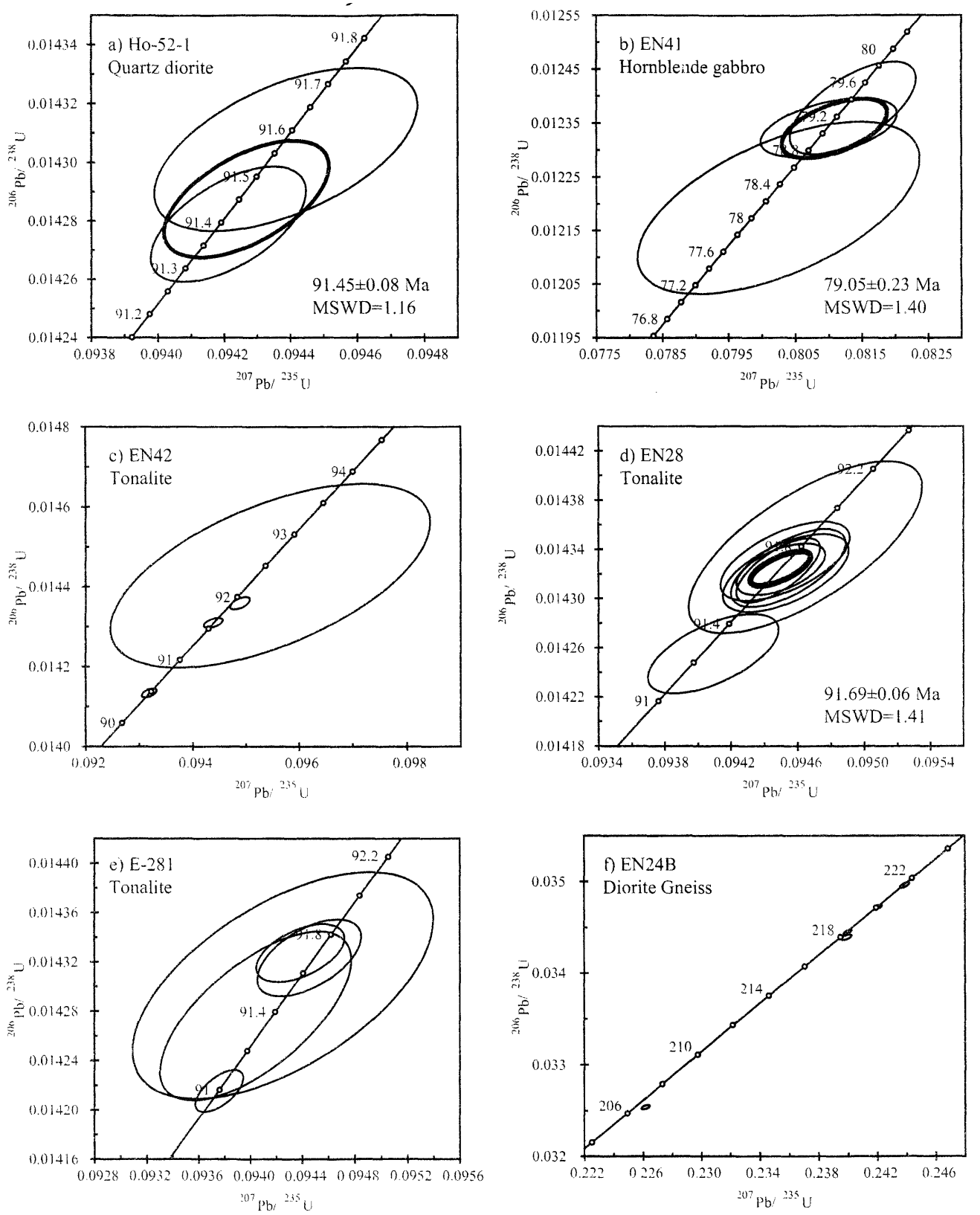

Figure 7. Concordia diagrams from all Seven-Fingered Jack and Entiat samples. Red ellipses are individual analyses, whereas heavy black ellipses are the concordia ellipses.

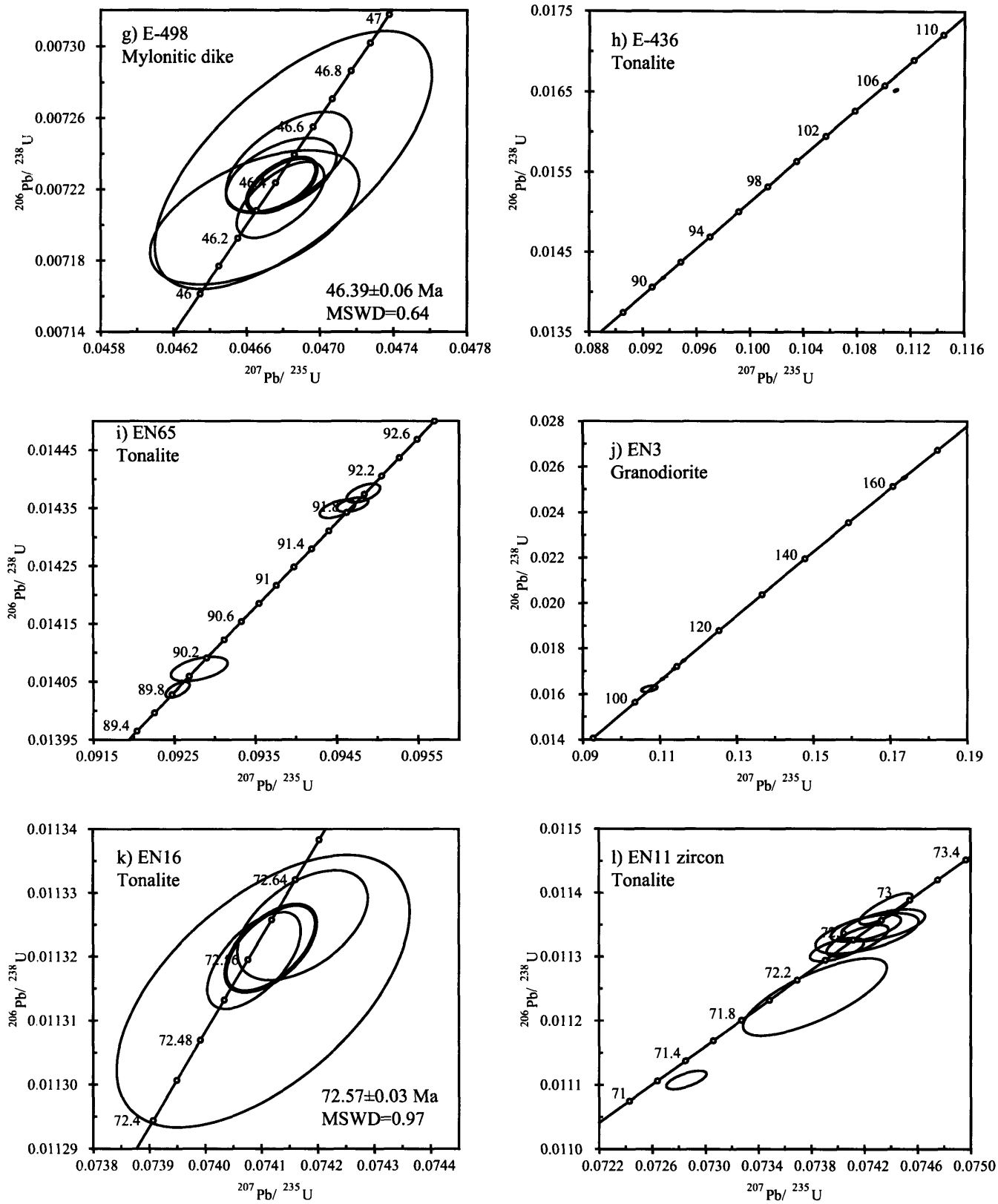

Figure 7 continued. Concordia diagrams from all Seven-Fingered Jack and Entiat samples. Red ellipses are individual analyses, whereas heavy black ellipses are the concordia ellipses.

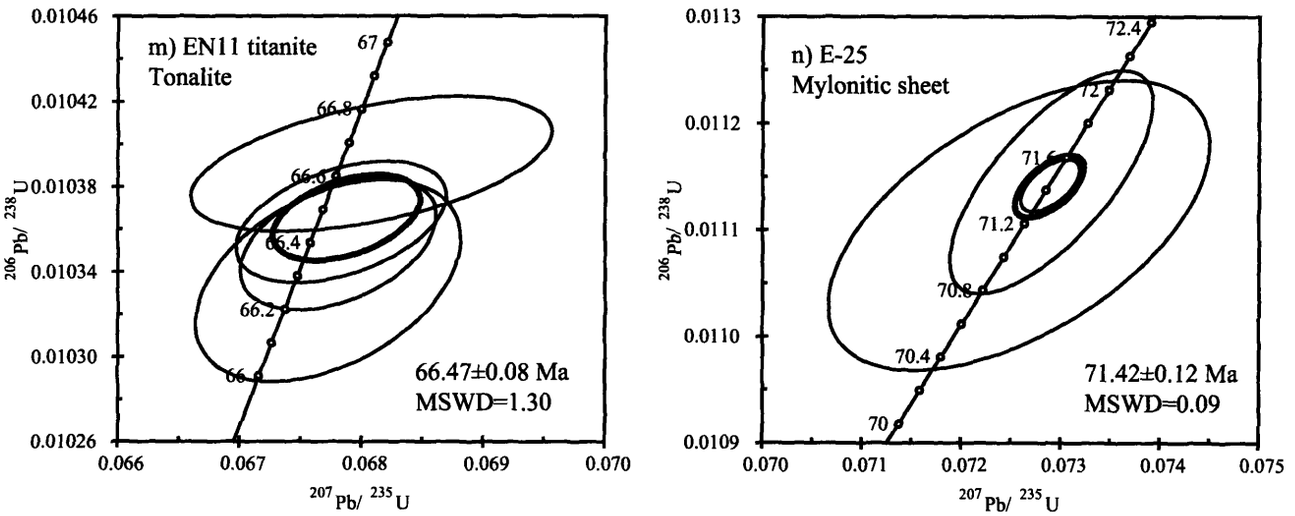

Figure 7 continued. Concordia diagrams from all Seven-Fingered Jack and Entiat samples. Red ellipses are individual analyses, whereas heavy black ellipses are the concordia ellipses.

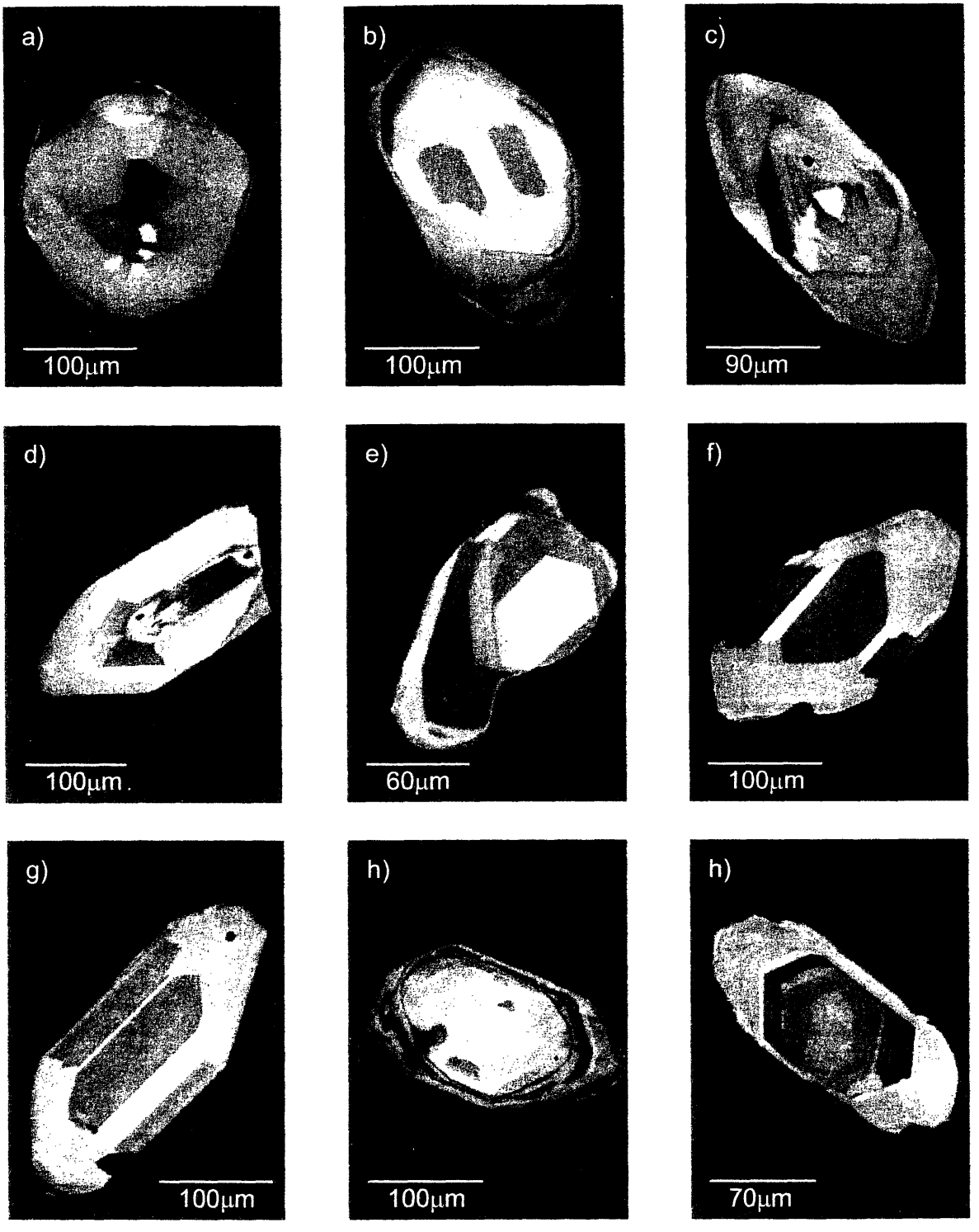

Figure x. Cathodoluminescence images of zircons from the Seven-Fingered Jack intrusion. (a-c) from sample EN24B, (d-e) from sample E-436, (f-g) from sample EN65, and (h-i) from sample EN3.

Table 1 U-Pb analyses from the Entiat Plutonic Complex.

	Composition						Isotopic Ratios								Dates (Ma)				
Frac[a]	Wt (μg)[b]	U (ppm)	Pb (ppm)	Th/U[c]	Pb*/Pbc[d]	Pbc[d] (pg)	$^{206}Pb/^{204}Pb$[e]	$^{208}Pb/^{206}Pb$[f]	$^{206}Pb/^{238}U$[f]	% err[g]	$^{207}Pb/^{235}U$[f]	% err[g]	$^{207}Pb/^{206}Pb$[f]	% err[g]	$^{206}Pb/^{238}U$[h]	$^{207}Pb/^{235}U$[h]	$^{207}Pb/^{206}Pb$[h]	corr. coef.	Discordance
Ho-52-1: Hornblende Quartz Diorite																			
z1	26.3	61.9	1.6	0.308	54.1	0.8	3543	0.099	0.026913	(.08)	0.18507	(.12)	0.049873	(.09)	171.20	172.41	189.1	0.638	9.6
z2	19.3	74.9	1.1	0.296	19.7	1.0	1307	0.095	0.014304	(.16)	0.09438	(.34)	0.047855	(.29)	91.56	91.58	92.1	0.543	0.5
z3	24.7	66.1	0.9	0.275	30.1	0.8	2004	0.088	0.014279	(.11)	0.09421	(.20)	0.047854	(.17)	91.40	91.42	92.1	0.582	0.7
EN41:Hornblende Gabbro																			
z1	2.4	147.1	1.8	0.268	8.2	0.5	558	0.086	0.012341	(.36)	0.08100	(1.03)	0.047605	(.92)	79.07	79.09	79.6	0.475	0.7
z2	2.1	164.6	2.0	0.261	5.2	0.8	360	0.083	0.012377	(.57)	0.08137	(.95)	0.047678	(.73)	79.30	79.43	83.3	0.642	4.9
z4	2.0	118.4	1.4	0.178	2.7	1.0	199	0.057	0.012192	(1.07)	0.08024	(2.16)	0.047736	(1.78)	78.12	78.37	86.2	0.570	9.5
EN42:Hornblende-Biotite Tonalite																			
z1	17.4	9.3	0.1	0.204	2.2	1.0	169	0.065	0.014428	(1.30)	0.09545	(2.55)	0.047982	(2.09)	92.34	92.57	98.4	0.578	6.2
z5	43.5	148.4	2.0	0.206	61.7	1.4	4169	0.066	0.014134	(.07)	0.09318	(.12)	0.047815	(.10)	90.48	90.46	90.2	0.561	-0.3
z6	18.5	170.9	2.4	0.284	39.1	1.1	2589	0.091	0.014359	(.09)	0.09489	(.16)	0.047928	(.13)	91.91	92.05	95.7	0.596	4.0
z7	16.1	190.0	2.6	0.194	52.0	0.8	3525	0.062	0.014309	(.07)	0.09439	(.15)	0.047840	(.13)	91.59	91.58	91.4	0.526	-0.3
EN28:Hornblende-Biotite Tonalite																			
z1	8.6	275.4	3.8	0.253	27.7	1.2	1856	0.081	0.014324	(.12)	0.09450	(.23)	0.047849	(.19)	91.68	91.69	91.8	0.560	0.1
z2	5.4	167.5	2.3	0.281	17.0	0.7	1140	0.090	0.014321	(.18)	0.09453	(.33)	0.047873	(.26)	91.66	91.71	93.0	0.593	1.4
z3	6.8	177.4	2.5	0.303	17.8	1.0	1182	0.097	0.014325	(.18)	0.09454	(.30)	0.047867	(.22)	91.69	91.73	92.7	0.652	1.1
z4	10.6	158.2	2.2	0.259	20.9	1.1	1403	0.083	0.014323	(.15)	0.09448	(.22)	0.047843	(.15)	91.68	91.67	91.5	0.712	-0.2
z5	5.3	170.8	2.4	0.311	16.8	0.8	1116	0.100	0.014330	(.18)	0.09452	(.33)	0.047839	(.27)	91.72	91.71	91.4	0.604	-0.4
z6	10.2	261.6	3.5	0.169	16.2	2.2	1120	0.054	0.014255	(.19)	0.09409	(.34)	0.047871	(.27)	91.25	91.31	92.9	0.606	1.8
z7	5.2	244.5	3.5	0.309	7.5	2.4	506	0.099	0.014342	(.40)	0.09465	(.61)	0.047863	(.43)	91.80	91.82	92.5	0.699	0.8
E-281: Hornblende-Biotite Tonalite																			
z1	8.0	775.5	11.0	0.337	7.9	11.2	528	0.108	0.014276	(.39)	0.09404	(.64)	0.047773	(.48)	91.38	91.26	88.0	0.664	-3.9
z2	11.6	387.5	5.4	0.271	23.8	2.6	1593	0.086	0.014327	(.13)	0.09438	(.29)	0.047779	(.25)	91.70	91.58	88.3	0.520	-3.9
z3	10.4	323.0	4.6	0.357	18.5	2.6	1208	0.114	0.014323	(.18)	0.09445	(.35)	0.047826	(.29)	91.68	91.64	90.7	0.557	-1.1
z4	5.8	413.6	5.5	0.122	6.2	5.2	447	0.039	0.014301	(.52)	0.09424	(1.00)	0.047795	(.82)	91.54	91.45	89.2	0.582	-2.7
z5	14.6	253.8	3.4	0.177	34.9	1.4	2385	0.056	0.014216	(.10)	0.09376	(.16)	0.047835	(.12)	90.99	91.00	91.1	0.636	0.1
EN24B: Hornblende Diorite Gneiss																			
z1	43.2	80.9	2.5	0.118	86.4	1.2	5959	0.039	0.032542	(.06)	0.22617	(.10)	0.050407	(.08)	206.44	207.03	213.8	0.629	3.5
z2	29.6	152.5	5.0	0.176	123.5	1.2	8378	0.056	0.034453	(.05)	0.23997	(.09)	0.050515	(.07)	218.36	218.39	218.7	0.643	0.2
z3	36.5	82.2	2.8	0.204	117.3	0.9	7890	0.065	0.034961	(.07)	0.24387	(.10)	0.050591	(.07)	221.52	221.58	222.2	0.708	0.3
z4	21.9	88.6	2.9	0.132	54.6	1.2	3755	0.043	0.034394	(.07)	0.23988	(.12)	0.050584	(.09)	217.99	218.32	221.9	0.627	1.8
z5	18.1	98.3	3.2	0.178	103.3	0.6	7002	0.057	0.034725	(.05)	0.24206	(.08)	0.050556	(.06)	220.05	220.10	220.7	0.630	0.3
E-498: Mylonitic Dike																			
z1	17.2	721.2	5.1	0.274	13.4	6.5	906	0.088	0.007214	(.24)	0.04678	(.42)	0.047035	(.33)	46.34	46.43	51.0	0.624	9.1
z3	7.5	858.0	6.2	0.345	14.6	3.2	963	0.110	0.007228	(.24)	0.04679	(.53)	0.046950	(.46)	46.43	46.43	46.7	0.502	0.6
z4	7.1	724.1	5.1	0.267	9.5	3.8	650	0.085	0.007235	(.32)	0.04683	(.60)	0.046940	(.48)	46.47	46.47	46.1	0.583	-0.7
z5	4.4	312.1	2.2	0.335	3.6	2.7	255	0.107	0.007236	(.82)	0.04685	(1.32)	0.046959	(.98)	46.48	46.49	47.1	0.669	1.4
z6	3.6	281.3	2.0	0.333	7.0	1.0	475	0.107	0.007204	(.43)	0.04664	(1.00)	0.046955	(.86)	46.27	46.29	46.9	0.523	1.4

Table 1 (continued). U-Pb analyses from the Entiat Plutonic Complex.

	Composition						Isotopic Ratios								Dates (Ma)				
Frac[a]	Wt (μg)[b]	U (ppm)	Pb (ppm)	Th[c] U	Pb*[d] Pbc	Pbc[d] (pg)	$^{206}Pb/^{204}Pb$[e]	$^{208}Pb/^{206}Pb$[f]	$^{206}Pb/^{238}U$[f]	% err[g]	$^{207}Pb/^{235}U$[f]	% err[g]	$^{207}Pb/^{206}Pb$[f]	% err[g]	$^{206}Pb/^{238}U$[h]	$^{207}Pb/^{235}U$[h]	$^{207}Pb/^{206}Pb$[h]	corr. coef.	Discord-ance
E-436:Hornblende-Biotite Tonalite																			
z3	9.2	2600	34.4	0.121	273.3	1.2	18847	0.039	0.014177	(.05)	0.09353	(.09)	0.047846	(.07)	90.75	90.78	91.7	0.634	1.0
z4	8.3	690.3	10.8	0.149	77.1	1.2	5279	0.048	0.016523	(.06)	0.11087	(.10)	0.048665	(.07)	105.64	106.76	131.7	0.660	19.9
z5	12.5	252.5	8.5	0.336	183.1	0.6	11855	0.107	0.033891	(.05)	0.23568	(.08)	0.050436	(.07)	214.85	214.88	215.1	0.589	0.1
z6	5.4	119.1	3.9	0.192	23.2	0.9	1585	0.059	0.034115	(.13)	0.23669	(.21)	0.050319	(.16)	216.25	215.71	209.7	0.657	-3.2
EN65:Hornblende-Biotite Tonalite																			
z1	22.3	178.4	2.5	0.288	62.1	0.9	4095	0.092	0.014356	(.07)	0.09469	(.17)	0.047840	(.14)	91.89	91.87	91.4	0.488	-0.6
z2	14.0	112.8	1.6	0.347	41.9	0.5	2725	0.111	0.014348	(.09)	0.09451	(.19)	0.047772	(.16)	91.84	91.70	88.0	0.521	-4.4
z3	13.5	160.9	2.2	0.263	29.3	1.0	1953	0.084	0.014072	(.12)	0.09281	(.31)	0.047833	(.27)	90.08	90.11	91.0	0.476	1.0
z4	14.5	192.5	2.6	0.258	46.7	0.8	3108	0.083	0.014036	(.08)	0.09254	(.13)	0.047815	(.11)	89.85	89.86	90.1	0.610	0.3
z5	17.6	116.1	1.7	0.325	38.4	0.8	2518	0.104	0.014376	(.09)	0.09483	(.18)	0.047840	(.15)	92.01	91.99	91.4	0.557	-0.7
EN3:Biotite Granodiorite																			
z1	5.7	263.0	4.2	0.181	20.9	1.1	1436	0.058	0.016666	(.15)	0.11070	(.25)	0.048174	(.19)	106.55	106.61	107.9	0.636	1.2
z2	4.8	508.8	8.0	0.143	40.2	1.0	2768	0.046	0.016774	(.09)	0.11165	(.14)	0.048273	(.10)	107.24	107.47	112.7	0.643	4.9
z3	9.1	75.0	1.3	0.375	16.9	0.7	1102	0.120	0.017111	(.19)	0.11371	(.30)	0.048195	(.22)	109.37	109.35	108.8	0.685	-0.5
z4	5.4	214.4	5.6	0.406	14.5	2.1	939	0.129	0.025529	(.22)	0.17370	(.29)	0.049347	(.19)	162.50	162.62	164.4	0.769	1.2
z5	3.1	141.8	2.2	0.199	4.1	1.7	294	0.063	0.016232	(.71)	0.10726	(1.58)	0.047926	(1.34)	103.80	103.46	95.6	0.537	-8.6
z6	4.7	252.7	4.4	0.309	14.1	1.4	941	0.099	0.017471	(.21)	0.11615	(.31)	0.048217	(.22)	111.65	111.58	109.9	0.715	-1.6
EN16: Fine-grained Tonalite																			
z1	42.2	138.4	1.6	0.511	24.2	2.8	1514	0.164	0.011315	(.15)	0.07410	(.29)	0.047499	(.23)	72.53	72.58	74.4	0.577	2.5
z2	38.3	130.7	1.6	0.540	149.0	0.4	9150	0.173	0.011325	(.06)	0.07417	(.13)	0.047502	(.11)	72.59	72.65	74.5	0.502	2.5
z3	22.2	365.9	4.2	0.453	238.9	0.4	15006	0.145	0.011319	(.05)	0.07409	(.09)	0.047470	(.07)	72.56	72.57	72.9	0.609	0.5
EN11:Hornblende-Biotite Tonalite																			
z2	12.0	219.0	2.6	0.504	19.2	1.6	1208	0.161	0.011349	(.18)	0.07434	(.34)	0.047509	(.28)	72.75	72.81	74.9	0.574	2.9
z3	5.0	403.4	4.6	0.407	6.9	3.3	459	0.131	0.011237	(.44)	0.07383	(.60)	0.047650	(.39)	72.03	72.32	82.0	0.756	12.2
z4	15.8	147.3	1.7	0.458	13.7	2.0	877	0.147	0.011336	(.23)	0.07422	(.43)	0.047485	(.34)	72.67	72.70	73.7	0.598	1.4
z5	24.7	143.0	1.7	0.477	21.2	1.9	1338	0.153	0.011345	(.15)	0.07421	(.29)	0.047445	(.23)	72.72	72.69	71.7	0.592	-1.5
z6	17.3	201.3	2.3	0.416	26.9	1.5	1724	0.133	0.011311	(.13)	0.07399	(.23)	0.047446	(.18)	72.51	72.48	71.7	0.618	-1.1
z7	22.7	345.5	4.1	0.472	18.1	5.1	1152	0.151	0.011375	(.17)	0.07436	(.22)	0.047413	(.12)	72.91	72.83	70.1	0.819	-4.1
z8	17.4	315.7	3.4	0.294	34.2	1.7	2260	0.094	0.011108	(.10)	0.07286	(.17)	0.047571	(.13)	71.21	71.41	78.0	0.653	8.7
z9	25.4	217.0	2.5	0.467	18.2	3.5	1154	0.150	0.011325	(.18)	0.07415	(.26)	0.047485	(.18)	72.60	72.63	73.7	0.714	1.5
s1	34.6	127.0	3.1	0.034	0.6	66.9	62.9	0.011	0.010353	(.25)	0.06781	(.97)	0.047501	(.89)	66.40	66.62	74.5	0.414	10.9
s2	31.1	86.1	2.2	0.038	0.6	45.4	58.4	0.012	0.010336	(.38)	0.06773	(1.31)	0.047524	(1.20)	66.29	66.54	75.6	0.418	12.4
s3	63.8	75.2	1.7	0.046	0.7	64.5	69.0	0.015	0.010391	(.25)	0.06808	(1.78)	0.047519	(1.67)	66.64	66.87	75.4	0.489	11.7
s5	61.6	88.8	1.6	0.045	1.1	47.6	95.9	0.014	0.010363	(.22)	0.06783	(1.04)	0.047472	(.96)	66.46	66.64	73.0	0.432	9.0
E-25: Mylonitic Tonalite																			
z5	0.7	510.9	5.4	0.196	2.8	1.4	211	0.063	0.011104	(1.00)	0.07258	(2.16)	0.047404	(1.81)	71.19	71.14	69.6	0.554	-2.3
z7	2.1	582.0	6.0	0.069	15.9	0.8	1130	0.022	0.011142	(.18)	0.07289	(.33)	0.047447	(.27)	71.43	71.44	71.8	0.592	0.5
z8	0.6	585.6	6.2	0.201	3.7	0.9	269	0.064	0.011145	(.77)	0.07290	(1.14)	0.047442	(.81)	71.45	71.45	71.5	0.709	0.1

Table 1 (continued). U-Pb analyses from the Entiat Plutonic Complex.

[a] All zircon fractions (i.e. z1) are composed of a single grain or fragment of a grain.

[b] Sample weights were estimated to within 40% using measured grain dimensions and a nominal density of 4.5 g/cm ^{3} for zircon.

[c] Th contents calculated from radiogenic ^{208}Pb and the $^{207}Pb/^{206}Pb$ date of the sample, assuming concordance between U-Th-Pb systems.

[d] Pb* and Pbc represent radiogenic Pb and common Pb respectively.

[e] Measured ratio corrected for fractionation and spike; Pb fractionation was 0.12 ±0.04%/a.m.u. for Faraday detector or 0.20 ± 0.04%/a.m.u.for Daly detector analysis, based on daily analysis of NBS-981.

[f] Measured ratios corrected for fractionation, spike, blank, and initial common Pb; nominal U blank = 0.1 pg ± 50% (2 σ); nominal Pb blank = 2.0 pg ± 50% (2 σ) or where lowe the total common Pb of the analysis ±10% (2σ); measured laboratory Pb composition: $^{206}Pb/^{204}Pb = 19.10$, $^{207}Pb/^{204}Pb = 15.72$, $^{208}Pb/^{204}Pb = 38.65 \pm 0.01$ (2σ); initial Pb composition from model of Stacey and Kramers (1975) at the nominal age of the fraction (i.e. 0.1 Ga).

[g] Numbers in parentheses are the % errors reported at the 2 σ confidence interval, propagated using the algorithms of Ludwig (1980).

[h] Isotopic ages calculated using the decay constants of Jaffey et al. (1971): $\lambda(^{235}U) = 9.8485 \times 10^{-10}$ yr^{-1} and $\lambda(^{238}U) = 1.55125 \times 10^{-10}$ yr^{-1}.

GEOCHRONOLOGIC CONSTRAINTS ON GRANITIC MAGMATISM

INTRODUCTION

Granitoid rocks are the most volumetrically significant part of continental magmatic arcs and contain a complex record of magma generation, transport, and crustal growth. Processes by which heat and mass are exchanged between ascending magmas and pre-existing crust are intimately linked to the development of composition heterogeneities and their distribution within the crust. Understanding the evolution of these processes, therefore, provides insight into the dynamics of crustal growth. The important role of granites (*sensu lato*) in formation of continental crust was acknowledged by Hutton in 1785 in his book *The Theory of the Earth*, and many of the questions he posed are still relevant today. In the following sections, I will first provide a historical perspective on the study of magma generation and transport, followed by a brief summary of the data from chapters 4 and 5. I will then discuss how these data provide insight into the construction and evolution of intrusive magmatic systems and the effect of these systems on the thermal structure of a continental magmatic arc.

GRANITE CONTROVERSIES: A HISTORICAL PERSPECTIVE

By the 1830s, geologists had reached the consensus that granite slowly crystallized at great depth from "subterranean lava" (see Pitcher, 1993). This consensus was pioneered by Charles Lyell and drew upon work by Poulett Scrope in 1825 that provided the first scientific basis to describe magma as a crystal suspension with an essential vapor content and a viscosity controlled by composition (see Pitcher, 1993). Over the last 50 years, several controversies have focused the debate on the processes by which granite forms and how it arrives at a certain position within the crust. One of the most contentious debates was argued between H.H. Read and N.L. Bowen in the 1950s. The central issue lay in the question: was granite formed by *in situ* transformation of other rock types (i.e. granitization), by partial melting of crustal rocks, or by fractional crystallization of mantle melts? Tuttle and Bowen (1958) determined phase relationships within the $NaAlSi_3O_8 - KAlSi_3O_8 - SiO_2 - H_2O$ system and concluded that granitic liquids may be generated from melting of quartzo-feldspathic rock but under conditions

that seemed unlikely to occur naturally. Not until the first experiments on dry melting in pelitic systems were carried out by Brown and Fyfe (1970) and Thompson (1982) was it demonstrated that granitic melts could be generated by incongruent melting of hydrous phases (micas and amphiboles). This work was consistent with field relationships linking pelitic migmatite to larger granitic bodies. Further experimental, geochemical, and isotopic work firmly established the crustal input to granite genesis and the role of mantle melts in the generation of intermediate composition granitoids (e.g., Patiño Douce, 1995, 1999; Pitcher, 1982; Chappell and White, 1974).

Another long-standing controversy that has dominated geologic debate is the so-called "room problem": the question of how space is created for the intrusion of magma into the upper crust. Proponents of granitization argued that space-generating mechanisms were not necessary, whereas others cited field evidence for forceful emplacement of magma. This controversy can be traced back to lively field discussions in 1835 by Norwegian petrologist Baltazar Keithau and Charles Lyell (see Pitcher, 1993). In the 1930s, Hans Cloos and co-workers focused on structural investigations of granitic rocks, and these developments were combined with microfabric studies (see Castro et al., 1999). Structural studies focused on the role of stoping, magma emplacement along structural discontinuities, and the interaction between intruding magma and the deforming envelope of country rock.

In the late 1970s and 1980s, new developments in structural geology concerning theories of flow and deformation in geologic materials led to a renewed interest in the room problem. Increasingly sophisticated analogue and computational models describing the rheological development of both magma and host rock have focused the modern debate. A key issue is whether magma ascent is accommodated by diapiric rise or ascent through dikes. The traditional idea of a buoyant granitic magma ascending through the continental crust as a slow-rising, *hot Stokes diapir* or by stoping was called into question. Marsh (1982) numerically modeled the effects of heat transfer between a rising diapir and the surrounding rock using a hot Stokes flow model whereby host rock is heated enough to ductilely flow around the diapir. Mahon et al. (1988) performed a similar study with ascent through a temperature-varying, non-isoviscous wall rock. Both studies reached the conclusion that diapiric ascent velocities at normal crustal

temperatures are so low that ascent into upper crustal levels is not possible on timescales less than the freezing times of large plutons (i.e., ~10^5 yrs). In contrast, Weinburg and Podladchikov (1994, 1995) show that heat transfer alone need not be the rate-limiting step controlling diapiric ascent, and the process is more effective if the rheology of the crust is considered non-Newtonian. In this model, the mechanism required to soften the crust is not thermal, as in the hot Stokes case, but dependent upon strain rate, which lowers host rock viscosity in the vicinity of the rising diapir. These *power-law diapirs* are proposed to reach within 10 km of the surface. Miller et al. (1999) proposed the new term *visco-elastic diapir* to describe magma ascent through host rocks with a complex rheology that ranges from elastic to viscous and varies both temporally and spatially. These diapirs may consist of one or more magma batches. Host rock deforms by both brittle and ductile processes, and ascent is driven by buoyancy plus regional stress.

An alternative to diapirism is ascent through narrow conduits, either as self-propagating dikes (Clemens and Mawer, 1992), along pre-existing faults (Hutton, 1992; Petford, 1996) or as an interconnected network of active shear zones and dilational structures (Brown and Solar, 1998; Collins and Sawyer, 1996; D'Lemos et al., 1993). The greatest difference between these models and diapiric ascent is the difference in magma ascent rate. Ascent in dikes may be up to a factor of 10^6 faster depending on the viscosity of the magma and the conduit width (Clemens, 1998; Petford, 1996). Given the possible rapid ascent of magma in dikes, timescales of pluton growth could also be geologically fast (<<1 Myr), even for large plutons (i.e., 1000-3000 km^3) (Clemens and Mawer, 1992; Petford, 1996), unless growth is limited by magma supply or by the mechanics of magma emplacement (Clemens, 1998; Johnson et al., 2001). In addition, chemical and thermal interactions between magma within dikes and the host rock are minimal, and there may be little evidence of the passage of large volumes of magma through the crust.

Even with centuries of study and debate, several important aspects of magma generation and transport are still unknown. Questions include: 1) Are composite intrusions constructed by continuous emplacement of small magmatic pulses or during more punctuated intervals? 2) At what level in the crust is textural and chemical homogeneity developed? 4) How long can a viscous mixture of melt and crystals reside

in the middle crust? Recent advances in geochronological techniques have made it possible to address these questions with high-precision temporal constraints. Modern low-blank, high-precision U-Pb geochronology permits the determination of crystallization ages of igneous rocks to a precision approaching 0.1%, but application of these techniques to the study of magma generation and transport has been underutilized. Specifically, unresolved issues that will influence the debate include the duration, episodicity, and rates at which individual intrusions are constructed, and the scale of compositional and temporal heterogeneity of a given magmatic system. Only when we can accurately and precisely describe the temporal evolution of magmatic systems, can we begin to make progress in solving the questions listed above. For this reason, I used high-precision U-Pb geochronology to elucidate the magmatic history of four composite intrusions within the Cretaceous North Cascades arc.

SUMMARY OF RESULTS FROM THE NORTH CASCADES

Chapters 4 and 5 present data from four composite intrusions in the North Cascades. These intrusions include the 3-4 kbar Mount Stuart batholith (MSB), the 7-9 kbar Tenpeak intrusion, and the 6-7 kbar Entiat and Seven-Fingered Jack intrusive suites (previously mapped as the Entiat pluton). Each intrusion displays a distinctive intrusive history that gives insight into the nature of magmatic systems.

Twelve samples from the MSB indicate that magma was emplaced during four punctuated intervals over a ca. 5.6 Myr time period (Chapter 4 – Fig. 12). These emplacement intervals occurred at 96.4-95.7 Ma, 94.6-94.5 Ma, 92.8-92.6 Ma and 91.0-90.8 Ma (Chapter 4). The oldest phases crop out in the NW hook-shaped region and the youngest phases crop out in the SE mushroom-shaped region. This intrusion exhibits gradational contacts between magma pulses of the same age but differing composition. The boundaries between age domains are poorly constrained because the predominantly tonalitic magmas are texturally and mineralogically similar even though they formed at significantly different times. Titanite analyses from primary grains in the hook and sill regions of the batholith approximate the time that these magma pulses cooled to near-solidus conditions. The titanite analyses yield dates that are within 1.5 Myr of the zircon crystallization age of the samples (Chapter 4 – Fig. 10), suggesting that magma within

each age domain had cooled below the closure temperature of titanite (i.e., ~650°C; Hodges, 2003) and near the H_2O-saturated solidus (Wyllie, 1983) before emplacement in the adjacent age domain.

Eight samples from the Tenpeak intrusion were collected from a range of composition and textural phases (Chapter 4). These phases have been mapped as discrete bodies that comprise a single pluton, and contacts between the bodies vary from gradational to sharp (Cater and Crowder, 1967; Crowder et al., 1966; Dragovich and Norman, 1995; Tabor et al., 2002; Tabor et al., 1987). Distinct textural and mineralogical differences such as plagioclase grain shapes and percentage of biotite versus hornblende define boundaries between magma pulses. The total duration of magma accumulation documented by these samples is 2.7 Myr, and the distribution of dates indicate that magma was emplaced at regular intervals with only short time periods (<0.5 Myr) between magma pulses (Chapter 4 – Fig. 12). Field relationships indicate that magma pulses were rheologically distinct from each other. The ca. 91.9 Ma internally-sheeted zone and the ca. 92.2-92.4 Ma Schaefer Lake tonalite are clearly truncated by later ca. 89.7 Ma Indian Creek tonalite.

In contrast to the Mount Stuart and Tenpeak intrusions, the Entiat and Seven-Fingered Jack intrusive suites are comprised of multiple elongate magma bodies/sheets that range in composition from gabbro to biotite granodiorite. These two intrusions had previously been mapped as one pluton; however, U-Pb zircon dates from fourteen samples indicate that these sheets were emplaced over at least three distinct time periods (Chapter 5). At the northwestern end of the body, the oldest sheets are coeval with the Triassic Dumbell plutons and should be considered part of that magmatic system. Sheets with ca. 90-92 Ma crystallization ages comprise the Seven-Fingered Jack suite and extend from the northwestern tip of the body and potentially most of the length of the body. Sheets with ca. 71-73 Ma crystallization ages comprise the Entiat intrusive suite and make up the more homogeneous southeastern end of the body. I was unable to obtain precise crystallization dates from several samples because of the presence several different age populations of zircon within a sample. The implications of these results for the origin and evolution of sheeted magmatic bodies are discussed below.

NATURE OF INTRUSIVE MAGMATIC SYSTEMS

Characteristics of Magma Reservoirs

The first question one must ask when studying intrusive magmatic systems is what constitutes a batholith, pluton or magma chamber? These terms are commonly used in the geologic literature, but their connotations are often unclear and their definitions need to be revised. The standard definition of a *batholith* (Bates and Jackson, 1987) is a large, generally discordant plutonic mass that has more than 100 km^2 of surface exposure and no known floor. Technically, a batholith only differs from a pluton in its size, but more commonly, the term batholith implies an intrusion composed of multiple plutons representing multiple magma pulses in a chemically related system. Earlier plutons may cool and solidified before emplacement of the next pulse, but all plutons are temporally or chemically related.

The term *pluton* was coined during the late 18^{th} century debate between Neptunists who argued that granite formed as a chemical precipitate from a primordial ocean, and Plutonists who argued that granite formed as a consequence of fluid and heat. The standard definition of a *pluton* – an igneous intrusion (Bates and Jackson, 1987) – is non-specific and originally signified only deep-seated or plutonic bodies of granitoid texture. However, the use of this term in the geologic literature generally implies that a pluton is composed of a single magma pulse or multiple magma pulses that were emplaced closely enough in time that the entire volume of the pluton existed in a magmatic state as one large magma chamber. This long-held view has been challenged recently by Glazner et al. (2004), and data from this thesis bear on this issue as discussed below.

Perhaps a more appropriate description of a pluton is a *magma reservoir* (c.f. Reid, 2003; Fig. 1). A magma reservoir consists of two portions – liquid and mush (e.g., Marsh, 1989; Reid, 2003; Sinton and Detrick, 1992; Vigneresse et al., 1996). The *liquid* regime behaves as a liquid in the mechanical sense and may contain up to 25-40% crystals, whereas the *mush* regime consists of a dense suspension containing up to 50-75% crystals that can resist shear deformation (Reid, 2003). A magma reservoir is distinct from a *magma chamber* in that the latter term implies an enclosed space more aptly compared to the liquid regime of the reservoir. As defined by Reid (2003), the

magma reservoir does not include the *melt-impregnated* regime (<25-50% melt) that is closer to the magma solidus than the mush state. As depicted in figure 1, only a limited portion of the magma reservoir is liquid at one time, and the boundaries of the magma reservoir are transient features. These boundaries broadly correspond to the conditions at which differential movement of crystals and melt, and therefore appreciable chemical modification of the magma, is likely to cease (Reid, 2003). In this more dynamic view of a pluton/magma reservoir, multiple pulses of magma are both spatially and temporally distinct, and multiple liquid reservoirs may exist in communication with the mush and melt-impregnated regimes.

Figure 1 likely represents a snapshot at any one time in the history of the Tenpeak or Mount Stuart intrusions. In the case of the Tenpeak intrusion, early-formed phases such as the Schaefer Lake tonalite intruded and then formed a mush region in which later sheets (i.e., elongate magma pulses) were emplaced as the sheeted zone and proto-mylonitic gneiss. Eventually these phases crystallized to the point that later pulses such as the Indian Creek tonalite truncated, rather than mixed with, earlier phases of the intrusion. These rheological and temporal differences suggest that the Tenpeak intrusion never existed as a single, convecting magma chamber.

The MSB also experienced a similar intrusive history, although longer time intervals existed between intrusion of different magma pulses. Titanite analyses suggest that magma pulses within the hook and sill domains had reached near solidus temperatures and effectively ceased to be part of the magma reservoir before the emplacement of the mushroom domain. Zircon dates from the mushroom-shaped domain range from 90.79±0.13 Ma to 91.02±0.10 Ma and constrain potential rates of magma emplacement into the MSB reservoir at its largest volume (~520 km^3; Chapter 4, Table 5). This magma reservoir comprised several different magma pulses that range in composition from gabbro to granodiorite and must have co-existed over the 230±130 kyr time span represented by these dates. Magma emplacement rates for just the mushroom-shaped domain are estimated at $2.4x10^{-3}$ km^3/yr, which is comparable to rates derived from other batholithic belts (Crisp, 1984). This rate estimate is also of the same order of magnitude as that derived from estimates of the rates of magma influx into the Mt. Shasta reservoir, the largest volcano of the Cascades chain, at $6.3x10^{-3}$ km^3/yr over the last 200

kyr (Grove et al., in press). The long term emplacement rates of the entire MSB and the Tenpeak intrusion are approximately an order of magnitude less at $0.2x10^{-3}$ km^3/yr and $0.1x10^{-3}$ km^3/yr, respectively (Chapter 4, Table 5).

The construction of the Entiat and Seven-Fingered Jack magma reservoirs most likely differed from figure 1 in that the contacts between magma pulses and host rock are steep and form sheets that are elongate in the vertical direction (Miller and Paterson, 2001; Paterson and Miller, 1998b). In this case, there is no clear evidence of where "ascent" processes ended and "emplacement" processes began. Multiple magma sheets coalesce to form elongate bodies that are 1-2 km in width. Sheets contacts within these elongate bodies are often cryptically marked by trails of host rock inclusions, zones of schlieren and/or subtle changes in orientation of magmatic foliation across planar boundaries.

These four systems present several different views of what constitutes a magma reservoir. All are composed of multiple magma pulses of varying composition, texture, and shape. Each system was constructed over at least 2 Myr up to 5.6 Myr time period. The differences between the systems relate to their internal magmatic contacts and the episodicity of magmatism. These differences may result from differing rates of intrusion or magma supply. At relatively slow rates of intrusion relative to cooling, magmatic systems may consist mostly of mush and relatively evolved melt (Shaw, 1985; Sinton and Detrick, 1992). At higher rates of intrusion, magma recharge may be frequent, which sustains the magma reservoir and may result in appreciable magma mixing (Koyaguchi and Kaneko, 2000; Reid, 2003). The Tenpeak system, and to some extent the Mount Stuart system, are more likely examples of a slow rate of intrusion because higher proportions of mush relative to liquid inhibit mixing and result in texturally distinct magma pulses. Less frequent recharge also implies a greater degree of cooling between magma pulses, also encouraging distinct textures. The Entiat and Seven-Fingered Jack intrusions more likely represent the case of higher rates of intrusion to cooling. This is supported by evidence of transfer of zircon crystals between different regimes of the magma reservoir as discussed in the next section. The ultimate control on the rate of intrusion may be a result of the rate of melt generation and magma supply (Petford et al., 2000). In cases where melt generation is limited, slow rates of intrusion may result.

Physical Processes within Magma Reservoirs

The geochronologic data from these four magmatic suites also constrain the timescales over which the magma reservoir evolves. In figure 1, different possible sources of crystals entrained in magma are depicted. Crystals such as zircon may be inherited from the surrounding country rock during ascent or upon emplacement. Crystals may also be transferred into the liquid regime from both the mush regime and the solidified margins of earlier phases depending upon the temperature of the mush and melt-impregnated regimes, the viscosity and volatile content of the magma and the extent of syn-magmatic deformation (Barboza and Bergantz, 2000; Renner et al., 2000; Vigneresse et al., 1996). These co-genetic crystals may be discernible from co-magmatic crystals (crystallized within the liquid regime) if there is a large enough age difference between the mush and melt-impregnated regimes and the liquid.

Transfer of crystals between the mush, melt-impregnated and liquid regime may be accomplished in several ways. Bergantz (2000) modeled the dynamics of mixing by recharge of a magmatic system. This modeling indicated that preservation of sharp internal contacts between magma pulses requires not just a large rheological contrast, but a high absolute viscosity of the host magma/mush. This, in turn, requires that the host magma/mush has a sufficiently low melt fraction so that grain-grain contiguity occurs. If the melt fraction is high enough within the mush regime, intrusion of a new magma pulse results in mixing and transfer of crystals between the liquid and mush. Along the nearly-solidified margin of the intrusion, emplacement of a new magma pulse may erode, or scour this contact back to a region where the solid fraction is high enough to be effectively rigid. This scouring would disaggregate portions of the mush and melt-impregnated regime and mix it with the intruding magma (Bergantz, 2000).

The timescales over which mixing occurs following reintrusion are on the order of the cooling time for the body of host magma/mush. The time, t, it takes for a magma sheet of thickness $2a$ and initial temperature, T_0, to cool below its solidus, T_s, at the center of the sheet can be described by the equation:

$$T_s = T_{hr} + B\frac{T_0 - T_{hr}}{2}\left[erf\left(\frac{a}{2\sqrt{\alpha t}}\right)\right]$$

where T_{hr} is the temperature of the host rock or mush, B is a constant that accounts for the latent heat of crystallization, and α is the thermal diffusivity (i.e. ~10^{-6} m^2/s). If I assume T_0=800°C, T_{hr}=600°C (i.e., just below the solidus), and T_s=650°C, then a sheets that is 1.75 km thick will cool below the solidus in 1 Myr. The cooling rate will increase with convection in the sheet, fluid circulation in the host rock and/or other shapes of magma pulses that allow for heat loss out of the sides of the body.

Another mechanism that has been proposed to rejuvenate or remobilize mush and nearly solidified portions of the magma reservoir is referred to as gas sparging (Bachmann and Bergantz, 2003). Rejuvenation, and hence the potential for mixing between partially-solidified and newly intruded magmas, occurs by the upward percolation of hot gas which acts as a "defrosting" agent for mush that has reached its rheological locking point. This mechanism is proposed to operate by shallow intrusion of volatile-rich mafic magma that stalls at the base of cooler, more silicic mush and exsolves a vapor phase. The vapor then advects heat upward through the mush at a potentially faster rate than by pure conduction. Numerical simulations show that if the temperature increase required for remobilization is limited to a few tens of degrees and the crystallinity of the mush is <70%, the volume of the volatile-rich mafic recharge required to cause rejuvenation is ~40% of the mush volume. The process by which mixing is thought to occur within the remobilized mush is referred to as convective self-mixing (Couch et al., 2001). Gas sparging may be an effective process for rejuvenation of shallow crustal magma reservoirs, such as proposed for the Fish Canyon tuff (Bachmann et al., 2002), but its effectiveness for remobilizing mid-crustal or deeper magma chambers remains to be proven.

In the case of the Tenpeak intrusion, nearly all samples display a tight cluster of concordant U-Pb zircon analyses as indicated by MSWDs near one (Chapter 4 – Figs. 14 and 15, Table 3), suggesting that each sample contains only one age population of zircon. This, in turn, suggests that the dates represent a single zircon crystallization event rather than zircon crystallization over a time period greater than the uncertainty on individual dates (typically ±0.28 Myr). Communication between the liquid and older, solidified parts of the system must also have been limited. In contrast, samples from the Mount

Stuart, Entiat and Seven-Fingered Jack intrusions show varying degrees of communication between different parts of the system.

Cathodoluminescence (CL) images of zircon from two samples from the hook region of the MSB (*MS5* and *MS6*) show brightly luminescent magmatic cores with dark magmatic rims (Chapter 4 – Fig. 6). U-Pb zircon dates from core and rim fragments plot on poorly-constrained discordia lines between a ca. 96 Ma lower intercept defined by rim fragments and a Middle Proterozoic upper intercept. These results suggest that the zircon cores were inherited from the host rock. One other sample from the MSB (PC-F) displays a range of zircon crystallization dates from 94.20±0.61 Ma to 94.92±0.58 Ma (Chapter 4 – Fig. 8, Table 1). This distribution suggests that sample PC-F contains more than one zircon age population, and may represent mixing between different pulses in the liquid regime of mixing between liquid and mush. The remaining samples form the MSB exhibit tight, concordant clusters of analyses similar to the Tenpeak samples (Chapter 4 – Figs. 7-9, Table 1).

The MSB differs from the Tenpeak intrusion in that even though the zircon dates suggest only limited transfer of crystals between liquid and mush regimes (PC-F), tonalitic magmas emplaced at distinctly different time periods in the MSB are texturally and mineralogically similar such that discrete contacts between age domains are difficult to define. One of the more surprising results of this study is that such similar and homogeneous tonalitic magmas were emplaced over the 5.6 Myr duration of MSB magmatism, whereas the Tenpeak intrusion developed varying textures over a shorter duration. Because the titanite data suggest that earlier magma pulses had cooled below the solidus prior to emplacement of later, adjacent magma pulses, then the observed textural homogeneity cannot be explained by magma mixing processes at the level of emplacement. This implies that such homogeneity was either inherited from the source region or developed during ascent.

The mineralogic and textural characteristics of the Entiat and Seven-Fingered Jack intrusive suites present a different picture. Three samples from the Seven-Fingered Jack intrusion yielded ca. 220 Ma dates or dates that can be explained by mixing between ca. 220 Ma cores and ca. 92-90 Ma magmatic overgrowths (Chapter 5 – Fig. 8). Zircon from three other Seven-Fingered Jack sheets (EN42, E-281, and EN65) and one sample

of the Entiat intrusion (EN11) show a 1-2 Myr range of crystallization dates that suggests they are co-genetic crystals remobilized from the mush or partially solidified parts of the magma reservoir. CL images from one of these samples (Chapter 5 – Fig. 8) lack any evidence of partial resorption of grains or magmatic overgrowths. The lack of these features suggests that the zircon grains introduced from the mush or melt-impregnated regime may have been isolated from the liquid inside early formed crystals. This distribution of dates indicates that remobilization of a partially-solidified reservoir is possible on timescales between 0.7 to 2.2 Myr. This distribution of dates also indicates that mixing and homogenization were occurring in the magma reservoir at the level of emplacement in constrast to the MSB system.

GEOTHERMAL GRADIENTS IN ARCS

The thermal structure of the crust plays a key role in the rheological, geochemical, and isotopic evolution of continental magmatic arcs. The distribution of heat influences the locations of crustal melting and strain partitioning (e.g. Paterson and Tobisch, 1992; Wyllie, 1979), and exhumation histories derived from thermochronology are dependent upon assumptions about how temperature changes with depth (i.e., the geothermal gradient or geotherm) (e.g., McDougall and Harrison, 1988). Estimating geotherms in arcs is complicated by the fact that much of the heat is advected by magma. The thermal histories that result from such heating differ from those of classical metamorphic terranes, where regionally extensive heat sources in the lower crust or upper mantle drive metamorphism (e.g., England and Thompson). Numerical models that aim to explain the evolution of continental magmatic arcs do not account for simultaneous crustal thickening, exhumation and advection of heat by magmatism. A key question is how the emplacement of voluminous magmatic intrusions influences the geothermal gradients of arcs.

The absence of well-studied examples of the deeper crustal levels of arcs requires extrapolation of geothermal gradients inferred from shallow depths (up to 10-15 km) to higher pressures. Shallow geothermal gradients are estimated from surface heat flow measurements in active arcs (e.g., Blackwell et al., 1982, 1990; Morgan, 1984) and low-pressure thermobarometric data (e.g., Turner, 1981). These estimates range from 30-

35°C/km in the upper 35 km (Giese, 1994; Morgan, 1984) and up to ~50°C/km in the upper 12 km (Henry and Pollack, 1988). However, seismic velocities and other geophysical data indicate that these geotherm estimates do not translate sensibly to the lower crust because they predict widespread melting and temperatures in excess of 1200°C at the base of the crust (Giese, 1994). These observations suggest that geothermal gradients are not constant with depth in active arcs, and that shallow geothermal gradients reflect a perturbation from some steady-state geotherm.

The emplacement of plutons in the crust creates thermal perturbations of host rock, and the magnitude of the perturbations varies depending upon the proximity to the pluton. As a result, the crust experiences localized contact metamorphism during short-lived events that, when integrated over the life of the arc, give the appearance of a regionally metamorphosed terrane at moderate to high temperatures (Barton and Hanson, 1989; Rothstein and Manning, 2003). In reality, there is a "background" advective geothermal gradient in the arc that characterizes much of the crust throughout the duration of magmatism. At any given time, only a fraction of the crust is at temperatures elevated above this background geotherm, and host rock temperatures will return to the background geotherm after being perturbed by magmatism (Rothstein and Manning, 2003). Because peak metamorphic temperatures decrease with distance from a pluton, the minimum host rock temperatures will represent the smallest excursion from the ambient host rock temperature during magmatism. These minimum host rock temperatures then define a maximum background geotherm that represents the highest possible *ambient* temperature at a given depth during magmatism.

Rothstein and Manning (2003) utilized thermobarometric data from several continental magmatic arcs to estimate this background geotherm. These P-T data defined a maximum background geotherm of ~22°C/km at depths of 10-25 km. The actual background geotherm lies somewhere between the upper limit defined by the maximum background geotherm and a geothermal gradient that was present prior to the magmatism. They take 18°C/km as a conservative lower limit because it is broadly characteristic of a stable continental lithosphere.

Thermobarometric data from the host rocks of the Mount Stuart and Tenpeak intrusions yield geothermal gradients consistent with the observations of Rothstein and

Manning (2003). Peak P-T data adjacent to the 3-4 kbar MSB (Bendixen, 1994; Brown and Walker, 1993; Evans and Berti, 1986; Stowell and Tinkham, 2003) yield a transient geotherm of 30-35°C/km to locally ~55°C/km. P-T data at a deeper level of the arc from host rock of the 7-9 kbar Tenpeak pluton (Valley et al., 2003) yield a geothermal gradient of ~20°C/km, which much more closely approximates the geotherm of Rothstein and Manning (2003). The duration of magmatism represented by the MSB and Tenpeak intrusion place time constraints on the longevity of the thermal perturbations to the crust. The overall duration of these magmatic systems ranges from 3 to 6 Myr, but the input of individual pulses is on the order of 1 Myr or less.

The continental magmatic arcs that Rothstein and Manning (2003) used to constrain their model were selected because they represented a range of crustal depths and the available structural and thermochronologic constraints indicated relatively simple thermal histories dominated by magmatic heating rather than tectonic thickening. These arc terranes include the eastern Peninsular Ranges batholith of southern California and Baja California, the Sierra Nevada batholith, and the Ryoke metamorphic belt, Japan. The North Cascades arc does not have such a simple tectonic history. Deformation in the Mount Stuart region occurred pre-, syn- and post-emplacement (Miller and Paterson, 1992; Paterson and Miller, 1998a). Syn- to post-magmatic tectonism will, to varying degrees, result in departures from the idealized thermal structure assumed by this model; however, the fact that the geothermal gradient estimated from the deep levels of the arc closely approximate the background geotherm defined by Rothstein and Manning (2003) suggests that crustal thickening in the North Cascades does not invalidate the model.

CONCLUSIONS

The data presented in chapters 4 and 5 provide high-precision temporal constraints on the intrusive histories of four contrasting magmatic systems in the North Cascades arc. These data support the view that magma reservoirs consist of a mush regime and potentially one or more liquid regimes. Communication between regimes may be limited if the rate of intrusion or magma recharge is slow relative to cooling. The Tenpeak intrusion likely represents this type of system, whereas the Entiat and Seven-Fingered Jack intrusions have characteristics more typical of a fast rate of intrusion or

magma recharge. Zircon grains from several samples of the Entiat and Seven-Fingered Jack intrusion display a range of crystallization ages within a given sample. These results suggest that zircon crystals were transferred between the mush and/or melt-impregnated regimes into the liquid phase. This transfer may have occurred by scouring of virtual "walls" created by the liquid-mush transition during recharge (i.e., Bergantz, 2000).

These data have implications for the questions posed within the granite controversies section and are addressed below:

1) *Are composite intrusions constructed by continuous emplacement of small magmatic pulses or during more punctuated intervals?* These intrusions contain abundant evidence that they were constructed from multiple pulses of magma. The geochronologic data from the MSB and Tenpeak intrusion suggest that these pulses remained distinct phases and challenge the view that these systems ever formed a single, convecting magma chamber. At the resolution of these dates, emplacment processes appear more episodic than continuous, which supports that idea that magma is emplaced in discrete batches.

2) *At what level in the crust is textural and chemical homogeneity developed?* Geochronologic data from the Entiat and Seven-Fingered Jack systems suggest that mixing between different regimes of the magma reservoir took place at the level of emplacement. In contrast, the lack of distinct internal contacts between tonalite of different age domains in the MSB suggests that, in this case, textural and chemical homogeneity was either inherited from the source region or developed during ascent. In addition, samples from both the Seven-Fingered Jack intrusion and the MSB contain zircon grains that have cores inherited from the surrounding country rock; however, the depth at which these crystals were introduced into the magma system is unconstrained.

3) *How long can a viscous mixture of melt and crystals reside in the middle crust?* Thermal models predict that with frequent recharge silicic liquid and/or mush may be maintained in the crust for several Myr (Annen and Sparks, 2002; Koyaguchi and Kaneko, 2000); however, the exact timescales are controlled by several assumptions including the frequency of recharge, geothermal gradient, and the temperatures of mush and recharge magma. The Entiat and Seven-Fingered Jack intrusions represent natural examples of magma reservoirs that remained active for 0.7 Myr to up to 2.2 Myr. These reservoirs may have existed entirely in the mush regime until recharge disaggregated the

mush and mixed with co-genetic, but distinctly older crystals. Natural examples such as these form important constraints on the longevity of magmatic systems.

In continental magmatic arcs, magmatic advection is the predominant heat transport mechanism that influences temperatures in the upper and middle crust (Barton and Hanson, 1989), and estimating geothermal gradients from metamorphic P-T-t paths in continental magmatic arcs is complicated by this fact. Thermobarometric data from the Mount Stuart region are consistent with shallow level, advective geotherms estimated from surface heat flow measurements in active arcs (Blackwell et al., 1982; Blackwell et al., 1990; Morgan, 1984). In contrast, P-T data from the Tenpeak region yield a ~20°C/km gradient, which is consistent with the maximum background geotherm of Rothstein and Manning (2003). The duration of magmatism represented by the MSB and Tenpeak intrusion place time constraints on the timescales of the thermal perturbations to the crust. These data also suggest that it is inappropriate to use geothermal gradients inferred from short-lived peak temperatures recorded in contact metamorphic assemblages to interpret exhumation processes that operate over longer timescales.

FUTURE WORK

The application of high-precision U-Pb geochronology has proved a useful tool in the study of the nature of magmatic systems and crustal evolution processes. The geochronologic results from chapters 4 and 5 reveal several new avenues of research that can be explored. In particular, interpretation of U-Pb zircon dates would be greatly enhanced if the petrographic setting of each grain could be defined prior to analysis. With this knowledge, we may be able to determine when in the crystallization history zircon began to crystallize and how this relates to the rheological state of the magma. It may also be possible to distinguish zircon grains from different parts of the magma reservoir based on their inclusion in specific minerals.

Future work must also focus on the development of realistic numerical models that describe the timescales of cooling of these magma systems. The models need to address variations in shape of magma pulses, rates and episodicity of recharge and an accurate assessment of host rock temperatures. These parameters can be better constrained with more detailed thermochronology. Titanite data from the MSB and

Tenpeak intrusion yielded important controls on the magmatic evolution of these systems; however, careful consideration of the nature of titanite growth (i.e., primary or secondary) is necessary to interpret the results.

Finally, a multi-disciplinary approach must be taken to further develop our understanding of magmatic systems. Advances in geochronology techniques have added a sophisticated tool with which to study intrusions, but these data need to be fully integrated with field, geophysical, isotopic, geochemical and rheological studies.

REFERENCES

Annen, C., and Sparks, R. S. J., 2002, Effects of repetitive emplacement of basaltic intrusions on thermal evolution and melt generation in the crust: Earth and Planetary Science Letters, v. 203, p. 937-955.

Bachmann, O., and Bergantz, G. W., 2003, Rejuvenation of the Fish Canyon magma body: a window into the evolution of large-volume silicic magma systems: Geology, v. 31, p. 789-792.

Bachmann, O., Dungan, M. A., and Lipman, P. W., 2002, The Fish Canyon magma body, San Juan volcanic field, Colorado: rejuvenation and eruption of an upper-crustal batholith: Journal of Petrology, v. 43, p. 1469-1503.

Barboza, S. A., and Bergantz, G. W., 2000, Metamorphism and anatexis in the mafic complex contact aureole, Ivrea Zone, northern Italy: Journal of Petrology, v. 41, p. 1307-1327.

Barton, M. D., and Hanson, R. B., 1989, Magmatism and the development of low-pressure metamorphic belts: implications from the Western United States and thermal modeling: Geological Society of America Bulletin, v. 101, p. 1051-1065.

Bates, R. L., and Jackson, J. A., 1987, Glossary of Geology: Alexandria, Virginia, American Geological Institute, 788 p.

Bendixen, J., 1994, Thermobarometry and structural history of the pelitic Chiwaukum Schist, northern Cascades, Washington [M.S. thesis]: University of Southern California, Los Angeles.

Bergantz, G. W., 2000, On the dynamics of magma mixing by reintrusion: implications for pluton assembly processes: Journal of Structural Geology, v. 22, p. 1297-1309.

Blackwell, D. D., Bowen, R. G., Hull, D. A., Riccio, J., and Steele, J. L., 1982, Heat flow, arc volcanism, and subduction in northern Oregon: Journal of Geophysical Research, v. 87, p. 8735-8754.

Blackwell, D. D., Steele, J. L., Kelley, S., and Korosec, M. A., 1990, Heat flow in the State of Washington and thermal conditions in the Cascade Range: Journal of Geophysical Research, v. 95, p. 19,495-19,516.

Brown, E. H., and Walker, N. W., 1993, A magma-loading model for Barrovian metamorphism in the Southeast Coast Plutonic Complex, British Columbia and Washington: Geological Society of America Bulletin, v. 105, p. 479-500.

Brown, G. C., and Fyfe, W. S., 1970, The production of granitic melts during ultrametamorphism: Contributions to Mineralogy and Petrology, v. 28, p. 310-318.

Brown, M., and Solar, G. S., 1998, Granite ascent and emplacement during contractional deformation in convergent orogens: Journal of Structural Geology, v. 20, p. 1365-1393.

Castro, A., Fernández, C., and Vigneresse, J. L., 1999, Understanding granites: integrating new and classical techniques, *in* Castro, A., Fernández, C., and Vigneresse, J. L., eds., Understanding Granites: Integrating New and Classical Techniques: London, Geological Society of London, p. 278.

Cater, F. W., and Crowder, D. F., 1967, Geologic map of the Holden Quadrangle, Snohomish and Chelan counties, Washington: U. S. Geological Survey.

Chappell, B. W., and White, A. J. R., 1974, Two contrasting granite types: Pacific Geology, v. 8, p. 173-174.

Clemens, J. D., 1998, Observations on the origins and ascent mechanisms of granitic magmas: Journal of the Geological Society of London, v. 155, p. 843-851.

Clemens, J. D., and Mawer, C. K., 1992, Granitic magma transport by fracture propagation: Tectonophysics, v. 204, p. 339-360.
Collins, W. J., and Sawyer, E. W., 1996, Pervasive granitoid magma transfer through the lower-middle crust during non-coaxial compressional deformation: Journal of Metamorphic Geology, v. 14, p. 565-579.
Couch, S., Sparks, R. S. J., and Carroll, M. R., 2001, Mineral disequilibrium in lavas explained by convective self-mixing in open magma chambers: Nature, v. 411, p. 1037-1039.
Crisp, J. A., 1984, Rates of magma emplacement and volcanic output: Journal of Volcanology and Geothermal Research, v. 20, p. 177-211.
Crowder, D. F., Tabor, R. W., and Ford, A. B., 1966, Geologic map of the Glacier Peak quadrangle, Snohomish and Chelan counties, Washington: U. S. Geological Survey.
D'Lemos, R. S., Brown, M., and Strachan, R. A., 1993, Granite magma generation, ascent and emplacement within a transpressional orogen: Journal of the Geological Society of London, v. 149, p. 487-490.
Dragovich, J. D., and Norman, D. K., 1995, Geologic map of the west half of the Twisp 1:100,000 Quadrangle, Washington, scale 1:100,000.
England, P. C., and Thompson, A. B., 1984, Pressure-temperature-time paths of regional metamorphism, I: Heat transfer during the evolution of regions of thickened continental crust: Journal of Petrology, v. 25, p. 894-928.
Evans, B. W., and Berti, J. W., 1986, Revised metamorphic history for the Chiwaukum Schist, North Cascades, Washington: Geology, v. 14, p. 695-698.
Giese, P., 1994, Geothermal structure of the Central Andean crust; implications for heat transport and rheology, *in* Reutter, K. J., Scheuber, E., and Wigger, P. J., eds., Tectonics of the southern Central Andes: structure and evolution of an active continental margin: Berlin, Springer-Verlag, p. 69-76.
Glazner, A. F., Bartley, J. M., Coleman, D. S., Gray, W., and Taylor, R. Z., 2004, Are plutons assembled over millions of years by amalgamation from small magma chambers?: GSA Today, v. 14, p. 4-11.
Grove, T. L., Baker, M. B., Price, R. C., Parman, S. W., Elkins-Tanton, L. T., Chatterjee, N., and Müntener, O., in press, Magnesian andesite and dacite lavas from Mt. Shasta, northern California: Products of fractional crystallization of H_2O-rich mantle melts: Contributions to Mineralogy and Petrology.
Henry, S. G., and Pollack, H. N., 1988, Terrestrial heat flow above the Andean subduction zone in Bolivia and Peru: Journal of Geophysical Research, v. 93, p. 15,153-15,162.
Hodges, K. V., 2003, Geochronology and thermochronology in orogenic systems, *in* Rudnick, R. L., ed., Treatise on Geochemistry: Amsterdam, Elsevier, p. 263-292.
Hutton, D. H., 1992, Granite sheeted complexes: evidence for the dyking ascent mechanism: Transactions of the Royal Society of Edinburgh: Earth Sciences, v. 83, p. 377-382.
Johnson, S. E., Albertz, M., and Paterson, S. R., 2001, Growth rates of dike-fed plutons: are they compatible with observations in the middle and upper crust?: Geology, v. 29, p. 727-730.
Koyaguchi, T., and Kaneko, K., 2000, Thermal evolution of silicic magma chambers after basalt replenishments: Transactions of the Royal Society of Edinburgh: Earth Sciences, v. 91, p. 46-60.
Marsh, B. D., 1982, On the mechanics of igneous diapirism, stoping, and zone-melting: American Journal of Science, v. 282, p. 808-855.
Marsh, B. D., 1989, Magma chambers: Annual Review of Earth and Planetary Sciences, v. 17, p. 439-474.
McDougall, I., and Harrison, T. M., 1988, Geochronology and thermochronology by the $^{40}Ar/^{39}Ar$ method, Oxford Monographs on Geology and Geophysics, 212 p.
Miller, R. B., and Paterson, S. R., 1992, Tectonic implications of syn-emplacement and postemplacement deformation of the Mount Stuart batholith for mid-Cretaceous orogenesis in the North Cascades: Canadian Journal of Earth Sciences, v. 29, p. 479-485.
Miller, R. B., and Paterson, S. R., 1999, In defense of magmatic diapirs: Journal of Structural Geology, v. 21, p. 1161-1173.
Miller, R. B., and Paterson, S. R., 2001, Construction of mid-crustal sheeted plutons: Examples from the north Cascades, Washington: Geological Society of America Bulletin, v. 113, p. 1423-1442.
Morgan, P., 1984, The thermal structure and thermal evolution of the continental lithosphere, *in* Pollack, H. N., and Murthy, V. R., eds., Structure and evolution of the continental lithosphere, Physics and Chemistry of the Earth, p. 107-193.

Paterson, S. R., and Miller, R. B., 1998a, Magma emplacement during arc-perpendicular shortening: An example from the Cascades crystalline core, Washington: Tectonics, v. 17, p. 571-586.
Paterson, S. R., and Miller, R. B., 1998b, Mid-crustal magmatic sheets in the Cascades Mountains, Washington: implications for magma ascent: Journal of Structural Geology, v. 20, p. 1345-1363.
Paterson, S. R., and Tobisch, O. T., 1992, Rates of processes in magmatic arcs: Implications for the timing and nature of pluton emplacement and wall rock deformation: Journal of Structural Geology, v. 14, p. 291-300.
Patiño Douce, A. E., 1995, Experimental generation of hybrid silicic melts by reaction of high-Al basalt with metamorphic rocks: Journal of Geophysical Research, v. 100, p. 15,623-15,639.
Patiño Douce, A. E., 1999, What do experiments tell us about relative contributions of crust and mantle to the origin of granitic magmas?, *in* Castro, A., Fernández, C., and Vigneresse, J. L., eds., Understanding Granites: Integrating New and Classical Techniques: London, Geological Society of London, p. 55-75.
Petford, N., 1996, Dykes or diapirs?: Transactions of the Royal Society of Edinburgh: Earth Sciences, v. 87, p. 105-114.
Petford, N., Cruden, A. R., McCaffrey, K. J. W., and Vigneresse, J. L., 2000, Granite magma formation, transport and emplacement in the Earth's crust: Nature, v. 408, p. 669-673.
Pitcher, W. S., 1982, Granite type and tectonic environment, *in* Hsue, K. J., ed., Mountain Building Processes: Zurich, Switzerland, Academic Press, p. 19-40.
Pitcher, W. S., 1993, The nature and origin of granite: London, Chapman & Hall, 321 p.
Reid, M. R., 2003, Timescales of magma transfer and storage in the crust, *in* Rudnick, R. L., ed., Treatise on Geochemistry: Amsterdam, Elsevier, p. 263-292.
Renner, J., Evans, B., and Hirth, G., 2000, On the rheologically critical melt fraction: Earth and Planetary Science Letters, v. 181, p. 585-594.
Rothstein, D. A., and Manning, C. E., 2003, Geothermal gradients in continental magmatic arcs: constraints from the eastern Peninsular Ranges Batholith, Baja California, Mexico, *in* Johnson, S. E., Paterson, S. R., Fletcher, J. M., Girty, G. H., Kimbrough, D. L., and Martin-Barajas, A., eds., Tectonic evolution of northwestern Mexico and the Southwestern USA: Boulder, Colorado, Geological Society of America, p. 337-354.
Shaw, H. R., 1985, Links between magma-tectonic rate balances, plutonism, and volcanism: Journal of Geophysical Research, v. 90, p. 11,275-11,288.
Sinton, J. M., and Detrick, R. S., 1992, Mid-ocean ridge magma chambers: Journal of Geophysical Research, v. 97, p. 197-216.
Stowell, H. H., and Tinkham, D. K., 2003, Integration of phase equilibria modelling and garnet Sm-Nd chronology for construction of P-T-t paths: Examples from the Cordilleran Coast Plutonic Complex, USA, *in* Vance, D., Muller, W., and Villa, I., eds., Geochronology: Linking the Isotopic Record with Petrology and Textures, Geological Society of London, p. 119-145.
Tabor, R. W., Booth, D. B., Vance, J. A., and Ford, A. B., 2002, Geologic map of the Sauk River 30- by 60-minute quadrangle, Washington: U.S. Geological Survey, scale 1:100000.
Tabor, R. W., Frizzell, V. A., Jr., Whetten, J. T., Waitt, R. B., Jr., Swanson, D. A., Byerly, G. R., Booth, D. B., Hetherington, M. J., and Zartman, R. E., 1987, Geologic map of the Chelan 30' by 60' Quadrangle, Washington: U. S. Geological Survey, scale 1:100,000.
Thompson, A. B., 1982, Dehydration melting of pelitic rocks and the generation of H_2O-undersaturated granitic liquids: American Journal of Science, v. 282, p. 1567-1595.
Turner, F. J., 1981, Metamorphic petrology: mineralogical, field, and tectonic aspects, International series in the Earth and planetary sciences: New York, McGraw-Hill, 524 p.
Tuttle, O. F., and Bowen, N. L., 1958, Origin of granite in the light of experimental studies in the system $NaAlSi_3O_8$ - $KAiSi_3O_8$ -SiO_2 - H_2O: Geological Society of America Memoir, v. 74, p. 153.
Valley, P. M., Whitney, D. L., Paterson, S. R., Miller, R. B., and Alsleben, H., 2003, Metamorphism of the deepest exposed arc rocks in the Cretaceous to Paleogene Cascades belt, Washington: evidence for large- scale vertical motion in a continental arc: Journal of Metamorphic Geology, v. 21, p. 203-220.
Vigneresse, J. L., Barbey, P., and Cuney, M., 1996, Rheological transitions during partial melting and crystallization with application to felsic magma segregation and transfer: Journal of Petrology, v. 37, p. 1579-1600.

Weinberg, R. F., and Podladchikov, Y., 1994, Diapiric ascent of magmas through power law crust and mantle: Journal of Geophysical Research, v. 99, p. 9543-9559.
Weinberg, R. F., and Podladchikov, Y. Y., 1995, The rise of solid-state diapirs: Journal of Structural Geology, v. 17, p. 1183-1195.
Wyllie, P. J., 1979, Petrogenesis and the physics of the Earth, *in* Yoder, H. S., Jr., ed., The evolution of the igneous rocks: Princeton, Princeton University Press, p. 483-520.
Wyllie, P. J., 1983, Experimental and thermal constraints on the deep-seated parentage of some granitoid magmas in subduction zones, *in* Atherton, M. P., and Gribble, C. D., eds., Migmatites, melting and metamorphism: Proceedings of the Geochemical Group of the Mineralogical Society of the University of Glasgow: Glasgow, United Kingdom, Geochemical Group of the Mineralogical Society of the University of Glasgow, p. 37-51.

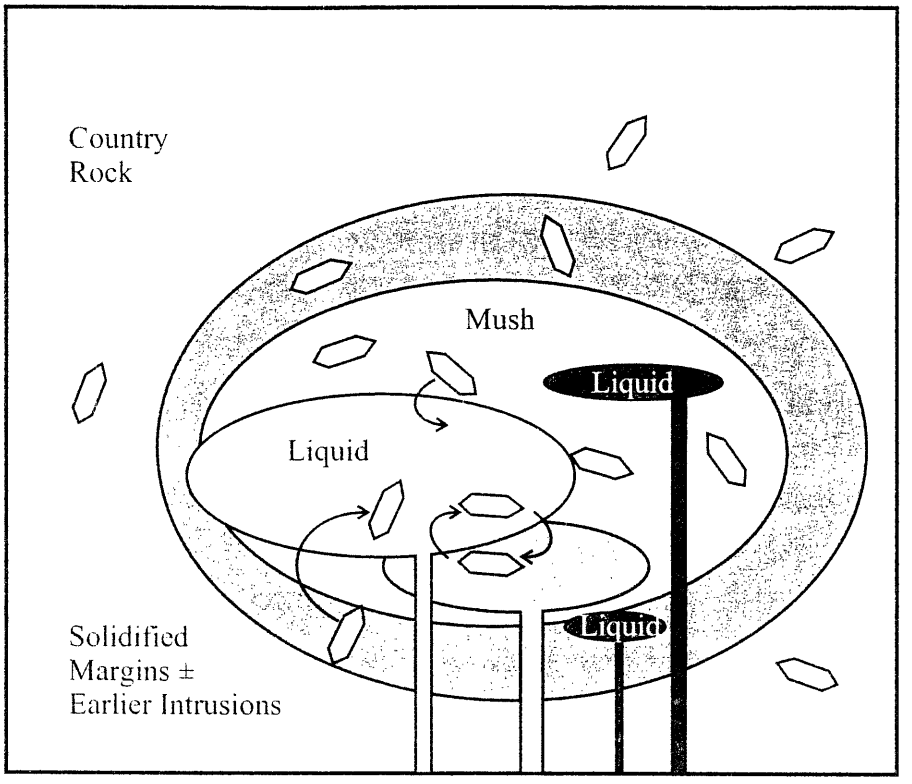

Figure 1. Cartoon of a magma reservoir illustrating the possible sources of crystals contained within a magma (after Reid, 2003).